UNIVERSITY OF SOUTHAMPTON

FACULTY OF NATURAL AND ENVIRONMENTAL SCIENCES

School of Ocean and Earth Science

Dissolved Manganese in Ocean Waters: Analytical and Biogeochemical Studies

by

Farah Akmal Idrus

Thesis for the degree of Doctor of Philosophy

June 2013

UNIVERSITY OF SOUTHAMPTON

ABSTRACT

FACULTY OF NATURAL AND ENVIRONMENTAL SCIENCES
School of Ocean and Earth Science

Doctor of Philosophy

Dissolved Manganese in Ocean Waters: Analytical and Biogeochemical Studies

By Farah Akmal Idrus

The aim of this study was to improve our understanding of the natural sources and processes of the dissolved manganese associated with the Southern Ocean and the Tropical North-Eastern (NE) Atlantic Ocean.

A flow injection analyser (FIA) with chemiluminescence (CL) detection was first set up for the determination of dissolved manganese (DMn, ≤ 0.2 µm). Extension work was undertaken to solve problems relating to our limited level of understanding of the CL reaction, and the behaviour of the resins used to either preconcentrate the manganese (*i.e.* Toyopearl AF-Chelate 650M) or to remove the interfering elements (cleaning resin, i.e. NTA Superflow and 8-Hydroxyquinoline). Using the system built in our laboratory, the determination of the interference of other dissolved trace metals (e.g. Fe, Ni, Cu, Co, Zn and Cd) were possible with dissolved manganese measurement in order to obtain a good measurable CL peak for dissolved manganese.

The distribution of manganese around the Crozet Islands was examined and was used to provide a conceptual framework for future studies. Dissolved manganese concentrations were measured in samples collected from nine vertical profiles taken across the Crozet Plateau (80 - ~4500 m water depth) that show evidence of a range of processes influencing the manganese distributions. Dissolved manganese varied between 0.1 and 2.44 nM, and the resulting detailed section showed evidence of an island souce is identified which suggests that the plateau and the associated sediments are a source of manganese. Waters further north also appear to be affected by this input of both coastal and shelf origin, although dissolved manganese decrease as a function of distance to the north of the plateau with a gradient of 0.096 nM/km as a result of dispersion and mixing. This gradient was then combined with short-lived Radium isotopes profiles, allowing the determination of a lateral advective flux of manganese (up to 538 nmol/m^2/d). Estimates of atmosphere and vertical fluxes of manganese to surface waters were also calculated. It was then possible to estimate a pre-bloom concentration of ~0.4 nM.

A set of surface samples were collected from the Tropical NE Atlantic Ocean, and were analysed for dissolved manganese. Results suggest the land-sources of manganese near to the Canary Islands, the Cape Verde Islands and the African Continent, where high dissolved manganese concentrations were determined, with the highest is ~3.90 nM. The lateral advective flux of manganese was higher (47 µmol/m^2/d) than the atmospheric flux of manganese (0.17 µmol/m^2/d), thus making the shelf+sediment as the most prominent sources of dissolved manganese in the seawater close to the islands. From this atmospheric flux of manganese, it was then possible to estimate the manganese enrichment around the further offshore dust event regions of 0.73 nM/yr and consistent with the dissolved manganese background concentrations. This support the low residence time calculated in dust event regions of around 1 year.

LIST OF CONTENTS

LIST OF FIGURES

CHAPTER I.

CHAPTER II.

CHAPTER III.

CHAPTER IV.

CHAPTER V.

LIST OF TABLES

CHAPTER I.

CHAPTER II.

CHAPTER III.

CHAPTER IV.

CHAPTER V.

LIST OF APPENDICES

DECLARATION OF AUTHORSHIP

I, Farah Akmal Idrus, declare that the thesis entitled:

Dissolved Manganese in Ocean Waters: Analytical and Biogeochemical Studies

and the work presented in the thesis are both my own, and have been generated by me as the result of my own original research. I confirm that:

- this work was done wholly or mainly while in candidature for a research degree at this University;
- where any part of this thesis has previously been submitted for a degree or any other qualification at this University or any other institution, this has been clearly stated;
- where I have consulted the published work of others, this is always clearly attributed;
- where I have quoted from the work of others, the source is always given. With the exception of such quotations, this thesis is entirely my own work;
- I have acknowledged all main sources of help;
- where the thesis is based on work done by myself jointly with others, I have made clear exactly what was done by others and what I have contributed myself;
- none of this work has been published before submission

Signed: Farah Akmal Idrus
Date: **7th June 2013**

Acknowledgements

My journey began when I was given the opportunity back in 2007 by Professor Peter J. Statham came over to a very different country than the one I grew up. And it was a beautiful journey indeed, full of experiences, memories and hard times. So how can I not be very grateful to Professor Peter J. Statham, who with his intense and rigorous efforts helped me become an independent researcher. His continuous guidance and pressure helped me progress and provided serious work. He also always there to help me in my work through the endless discussions on my subject that helped in expand my view. I also would like to thank Dr Denise Smythe-Wright and Dr Doug Connelly not only because they were there to help me expanding my view of my work, but more importantly for the moral support that I needed to keep going. Special thanks are also owe to Professor Harry Bryden who gave me moral support and motivation that I needed when I was ready to give up, that encouraged me to keep going. The best and most exciting time during my PhD was my participation in the Extended Ellet Line 2010 Cruise D351 and I really thank Professor Eric Achterberg for that but also reminding me that science is also fun. During that cruise there was not a person I could not thank either researchers or member of the crews because without them it would have been impossible to make it through. However special thanks had to go to Dr Sebastian Steigenberger for all the help with the clean technique of samples collection on the cruise. I also would like to thank Dr Duncan Purdie, Dr Micha Rijkenberg, and Dr Sebastian Steigenberger for providing me with their results. I would also like to thank everyone who helped during my long hours in the laboratory either by showing something or just coming to greet me like Dr Alexandra Xylouri, Dr Mattew Patey, Dr Sebastian Steigenberger, Dr Khairul Nizam, Dr Ibrahim Muhammed, Dr. Pornsri Mingkwan, and probably others that I am forgetting to mention here. Special thanks too to my dear friends Dr Aazani Mujahid, Dr Lailatul Qadri, Dr Nurlida Basir, Dr Hayati Yusof, Dr Nabilah Ramli who helped me so much in many levels of my life, career and personal. I also wanted to thank my beloved parents and family, especially to my father Dr Idrus Isa, who gave me everything and more importantly freedom and support to follow my dreams. Until his last breathe on October 19, 2011, my father still encouraged me not to give up on completing my PhD. Lastly, I need to thank my husband, Mr. Nazrul Faris, who never lost faith in me and made me believe in myself.

Chapter I: Introduction and Objectives

Why is manganese important in the oceans? What is the biogeochemistry of manganese in seawater? What does this thesis aim to do?

These are questions that this chapter aims to answer, and in doing so demonstrate the relevance of this study to ocean and earth science. Firstly, an overview of why manganese plays an important role in biogeochemical processes in the ocean is given together with information on its speciation, concentrations and distributions. Then mechanisms controlling the input, removal and recycling of manganese in seawater throughout the oceans will be presented, and the oceanic waters investigated here that require more research to better understand processes controlling Mn concentrations are introduced. At the end of the chapter, the project aims and objectives of this study will be outlined, along with an overview of the chapters that follow to address these goals.

1 The importance of manganese in the oceans

Manganese plays an important role in both inorganic and biological processes in the ocean. Removal of a range of trace elements from sea water during formation of oxidised solid forms of Mn has led to formation of concretions and deposits (Nicholson *et al.*, 1997) with implications for the marine geochemistry of these elements. Additionally dissolved manganese is vital for the metabolic functioning of many living organisms, where it is fundamental in oxidation and reduction processes in plants, such as the electron transport in photosynthesis and radical scavenging enzymes (Horsburgh *et al.,* 2002; Kernen *et al.,* 2002). Thus the synthesis of organic carbon directly from carbon dioxide using energy from light by phytoplankton in the ocean (*i.e.* through photoautotrophs such as algae, diatoms, and cyanobacteria) is dependent on manganese.

However, other factors, such as the presence of additional nutrients, also control the process of photosynthesis. Nutrients that are consumed by phytoplankton in large quantities are called macronutrients (*e.g.* ammonia, nitrate, phosphate and silicic acid) and nutrients that are required in small quantities are called micronutrients (mostly trace metal elements *e.g.* iron, manganese, zinc, copper, nickel). These micronutrients are not only required in small quantities, but are also present in seawater at typically low concentrations. Lack of availability of any of these nutrients may result in limitation of oceanic production. Alfred Redfield (Redfield *et al.,* 1963) initially developed a general concept of the ratio of the composition of major nutrients: **C: N: P = 106:16:1**. Subsequently researchers found that several trace metals *i.e.* iron, manganese, zinc, copper, nickel, cobalt and cadmium (*e.g.* Morel *et al.*, 2003; Bruland *et al.,* 1991) are also vital for phytoplankton growth as they are used as co-factors in many enzymes in vital

processes (*e.g.* (Sunda and Huntsman, 1983)). Later, the Redfield ratio formula was extended to:

$$(C_{124}N_{16}P_{1}S_{1.3}K_{1.7}Mg_{0.56}Ca_{0.5})_{1000}Sr_{5.0}Fe_{7.5}Mn_{3.0}Zn_{0.80}Cu_{0.38}Co_{0.19}Cd_{0.21}Mo_{0.03}$$

However, the stoichiometry of this extended ratio may vary between phytoplankton species (Twining *et al*., 2004).

Manganese in organisms is a constituent of essential metalloenzymes, including the antioxidant defense enzyme Mn-superoxide dismutase (Mn-SOD), that protects phytoplankton cells by deactivating free radicals which can destroy phytoplankton tissues (Bascik-Remisiewicz *et al*., 2009). Manganese is also required in the dark reaction of photosynthesis to activate the enzyme Rubisco (Ribulose 1-5-bisphophate carboxylase oxygenase) (Morel *et al.,* 2003 and references therein).

However, manganese is crucial in Photosystem II (PSII), where four manganese ions of oxidation states between +3 and +5, and divalent calcium ions, are required in the "Manganese Centre" or the oxygen evolving centre (Umena *et al.,* 2011). During photosynthesis, the photonic energy of light is collected by the light harvesting chlorophyll complex II (LHCII). Excitation energy is transferred from LHCII to a chlorophyll molecule (P680) in the reaction centre of PSII, where the primary charge separation takes place between P680 and pheophytin (Pheo) molecules. At this point, the primary radical initiates the "Manganese Centre" to oxidize water, producing oxygen (O_2) gas, protons, and electrons, and can be written as the following simplified chemical reaction (Equation 1):

$$2H_2O \rightarrow O_2 + 4e^- + 4H^+ \qquad (1)$$

The electrons from the oxidized water molecules are transported to the tyrosine sidechain (D1-Yz) which then replace electrons in the P680 that have been removed into the Pheo molecules and onto plastoquinone (Q_A and Q_B). The protons are released into the thylakoid contributing to the production of proton gradient across the thylakoid membrane. This proton gradient then initiates the ATP synthesis that produces chemical energy for the phytoplankton cells. This PSII reaction is shown in Figure I1, as described in Kato and Sakamoto (2009).

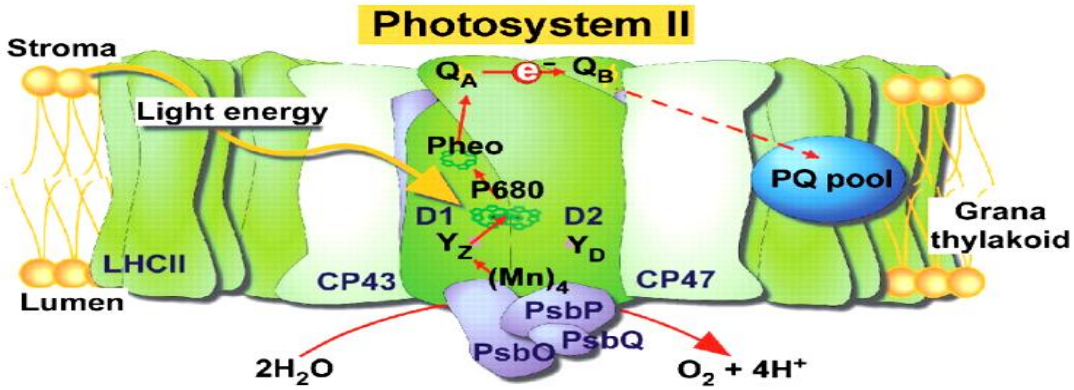

Figure I1. Schematic model demonstrating the biochemical processes of the PSII of phytoplankton. LHCII: Light harvesting chlorophyll complex II; CP43 and CP47: the inner antennae proteins; PsbO, PsbP and PsbQ: the extrinsic proteins involved in stabilization of the Mn cluster; $(Mn)_4$: Mn Centre; D1 and D2: the reaction center proteins bind the electron carriers involved in transferring electrons to plastoquinone; Y_z and Y_D: tyrosine; P680: reaction center chlorophyll; Pheo: pheophytin; QA and QB: plastquinone; PQ pool: plastquinone pool. The schematic is given only as a guide to the importance of Mn to organisms (Taken from Kato and Sakamoto, 2009).

2 Speciation of manganese

Manganese is the twelfth most abundance element in the Earth's crust (Wedepohl, 1995; Middag *et al.,* 2011a), and comprises approximately 0.1 wt% of this part f the planet. In the marine environment, manganese commonly occurs in two stable oxidation states, soluble Mn^{2+} (Mn(II)) (stable at low pH), and insoluble Mn^{4+} (Mn(IV)) in the form of MnO_2 at high pH (Stumm and Morgan, 1996). The unstable Mn^{3+} (Mn(III)) is an unlikely oxidation state because it will simultaneously oxidize and reduce to Mn(II) and Mn(IV) (Equation 2).

$$2\,(Mn^{3+} + e^- \rightarrow Mn^{2+})$$
$$\underline{Mn^{2+} \rightarrow Mn^{4+} + 2e^-}$$
$$2\,Mn^{3+} \rightarrow Mn^{2+} + Mn^{4+} \qquad (2)$$

However Mn(III) has been identified in sub oxic waters (Tebo *et al.,* 2010). Under typical ocean conditions, manganese in seawater can be found in these three oxidation states: Mn(II), Mn(III), and Mn(IV), in dissolved and fine particulate forms. In sediment, solids phases include manganese carbonates, oxides, and oxyhydroxides, for example, Mn(III) phases: MnOOH polymorphs (manganite, groutite, and feitknechtite); Mn(IV) phases: MnO_2 (todorokite, pyrolusite); Mn(III/IV) intermediate form: birnessite; and Mn(II/III) intermediate form: hausmannite (Anschutz *et al.,* 2005). These manganese forms are incorprated in the "manganese triangle" cycle (Figure I2).

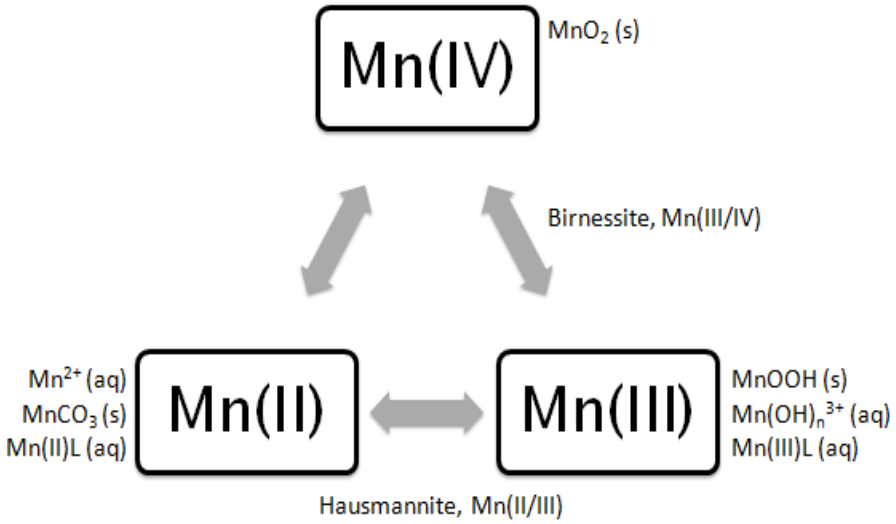

Figure I2. The manganese speciation cycle in the marine environment

The ambient oxygen concentration, and pH (oxidation increases with increases basicity) in aqueous systems are the most important factor for redox reactions (see also Section 5), as shown in Equation 3:

$$4Mn^{2+}(aq) + O_2(aq) + 6H_2O \rightarrow 4MnOOH(s) + 8H^+ \quad (3)$$

Redox reactions thus influencing the solubility of manganese in seawater (Anschutz *et al.,* 2005), and control the distributions and concentrations of (dissolved and particulate) manganese in seawater. Concentrations and distributions of dissolved manganese are further discussed below.

3 Concentrations and distributions of dissolved manganese in the oceans

Concentrations of dissolved manganese in seawater fall within a range of nanomolar to micomolar (nM- µM) in surface water, especially close to the coastal region, extending to a range of picomolar to nanomolar (pM-nM) at full ocean depth. Manganese in seawater can exist in particulate and dissolved forms. However, there is still much debate on what is the definition of true soluble manganese. The separation between the particulate and dissolved forms is defined by physical separation rather than biological measures. The existence of colloids make the dissolved particle size boundary difficult to establish, varying from 0.1 to 0.4 µm. In earlier years, dissolved manganese was defined as the fraction of manganese that passes through a 0.4 µm (Statham *et al.,* 1998) pore size filter. Recently, the recommended pore size has been decreased to 0.2 µm (Xylouri, 2009). Thus, the particulate manganese is then defined as the fraction of manganese that is retained on the 0.4 or 0.2 µm pore size filter (Statham *et al.*, 1998; Xylouri, 2009; Tebo *et al.,* 2010).

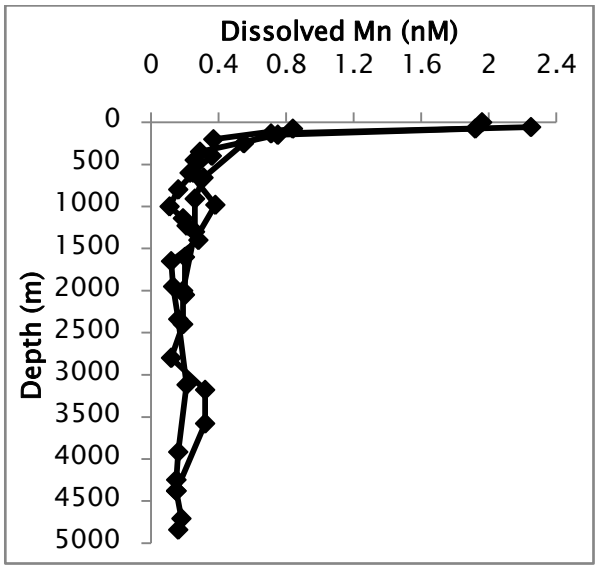

Figure I3. Typical scavenged type profile of dissolved manganese (0.4μm filter pore) in the Eastern Atlantic Ocean (data replotted from Statham *et al.* (1998) of Stations 4, 5 and 7 (dissolved manganese analysis were done at the University of Southampton, Department of Oceanography (SUDO) (now known as National Oceanography Centre, Southampton)). Input of deep water from the western North Atlantic contributed to elevated concentrations of dissolved manganese at ~3000-3500 m.

The concentrations and distributions of manganese in seawater are controlled by a combination of processes, including the inputs, cycling and removal mechanisms. The distribution profile of dissolved manganese in oceanic water is a scavenged type (Figure I3). Generally, profiles of dissolved manganese show the highest concentration in the surface mixed layer, and then rapidly decrease to uniform deeper water concentrations. Lower concentrations of dissolved manganese in deep water are due to continual particle scavenging (removal onto particles). Dissolved manganese concentrations also tend to be maximal near major sources, such as atmospheric dust, fluvial discharges, hydrothermal vents and bottom sediments, and decrease with distance from these sources.

Table I1 shows the distribution of the concentration of dissolved manganese in surface and deep water of different oceanic regions. Overall, the concentrations of dissolved manganese are >40 pM. The lowest surface concentration is in the Atlantic Sector of the Southern Ocean with 40 pM (detection limit= <10 pM) (Middag *et al.,* 2011a) and the highest surface concentration is in the Laptev Sea of the Arctic Ocean with 20 nM due to the fluvial input (Middag *et al.,* 2011b). The deep water concentrations of dissolved manganese are in a range between 50 pM (in the deep Makarov Basin of the Arctic Ocean, Middag *et al.,* 2011b) and 12 nM (detection limit= 90 pM) (due to hydrothermal input in the Eastern Tropical Pacific Ocean, (Landing and Bruland, 1987). However, seawater around the Kerguelen Islands which are remote islands in the Southern Ocean, are reported to have exceptionally high concentrations of dissolved manganese in surface waters (surface near coastal: up to 9 nM; surface offshore: up to 3 nM), and even deep water values are high (near coastal: ~6.40 nM; offshore: 2.30 nM) with the lowest concentration being 0.54

nM in the offshore deep water. It is believed that the main source of the manganese in this region is the island system itself, as the soils and rocks of the Kerguelen Islands are rich in silicate minerals (Bucciarelli *et al.,* 2001), and it is argued the coastal zone of Kerguelen is clearly affected by material from the islands (riverine discharges, soil leaching by rain waters, aeolian inputs), as well as by inputs from the sediments (effluxes from the sediment–water interface, resuspension from the sediments; Bucciarelli *et al.,* 2001). Overall It has been concluded that the variations of dissolved manganese concentrations are strongly dependent on manganese sources to the oceans, combined with a complex mixture of interactions including removal, internal cycling, and physical transport. Thus, it is essential to determine the importance of the input, removal and recycling processes for Mn in the ocean in order to understand appropriately its distribution.

Table I1. Concentrations of dissolved manganese (nM) for various coastal and oceanic environments.

Ocean	Region	Depth	DMn concentration (nM)	Reference
Atlantic	Eastern	[surface] [deep]	1.10-3.20 0.2-0.5	Statham *et al.*, 1998 Statham and Burton, 1986
	North-Eastern	[surface] [deep]	~0.4-1.10 0.1-0.4	De Jong *et al.*, 2007
	Western	[deep]	<0.5	Saager *et al.*, 1997
Pacific	North	[surface] [surface] [surface] near coastal [deep] [deep]	1.0-1.5 0.6-1.0 6-12 <0.25 0.2-1.0	Landing and Bruland, 1987 Landing and Bruland, 1980 Landing and Bruland, 1980 Landing and Bruland, 1987 Landing and Bruland, 1980
	Western	[surface] [deep]	2.0 <0.5	Landing and Bruland, 1987
	South	[surface] [deep]	~0.5 ~0.2	Nakayama *et al.*, 1995
	Equatorial	[surface]	<0.5-2.5	Nakayama *et al.*, 1995
	Eastern-Tropical	[surface] [deep]	5.0 ~12	Landing and Bruland, 1987
Indian	South-Western	[surface] [deep]	0.69-1.30 <0.4	Morley *et al.*, 1993
	North-Western	[surface] [deep]	2.0-4.3 0.7-1.5	Saager *et al.*, 1989
Southern	Atlantic Sector	[surface] [deep]	0.04-0.64 0.07-0.23	Middag *et al.*, 2011a
	Kerguelen Islands	[surface] near coastal [deep] near coastal [surface] open ocean [deep] open ocean	4.48-8.54 5.24-6.35 0.68-2.88 0.54-2.30	Bucciarelli *et al.*, 2001
	Ross Sea	[surface] [surface]	0.2-1.0 ~0.10-6.60	Sedwick *et al.*, 2000 Grotti *et al.*, 2001
Arctic	Lapter Sea	[surface]	Up to 20.0	Middag *et al.*, 2011b
		[surface] over deep basins	Up to 6.0	Middag *et al.*, 2011b
	Makarov Basin	[deep]	~0.05	Middag *et al.*, 2011b
	Eurasian Basin	[deep]	~0.10	Middag *et al.*, 2011b

4 Inputs of manganese to the oceans

Manganese is a natural component of the Earth, and release of dissolved manganese results from erosion and weathering of rocks and soils. Manganese occurs in streams, rivers, atmospheres, and hydrothermal fluids in dissolved forms and also associated with particulate materials, and aerosols. The biogeochemical cycle of manganese is presented in Figure I4. There are three major pathways by which manganese is now known to enter the oceans:

(1) river discharge and terrestrial run-off,
(2) hydrothermal discharge,
(3) atmospheric (dry/wet) deposition.

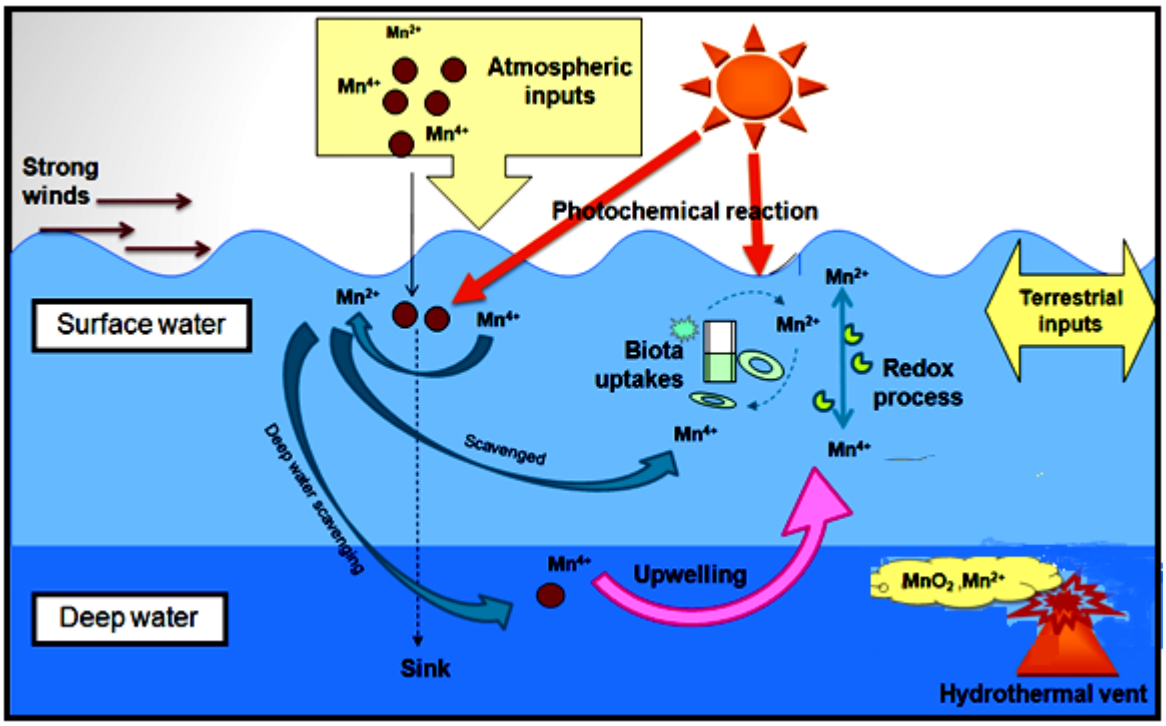

Figure I4. The biogeochemical cycle of manganese in the ocean's system, including inputs (yellow arrows and cloud), internal processes (blue arrows), upwelling/vertical mixing (pink arrow), photochemical reaction (orange arrows), wind blow (brown arrows) and sinking (black arrows).

4.1 River discharge and terrestrial run-off

Dissolved manganese concentrations in rivers reflect the combined effects of weathering of local geology, floodplain, tributary inputs, anthropogenic inputs, water chemistry and hydrology, and therefore the concentrations of dissolved manganese tend to be higher in the rivers than the oceans. Several influences, such as river discharge and season, on dissolved manganese concentrations can cause temporal variability. For example, pulses in river flow during winter and spring in the Columbia River, appear to reduce nutrients (macro- and micro-nutrients) concentrations in summer (Aguilar-Islas and Bruland, 2006), suggesting that a constant input is diluted by cleaner run-off. In estuaries, where

freshwater meets the sea, the concentrations of dissolved manganese are influenced by processes that remove dissolved manganese from solution and by the salinity gradient that characterizes the mixing of a river with its oceanic receiving waters. Thus, the concentrations of dissolved manganese are at maximum at low salinities as shown in the Columbia River estuary (Aguilar-Islas and Bruland, 2006) and Seine River estuary (Ouddane *et al*., 1999) due to: (i) the solid-solution partitioning of Mn being very sensitive to salinity by the formation of stable dissolved chloride and sulfate complexes; (ii) competitive exchange equilibria between dissolved Ca^{2+} and Mg^{2+} and the manganese embedded in calcium carbonate's lattice as a solid solution within an estuary (Ouddane *et al.,* 1999).

River outflow can indirectly supply manganese in dissolved (Mn(II)) and particulate (Mn(III) and Mn(IV)) forms to the ocean systems by transporting Mn-rich particles to coastal waters. Resuspension or effluxes at the Mn-rich sediment-water interface in near-shore regions resulted in higher concentrations of dissolved manganese (Beck *et al.,* 2002a; Corami *et al*., 2005) compared to the offshore regions. Furthermore, manganese is known to have a benthic source on continental shelves from reducing sediments (*e.g.,* Tappin *et al.* ; 1993) which further increases its concentration in shelf waters. At the shelf edge, the presence of a correlation between manganese and salinity, combined with a measurable gradient of concentration, suggests that the shelf (Chase *et al.,* 2005) is an important source of manganese for the open ocean as demonstrated in several continental margins for example western South Pacific Ocean (Obata *et al*., 2008), New Zealand (Croot and Hunter, 1998), eastern North Atlantic Ocean (Le Gall *et al.,* 1999), European shelf (Kremling, 1985), and Arctic Ocean (Middag *et al.,* 2011b). Manganese enrichments have also been reported in water masses over the shelf regions of oceanic islands *e.g*. the Kerguelen Plateau of the Southern Ocean (Bucciarelli *et al*., 2001), and the Galapagos Archipelago of the Equatorial of the Pacific Ocean (Gordon *et al*., 1998).

4.2 Hydrothermal discharge

Hydrothermal inputs are a crucial source of manganese to the deep-ocean (Klinkhammer *et al.,* 2001; Middag *et al.,* 2011b) especially along the mid-ocean ridges (Coale *et al.,* 1991). The most enriched metals in hydrothermal vent fluids are iron and manganese, and these elements participate in redox reactions and change between reduced dissolved forms (Fe^{2+} and Mn^{2+}) and oxidized forms (Fe(III), Mn(III,IV) precipitates), which are stable in the open ocean (German and Von Damm, 2003), with the (Mn) reaction (Equation 4) (Burton and Statham, 1988):

$$MnO_2\ (s) + 4H^+ + 2e^- \leftrightarrow Mn^{3+} \leftrightarrow Mn^{2+} + 2H_2O \qquad (4)$$

Hydrothermal activity is usually found by looking at light scattering (transmission or turbidity), temperature and enhanced manganese concentration (Klinkhammer *et al.,* 2001), as observed in the Central Basin of Bransfield Strait, Antarctica (DMn_{max}=~22nM)

(Klinkhammer *et al.,* 2001); over the Gakkel Ridge, Arctic Ocean (DMn_{max}=~5nM) (Figure I5) (Middag *et al.,* 2011b); and over the Bouvet Triple Junction Ridge, Southern Ocean (DMn_{max}=1.5nM) (Middag *et al.,* 2011a), with the elevated manganese concentrations coinciding with maxima of iron and temperature and a transmission minimum (Middag *et al.,* 2011b).

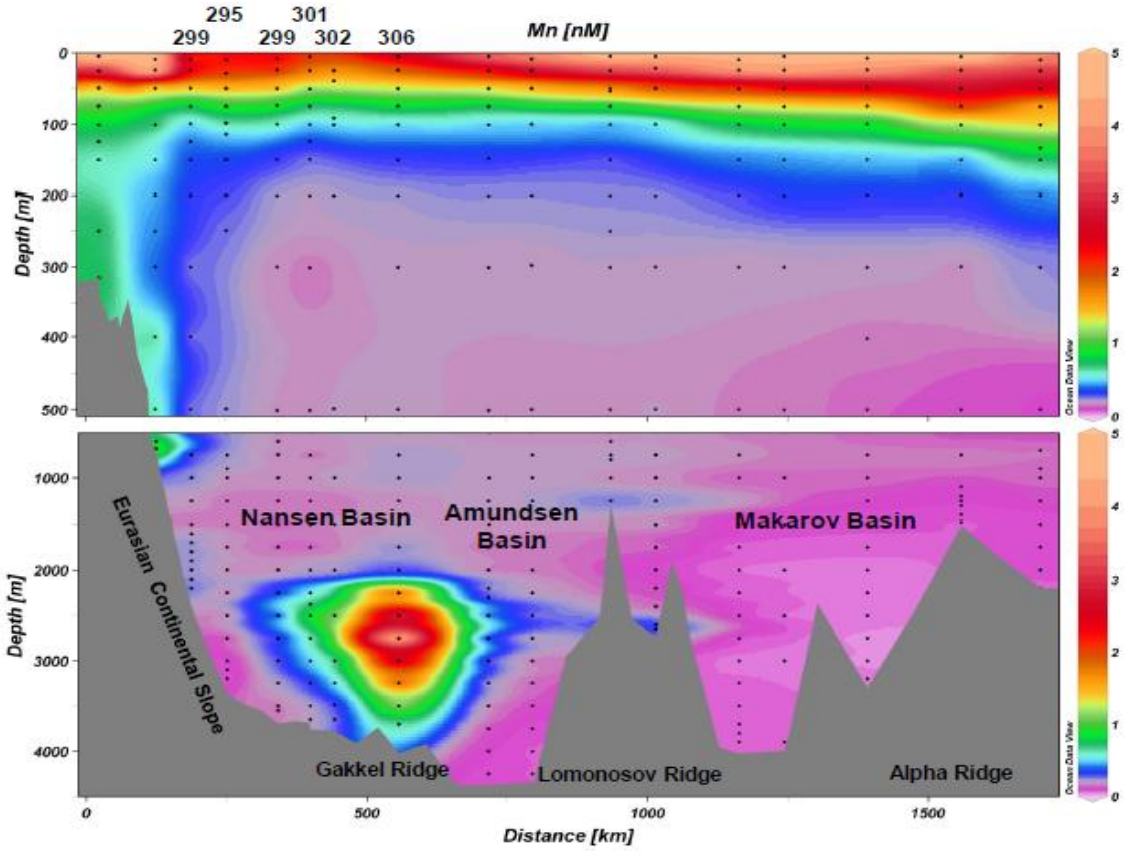

Figure I5. Concentrations of dissolved manganese in the upper 500 m of the water column (upper panel) and over the entire water column (lower panel) in the Eurasian and Makarov basin and extending onto the Makarov Ridge of the Arctic Ocean. There was a very clear maximum around 2500 m over the Gakkel Ridge of the Nansen basin, indicated the hydrothermal input (taken from Middag *et al.,* 2011).

Therefore, as iron and manganese are enriched in hydrothermal vent fluids, with total (dissolved and particulate) iron and manganese concentrations orders of magnitude greater than normal water column values, both elements can be used as good tracers of hydrothermal activity (German and Von Damm, 2003). In addition to manganese and iron, other elements i.*e.* $Ca^{2+,}$ Cu^{2+}, Zn^{2+}, Si can also be added to the ocean through hydrothermal venting (Millero, 2003).

4.3 Atmospheric (dry/wet) deposition

Atmospheric inputs are the main source of manganese and other trace metal elements (in particulate and dissolved forms) to the open ocean (Spokes *et al.,* 2001; Statham and Chester, 1988; Statham and Burton, 1986; Jickells *et al.,* 1994; Guieu *et al.,* 1994) whether

by rain (wet) or/and by dust (dry) deposition, and the most important source for dust inputs into the oceans are deserts (Jickells *et al.,* 1994). The effect of the atmospheric inputs can be clearly seen in central ocean gyres (Atlantic and Pacific Oceans), which has led to suggestions that these inputs may influence the primary production of the oceans (Jickells *et al.*, 1994; de Jong *et al.,* 2007; Mendez *et al.,* 2010). The Sahara and Sahel desert regions in Africa are the largest sources of dust in the Atlantic Ocean, and they are estimated to range between 220 and 1000 x 10^{12} g y^{-1} (Duce *et al.,* 1991; Jickells and Spokes, 2001). The Asian deserts (*e.g.* Gobi) are the main dust sources in the North Pacific Ocean (Jickells *et al.,* 2005) and the Australian deserts are the main dust inputs to the South Pacific Ocean (Jickells *et al.,* 2005; Obata *et al.,* 2008); the Arabian deserts are the main dust sources to the Northwestern Indian Ocean (Saager *et al.,* 1989). The main deserts in the world are shown in Figure I6.

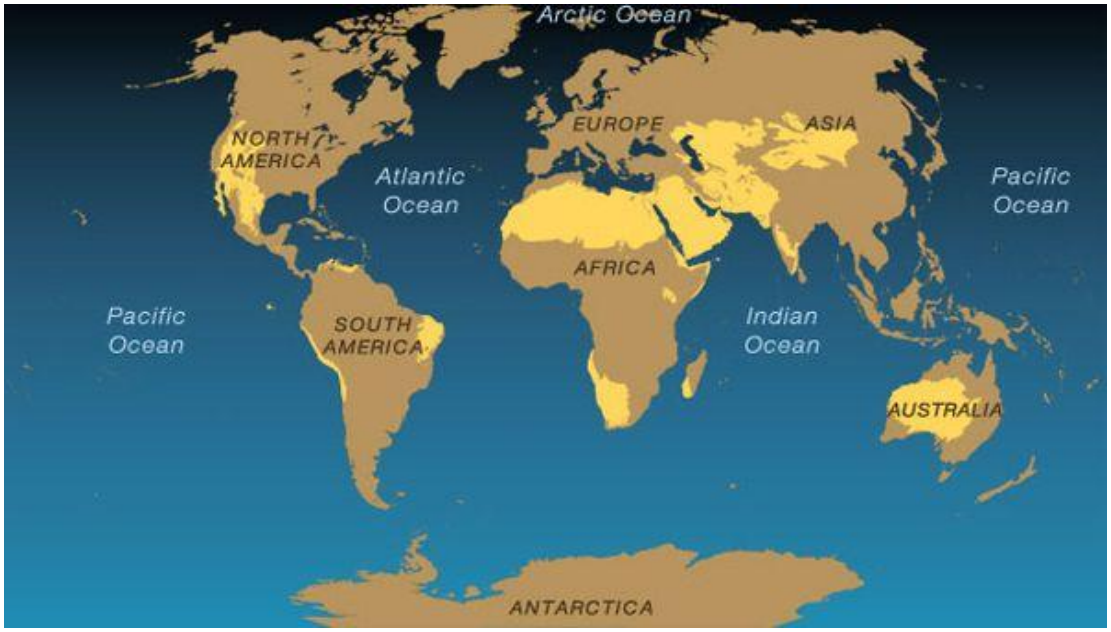

Figure I6. Locations of the desert regions in the world are showed in world map above (yellow patches), as deserts are the major sources of atmospheric dust to the world oceans. The map is given as a guide to the dust sources which also bring manganese to the ocean regions. (Map taken from the Matrix web portal: (http://coursesa.matrix.msu.edu/~fisher/HST140_2008/MapDeserts.html)).

Dust can travel hundred miles away from their origins by strong winds, and inputs are dependent on meteorological conditions and emission patterns (Prospero *et al.,* 1996). Thus, the spatial and temporal effect of atmospheric inputs on surface ocean biogeochemistry may be seen even in remote oceanic areas.

However, Mendez and co-workers (2010) report that manganese has more complicated profiles relative to other trace metals (*e.g.* Fe, Al and Co) in the ocean regions which receive high dust inputs. The dissolution of manganese in these regions is really dependent upon the dust concentrations (Mendez *et al.,* 2010). After dust containing

particulate and dissolved manganese enters the ocean surface water, they are involved in various biogeochemical processes (Figure I4). There is evidence that manganese dissolves readily from dust in surface seawater (Statham and Chester, 1988; Guieu *et al*., 1994), and that complex photochemical reactions reduce the oxidized and insoluble Mn(IV) to soluble Mn(II). Light in the surface ocean promotes an electron transfer between organics, such as humic material and Mn, while, the middle reduction state, Mn(III), readily disproportionates to Mn(II) and Mn(IV). As a result, the concentration of soluble Mn in the oceanic surface water can be as high as 30 nM after rain events (Mendez *et al.,* 2010) and available for biological use. Particulate manganese from dust may also be reduced during ingestion by zooplankton, that releases the dissolved form of manganese back into the surface water column (Sunda and Huntsman, 1998). As redox processes are the most important processes controlling manganese removal and cycling in seawater, they are further discussed in the next Section.

5 Removal and internal cycling of manganese

In general, manganese is removed from the water column by adsorption onto or incorporation into particles (Burton *et al.,* 1993; Tappin *et al.,* 1993; Le Gall *et al*., 1999), bacteria (Schoemann *et al.,* 1998; Beck *et al.,* 2002a) and phytoplankton (Schoemann *et al.,* 1998; Roitz *et al.,* 2002), which involves complex redox processes. The redox processes of manganese are usually dominated by the Mn(II) and Mn(IV) oxidation states in two ways:

1. partly by direct adsorption and scavenging as Mn(II), followed by oxidation to Mn(IV) on particle surfaces;
2. partly by direct oxidation to particulate Mn(IV) in colloidal form, which is then scavenged by larger particles.

However, in both cases, particulate Mn(IV) can only be reduced to soluble Mn(II) again if the particle encounter an oxygen-deficient (anoxic) environment. However, manganese concentrations can also be reduced in the water column by other factors such as physical mixing with lower Mn waters, and active uptake by biota.

5.1 Fate of manganese in upper water column

The fate of manganese once it enters seawater is influenced by complex biogeochemical processes. Waters in the euphotic zone are exposed to sunlight that allows phytoplankton blooms to occur, which can influence the manganese concentrations in the surface seawaters (Middag *et al.,* 2011b).

Unlike most other trace metal elements which are depleted in surface water due to biological removal processes; dissolved manganese demonstrates a distinct surface

maximum (*e.g*. Morley *et al.,* 1993; Statham *et al.,* 1998). This maximum is associated with a minimum concentration of manganese oxides (particulate manganese), as a result of indirect photochemical reductive dissolution of manganese oxide (Sunda and Huntsman, 1988; Morel *et al.,* 2003), suggesting that it results at least partially from a decrease in particule scavenging rates. These conditions however, are often seasonally variable and depend on the reduction-oxidation potential in the system (Statham *et al.,* 1998). For example, during winter, deeper water mixing and the aeration of the sediment resulting in low surface concentrations of dissolved manganese due to oxidation, and particulate excess manganese concentrations were relatively high due to oxidation of the dissolved phases, resuspension, adsorption, and lateral transport, as showed in the Adriatic Sea (Tankere *et al.,* 2000). Although thermodynamically favourable, the chemical oxidation of Mn(II) to Mn(IV) by oxygen is exceedingly slow at seawater pH. The oxidation of Mn(II) in the surface ocean is therefore largely bacterially mediated (Sunda and Huntsman, 1988).

However, during summer, high dissolved manganese concentrations are obtained in surface seawater, where particulate manganese concentrations are low (Tankere *et al.,* 2000), due to photoinhibition of Mn(II) oxidation by bacteria (Sunda and Huntsman, 1988), and high rates of Mn oxide reductive dissolution occurs (Tankere *et al.,* 2000). Sunlight increased the dissolution rate of manganese oxide (MnO_x) in seawater to values of 6-13 % h^{-1}, 6-70 times higher than rates in the dark (Sunda and Hunstman, 1988). The lack of oxides near the surface results in low manganese removal rates by aggregation and sinking of Mn oxide particles. These low scavenging rates and photoinhibition of the bacteria, in turn, increase the residence time of the photoproduced Mn(II) in surface seawater and thereby contribute to surface maxima in dissolved manganese concentrations which happen over wide areas of the world's oceans (Sunda and Huntsman, 1988, 1990). The residence time of manganese is defined as the average amount of time that manganese spends in the surrounding waters by assuming in a dynamic steady state condition, and can be calculated using Equation 5:

$$\text{Residence time } (\tau) = \frac{total\ mass\ of\ dissolved\ manganese\ \ in\ the\ oceans}{rate\ of\ supply\ \ (or\ removal\ )of\ manganese} \qquad (5)$$

The residence times of dissolved manganese variy according to the oceanic region and the local sources of manganese. For examples, reported values in the Pacific Ocean are 50 years (North Pacific) (Landing and Bruland, 1980), 3 – 74 years (Northeast Pacific) (Landing and Bruland, 1987), and 20 - 40 years (Central North Pacific) (Bruland *et al.,* 1994). In the Atlantic Ocean, the reported values are 20 years (Sargasso Sea, Atlantic Ocean) (Sunda and Huntsman, 1988), 1.0 – 3.8 years (Northeast Atlantic) (de Jong *et al.,* 2007), and 19 years (tropical Northeast Atlantic) (Statham and Chester, 1988); and 4 – 20 years in the Southern Ocean (Middag *et al.,* 2011a). The different concentrations and residence times of the dissolved manganese also reflect the different water masses and basins, the origin and age

of the water masses, and regional biogeochemical processes (Statham *et al.*, 1998; Middag *et al.,* 2011a). Questions remain however, about an equilibrium or dynamic steady state with a solid phase which is suggeted to be important in the control of dissolved manganese concentrations in older deep waters (Statham *et al.*, 1998).

In shallow waters (<600 m), where the physical disturbance (*e.g.* internal tide and wave currents) and bioturbation are strong enough to disturb sediments, enhanced concentrations of dissolved manganese that coincide with turbidity maxima are seen. The manganese is produced as a result of reducing conditions caused by the decomposition of organic matter leading to reduction of Mn oxides and release of dissoveld Mn (II) (Laes *et al.*, 2007). Such Mn release has been observed over the continental slope, for example on the Iberian continental margin of the Northeastern Atlantic Ocean (Van der Zee *et al.,* 2001, 2002) and the European continental shelf of the eastern North Atlantic Ocean, Bay of Biscay (Laes *et al.,* 2007).

5.2 Fate of manganese in deeper water column

Near the bottom of the euphotic zone, the concentrations of dissolved manganese (Mn(II)) decrease. Direct chemical oxidation (abiotic pathway) of Mn(II) to Mn(IV) is very slow, thus it must be catalyzed by enzymes or enzyme complexes involving a multi-copper oxidase (Webb *et al.*, 2005) that is present in bacteria. Thus dissolved Mn(II) is oxidized to insoluble Mn(III) intermediates, that convert to insoluble Mn(IV), by Mn(II)-oxidizing bacteria (Sunda and Huntsman, 1998) in oxic waters. Bacteria-catalysed oxidation rates are up to five orders of magnitude greater than the abiotic pathway rates (Tebo *et al.,* 2005). Where sunlight can penetrate some oxide reduction can occur, whilst at night Mn(II) oxidation rates are higher so a pronounced diurnal cycle in oxidation rates can occur (Sunda and Huntsman, 1990). This dynamic cycle is repeated many times before manganese leaves the mixed layer. The number of Mn-oxidizing bacteria in the water column increases during bloom events because they used carbon generated by the bloom. This bacterial oxidation mechanism was originally suggested by Beck *et al.* (2002a) to explain the loss of dissolved manganese (~80%) observed during microcosm simulations of the annual spring diatom bloom in South San Francisco Bay.

Where a water column has a distinct anoxic deep layer underlying an oxic layer in contact with the atmosphere, manganese oxides (derived mostly from margin sediments) are reduced to Mn(II) just below the oxic zone. Therefore Mn(II) profiles in such regions typically show a sharp increase at the redox boundary. The increase occurs because Mn^{2+} is produced at the boundary by reduction, and elevated dissolved values below this layer reflect further dissolution of particles. Just above the interface in oxic waters oxide formation and scavenging leads to a maximum in the Mn particle phase. This type of profile can be seen in the oxygen minimum zone for examples in the North Pacific (Bruland

et al., 1994), and in anoxic water columns such as the Black Sea (Konovalov *et al*., 2004; Alkan and Tufekci, 2009). As indicated above, in anoxic waters, significant manganese oxide precipitation (Mn-rich particles) occurred when dissolved manganese dispersed to the upper, oxygenated layers of the water column, for examples, amorphous and dendritic (stellate) particles; and these Mn-rich particles are associated with large aggregates which also contain organic matter (Neretin *et al.,* 2003). Most trace metals (*e.g.* Co^{2+}, Cu^{2+}, Zn^{2+}, Pb^{2+}, Ni^{2+}, Cd^{2+}, Mn^{2+}) have a strong adsorptive affinity for manganese oxides, where those metals are adsorbed onto the large surface areas of the Mn-rich particles (Tonkin *et al.,* 2004). Any adsorbed metals are released into solution in the reducing environments containing reductants such as sulphide and iron(II) (Neretin *et al.,* 2003). Reduction of oxidized particulate phases in suboxic or anoxic waters produces high concentrations of dissolved manganese, which can mix horizontally into the oxygenated ocean's interior (Bruland *et al.,* 1994).

Manganese also can be scavenged onto a wide range of both living and dead organisms, *e.g.* accumulation in phytoplankton colonies (Lubbers *et al.,* 1990; Schoemann *et al*., 2001), and skeletal materials, which then sink into the deep water of the ocean. Sinking and decomposition of the bloom to the seafloor released Mn from Fe and Mn hydroxides in surficial sediments (Schoemann *et al*., 1998). When the bloom material sinks to the bottom, bacteria first use oxygen to decompose the organic material (Schoemann *et al*., 1998). Beck and Bruland (2000) recognized that when conditions become suboxic, bacteria can use other elements such as Mn(IV), as electron receptors. By reducing particulate Mn(IV) to soluble Mn(II), bacteria in suboxic conditions can increase dissolved Mn concentrations (Schoemann *et al*., 1998; Beck and Bruland, 2000), and this Mn enriched waters are believed to be transported back to the upper water column by upwelling or vertical mixing (Chase *et al.,* 2005). Manganese oxide particles which may also transported to the surface water are then photo-reduced to soluble Mn(II) (Figure I7, De Schamphelaire *et al*., 2007). Roitz *et al*. (2002) and Schoemann *et al*. (1998) used this mechanism to explain enhancement in dissolved Mn concentrations after the phytoplankton bloom in the North Sea and South San Francisco Bay, respectively. Attempts have been made by Luengen *et al.* (2007) in South San Francisco Bay to validate this mechanism as an important process of reduction and dissolution of Mn(IV) in suboxic sediments, that leads to remarkably high dissolved Mn during the spring phytoplankton bloom. What is unclear is whether the much higher dissolved Mn concentrations are the result of higher rates of input of sediment derived manganese oxides or the result of faster rates of manganese oxide reduction.

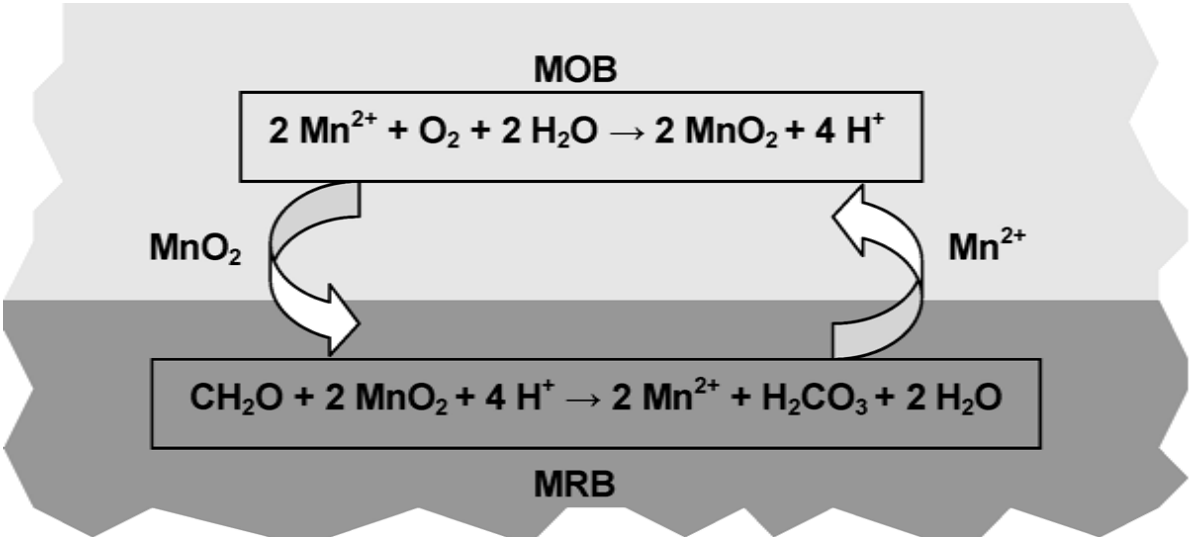

Figure I7. Manganese cycle occurring in marine systems. The manganese oxidation is performed by manganese oxidizing bacteria (MOB) in an oxic zone, while the manganese reduction is performed by manganese reducing bacteria (MRB)–with concomitant oxidation of organic matter—in an anoxic zone (taken from De Schamphelaire *et al.*, 2007).

6 Overview of the study regions

Certain oceanic regions are particularly appropriate for studying Mn biogeochemistry. Here the two chosen regions, and for which samples were available, are the Tropical NE Atlantic Ocean and the Crozet Islands on the edge of the Southern Ocean. The Atlantic region has some of the highest atmospheric dust inputs in the world (thus appropriate for study of impacts of aeolian deposition on Mn) whilst the Crozet islands provide an opportunity to study Mn cycling and inputs in a remote part of the global ocean with extremely low concentrations of Mn and other trace metals, and potential island inputs.

6.1 The Crozet Islands of the Southern Ocean

The Southern Ocean is a very important region of the Earth where ocean currents circle the globe unimpeded and it is the source region of Antarctic Bottom Water (AABW) (Foster and Carmack, 1976; Orsi *et al*., 1993; Farchbach *et al*. 1994). Moreover, the Southern Ocean is the largest High Nutrient Low Chlorophyll (HNLC) region on the world's oceans (Pollard *et al.,* 2007a). The existence of a plentiful supply of primary nutrients such as nitrate and phosphate in HNLC regions should lead to seasonal phytoplankton blooms in the austral spring, but the blooms do not occur, with iron limitation of primary production now known to be a major control on biogeochemical processes in the region (Martin *et al.,* 1990, 1994). Within this Southern Ocean HNLC area, there are hotspots (*i.e.* South Georgia, Crozet and Kerguelen) of primary productivity observed every year (Figure I8).

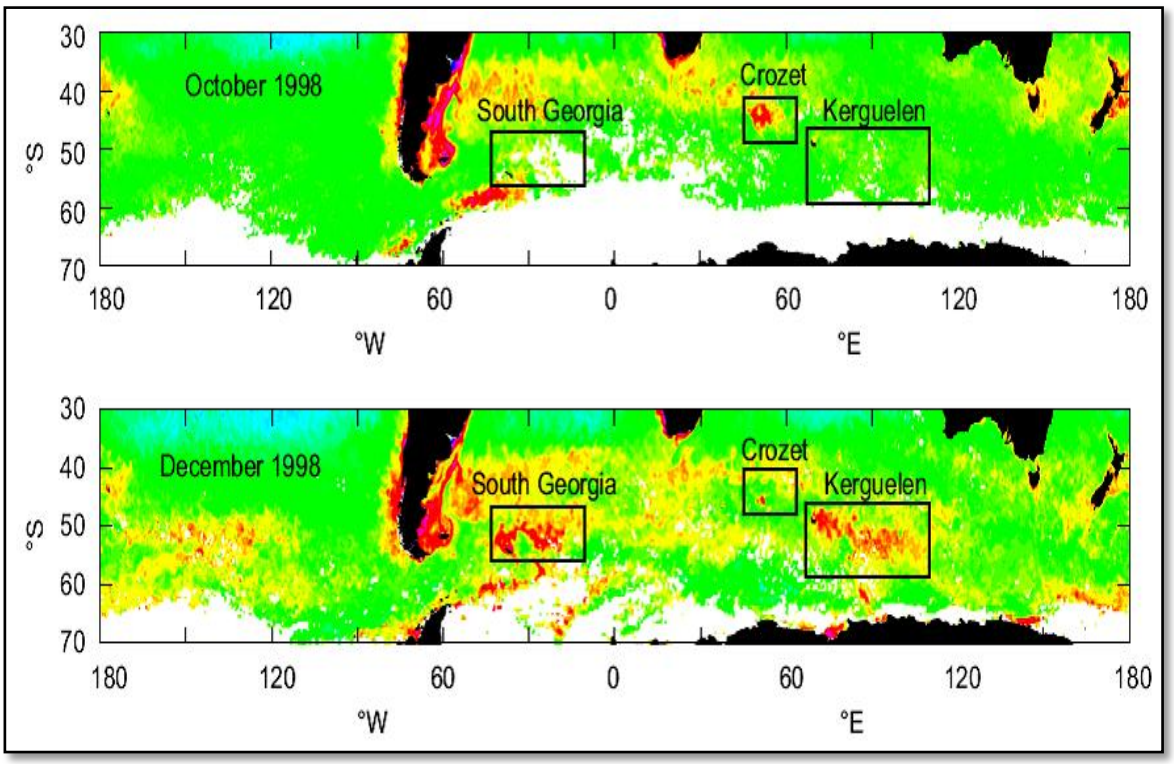

Figure I8. Southern Ocean HNLC region showing localized on high productivity in association with some mid ocean islands including Crozet, Kerguelen and South Georgia Islands (Pollard *et al.,* 2007a).

The Crozet Islands, or also known as Crozet Bank (Recq *et al.,* 1998; Stein and Herzen, 2007), the easternmost region of the Crozet Plateau, is located in the Southern Ocean HNLC region, with two main islands, which form the Crozet Archipelago (Figure I9):

1. Eastern Group: Ile de la Possession and Ile de l'East, and three small islands;
2. Western Group: Ile aux Cochons, Ile des Pingouins, and Ilots des Apotres.

Between the two groups of islands is the Indivat Basin, which disects the Crozet Bank into two separate domains (Recq *et al.,* 1998). The distance between the Eastern and the Western Groups is ~100 km (Giret *et al.,* 2002). The shallow Crozet Bank appears to have been situated on old and mechanically thick crust which is of volcanic and basalt origin, different from the adjacent Del Cano Rise, which formed on or near the Southwest Indian Ridge (Recq *et al.,* 1998; Stein and Herzen, 2007). Mostly showing magmatic fractionation from picritic to tephritic types (Giret *et al.*, 2002), the Eastern Group of islands is volcanic and plutonic rocks, and the Western Group of islands is only volcanic with sedimentary levels (Giret *et al.,* 2002).

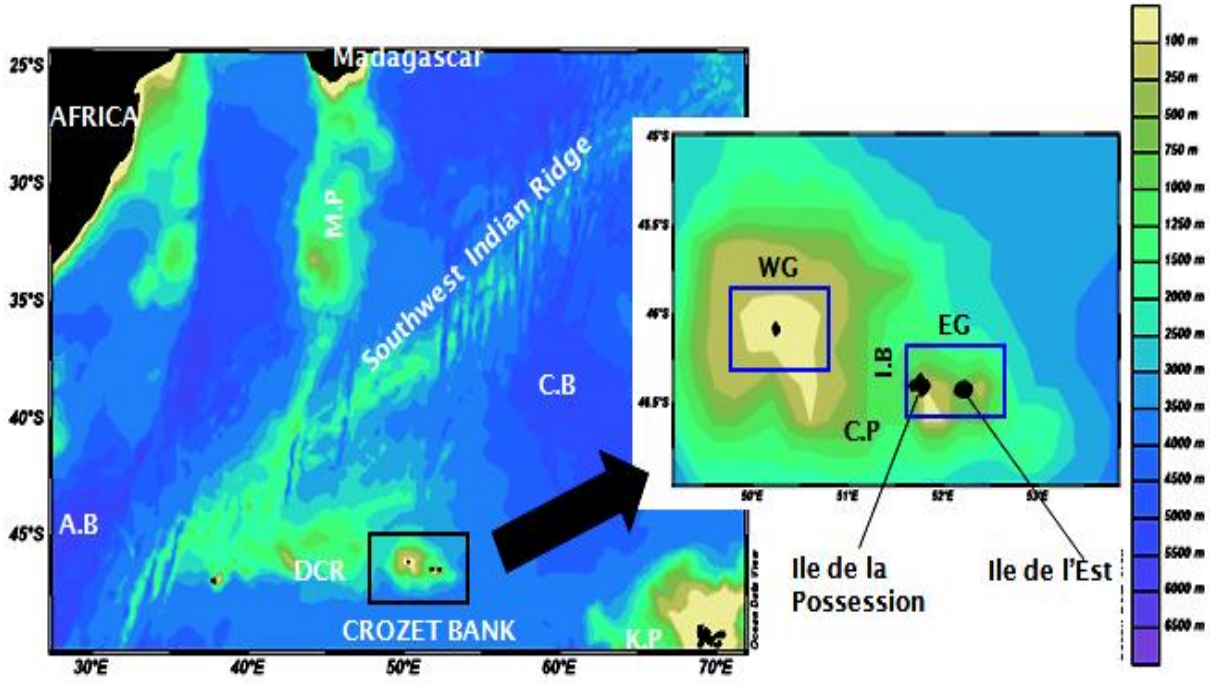

Figure I9. The inset shows the location of the Crozet Archipelago relative to the Southwest Indian Ridge. The enlarge map shows the Eastern and Western Groups of the Crozet Islands, which separated by the Indivat Basin. The big islands of the Eastern Group, I'le de la Possession and Ile de l'Est, are showed in the enlarge map. M.P: Madagascar Plateau; A. B: Agulhas Basin; C.B: Crozet Basin; K.P: Kerguelen Plateau; DCR: Del Cano Rise; W.G: Western Group; E.G: Eastern Group; I.B: Indivat Basin; C.P: Crozet Plateau.

Every year, there are phytoplankton bloom events recorded to the north of the Crozet Plateau (Figure I10, Pollard *et al.*, 2007a) with the first bloom between October and November; and the second bloom between December and January. The most logical hypothesis to explain these blooms are they are supported by a natural source of iron most likely the shallow sediments of the Plateau (Planquette *et al.*, 2007). The bloom is

located in the Polar Frontal Zone (PFZ) with macronutrients were not the limiting factor at the end of the winter (Pollard *et al*., 2007b). Nitrates were not limiting over the sampling period (Lucas *et al*., 2007), but silicate concentrations were almost fully depleted in December.

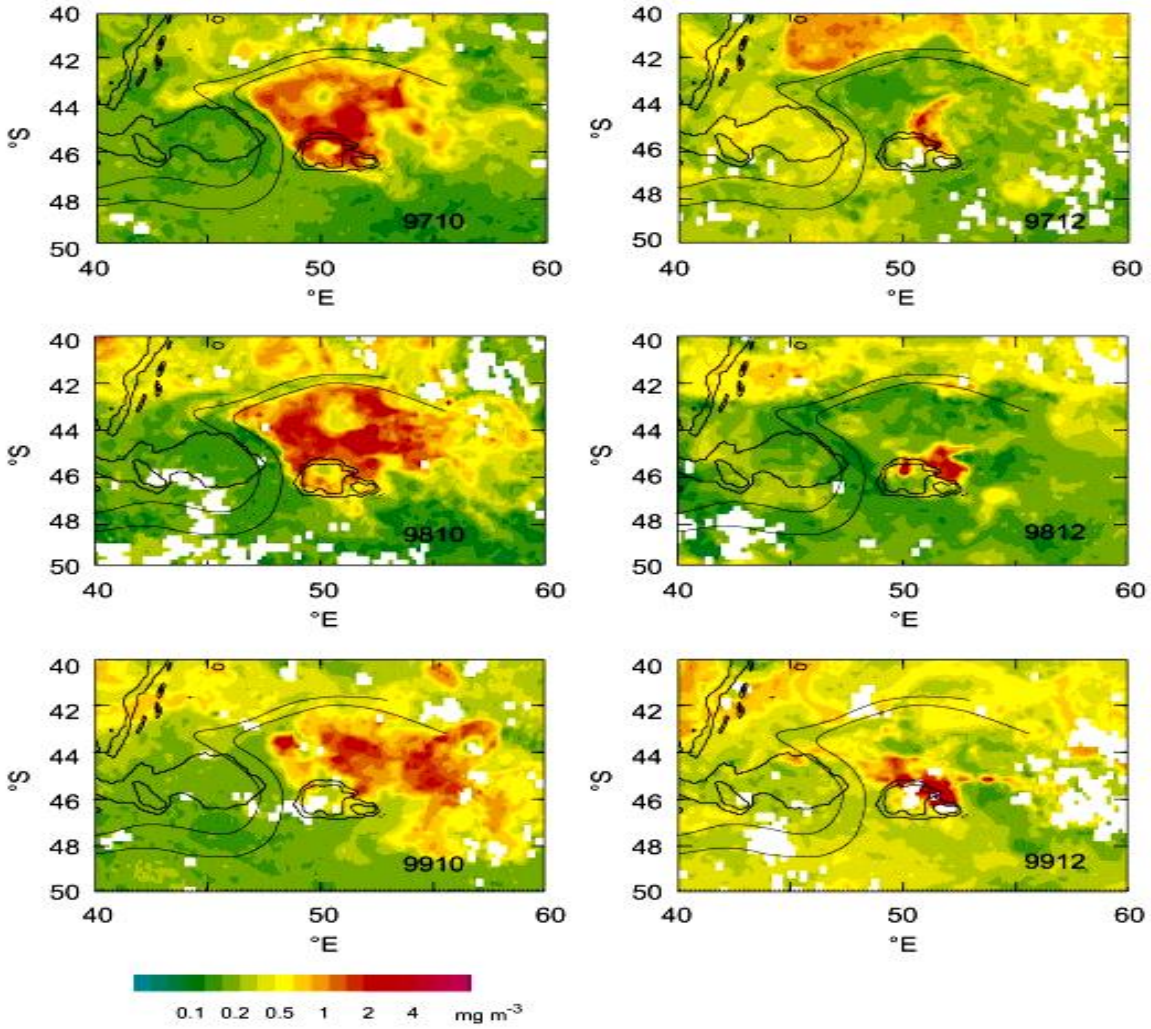

Figure I10. The SeaWiFS chlorophyll images for the annual phytoplankton blooms occur to the north of the Crozet Plateau in October and December of 1997, 1998, and 1999. The Crozet Plateau is represented by a light black solid line. The Sub Antarctic Front is also represented by a thin black line. Satellite images were taken from Pollard *et al*. (2007a).

According to Bucciarelli *et al.* (2001), atmospheric input is not the major source of manganese in the remote Southern Ocean region. However, we know the major source of iron in the remote region was the plateau *e.g.* Planquette *et al.* (2007). There is a possibility that the plateau also supplies manganese to the surrounding waters, as the sources of the redox metals iron and manganese are usually similar, as shown for the Kerguelen Islands region (Bucciarelli *et al.,* 2001). In a study by Marsh *et al.* (2007) total manganese concentrations were determined in sediments at Crozet Stations represent contrasting productivity regimes; (1) to the north of the Plateau: is within a high-productivity region, (2) to the south of the Plateau: is within ambient HNLC waters, and (3) central of the Plateau: is within a region of intermediate. The total manganese

concentrations varied between 373-804 ppm (central Plateau), 348-1906 ppm (south Plateau), 87-490 ppm (north Plateau), and 1300 ppm (Crozet Islands) (Marsh *et al.,* 2007).

Constant Mn/Fe ratios obtained in these sediments indicate oxic conditions, with no fractionation of these elements (Marsh *et al.,* 2007). There is very little organic matter present in the sediment (ranging from 0.26% to 0.60%) and no sulphides are detectable (Marsh *et al.,* 2007), meaning that there is a limited supply of electron donors to reduce the manganese present to Mn(II) and transport this via diffusion to the redox boundary.

Sediments from this region are mixtures of biogenic components and lithogenic inputs (Marsh *et al.,* 2007) because the Crozet Plateau is surrounded by the PFZ, and the volcanic islands and steep topography provide a considerable source of lithogenic material to the deep sea (Dezileau *et al*., 2000). Thus, the Crozet Plateau sediments can provide a good record of accumulation under a gradient from Mn-deplete to Mn-replete conditions that provide an insight into the impact of manganese supply on biogeochemical cycles.

However, there is no data on dissolved manganese around the Crozet Islands until the present work. Numerous studies in Southern Ocean have focused on the iron hypothesis where iron can act as the limiting micro-nutrient in HNLC waters, and experiments have demonstrated that the addition of iron does causes an increase in phytoplankton productivity. However, iron and manganese behave differently in seawater. Different source signals of manganese are more visible than that of iron (Bucciarelli *et al.,* 2001) due to the longer residence time of manganese. Hence, a study of manganese is necessary to understand the behaviour and the biogeochemistry of manganese in term of sources, sinks and cycling, in the Southern Ocean which is a sparsely studied region.

Therefore, seawater samples collected for trace metals analysis during the CROZet natural iron bloom and EXport experiment (CROZEX) cruises (D285 and D286) on board *RRS Discovery* during the austral summer between 3 November 2004 and 21 January 2005 provided an excellent opportunity to study how the natural sources of dissolved manganese (either directly from the islands or from the surrounding sediments) may impact concentrations in surrounding waters and possibly affect the growth of phytoplankton. Details of this study are further discussed in Chapter IV.

6.2 The tropical North-Eastern (NE) Atlantic Ocean

The tropical NE Atlantic Ocean region receives high atmospheric inputs every year, with an estimated 195 Tg of annual dust deposition (Jickells *et al.,* 2005). Satellite and model data show that the largest and most intense dust sources come from the Saharan desert region (Jickells *et al.,* 2005). Atmospheric transport of dust and its deposition in the surface ocean is considered to be an important supply of nutrients and trace metals to the euphotic zone

of open ocean regions (Baker *et al*., 2006; Baker *et al.,* 2007; Sarthou *et al.,* 2003). Dust originating from the Saharan desert can be transported by strong winds and are entrained into the atmosphere. The dust lifetime ranges from a few minutes (for particles larger than 10 μm) to several weeks (for particles in the sub μm size range). Once dust particles are lifted into the atmosphere, they can be transported hundreds miles away from their origin (Mahowald *et al.,* 2005), for example in Figure I11, dusts from African deserts (*e.g*. Sahara and Sahel) can readily reach the Caribbean, southern Florida, and the eastern United States (Prospero *et al.,* 1981).

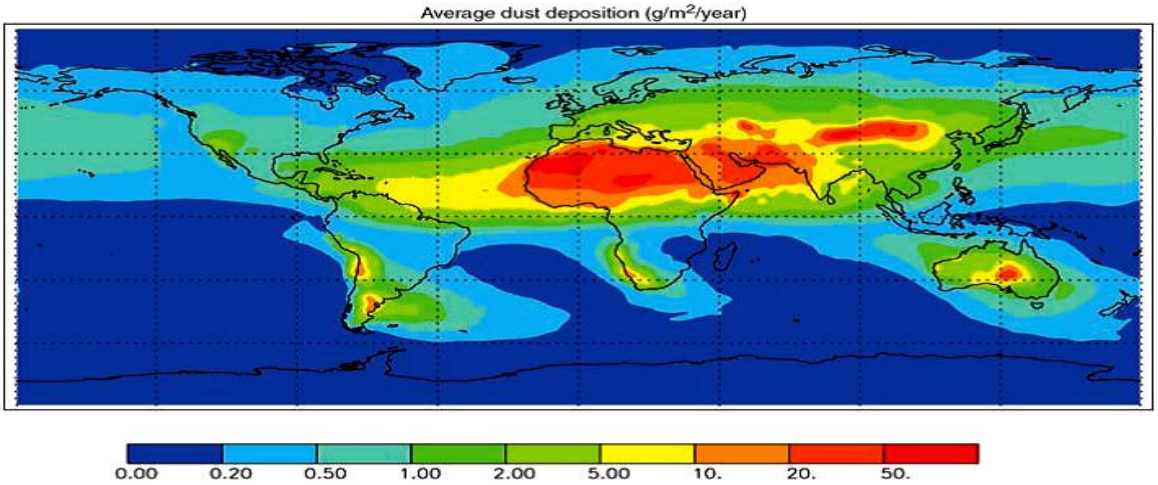

Figure I11. Average dust fluxes to the world oceans; based on a composite of three published modelling studies. Taken from Jickells *et al.* (2005).

Dust deposition occurs through dry and/or wet deposition and is strongly seasonal and episodic (Gao *et al.,* 2001). Dry deposition, mainly from soil particles that have been mobilized by strong winds and are entrained into the atmosphere, takes place after dust has travelled in the marine boundary layer (Jickells *et al.,* 2005) with the coarser particles, having diameters >100μm, being lost quite rapidly by gravitational settling whilst the finer ones, with average diameter ~6μm, can be transported great distances. Dust deposition is influenced by season, soil dryness in the source area, and natural climate variability (Xylouri, 2009), but, in the context of biogeochemical processes, the soluble or potentially bioavailabe trace metal fraction that is relased in the surface ocean is the most crucial (Jickells *et al.,* 2005). Dust events are triggered when near-surface wind speeds exceed 10 m/s, and are associated with synoptic-scale variability in the large-scale atmospheric circulation (Mahowald *et al.,* 2005).

Dust particles are eroded soils, and their chemical composition and mineralogy may be similar to that of parent crustal rock. The most abundant minerals in the dust from the Saharan are illite, carbonates, chlorite and palygorskite, whereas dust from the South Saharan contains more kaolinite and hematite (Usher *et al.,* 2003). In previous work, dust samples were collected from the Sal Island and the Cape Verde Islands to identify their distinct source regions by using a combination analysis and air-mass back trajectory

calculations (Chiapello *et al.,* 1997). Three different source regions were recorded: north and west Sahara; south and central Sahara; and the Sahel. Dust originating from north and west Sahara contains high amounts of calcite and the ratio of the clay minerals illite/kaolinite provides a good indicator of dust source, due to the higher abundance of kaolinite in the Sahel than in the Sahara. Rare earth element (REE) patterns and strontium isotopes have also been used to identify source regions of African dust (Chavagnac *et al.,* 2007).

The latitude of maximum dust transfer from Saharan region to the tropical NE Atlantic Ocean region changes between winter and summer, and is determined by the seasonal migration of the Inter Tropical Convergence Zone (ITCZ) (Prospero *et al.,* 1981). At the Cape Verde Islands, the highest dust deposition occurs in winter, as a result of dust transport in the lower air masses of the trade winds (Chiapello *et al.,* 1995). Saharan dust can reach the American continent (Prospero *et al.,* 1981) in summer, as it is transported at higher altitude within the Saharan Air Layer (1.5-6 km).

In addition to simple dry deposition wet deposition can also occur via rainfall where the particles are scavenged by being entrained within raindrops in the atmosphere, prior to transport to the sea surface. In a previous study by Xylouri (2009), she concluded that manganese could dissolve in cloud water at low pH, and remained dissolved and readily available for phytoplankton upon reaching the seawater. These observations are in line with those of Statham and Chester (1988) and Guieu (1994).

An opportunity to study the impact of atmospheric deposition of Mn in the NE Atlantic arose through analysis of samples collected during a research cruise in this area. The UK SOLAS cruise (D326) in the tropical NE Atlantic Ocean on board *RRS Discovery* between 5 January and 5 February 2008, started and finished at Santa Cruz, Tenerife (Canary Islands) and covered an oceanic area between 12 °N – 27 °N and 17 °W – 36 °W (Figure I13), During the crusie 189 underway surface seawater samples were collected for dissolved manganese analysis. No rainfall was recorded during the cruise (Patey, 2010); whilst two dust deposition events were noticeable. The first event was in the period from 17 to 22 January 2008 and a second more intense and prolonged dust event was encountered between 25 January and 1 February 2008. Aluminium (Al) and iron (Fe) are commonly used as indicators of a dust event, and concentrations of Al and Fe in aerosol increased sharply at the same time as the dust events (Figure I12).

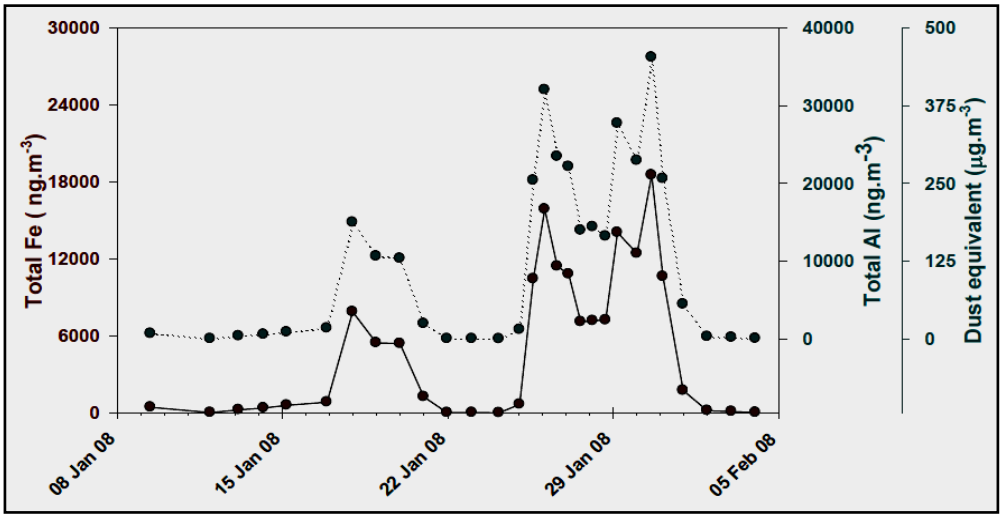

Figure I12. Total Fe and Al concentrations from aerosol samples collected aboard RRS Discovery during a research cruise (D326) in the tropical NE Atlantic between 8 January and 4 February 2008. Estimated mineral dust concentrations are indicated using the Al data with the additional vertical axis (Taken from Patey (2010)).

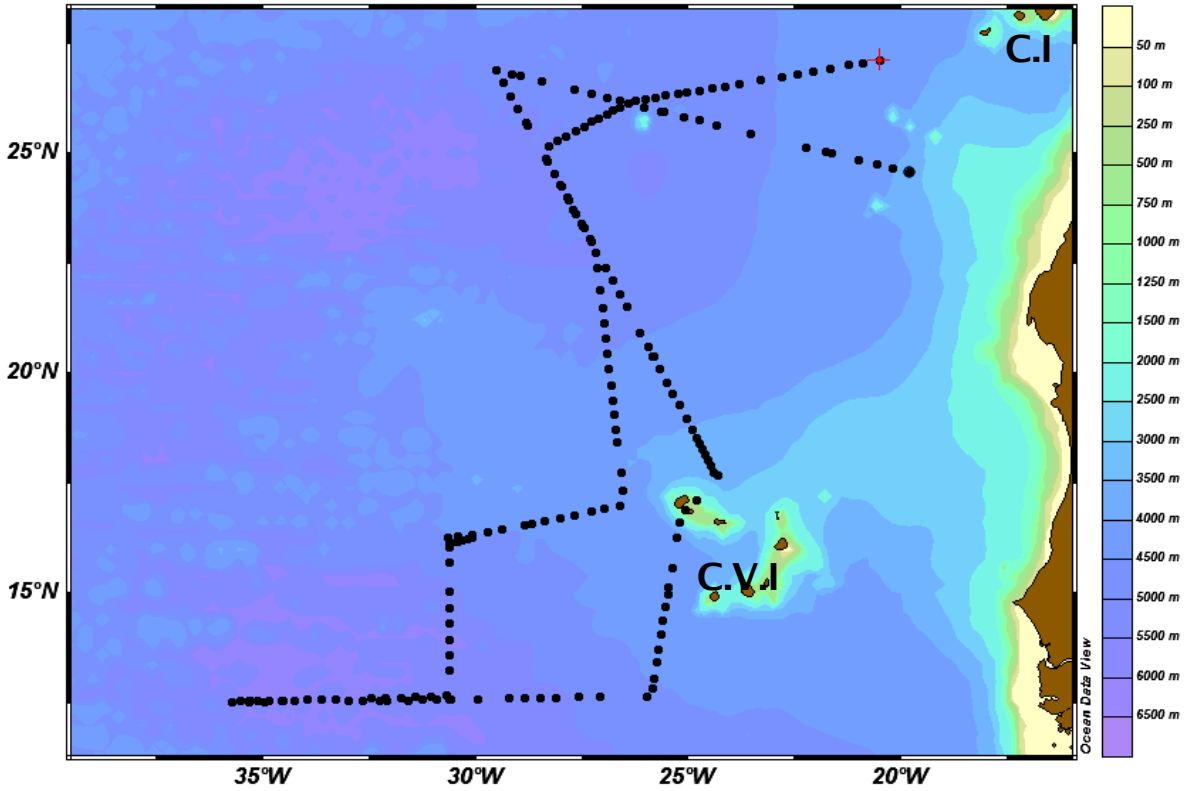

Figure I13. The map shows the Underway stations of the UK SOLAS Discovery 326 cruise (black dots). C.I: Canary Islands; C.V.I: Cape Verde Islands.

This study is therefore important in improving our understanding of the complex biogeochemistry of dissolved manganese concentrations in surface waters receiving high atmospheric dust deposition; details of this work are given in Chapter IV.

7 Aims and Objectives

The principal aim of this project is to improve our understanding of the marine manganese cycle by investigating the processes influencing the dissolved manganese distribution in two different regions where samples were collected for use in this project: the high nutrient low chlorophyll (HNLC) Crozet Islands of the Southern Ocean, and the high dust input area of the tropical North-Eastern (NE) Atlantic Ocean. To this end there were the following objectives:

- To construct a working analyser for nanomolar–picomolar dissolved manganese analysis that could reduce the risks of contamination and interference. The chosen technique was a flow injection analyser (FIA) with chemiluminescence (CL) detection.
- To characterise any interferences from other trace metals on manganese measurements made with the nanomolar–picomolar analyser and to investigate other factors (e.g. sample handling, and protocol in preparation of reagents) that can affect dissolved manganese measurements, particularly at ultra-low concentrations.
- To apply the developed analyser to determine dissolved manganese concentrations in seawater samples collected from the Southern Ocean (Crozet Islands) and from the tropical NE Atlantic Ocean.

8 Thesis structure

Chapter II describes the clean seawater sampling procedures for dissolved manganese (and other elements) during the cruises aboard RRS Discovery (D285 and D286, between 3 November 2004 and 21 January 2005) and also during the cruise aboard RRS Discovery D326 during January-February 2008. It describes the equipment, used for sampling, and sample storage.

Chapter III is concerned with the analysis of nanomolar-picomolar concentrations of dissolved manganese in seawater. The chapter begins with a review of the field and compares the relative merits of the various available methods for dissolved manganese analysis. An instrument for the laboratory measurement (Flow Injection Analyser with Chemiluminescence detection (FIA-CL)) of nanomolar-picomolar dissolved manganese that was developed for this study is described in detail. The chapter also contains a discussion of various problems and interferences (with solutions for each of problems and interferences that occurred) with the measurement of nanomolar-picomolar dissolved manganese concentrations.

Chapter IV and V present discussions of the data from seawater samples collected around the Crozet Islands during the CROZEX cruises (D285 and D286), and during the UK SOLAS project cruise (D326) in the tropical North-Eastern Atlantic Ocean on board *RRS Discovery*. In Chapter IV depth profiles of dissolved manganese around Crozet are presented, and an island source is identified. Estimates of manganese fluxes to the Crozet region are also calculated. Chapter V focuses on the concentrations of dissolved manganese in the surface seawater of the tropical NE Atlantic Ocean associated with dust deposition in relation of other factors (*e.g.* physical and biological). Estimates are calculated of soluble manganese fluxes to the tropical NE Atlantic.

Chapter VI brings together the principal findings from the work described in this thesis and describes further work that could be carried out on the datasets. Finally, this work is put in the more general context of future research directions in manganese biogeochemistry.

Chapter II: Methodology for sampling and background parameters

This chapter is divided into three sections: (1) sampling (*e.g.* sampling preparation and clean seawater sample collection), (2) sample acidification, and (3) analytical methods used for macronutrients and chlorophyll *a* (Chl-*a*). Methods associated with the measurement of nanomolar-picomolar concentrations of dissolved manganese are dealt with Chapter III.

Seawater samples used in this study for dissolved manganese analysis were collected by Dr. Helene Planquette during CROZEX project in Crozet waters, and by Dr. Alex Xylouri during SOLAS project in the tropical NE Atlantic waters. I was unable to join the cruises as for the CROZEX cruises: I had not yet enrolled as a student, and at the time of the SOLAS cruise: I was still pursuing an MSc. programme. However, I was given the opportunity to learn about the ultra-clean sampling procedures for trace metals in the final year of my studies on the RRS Discovery (D351) cruise to the North Atlantic Ocean during the Extended Ellet Line Project. The report for this D351 cruise is attached at Appendix 4. I am grateful to both Dr. Helene Planquette and Dr. Alexandra Xylouri for their sampling work, and information here on sampling protocols in this chapter are based on their work.

1 Pre-treatment and sampling procedures

1.1 Procedures for Cleaning Bottles and equipment

Implementation of ultra clean sampling and sample handling procedures are very important in trace metal studies to prevent contamination during sampling and storage before the analysis step. Prior to the cruises, the low density polyethylene (LDPE, Nalgene) sample bottles (1L, 500mL) were soaked for a week in ~2% Decon detergent solution, then a week in 50% HCl (v/v), and finally in 50% HNO_3 (v/v) acid bath for one more week. In between each step the bottels were rinsed four times with MQ water (18.2 MΩ cm). Finally the bottles were rinsed four times with MQ water and were filled with MQ water and spiked with HCl at 1µl/ml. The sample bottles were stored in double clean zipper seal polyethylene bags and placed in a clean plastic box to reduce potential contamination during handling and transferring samples.

All other materials used for the experiments such as syringes and measuring cylinders, were cleaned initially with 2% Decon detergent and after being rinsed with MQ water were acid cleaned with 50% HCl (v/v) acid. All the filters (e.g. polycarbonate filters) used for removing the particles were soaked with 10% HCl (v/v) for ~14 days and rinsed and stored in MQ water. In this work, HCl and HNO_3 were purified using a quartz sub-boiling

distillation unit that relies upon vaporising the reagent with a heating element, and using a 'cold finger' for condensation of acid vapours. Teflon bottles (1L) were used to collect and store the clean acids. The sub-boiled acids when prepared at the clean room laboratory of the National Oceanography Centre were found to provide very satisfactory results for almost all trace metals examined at low nanomolar to picomolar levels.

1.2 Sampling and filtration

Water column samples were collected using a titanium-frame CTD (conductivity, temperature, depth) (Figure II1) rosette system fitted with trace metal clean 10L OTE (Ocean Technology Equipment) sampling bottles with external springs that had been specifically modified for trace metal work.

Figure II1. Example of Titanium-frame CTD rosette system as used to collect water column samples for trace metal work.

The recovered trace metal sampling bottles were transferred to a clean van (equipped with a class 100 laminar flow bench) on the back deck for sample processing (Figure II2). Inside the clean container, OTE bottles were put on the rack using Delrin clamps. The OTE bottles were put under a slight positive pressure (~0.8 atm) (oxygen-free N_2). After opening the Teflon tap, samples were filtered in line using acid washed silicone rubber tubing with Teflon connections and acid washed Teflon filter holders, containing Nuclepore filters. Polycarbonate Nuclepore 0.2 µm filters were used during the sampling. The filtered samples were collected in the 0.5 L or 1L storage bottles, after rinsing three times with the seawater sample.

Figure II2. Left: OTE bottles for the filtration of dissolved manganese. Right: trace metals sampling work in the clean container.

Samples were collected at CTD stations reported here at up to sixteen depths, depending on water depth at each of the Crozet station (*see* Crozet map in Section 2, Chapter IV).

Table II1. Station locations, water depths, and sampling date during D285 and D286 cruises around the Crozet Islands.

Station	Date	Water depth (m)	Latitude (°S)	Longitude (°E)
M3 (496)	13/11/2004	2287	46.06809	51.78529
M3 (572)	22/12/2004	2375	46.06223	51.78169
M3 (622)	10/01/2005	2322	46.03412	51.86656
M1 (491)	11/11/2004	3118	43.92049	50.26742
M7 (524)	27/11/2004	2749	45.49943	49.00242
M10 (563)	21/12/2004	2943	44.52528	49.96059
M2 (502)	19/11/2004	3870	47.79537	52.86216
M6 (511)	22/11/2004	4275	49.00557	51.50046
M6 (598)	03/01/2005	4214	48.99900	51.53800
BA (567)	22/12/2004	83	46.36854	51.82754
BA+1 (568)	22/12/2004	379	46.32332	51.89459
BA+2 (569)	22/12/2004	1491	46.26997	51.97083

The underway surface samples used to provide the surface dissolved manganese data presented in Chapter V, were collected every one to two hours during transit between stations (*see* map in Section 2 of Chapter V). Underway surface seawater was sampled by pumping it into a trace metal clean container laboratory using a Teflon diaphragm pump (Almatec A-15, Germany) connected by an acid-washed braided PVC tubing to a towed fish

positioned at approximately 2 m depth alongside the ship (Figure II3). The seawater was filtered in-line through an acid-washed Sartobran 300 MF 0.2 µm filter cartridge, and collected in Nalgene LDPE bottles after being rinsed three times with the seawater sample. Table II2 shows surface underway stations location and sampling period.

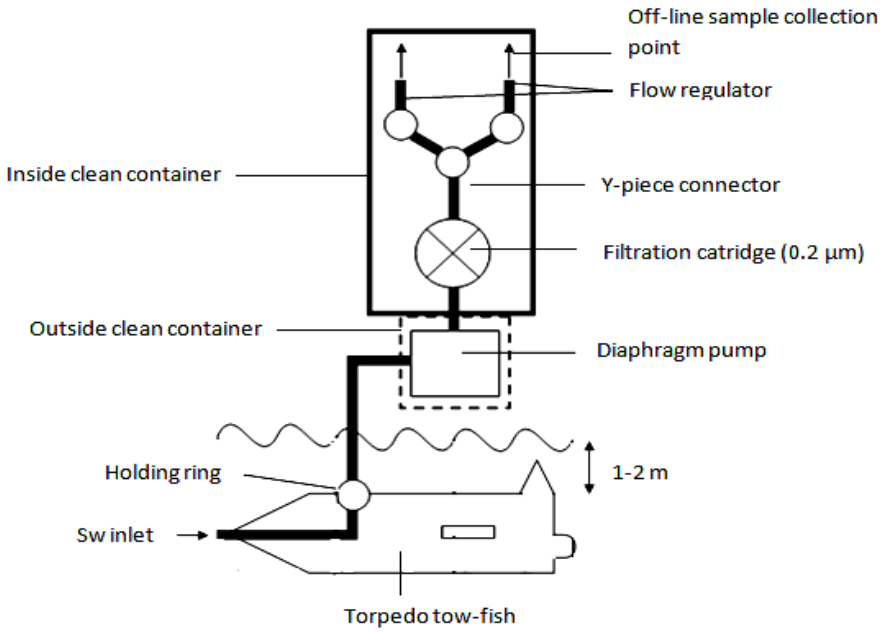

Figure II3. Above: An Underway Trace Metal Sampling (TMS) torpedo tow-fish. Below: The schematic of the flow design used for the collection of surface seawater (~2m) with a torpedo tow-fish, diaphragm pump and filtration system.

Table II2. List of surface underway stations location and sampling date during D326cruise around the tropical NE Atlantic Ocean

Station (UT)	Date	Time	Latitude (°N)	Longitude (°W)
1	07/01/2008	17:05:00	24.5637	19.7997
2	07/01/2008	18:56:00	24.6433	20.1804
3	07/01/2008	20:52:00	24.7375	20.5712
4	07/01/2008	22:57:00	24.8369	20.9874
5	08/01/2008	02:10:00	24.9928	21.6232
6	08/01/2008	02:58:00	25.0301	21.7780

7	08/01/2008	05:20:00	25.1443	22.2299
8	08/01/2008	17:00:00	25.4537	23.5338
9	08/01/2008	19:00:00	25.6481	24.3456
10	09/01/2008	01:00:00	25.7445	24.7454
11	09/01/2008	02:55:00	25.8352	25.1255
12	09/01/2008	05:08:00	25.9419	25.5689
13	09/01/2008	09:00:00	25.9514	25.6334
14	09/01/2008	11:00:00	26.0546	26.0347
15	09/01/2008	12:50:00	26.1421	26.4074
16	09/01/2008	17:07:00	26.1921	26.6120
17	09/01/2008	19:08:00	26.2655	26.9037
18	09/01/2008	21:00:00	26.3526	27.2838
19	09/01/2008	23:00:00	26.4475	27.6821
20	10/01/2008	02:55:00	26.6356	28.4687
21	10/01/2008	05:20:00	26.7526	28.9467
22	10/01/2008	11:00:00	26.7971	29.1467
23	10/01/2008	12:50:00	26.8812	29.5123
24	10/01/2008	23:00:00	26.5956	29.3464
25	11/01/2008	01:00:00	26.3053	29.1782
26	11/01/2008	02:58:00	26.0107	29.0076
27	11/01/2008	05:05:00	25.6892	28.8228
28	11/01/2008	09:00:00	25.6283	28.7792
29	11/01/2008	12:45:00	24.8205	28.3263
29	11/01/2008	19:00:00	24.8205	28.3263
30	11/01/2008	21:00:00	24.5276	28.1587
31	11/01/2008	23:00:00	24.2690	28.0102
32	12/01/2008	01:00:00	23.9980	27.8578
33	12/01/2008	02:58:00	23.7275	27.7041
34	12/01/2008	05:05:00	23.4149	27.5269
35	12/01/2008	09:00:00	23.3429	27.4835
36	12/01/2008	11:00:00	23.0621	27.3289
37	12/01/2008	19:04:00	22.3869	26.9489
38	12/01/2008	21:00:00	22.1025	26.7903
39	12/01/2008	23:00:00	21.8079	26.6258
40	13/01/2008	01:00:00	21.5164	26.4636
41	13/01/2008	05:00:00	20.9192	26.1322
42	13/01/2008	11:15:00	20.5917	25.9496
43	13/01/2008	12:45:00	20.3752	25.8336
44	13/01/2008	19:00:00	20.3771	25.8224
45	13/01/2008	21:00:00	20.0919	25.6742
46	13/01/2008	23:10:00	19.7878	25.5066
47	14/01/2008	01:00:00	19.5363	25.3684
48	14/01/2008	02:56:00	19.2695	25.2216
49	14/01/2008	05:11:00	18.9581	25.0507
50	14/01/2008	11:05:00	18.7286	24.9266
51	14/01/2008	12:35:00	18.5127	24.8088
52	14/01/2008	17:00:00	18.4024	24.7508

53	14/01/2008	19:04:00	18.2623	24.6747
54	14/01/2008	21:00:00	18.1329	24.6040
55	14/01/2008	22:59:00	18.0116	24.5376
56	15/01/2008	01:00:00	17.8881	24.4694
57	15/01/2008	02:56:00	17.7543	24.3951
58	15/01/2008	15:00:00	17.6714	24.3074
59	15/01/2008	19:10:00	17.0977	24.8009
60	15/01/2008	20:56:00	16.9015	25.0686
61	15/01/2008	23:00:00	16.5938	25.2116
62	16/01/2008	01:00:00	16.2562	25.2697
63	16/01/2008	05:10:00	15.5624	25.3898
64	16/01/2008	12:10:00	15.1392	25.4630
65	16/01/2008	17:25:00	14.9569	25.4840
66	16/01/2008	19:04:00	14.6798	25.5412
67	16/01/2008	21:00:00	14.3605	25.5970
68	16/01/2008	22:58:00	14.0453	25.6502
69	17/01/2008	01:00:00	13.7258	25.7050
70	17/01/2008	02:55:00	13.4218	25.7583
71	17/01/2008	05:00:00	13.0634	25.8186
72	17/01/2008	11:12:00	12.8300	25.8593
73	17/01/2008	12:45:00	12.6540	25.9957
74	17/01/2008	23:00:00	12.6449	27.0836
75	18/01/2008	05:00:00	12.6375	27.5947
76	18/01/2008	11:43:00	12.6260	28.1141
77	18/01/2008	19:00:00	12.6186	28.4816
78	18/01/2008	21:00:00	12.6131	28.8536
79	18/01/2008	23:00:00	12.6052	29.2273
80	19/01/2008	01:00:00	12.5735	30.6031
81	19/01/2008	02:56:00	12.5919	29.9712
82	19/01/2008	05:05:00	12.5812	30.9391
83	19/01/2008	19:16:00	12.5755	31.2625
84	19/01/2008	21:05:00	12.5812	31.5992
85	19/01/2008	23:00:00	12.5677	32.1126
86	20/01/2008	00:58:00	12.5649	32.2777
87	20/01/2008	02:55:00	12.5526	32.6575
88	20/01/2008	05:05:00	12.5486	32.9970
89	20/01/2008	11:07:00	12.5376	35.3221
90	20/01/2008	12:43:00	12.5378	35.1547
91	20/01/2008	17:00:00	12.5266	34.8609
92	20/01/2008	19:00:00	12.5307	34.5507
93	20/01/2008	21:06:00	12.5210	34.9862
94	20/01/2008	23:00:00	12.5170	35.3569
95	21/01/2008	01:00:00	12.5113	35.7374
96	21/01/2008	02:58:00	12.5082	35.5342
97	21/01/2008	05:00:00	12.5038	35.3563
98	21/01/2008	11:06:00	12.5375	35.1547
99	21/01/2008	12:27:00	12.5400	34.8609

100	21/01/2008	17:00:00	12.5450	34.5604
101	21/01/2008	19:00:00	12.5512	34.2761
102	21/01/2008	21:02:00	12.5567	33.9554
103	21/01/2008	22:57:00	12.5639	33.6439
104	22/01/2008	01:00:00	12.5693	33.2897
105	22/01/2008	02:57:00	12.5759	32.4690
106	22/01/2008	05:05:00	12.5807	32.1401
107	22/01/2008	17:07:00	12.6136	31.7783
108	22/01/2008	19:00:00	12.6129	31.4200
109	22/01/2008	21:00:00	12.6259	31.0515
110	22/01/2008	22:58:00	12.6422	30.6934
111	23/01/2008	01:00:00	12.6583	30.6342
112	23/01/2008	02:57:00	12.6754	30.6337
113	23/01/2008	15:00:00	12.5677	30.6341
114	23/01/2008	18:57:00	13.2484	30.6331
115	23/01/2008	20:57:00	13.5898	30.6333
116	23/01/2008	22:55:00	13.9350	30.6333
117	24/01/2008	01:00:00	14.3044	30.6333
118	24/01/2008	03:00:00	14.6535	30.6338
119	24/01/2008	05:10:00	15.0271	30.6345
120	24/01/2008	09:00:00	15.6835	30.4358
121	24/01/2008	11:00:00	16.0360	30.1330
122	24/01/2008	17:15:00	16.1770	30.0756
123	24/01/2008	19:00:00	16.2496	30.1885
124	24/01/2008	21:07:00	16.2580	30.3187
125	24/01/2008	22:55:00	16.2347	30.4596
126	25/01/2008	00:57:00	16.2048	30.6284
127	25/01/2008	03:00:00	16.1693	30.6510
128	25/01/2008	05:10:00	16.1312	30.4103
129	27/01/2008	21:30:00	16.2494	30.0913
130	27/01/2008	23:00:00	16.2808	29.7338
131	28/01/2008	00:55:00	16.3210	29.3844
132	28/01/2008	03:00:00	16.3774	28.8674
133	28/01/2008	05:06:00	16.4451	28.7042
134	28/01/2008	08:07:00	16.5429	28.3737
135	28/01/2008	09:05:00	16.5745	28.0274
136	28/01/2008	11:00:00	16.6419	27.6715
137	28/01/2008	13:00:00	16.7067	27.2715
138	28/01/2008	15:00:00	16.7739	26.9778
139	28/01/2008	17:18:00	16.8511	26.6046
140	28/01/2008	19:00:00	16.9078	26.5397
141	28/01/2008	21:07:00	16.9802	26.5872
142	29/01/2008	02:56:00	17.3411	26.6680
143	29/01/2008	05:10:00	17.7402	26.7018
144	29/01/2008	09:18:00	18.4287	26.7415
145	29/01/2008	11:00:00	18.7094	26.7821
146	29/01/2008	13:00:00	19.0484	26.8234

147	29/01/2008	15:00:00	19.3896	26.8661
148	29/01/2008	17:00:00	19.7335	26.9056
149	29/01/2008	19:05:00	20.0962	26.9478
150	29/01/2008	21:00:00	20.4285	26.9915
151	29/01/2008	23:05:00	20.7905	27.0318
152	30/01/2008	01:00:00	21.1297	27.0819
153	30/01/2008	02:54:00	21.4704	27.1444
154	30/01/2008	05:10:00	21.8846	27.1863
155	30/01/2008	11:07:00	22.4034	27.2856
156	30/01/2008	13:00:00	22.7287	27.4642
157	30/01/2008	17:00:00	22.9791	27.6428
158	30/01/2008	19:00:00	23.2977	27.8166
159	30/01/2008	21:00:00	23.6131	27.9999
160	30/01/2008	23:00:00	23.9213	28.1607
161	31/01/2008	01:05:00	24.2442	28.3551
162	31/01/2008	02:55:00	24.5281	28.2843
163	31/01/2008	05:15:00	24.8666	28.0859
164	31/01/2008	11:20:00	25.1751	27.8697
165	31/01/2008	13:03:00	25.2787	27.6659
166	31/01/2008	15:00:00	25.3916	27.4559
167	31/01/2008	17:02:00	25.4968	27.2695
168	31/01/2008	19:10:00	25.6058	27.1023
169	31/01/2008	21:07:00	25.7112	26.9167
170	31/01/2008	23:00:00	25.7968	26.7735
171	01/02/2008	01:12:00	25.8880	26.5993
172	01/02/2008	02:58:00	25.9647	26.2466
173	01/02/2008	05:05:00	26.0513	26.0111
174	01/02/2008	11:01:00	26.2010	25.7879
175	01/02/2008	13:04:00	26.2386	25.5470
176	01/02/2008	15:00:00	26.2763	25.2340
177	01/02/2008	17:00:00	26.3094	25.0324
178	01/02/2008	19:30:00	26.3495	24.7554
179	01/02/2008	21:00:00	26.3768	24.4420
180	01/02/2008	23:00:00	26.4203	24.1488
181	02/02/2008	01:05:00	26.4715	23.8204
182	02/02/2008	02:58:00	26.5041	23.3206
183	02/02/2008	05:10:00	26.5730	22.8073
184	02/02/2008	11:00:00	26.6577	22.4354
185	02/02/2008	16:58:00	26.7439	22.0564
186	02/02/2008	19:00:00	26.8062	21.6760
187	02/02/2008	21:00:00	26.8733	21.2409
188	02/02/2008	23:00:00	26.9256	20.9093
189	03/02/2008	01:15:00	27.0047	20.4950

2 Sample acidification

All samples were acidified on board within 24 hours of sample collection to stabilise the metals present in solution. During Crozex and D326 cruises, samples initially were acidified with ultra clean HCl (Romil UHP grade) to pH~2, representing typically ~1mL 12M HCl per ~1L of seawater. This procedure limits manganese loss from solution by adsorption onto the walls of the container particularly when the samples were stored for a long period of time (weeks to years) and, to avoid any biological and chemical activity during the storage. All acidified samples were stored in double clean zipper resealable polyethylene bag, and placed in a clean crate container to reduce potential contamination during handling and transfer steps.

3 Analytical methods for chlorophyll *a* (Chl-*a*) and macronutrients

For chl-*a* approximately 100-200 mL of seawater sample at each depth and station was filtered onto a Whatman GF/F 25mm filter with a nominal pore size 0.7 µm (Seeyave *et al.,* 2007). The filters were placed in 20 mL glass scintillation vials and 10 mL 90% Acetone (HPLC grade, Fisher Chemical) was added for pigment extraction over 24 hours in a dark fridge. Chl-*a* pigment was measured fluorometrically on board, using a Turner Designs fluorometer following the Welschmeyer (1994) protocol. The Fluorometer was calibrated with a chl-*a* commercial grade standard (Sigma).

Nutrient analyses were processed on board (CROZEX) by Dr. Richard Sanders. In brief, samples for macronutrients (nitrate+nitrite (hereinafter nitrate), phosphate and silicate) were taken from the Stainless Steel CTD casts and analysed on-board using a Skalar San Plus autoanalyser following methods described by Sanders and Jickells (2000). Samples were drawn from Niskin bottles into 25ml sterilin coulter counter vials and kept refrigerated at 4 ˚C until analysis which commenced within 24 hours of sampling. Stations were run in batches of 1-3 with most runs containing 1 or 2 stations. Overall 40 runs were undertaken. An artificial seawater matrix (ASW) of 40 g/l sodium chloride was used as the intersample wash and standard matrix. The nutrient free status of this solution was checked by running Ocean Scientific International (OSI) nutrient free seawater on every run. A single set of mixed standards were made up at the start of the cruise and used throughout the cruise. These were made by diluting 5 mM solutions prepared from weighed dried salts in 1L of ASW into 1L plastic volumetric flasks that had been cleaned. Three low silicate standards were also used after several initial runs without them. OSI nutrient standard solutions were used sporadically during the cruise to monitor any degradation of these standards. Data processing was undertaken using Skalar proprietary software. Generally this was straightforward. The wash time and sample time were 75

seconds; the lines were washed daily with 0.25M NaOH (P) and 10% Decon (N, Si). Time series of baseline, bulk standard concentration, instrument sensitivity, calibration curve correlation coefficient, nitrate reduction efficiency and duplicate difference were compiled and updated on a daily basis.

Meanwhile, nutrient analyses for underway surface seawater samples from the D326 cruise were processed by Dr. Matthew Patey. In brief, analysis for nitrate+nitrite (hereinafter nitrate) and phosphate at nanomolar concentration were undertaken following a method described in Patey *et al.* (2008). A segmented-flow autoanalyser with liquid waveguide capillary flow cells each having a two-metre path-length enabled the detection of nanomolar levels of the nutrients. Two Tungsten-halogen light sources were used in conjunction with fibre-optic spectrometers to monitor the absorbance of the solution flowing through the waveguides. Samples were taken in HCl-washed 60 ml LDPE bottles.

Chapter III: Developing an analytical method for determining dissolved manganese in seawater

1 Introduction

During the last three decades, much progress has been made in understanding the biogeochemical cycling of manganese in seawater and its role in phytoplankton growth. Manganese is frequently present at sub nanomolar levels in seawater and this makes its detection challenging (Mallini and Shiller, 1993; Aballea *et al.,* 1998; de Jong *et al.,* 2007; Doi *et al.,* 2004). Early investigations had problems with attempting to measure these sub-nanomolar levels of manganese, as a result of sample contamination and insufficiently low analytical limits of detection. In this chapter the development of an analyser suitable for the relatively high surface water concentrations of Mn found in the Tropical NE Atlantic is described first. This analyser was used to generate the data discussed in the later chapter on the atmospheric imprint of Mn in the Atlantic waters. However, initial analyses of deep waters from around the Crozet islands using this method demonstrated that it was not sensitive enough and additionally subsequent work showed that there were interferences from other metal ions present. These problems were overcome and the modified technique was successfully used to mesure Mn in waters around the Crozet Islands and the interpretation of this data is given in Chapter IV. The development of the more sensitive and selective analyser is described in the second part of the present chapter.

1.1 Analytical Challenge: Contamination

Sample contamination was a major problem that occurred in attempts to measure trace metals in seawater. The impact of contaminant species includes not only an increase in the analyte concentration but there may also be interferences in the final determination stage. There are two main types of contribution to analyte contamination in the analysis: (1) random sources *e.g.* particles of dust which fall into the solution or a single faulty container in a batch, and (2) contamination from the reagent solutions and equipment used in the analytical procedure. Reduction of the number of handling steps and reagents used in the analysis thus reduces contamination.

2 Dissolved Manganese Analysis

Since the implementation of ultra clean sampling procedures, a variety of methods have been developed with the aim of generating good manganese data. These involve reduction of contamination, and development of more sensitive and flexible analytical methods, including real-time measurement of manganese in situ for e.g. hydrothermal systems.

Various techniques for determination of low level (<1 nM) trace metals in seawater have been developed that frequently include pre-concentration and separation techniques, such as ion exchange (Saager *et al.,* 1997), solvent extraction (Saager *et al*., 1997; Le Gall *et al.,* 1999) and chelating resin (Chapin *et al*., 1991; Mallini and Shiller, 1993; Hirano *et al*., 2001; Willie *et al*., 2001; Beck *et al*., 2002; Doi *et al*., 2004). As a result of these developments it is now possible to detect and determine manganese concentrations in seawater at picomolar levels.

After pre-concentration, manganese from seawater samples has been determined by various methods, for example inductively coupled plasma – optical emission spectrometry (ICP-OES) (Vassileva and Furuta, 2003); cathodic stripping voltametry (CSV) (Roitz and Bruland, 1997; Roitz *et al*., 2002); graphite furnace atomic absorption spectrometry (GFAAS) (Statham and Burton, 1986); inductively coupled plasma – mass spectrometry (ICP-MS) (Hirata *et al*., 2001; Bergquist and Boyle, 2006); ICP-MS (after pre-concentration with the chelating resin (Toyopearl AF-Chelate 650M; Milne *et al.,* 2010), or Nobias-Chelate PA1 (Sohrin *et al.,* 2008; Biller and Bruland, 2012). Additionally flow injection methods (FIA) have been coupled with pre-concentration chelating resins, for examples, 8-hydroquinoline (Bucciarelli *et al.,* 2001; Laes *et al*., 2007; de Jong *et al.,* 2007; Nakayama *et al.,* 1989; Obata *et al.,* 2007; Sedwick *et al.,* 1997; Aballea *et al.,* 1998), Toyopearl AF-Chelate 650M (Middag *et al.,* 2011a, 2011b), Fractogel-8-hydroxyquinoline (Malini and Shiller, 1993), MAF-IDA (Doi *et al*., 2004).

Table III1 gives an overview of the reported methods for the analysis of manganese in seawater at nanomolar concentrations, their detection limits, precision, and the pre-concentration columns used. Among these techniques, the most common recently used technique to determine manganese is FIA since low detection limits are achieved when these methods are coupled with pre-concentration techniques. As indicated above these techniques require care in the critical steps of sampling and analysis, and use ultra-clean sampling procedures (Bruland *et al.,* 1979) including use of acid washed bottles, working in clean rooms during sample collection and working on a laminar flow bench during the analysis; use of high purity reagents in order to maintain the sample integrity is also mandatory.

Table III1. Figures of merit of some techniques used to determine manganese concentrations in seawater. Limit of detection = 3 times the standard deviation of the blank (3 S.D.), unless specified otherwise

Mn measured	Technique used	Preconcentration column	Limit of detection (nM/nmol kg^{-1})	Precision	Reference
Dissolved Mn	FIA-CL	8-hydroxyquinoline	0.54 (n = 5)	4.0 % for concentration above 5 nM	**Bucciarelli *et al.*, 2001**
Dissolved Mn	FIA-CL	Toyopearl AF-Chelate 650M	~0.012 (n = 22)	1.3 – 3.5 %	**Middag *et al.*, 2011a, 2011b**
Total dissolved Mn	Online preconcentration and ICP-MS	Muromac A-1	2.33 at pH 3.0 0.13 at pH 5.0	~0.1 – 5.4 %	**Hirata *et al.*, 2001**
Total dissolved Mn	Online preconcentration and ICP-OES	Muromac A-1	0.02	1.32 ± 0.21 µ/g	**Vassileva and Furuta, 2003**
Dissolved Mn	FIA-colorimetric detection	8-hydroxyquinoline	0.0062 (n = 14)		**Laes *et al.*, 2007**
Dissolved Mn	FIA-colorimetric detection	8-hydroxyquinoline	0.09 (n = 7)	2.0 % at the 0.5 nM	**de Jong *et al.*, 2007**
Dissolved Mn	FIA-CL	8-hydroxyquinoline	0.05	1.2 %	**Nakayama *et al.*, 1989**
Dissolved Mn	Isotope dilution followed by $Mg(OH)_2$ coprecipitation and ICP-MS	–	0.15 (1 S.D.)	0.1 nM (1 S. D.)	**Bergquist and Boyle, 2006**
Dissolved Mn	GFAAS	–	0.15	~10.0 %	**Mackey *et al.*, 2002**

Total dissolved Mn	FIA-CL	8-hydroxyquinoline	0.05	1.2 % at 1 nM	**Obata *et al.*, 2007**
Dissolved Mn	FIA-colorimetric detection	8-hydroxyquinoline	-	20.0 %	**Sedwick *et al.*, 1997**
Dissolved Mn	CSV	–	6.00	4.0 %	**Roitz and Bruland, 1997** **Roitz *et al.*, 2002**
Dissolved Mn	GFAAS	–	0.36 0.10	0.22 ± 0.04 nM (1 S.D.)	**Statham and Burton, 1986**
Dissolved Mn	FIA-CL	MAF-IDA	0.005 (n = 10)	0.89 %	**Doi *et al.*, 2004**
Dissolved Mn	FIA-colorimetric detection	Fractogel-8-hydroxyquinoline	0.04	4.5 % at 1.7 nM (n = 10) 5.0 % at 0.47 nM (n = 5)	**Mallini and Shiller, 1993**
Dissolved Mn	FIA-colorimetric detection	8-hydroxyquinoline	0.05 for 10 min preconcentration 0.10 for 4 min preconcentration	5.0 % at 0.2 nM	**Aballea *et al.*, 1998**
Total dissolved Mn	ICP-MS	Toyopearl AF-Chelate 650M	0.007	4.6%	**Milne *et al.*, 2010**
Total dissolved Mn	ICP-MS	Nobias-Chelate PA1	0.09		**Sohrin *et al.*, 2008**
Total dissolved Mn	ICP-MS	Nobias-Chelate PA1	0.002		**Biller and Bruland, 2012**

3 Flow Injection Analysis (FIA)

Ruzicka and Hansen (1988) described FIA as an automated method based on injection of a liquid sample into a continuous flow of a suitable carrier solution (reagent) that mixes with other continuously flowing solutions before transport towards a detector that continuously records the absorbance or any other physical parameter. Recently, FIA has being an attractive technique in trace metal analysis due to its advantages. These advantages are: **(1)** it is rapid, and requires low volumes of sample and reagents; **(2)** the closed system reduces the risk of airborne contamination and **(3)** it also offers the possibility of low detection limits (Chapin *et al*., 1991; Mallini and Shiller, 1993; Hirano *et al.,* 2001) when use onboard for near real-time determinations. Thus, the FIA technique has excellent reproducibility compared with other off-line pre-treatment techniques (Hirano *et al*., 2001). This approach is an inexpensive alternative to other systems using complex analysis systems (*e.g.* ICP-MS) and provides a portable instrument that can be used in conjunction with a laminar flow bench where samples and reagents are placed, and under these conditions it is argued that a clean van is no longer necessary (de Jong *et al*., 2000).

In an FIA experimental system there are usually two kinetic processes that must occur simultaneously (Ruzicka and Hansen, 1988): (1) the physical processes of zone dispersion; and (2) the chemical processes resulting from reactions between sample and reagent species. When both conditions are at the optimum level, then the FIA analytical signal can be quantified based on either: (1) the peak height (*h*); (2) peak area (*a*); or (3) peak width (*w*). These parameters reflect the sensitivity and sample throughput of the system. Therefore, it is crucial to know how these parameters are influenced by variables in the FIA system. Theoretical principles can be used to optimize the system, but these quantitative relationships typically have a narrow range of application and thus, optimisation of an FIA system is often achieved through laboratory experimentation. The variations may be caused by several factors, for example the injection system, connectors, dead volumes, design of the flow cell and chemicals used. Furthermore, the mathematical relations that have been derived mostly focus on simple FIA manifolds (single or two lines). Consequently, these are not usually applicable to systems with more lines and several mixing points, or those involving the use of separation/pre-concentration devices.

An FIA system coupled with a chemiluminescence (CL) detection cell can determine trace metals through light emission during a chemical reaction with luminol. In the first part of this chapter, a FIA-CL system was developed to determine dissolved manganese in seawater at concentrations of ~0.5 nM or more. Before explaining in more detail about the FIA-CL technique, it is crucial to know the key factors affecting the manganese signal in the FIA-CL technique. In general, there are three important factors that should be considered: (1) the chemiluminescence reaction, (2) uptake by the resin, and (3) elution. Some

optimisation of the FIA-CL method also needs to be done to make this technique specific to manganese only. In this chapter, all the above factors will be discussed in detail, including the problems encountered during the analysis and their solutions.

4 Flow injection analysis with chemiluminescence detection (FIA-CL)

The FIA-CL technique generally involves three major analytical steps:
i) sample pre-treatment to determine which size fraction and oxidation state of manganese is analysed (see *Chapter II* for sample pre treatment);
ii) a resin pre-concentration step to a), remove interfering sea-salts and to b) collect and concentrate Mn(II) so as to lower the limit of detection;
iii) the detection step using the chemiluminescence reaction with luminol.

4.1 Pre-concentration

The preconcentration procedure in dissolved manganese analysis was very important in this study as seawater samples to be measured were at nanomolar-picomolar concentrations. Without the pre-concentration process, dissolved manganese was undetectable and also prone to interferences. A conventional 8-Hydroxyquinoline (8-HQ) resin which has often been used to separate metals from solutions was not initially used in the developed Mn-FIA-CL systems because of several factors. 8-HQ when coupled to a silica substrate has been found to be unstable at high pH (~9), whilst the optimum pH for collecting manganese is ~8.6 (Aguilar-Islas *et al*., 2006). At high pH, the 8-HQ chelating group tended to 'bleed' from the silica substrate as a result of hydrolysis and also this substrate breakdown can release contamination (Sturgeon *et al*., 1981). Also this resin is reported to leach colour when eluted with high concentrations of hydrochloric acid (HCl) (> 0.1 M) as used in the present study, and the leached functional group may cause masking effects (Obata *et al*., 1993; Weeks and Bruland, 2002). Additionally 8-HQ resins are not commercially available, and their synthesis produces resins of varying quality (Aguilar-Islas *et al.,* 2006), and for some manganese was poorly retained (Dierssen *et al.,* 2001).

Here the commercially available Toyopearl AF chelate-650M (hereafter called Toyopearl) was used by Aguilar-Islas *et al*. (2006) which have a high affinity for binding manganese ions at pH 8 to 9. This resin is based on the amino di-acetic acid functional group with a macroporous methacrylate backbone (Figure III1). The resin used had a bead size of 65 µm, a capacity of approximately 35 µmol ml^{-1} (Arslan and Paulson, 2003), and this resin is stable within wide extremes of pH (ranges from 2 to 13) and ionic strength. Furthermore, the quality of the resin was reproducible and overall its use simplifies system set up (Aguilar-Islas *et al.,* 2006).

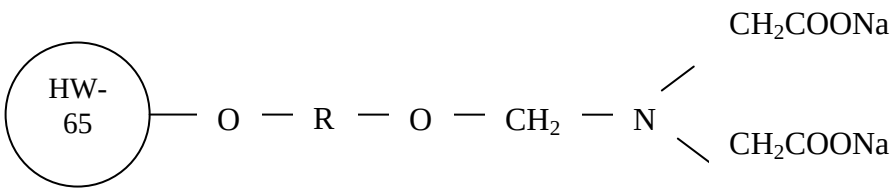

Figure III1. Toyopearl 650M AF chelating resin is based on the amino di-acetic functional group with a macroporous methacrylate backbone.

The seawater matrix is complex and may potentially create interferences during the detection step. Sea-salt ions such as Ca^{2+}, Mg^{2+} and Cl^{-} tend to significantly suppress (for cations) or increase (for halides) the chemiluminescence signal (Chang and Patterson, 1980; Bowie *et al*., 1998). These ions may also precipitate (*e.g.* to $Mg(OH)_2$) after mixing with basic luminol solution at a pH>10 and clog the detector (Nedelec, 2006). A rinsing step with MQ water after passing the sample through the column is therefore necessary to remove sea-salts still present in the dead volume of the column. According to the results of Aguilar-Islas *et al*. (2006), Willie *et al.* (2001), Warnken *et al.* (2000), Beck *et al*. (2002), and Milne *et al.* (2010), Mn(II) is quantitavely collected at a pH between 8 and 9. A number of studies have shown that several trace metals including Fe(II and III), Cr(III), Co(II), Cu(II), Ni(II), Zn(II), and Cd(II) can intefere with the chemiluminescence reaction (Nakayama *et al*., 1989; Okamura *et al*., 1998; Doi *et al*., 2004). However only Ni(II), Cu(II), and Cd(II) can be collected on the Toyopearl resin at a pH of 8.8 - >9 (Warnken *et al*., 2000). Mn(II) thus can be selected from other trace metals by carefully adjusting the pH to 8.5-8.6 (Willie *et al.,* 2001; Aguilar-Islas *et al.,* 2006).

The pre-concentration resin column is therefore important for separating manganese from other trace metals, and lowering the detection limit, as well as removing the seawater matrix. Several factors can impact the chelating efficiency onto the Toyopearl resin, such as the pH of the sample, the loading flow rate, the eluent concentration and pH, and column preconditioning (Aguilar-Islas *et al.,* 2006).

4.2 Chemiluminescence reaction of luminol

The chemiluminescence of luminol (5-amino-2,3-dihydro-1,4-phthalazinedione) was first described by Albrecht in 1928. This compound reacts with a potent oxidizing agent (*e.g*. H_2O_2) in the presence of a catalyst (generally a metal or metal-containing compound) in alkaline solution to produce 3-aminophthalate in an excited electronic state which returns to ground state with the production of light. The most obvious use of the reaction has been to determine oxidants or compounds which interact with oxidant, but it is possible to determine metal ions by their catalysis of the CL reaction.

4.2.1 The chemiluminescence reaction

Chemiluminescence (CL) is the emission of light during a chemical reaction. When luminol is oxidized by hydrogen peroxide (H_2O_2), some of the energy released in the reaction causes excitation of electrons in the products of the reaction and the CL is produced at a wavelength of 425 nm under many conditions (Rose and Waite, 2001). Due to its sensitivity and its potential selectivity, the CL reaction of luminol with H_2O_2 has been used as the baisis of analytical procedures to determine trace level of various metal ions as an alternative to other spectroscopic techniques. However, this technique is not actually detecting trace metals (*i.e.* manganese) directly. It is the manipulation of the chemical reactions and the metal collection during the analysis that actually makes the determination specific to a particular metal (*i.e.* manganese) in a seawater sample.

4.2.2 Decomposition of H_2O_2

Trace metals existing in the FIA-CL technique act as a catalyst, which enhances the decomposition of H_2O_2. Decomposition of H_2O_2 occurs in two ways: **(1)** a radical chain reaction catalysed by any cation having two or more oxidation states for example manganese, iron, copper, cobalt and nickel, which leads to the production of the hydroxyl radical ·OH in the alkaline solution (Nakayama *et al.*, 1989); and/or **(2)** a two electron oxidation where H_2O_2 initially reacts with free manganese (or other metals) species to form an intermediate complex Mn^{2+}–H_2O_2 (Xiao *et al.*, 2000). The resulting hydroxyl radical immediately oxidizes luminol to 3-aminophthalate dianion that emits light when going to the ground state, as explained in Section 4.2.

The catalytic activity of metal ions in the decomposition of H_2O_2 is more efficient when triethylenetetramine (TETA) is added because $Me(OH)^{2+}$ (Me is either Fe or Mn) decomposes H_2O_2 with great efficiency (Jarnagin and Wang, 1958). TETA is a strong ligand containing four amine groups which holds the metal ion close to the reactive centre. The polarization of the metal ion in TETA forms octahedral complexes. Four of the octahedral orbitals of the metal ion are used to bond with the tetramine and the other two remaining orbitals are used to bond with either hydroxide or hydroperoxide (H_2O_2) ions or both, as shown in Figure III2. Adding TETA into the experiment has been shown to distinctly enhance the CL intensity (Nakayama *et al.,* 1989; Okamura *et al.,* 1998). Previous studies discovered that Fe(III) and Mn(II) showed the highest catalytic activity for decomposition of H_2O_2 when TETA was added (Nakayama *et al.*, 1989; Nedelec, 2006 and references therein) as Fe(III) and Mn(II) acted as catalysts in the decomposition of H_2O_2 into the radical ·OH under the alkaline conditions used (Nakayama *et al.*, 1989). Therefore, this technique could be used to determine the concentration of dissolved manganese (as Mn(II) after removing other metals that may interfere).

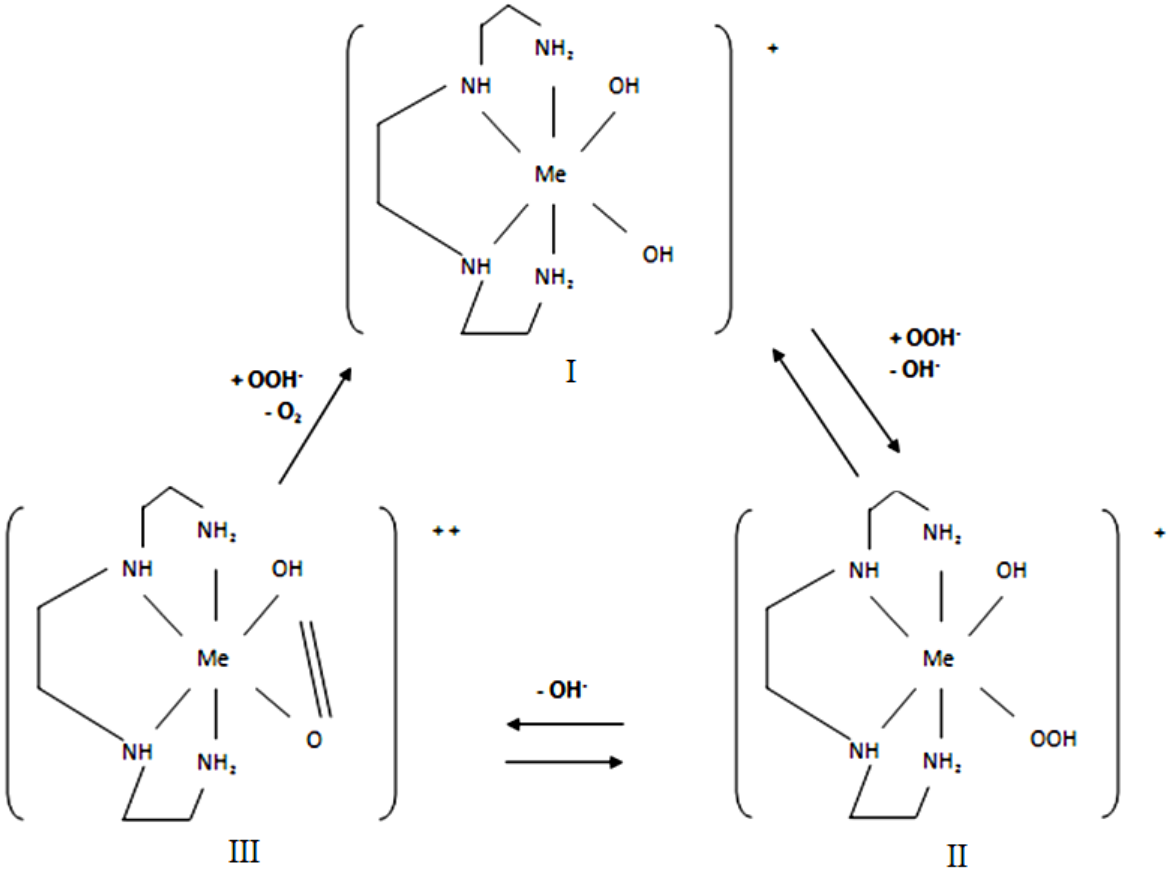

Figure III2. Mechanism of the catalytic decomposition of hydrogen peroxide by TETA-Me$(OH)_2^+$. Me is either Fe(II) or Mn(II) ion (after Jarnagin and Wang, 1958).

4.2.3 Oxidation of luminol

A sensible mechanism for the CL reaction is described in three basic steps (Figure III3) in the oxidation of luminol, as described by Rose and Waite (2001): **(1)** oxidation of luminol to the luminol radical by strong oxidants such as ·OH or its radical derivatives, but H_2O_2 alone is insufficient unless a trace metal (*e.g.* manganese, iron, cobalt, copper, and chromium), is present that can increase the rate of the photon emission; **(2)** oxidation of the luminol radical to α – hydroxyl hydroperoxide (α-HHP) producing luminol and diazaquinone which can react with the superoxide radical $\cdot O_2^-$, and **(3)** decomposition of α-HHP resulting in excitation of the 3-aminophthalate which emits light when going to the ground state. The amount of the 3-aminophthalate in the excited state is proportional to the concentration of Mn (II) under set conditions. Thus, the concentration of Mn (II) can be determined by measuring the CL intensity (Nakayama *et al.,* 1989).

However, the Mn (II)–CL reaction depended only on pH once the luminol α-hydroperoxide was formed (Rose and Waite, 2001). O'Sullivan *et al.* (1995) found that the optimum CL pH for seawater samples is 9.9 and for freshwaters, CL intensity has a broad maximum from pH 10.5 to 11, but a recent study showed that the optimum pH for CL is 10.2 (Doi *et al.*, 2004) as the efficiency of CL is increased at this pH. However, more alkaline

condition resulted in a higher background signal without any gain in sensitivity corresponding with a decreased in the fluorescence quantum yield of aminophthalate (Rose and Waite, 2001).

The addition of carbonate significantly enhances the CL signal (Nedelec, 2006). The carbonate reacts with hydroxyl radicals that is produced by Mn(II) oxidation or degradation of H_2O_2 catalysed by transition metal ions to form a carbonate radical $\bullet CO_3^-$. Various species (other than the luminol radical) are produced when luminol is oxidized by the $\bullet OH$ radical, as this radical is very reactive and reacts with several carbons on the aromatic ring of luminol (Xiao *et al.*, 2000). However, the $\bullet CO_3^-$ radical selectively reacts with luminol producing the luminol radical, which increases the CL efficiency by raising the steady-state concentration of the luminol radical (Xiao *et al.*, 2000).

As the oxidation of luminol to the luminol radical requires oxidizing agents, carboxylic acids (RCOOH) have been added. H_2O_2 can convert RCOOH (*e.g.* formic acid, as used by Doi *et al*. (2004)) into peroxy acids (RCOOOH), which are used as oxidizing agents. However, the CL detection is not selective. The CL signal produced may result from more than one cation being present, such as Cr(III,VI), Mn(II), Fe(II,III), Co(II), Ni(II) and Cu(II) (Obata *et al.,* 1993; Okamura *et al.,* 1998). Despite manipulation of the chemical reactions involved during the analysis, the interference of other metal elements may still need to be prevented and reduced, especially during the detection of low concentrations (picomolar–nanomolar) of manganese.

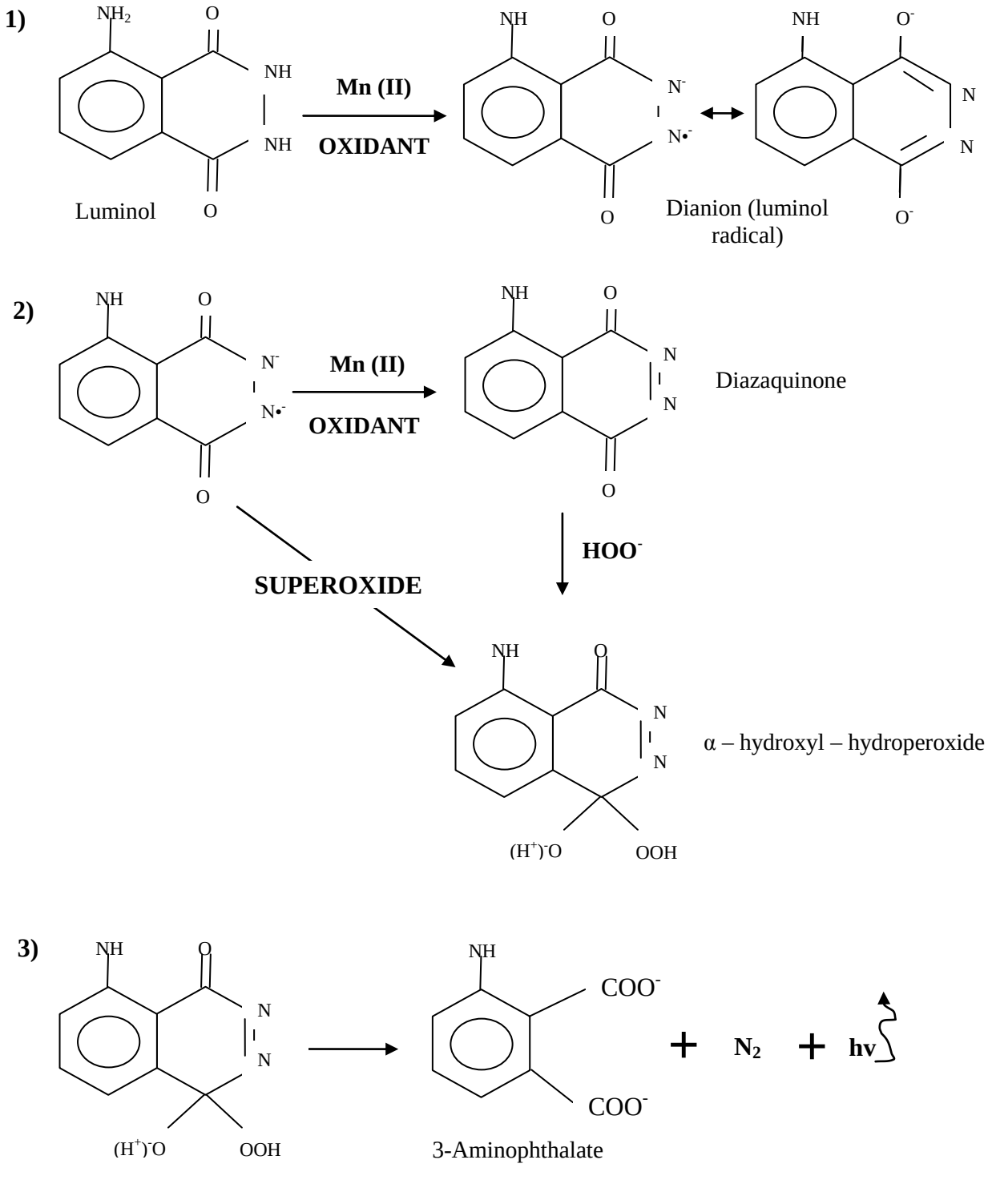

Figure III3. Three steps in the major pathway of the oxidation of luminol (after Rose and Waite, 2001).

5 Initial development of a Mn(II)-FIA-CL analyser to detect Mn(II) concentrations in seawater

Initially, a simple analyser to measure Mn(II) in MQ water was built in order to test the response from the photomultiplier tube and learn about the chemistry of the CL reaction. This first work on the analyser was undertaken in an open laboratory space without any particular precautions to avoid contamination, and used relatively high concentrations of manganese. This system was divided into two parts: **i)** the flow injection system including a peristaltic pump, an injection valve and an injection loop; and **ii)** the detection system including a flow cell, a photomultiplier tube, power supply, and a desktop computer for data acuisiition and control (Figure III4). Prior to a computer control system being available, the analyser was controlled manually. The buffered sample and the MQ water was changed manually to rinse the column. The injection valve was controlled by a two-position switching valve (valco system). Analyses were done using a new low-voltage photomultiplier tube (PMT) (H8443, Hamamatsu Photonics). This PMT had a separate power supply and the voltage signal was acquired through an electronic DAQ board (National Instruments DAQ-MX USB 6009). A Labview (version 7.1) virtual instrument (VI) was used to control the instrument and acquire and process data, and this VI was designed by Dr. Matt Mowlem (OED, NOCS). The PMT showed very good sensitivity to the CL reaction but also to ambient light. The high baseline (Figure III5) due to light entering the flow cell *via* the tubes and detected by the PMT was reduced by using black tubing to shield the PTFE tubing going to and from the flow cell.

Reagents (based on Doi *et al.* (2004)) – All solutions were prepared with deionized water (18 MΩ.cm) from a Milli-Q analytical reagent-grade water purification system (MQ water, Millipore). Luminol (Aldrich), TETA (Aldrich), formic acid (reagent grade, Merck), H_2O_2 (Suprapur, Merck), sodium carbonate (Na_2CO_3) (analytical reagent grade, Fisher Scientific), hydrochloric acid (SpA Romil), and ammonia solution (UpA Romil) were used without further purification. The carrier solution (eluent) was prepared by mixing 38.46 mL 0.1 M formic acid with 10 mL 0.1 M H_2O_2 and 13 mL 12 mM ammonia (pH~3 – ammonium formate buffer solution) and brought up to a final volume of 1 L with MQ water. A 0.06 mM luminol solution was prepared by diluting 600 µL luminol stock solution and 10 µL TETA in 1L MQ water. The luminol stock solution was prepared by diluting 270 mg 0.1M luminol and 500 mg 0.32 M Na_2CO_3 in 15mL MQ water. A 0.7 mM aqueous ammonia solution (208 mL) was diltued to 1L in MQ water, and used to adjust the CL reaction pH to ~10. MQ water was used as the cleaning solution to remove the residual sea-salt. A 1M HCl solution was prepared by diluting 86.20 mL 1M HCl to 1L, which was used to flush out any manganese residues in the manifold before and after daily analyses. A primary stock solution of 18.20 mM Mn(II) was prepared from a 1000 ppm Mn(II) standard solution (ASSURANCE certified reference material). 5 µM Mn(II) was prepared by diluting the primary stock solution in the

MQ water containing 50 µL borate buffer. Borate buffer was prepared by diluting 18.5 g boric acid and 27.7 g sodium borate in 1L MQ water.

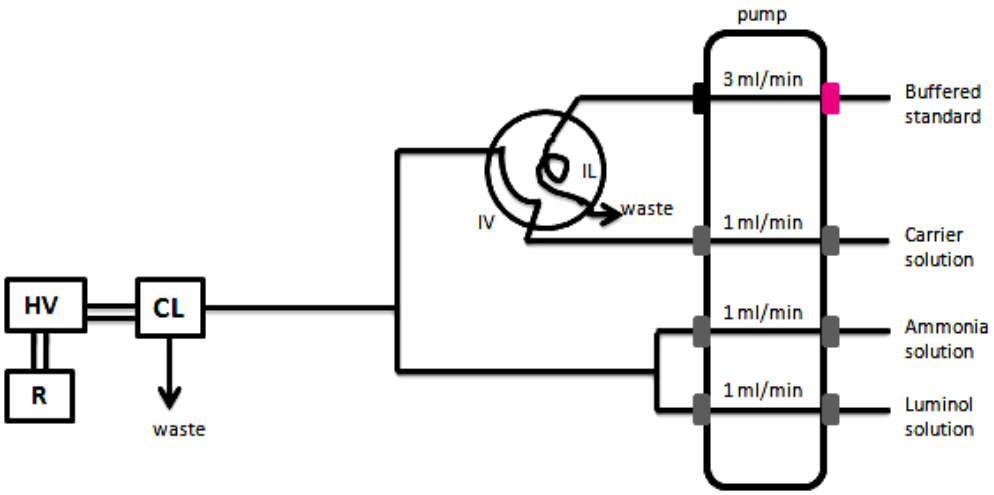

Figure III4. Schematic diagram of manual Mn-FIA-CL without any chelating resin. IL: injection loop; IV: injection valve; CL: a lab built flow cell and PMT, HV: power supply; R: recorder (desktop computer).

Procedure – The manifold set up is shown in Figure III4. The luminol and ammonia solutions were continuosly pumped during the analysis and went through the flow cell. When the injection valve was in the loading position, the buffered standard was pumped through the manifold, loaded in the injection loop, and excess solution went to waste. When the loop was filled, the valve was switched to elution position to allow the buffered standard solution in the loop to be carried by formic eluent carrier stream and mixed with the luminol and ammonia solutions, before entering the flow cell. The resultant stream passed through the flow cell coil of the PMT tube to allow the reaction to be completed and emitted light. The solution then went directly to waste.

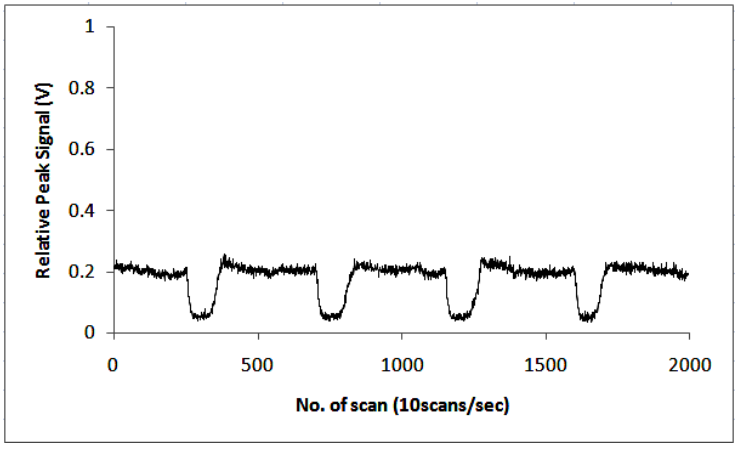

Figure III5. The high baseline due to light entering the flow cell *via* the tubes and detected by the PMT, thus reducing the peak CL signal.

5.1 Toyopearl AF-Chelate 650M resin to pre-concentrate dissolved manganese

Enhancement of the CL signal was observed when the pre-concentration resin column was added in the system (Doi *et al*., 2004). Pre-concentration of dissolved manganese is very important in this study as almost all seawater samples that would be analysed later are in nanomolar-picomolar concentrations. Thus, the commercially available Toyopearl AF-Chelate 650M resin (Tosohaas) (hereafter referred to as "Toyopearl") resin column was used to pre-concentrate manganese in this study (see earlier section). Packing the Toyopearl resin in the column was carried out very carefully in order to minimise the presence of the finest particles, which could lead to blockage, and backpressure problems. The resin was packed into a clear Perspex column (4.5 cm long, 2.0 mm i.d. and 10 mm o.d.; Figures III6). This column was fitted with two 3 mm diameter polyethylene frits at either end and when connected with flanged tubes and ¼" 28TPI fittings, this created a leak-proof unit. About 80 µL of Toyopearl resin was carefully pipetted into the column. Then, using a syringe, the supernatant was slowly removed and some more resin was added into the column until it was full. The seawater matrix may create interferences during the detection step and so a MQ rinsing step was included after passing the seawater sample through the Toyopearl column.

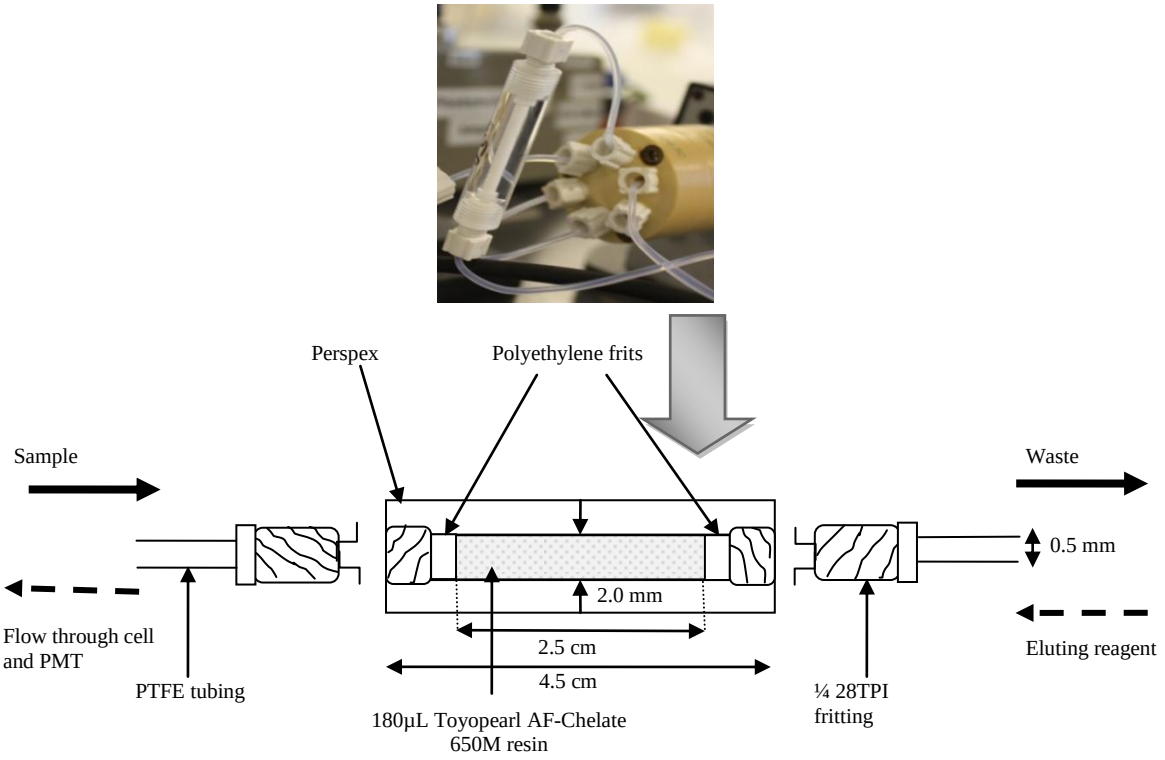

Figure III6. **Top**: Toyopearl AF-Chelate 650M resin column for pre-concentrating Mn(II) in seawater in the Mn-FIA-CL analyser. **Below**: Schematic diagram of the Toyopearl resin column. Solid arrows are in Position A (loading time), where Mn(II) ions are pre-concentrated onto the resin, and dash arrows are in Position B (elution time), where formic eluent are back-flushed the Mn(II) ions from the resin towards the flow cell and PMT.

5.2 Description and optimisation of the system

The analyser was controlled manually, where a solenoid valve was placed before the pump to switch between the buffered sample and the MQ water to rinse the column. The injection valve was changed for a 6-port injection valve, which was controlled by a National Instrument DAQ-MX USB 6009 card powered up when connected to the laptop. The desktop was changed for a laptop (Toshiba Satellite Pro). The injection loop was changed for a Toyopearl preconcentration column, as described above. The card also controlled the signal from the CL detector (a built-in flow cell and PMT).

Reagents – Most solutions were prepared as described above under section 5. However, based on the earlier experiments, luminol and Na_2CO_3 were very difficult to dissolve in MQ water even after shaking for more than 30 minutes. However, luminol seemed easier to dissolve in alkaline solution. For that reason, the luminol stock solution was prepared by diluting 500 mg 0.32 M Na_2CO_3 in 15mL MQ water, and after the Na_2CO_3 was dissolved, 270 mg 0.1M luminol was added into the solution; it took less than 10 minutes for the luminol to completely dissolve. The luminol-TETA solution was prepared as described earlier. The 18.20 mM Mn(II) primary stock solution was diluted to prepare nM Mn standard solutions; the final standards to be analysed were prepared in 25 mL MQ water containing 50 µL borate buffer (to get a pH~8.5).

Procedure - The luminol reagent was continuously pumped through the analyser and mixed with the eluent before the entrance of the flow cell. When the injection valve was in the load position (A, Figure III7 and Table III2), the buffered standard was first loaded onto the preconcentration column. The solenoid valve was switched to allow the resin to be rinsed with MQ water. The injection valve was then switched to the elution position (position B) and the eluted manganese was carried to the flow cell where it reacted with the luminol reagent. At the end of the elution step, the injection valve was switched back to position A to allow the preconcentration column to be rinsed with MQ water to remove any remaining acid. The solenoid valve was then switched to Position 1 to allow the standard to be loaded onto the column for a new cycle.

Table III2. Timing sequence of 3 minutes used with the Mn-FIA-CL analyser. Solenoid valves: Position 1 =sample (or standard); Position 2=Cleaning solution (MQ water). Injection Valve: Position A=Loading step; Position B =Eluting step.

Time	Solenoid valve position	Injection valve position	Process
60s	1	A	Loading Mn(II) onto the Toyopearl resin
30s	2	A	Rinsing column with MQ water
60s	2	B	Eluting Mn(II) from the Toyopearl resin
30s	2	A	Rinsing column with MQ water

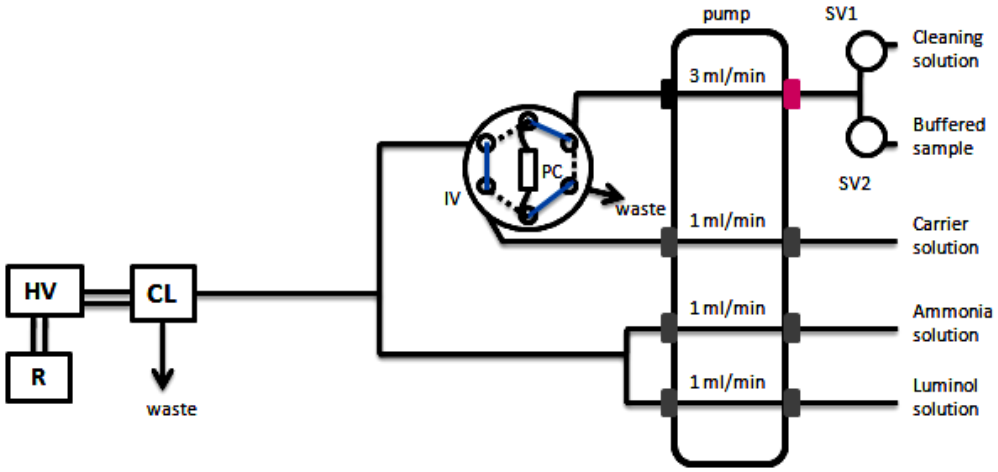

Figure III7. Schematic diagram of Mn-FIA-CL with preconcentration step. PC: preconcentration Toyopearl resin column; SV1 and SV2: solenoid valves; IV: injection valve; CL: a built-in flow cell and PMT, HV: power supply; R: recorder (laptop). Blue line is Position A (loading step) and dot line is Position B (eluting step).

During initial tests the baseline was high (Figure III8) and too unstable to allow detection of low-manganese concentrations, presumably because of low levels of manganese contamination of the reagents. It became clear that all reagents needed further purification.

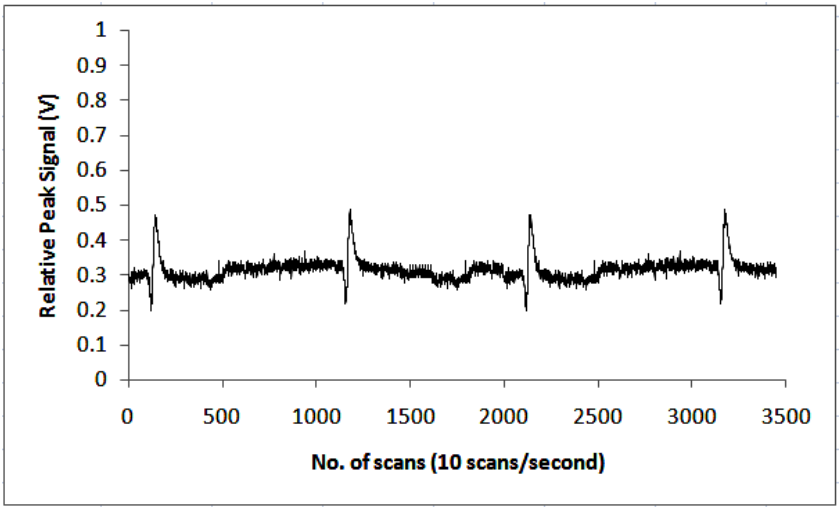

Figure III8. 20nM Mn(II) standard solution was analysed using the analyser in Figure III7. High and unstable baseline was detected during the initial tests, thus reducing the CL peak sensitivity.

5.2.1 Stabilisation of baseline

In order to enhance the sensitivity and stability of the CL reaction, several potential sources of contamination and their control were further examined. The tubing system was flushed for about an hour with 1M HCl before and after daily analysis, followed by rinsing with MQ

water. All reagent bottles, including seawater samples and Mn(II) standards, were placed on the clean laminar flow bench to prevent contamination from particles.

The luminol stock solution should be freshly made, stored in the dark and used within a week to degradation and to avoid particles from forming after dilution with the 0.32 M Na_2CO_3. Exposure to direct sunlight changed the colour of the solution from light and clear green ('new', freshly made) to dark green, after a week (Figure III9a). Using the 'old' luminol stock solution resulted in high and noisy baselines, shorter and broader CL peaks due to the reduced CL sensitivity. The luminol+TETA solution was made every day, and the solution bottle was placed in a dark tube (Figure III9b).

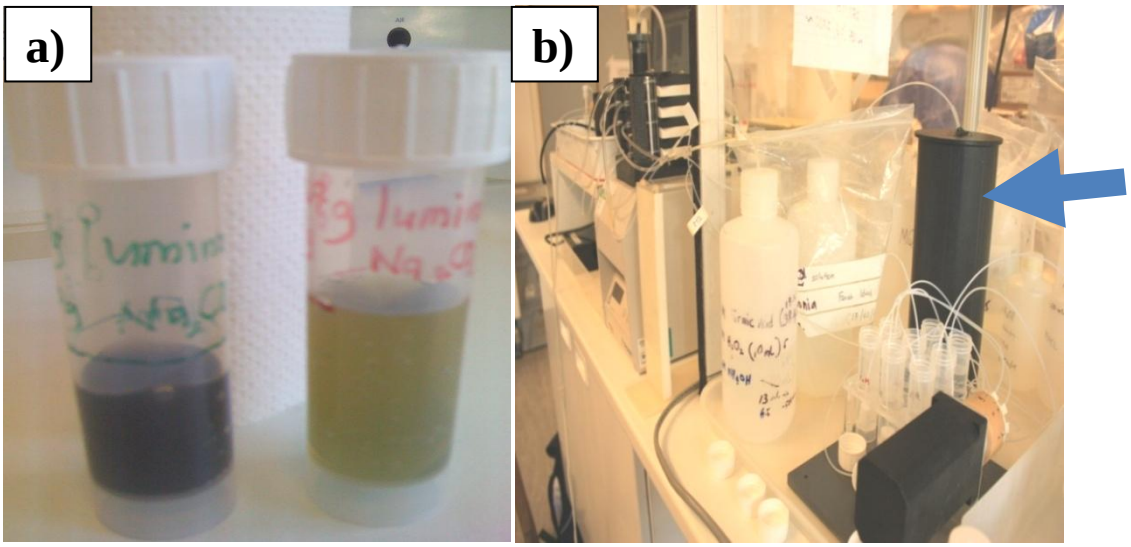

Figure III9. **a)** Light and clear green as in 'new' and freshly made luminol (right) turned to dark green of 'old' luminol (left) after prepared for more than a week, which using the 'old' luminol stock solution to make daily luminol solution caused significantly high and noisy baseline level, and yielded broader CL peak. **b)** Luminol+TETA solution bottle was placed in dark black tube (as pointed by the blue arrow) during the analysis to avoid oxidation of luminol.

The addition of formic acid to the H_2O_2 – NH_4OH solution produced excessive CO_2 bubbles in the solution (Xiao *et al.*, 2000), that created erratic shifts and instability in the baseline. To limit excessive bubble production in the manifold, the formic eluent was degassed using a vacuum pump (Figure III10) before every analysis, instead of using a heated water bath (Doi *et al.* (2004); Middag *et al.* (2011a,b).

Figure III10. Formic eluent was degassed before daily analysis to avoid the formation of excessive bubbles by using this vacuum pump.

As the CL reaction was not selective, interference by other metal elements could occur during the analysis, particularly Fe and Cu ions. This interference could be significantly reduced by adding a cleaning resin column(s) (*e.g.* nitrilotriacetic acid (NTA)) in the manifold to remove the Fe. Packing the cleaning resin in the Perspex column was carried out following the same technique explained in Section 5.1. Initially, the NTA resin was used in the system by placing after the Toyopearl resin column, and before entering the flow cell and PMT (Figure III11). The baseline level was reduced after the cleaning resin was added, thus lowering the blank and detection limit (Figure III12).

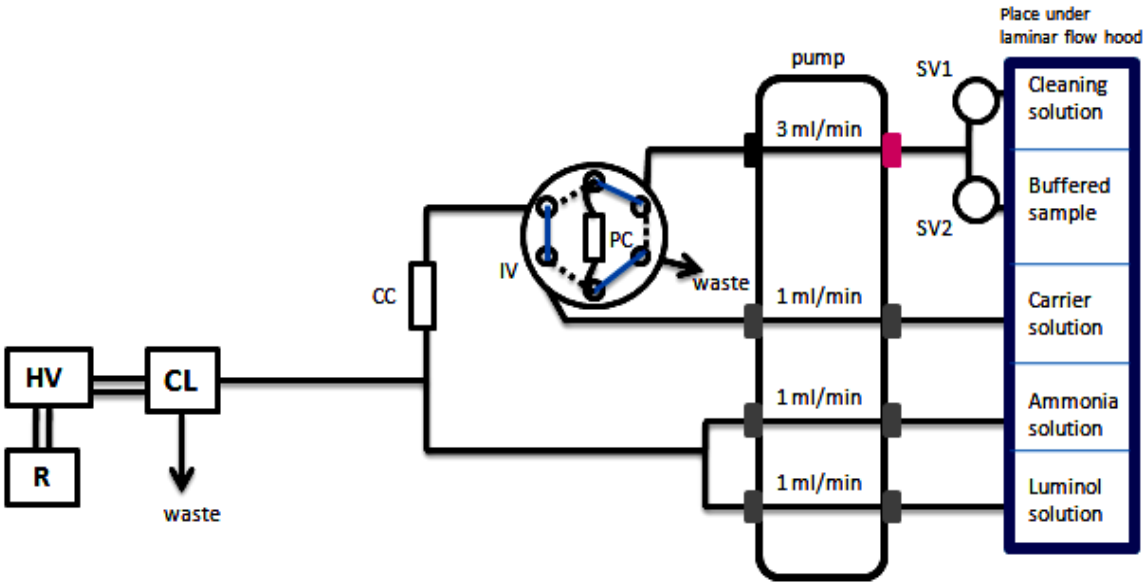

Figure III11. Schematic diagram of Mn-FIA-CL with preconcentration step and cleaning resin column. All reagents were placed under the laminar flow hood to prevent additional contamination from the airborne particles during the analysis. PC: preconcentration Toyopearl resin column; CC: cleaning resin column (NTA resin); SV1 and SV2: solenoid valves; IV: injection valve; CL: a built-in flow cell and PMT, HV: power supply; R: recorder (laptop). Blue line is Position A (loading step) and dot line is Position B (eluting step).

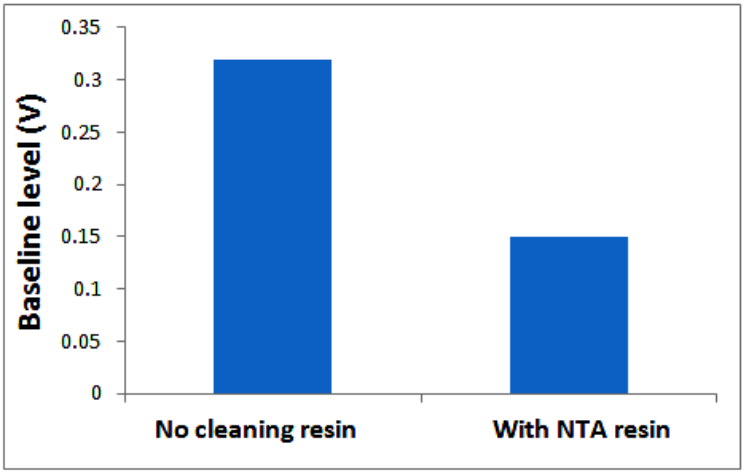

Figure III12. Baseline level without any cleaning resin (left) and with the NTA as a cleaning resin (right). The baseline level reduced from ~0.30 to ~0.15 V.

5.2.2 Enhancing CL peak signal - Mixing coil

To ensure a complete mixing of eluent and luminol solutions, a knotted mixing coil was used. It was very important to know the optimum length of this mixing coil for the CL reaction. The CL reaction with H_2O_2 is kinetically slow, and requires a long mixing time to enhance the reaction (Du *et al.*, 2001; Nedelec, 2006). According to Chapin *et al.* (1991), too little mixing resulted in higher background CL signals and increased the baseline noise, probably due to insufficient reagent mixing. Longer mixing coil length allowed for more complete oxidation of the H_2O_2 before it reacted with the Mn and consequently reduced sensitivity and wastes reagent. However, variables lengths are used in the literature, for example, 6.1 m (Okamura *et al.,* 1998), 10 m (Doi *et al.,* 2004; Obata *et al.,* 2007), 3m (Middag *et al.,* 2011a,b), and 6m (three 1m mixing coil, and one 3m reaction coil) (Aguilar-Islas *et al.,* 2006). A 1m mixing coil was initially tested and placed in the system before the PMT (Figure III13).

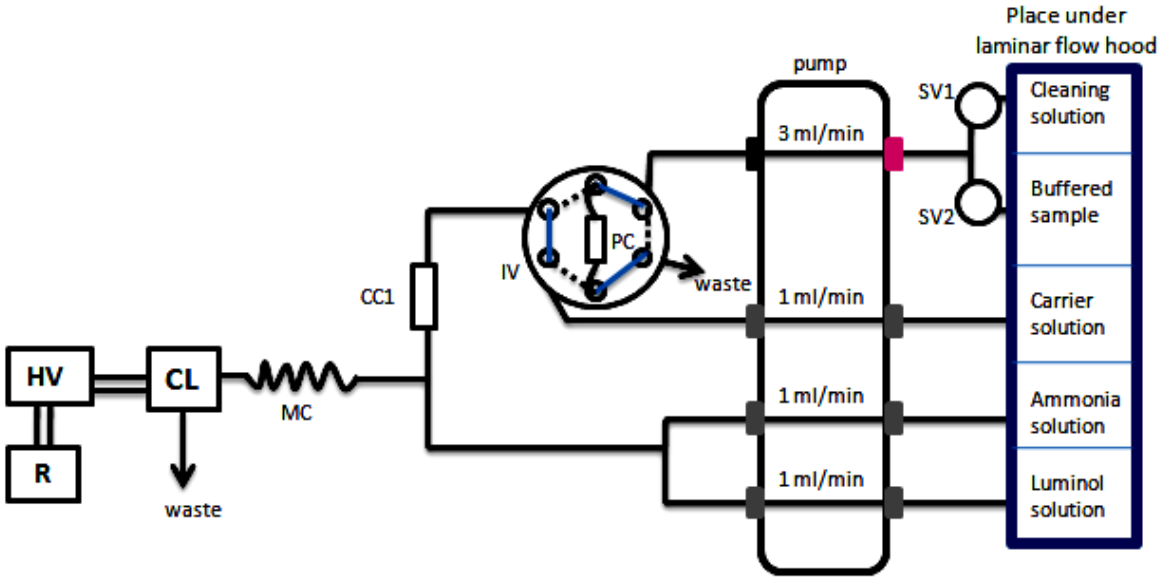

Figure III13. Schematic diagram of Mn-FIA-CL with preconcentration step, a cleaning resin column and 1m mixing coil. All reagents were placed under the laminar flow hood to prevent additional contamination from the airborne particles during the anaylysis. PC: preconcentration Toyopearl resin column; CC1: cleaning resin column (NTA resin); MC: 1m mixing coil; SV1 and SV2: solenoid valves; IV: injection valve; CL: a built-in flow cell and PMT, HV: power supply; R: recorder (laptop). Blue line is Position A (loading step) and dot line is Position B (eluting step).

High concentration of Mn(II) standards were analysed to test the analyser. A measurable CL peak signal was obtained with 40nM Mn(II) when a 1m mixing coil was placed in the system, as shown in Figure III14.

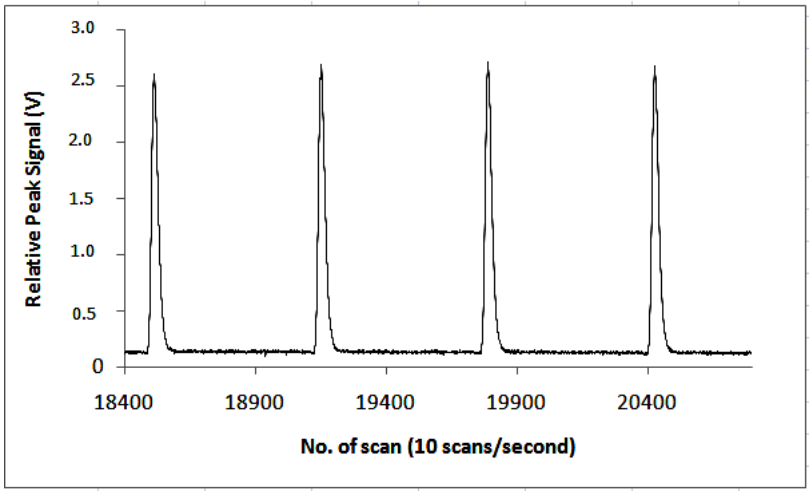

Figure III14. 40nM Mn(II) standard solution was analysed using the analyser in Figure III17. A measurable CL peak signal was obtained when 1m mixing coil was placed in the system.

5.2.3 Calibration with high concentration standards

Calibrations were carried out by standard additions to acidified (pH~1.7) filtered (0.2 µm) seawater. All standards were prepared in 25 mL seawater containing ~300 µL borate buffer

(to adjust the pH to ~8.5). MQ water was used as a reagent blank, and the pH of MQ water was also adjusted to ~8.5 by using 50 µL borate buffer. The timing sequences of the analyser were changed, as showed in Table III3.

Table III3. Timing sequence of 6 min used with the Mn-FIA-CL analyser. Solenoid valve: Position 1 =sample (or standard); Position 2=MQ water. Injection Valve: Position A=Loading step; Position B =Eluting step.

Time	Solenoid valve position	Injection valve position	Process
120s	1	A	Loading Mn(II) onto the Toyopearl resin
60s	2	A	Rinsing column with MQ water
120s	2	B	Eluting Mn(II) from the Toyopearl resin
60s	2	A	Rinsing column with MQ water

Both peak height and peak area were found to be linear functions of added Mn(II) in seawaters (Figure III15). Peak area was thus used for measurements in further method development and analytical work, since it resulted in less variability than the peak height.

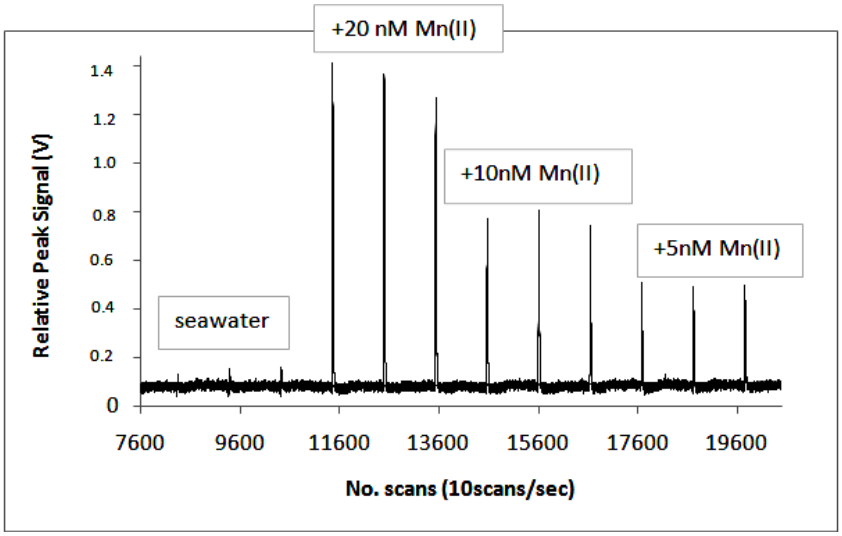

Figure III15. CL signals for calibration of high concentrations of Mn(II) standard additions. Slight variations occurred in the peak shape between replicates, but both peak height and peak area were found to be linear functions of added Mn(II) in seawaters.

5.3 Analytical Challenges and optimising the behaviour of the analyser

Extensive further work was undertaken to optimise conditions for the use of this version of the analyser to specifically enhance precision and the quality of calibration curves. This work included:

a) studying the impact of pH on uptake and elution from the Toyopearl resin, and on the CL reaction.

b) problems with peak shape and reproducibility
c) non linear calibrations

Major progress in the understanding of the FI-CL analyser for Mn was achieved through the extensive works carried out to optimise the system. Experiment were undertaken to improve performance of the system by focussing on precision and the calibration curve. Major improvements on precision were then made although the calibration remained poor. A significant number of experiments were carried out to try and to solve problems as they arose. To limit the length of the material presented here and for clarity, these results are presented classified relative to the problems encountered rather than chronologically. An overview of the main findings is given below.

5.3.1 Problem a: pH conditions

The CL reaction was dependent on the oxidation of luminol by H_2O_2 with manganese as a catalyst, as previously explained, and the CL efficiency was very dependent on the pH. The ideal pH for this reaction is ~10 as observed by Doi *et al*. (2004) and the optimum pH for manganese retention on the Toyopearl resin is ~8.6 (Aguilar-Islas *et al*., 2006). To obtain a final pH of ~10, it was important to adjust the pH of ammonia solution to be around 12 and the formic acid-hydrogen peroxide-ammonium hydroxide reagent pH to be around 3. Detailed studies were carried out to determine the pH effect **(1)** on the Mn(II) uptake onto the Toyopearl resin, **(2)** on the Mn(II) desorption from the Toypearl resin, and **(3)** on the CL signal reaction.

5.3.1.1 Adsorption of Mn(II) onto the Toyopearl AF-Chelate 650M resin

Previous studies showed that manganese in seawater was successfully quantitatively pre-concentrated on the Toyopearl AF-Chelate 650M resin at pH ranging from ~8.5 to 9 (8.8: Warnken *et al.,* 2000; 9.0: Beck *et al.,* 2002; 8.5: Aguilar-Islas *et al.,* 2006). To confirm the optimal pH conditions for pre-concentration, at which the resin collected Mn(II), low Mn acidified seawater (pH ~1.7) samples with the addition of 10 nM Mn(II) were examined. The seawater pH was adjusted to the desired pH (between 7.3 and 9.1) using ammonia solution.

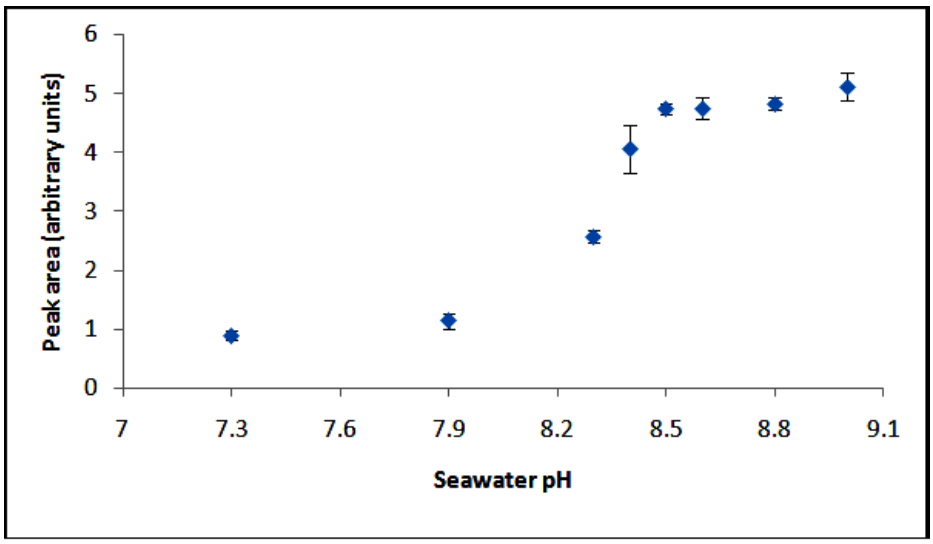

Figure III16.The relationship between seawater pH and peak area of Mn(II) concentration in seawater. 10 nM of Mn(II) concentration was added into every seawater vial. The Mn(II) was greatly adsorbed onto the Toyopearl resin at higher seawater pH (≥8.5). The pH of the formic eluent was 2.9, and the pH of the CL reaction was 10.2.

Figure III16 shows that the Mn(II) was more highly adsorbed onto the Toyopearl resin at higher seawater pH values (≥8.5). The optimal pH for collecting Mn on the Toyopearl AF-Chelate 650M resin was found to be between 8.5 and 9.0. The peak area (used in the study to show the amount of manganese present in the reaction) was not remarkably different at pHs between 8.5 and 9.0, as shown in Figure III16, giving some flexibility in the analysis. Warnken and co-workers (2000) found that at a higher pH (9.3) nickel was significantly adsorbed onto the Toyopearl resin, thus, increasing peak area at pH ≥9.0 probably due to nickel interference. Therefore, seawater samples were adjusted to pH ~8.5 by using the ammonia solution (Romil UpA) in this study, after considering that pH higher than 9.0 would have interference from nickel.

5.3.1.2 Elution of Mn(II) from the Toyopearl AF-Chelate 650M resin

The formic acid was preferable for eluting Mn^{2+} ions from the pre-concentration resin (*i.e.* Toyopearl). Formic acid can increase the CL signal efficiency by transferring the energy to the luminescing reagents. Furthermore, formic acid is a stronger acid than any other RCOOH (*e.g.* acetic acid) because the additional CH_3 group in RCOOH is an electron donor group, thus, the O–H bond is a bit stronger and less polar, hence, make it a weaker acid.

The formic eluent containing formic acid, H_2O_2, ammonia solution, and MQ water was prepared daily to elute Mn(II) from the Toyopearl AF-Chelate 650M resin. To optimize the pH conditions during the elution of Mn(II) from the Toyopearl AF-Chelate 650M resin, the relationship between the pH of the formic eluent and the peak area was investigated using seawater containing 10 nM of Mn(II). The formic eluent pH was adjusted from 2.4 to 3.3,

by passing through the Toyopearl resin. More Mn ions were eluted at pH2.9, resulted in higher peak area at this pH (Figure III17). The peak area decreased drastically in the pH more than 3. Therefore, pH 2.9 was chosen for formic eluent solution using in this study, in agreement with Doi *et al.* (2004).

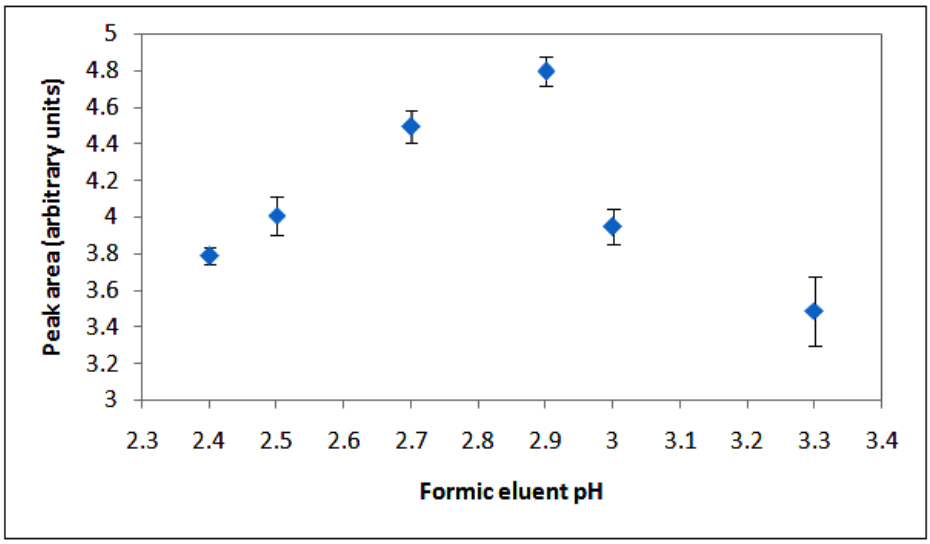

Figure III17. Effect of the formic eluent pH on desorption of the concentration of Mn (II) from the Toyopearl AF-Chelate 650M resin using the seawater sample containing 10 nM Mn(II) at pH 8.6 and the pH of the CL reaction was 10.2.

5.3.1.3 Optimal pH for chemiluminescence reaction

As discussed in the previous section, the luminol–H_2O_2–CL reaction is extremely dependent on the pH. O'Sullivan *et al.* (1995) found that the maximum CL intensity of seawater sample occurs at pH9.9. However, recent study by Doi *et al.* (2004) found that the maximum CL intensity occurs at pH10.2. Hence, it was necessary to conduct the reaction at the optimal pH values. The reaction pH was adjusted at a range of 9.8-10.7.

At pH values lower than 10, high baseline levels were observed together with a negative secondary peak during the rinsing step after Mn(II) was eluted from the Toyopearl resin. The decrease in CL signal at pH>10.3 matches the decrease in the fluorescence quantum yield of 3-aminophthalate. In seawater the maximum CL intensity occurs at pH~10.2 (Fig. III20), well before the decrease in the fluorescence quantum yield of 3-aminophthalate. The shift in the maximum in seawater is a result of precipitation of $Mg(OH)_2$ at pH>10.3. The precipitation of $Mg(OH)_2$ can suppress the CL intensity by scavenging of Mn(II) and/or by scattering of the CL emission. 20-30 µL of 0.7 M aqueous ammonium solution was used to adjust the pH to be 10.2 during the analysis. The mixing between 0.1 M formic eluent, 0.06 mM luminol solution and 0.7 M aqueous ammonium solution giving the maximum CL intensity at pH 10.2 (Figure III18) and agreed with Doi *et al.* (2004).

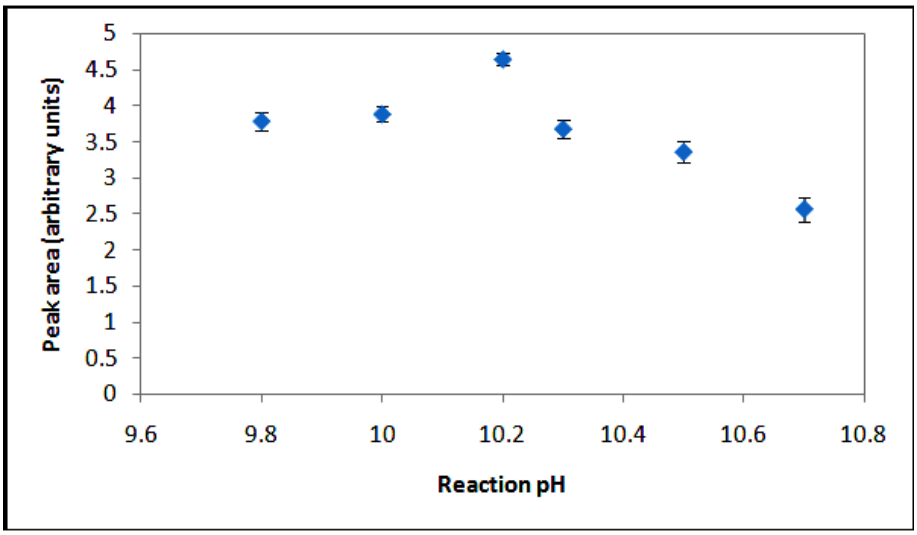

Figure III18. Effect of reaction pH on CL intensity. Conditions: sample: seawater containing 10 nM Mn(II) at pH 8.6; eluent: formic acid-ammonium formate buffer solution (pH 2.9) containing 0.1 M hydrogen peroxide; luminol, 0.06 mM; TETA, 0.075mM.

5.3.2 Problem b: double peaks and poor reproducibility

Problem of poor reproducibility and double peaks were identified when low Mn(II) concentrations (≤ 0.5 nM) in seawater samples (surface tropical North-Eastern Atlantic seawaters) were analysed (data see Chapter IV). There were several problems and limitation encountered (Figure III19):

1) Very small or no peak obtained – This reflected the low amount of Mn(II) concentrations presented in the seawater samples that reduced the sensitivity of the CL signal.
2) Negative peak formed before the CL peak - Negative peak(s) only obtained when low concentrations of Mn(II) in seawater samples or standards were analysed (≤0.5 nM). This negative peak was produced by the pH change of the elution solution sent into the PMT flow cell when a small amount of rinsing MQ water remained in the pre-concentration column and passed before the formic eluent.
3) Second peak appeared during the rinsing step when the valve changed position.
4) Bigger baseline noise made it difficult to distinguish between the peak and the baseline.

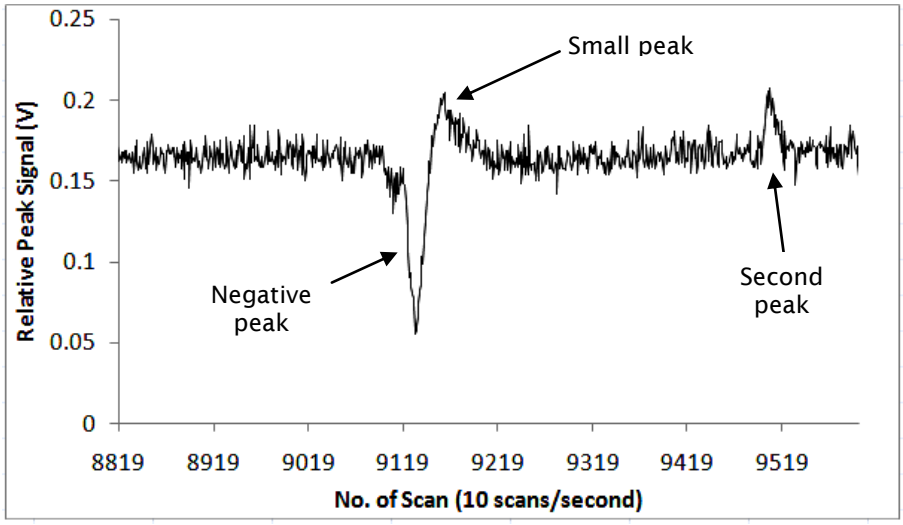

Figure III19. The enlarge peak of seawater sample with concentration of Mn(II) was ≤0.5 nM, with small peak, negative peak, and second peak observed.

Several components and parameters of the system which may influence reproducibility were thus tested, and their influence on precision was reported when possible. Almost all mechanical components of the system were tested to check for variations in their repetitive functioning. As flow is extremely important in FIA, thus, when issues arise with the FIA analyser, they were often related to flow. Flow issues are usually related to tubing. Air bubbles were observed in the standard/sample tubing when solenoid valves were changed between SV1 (cleaning solution (MQ water)) and SV2 (standard/sample). Thus, only one solenoid valve was used and one other valve were removed from the system (Figure III20). These modifications slightly improve the CL peak signal with the second peak disapeared.

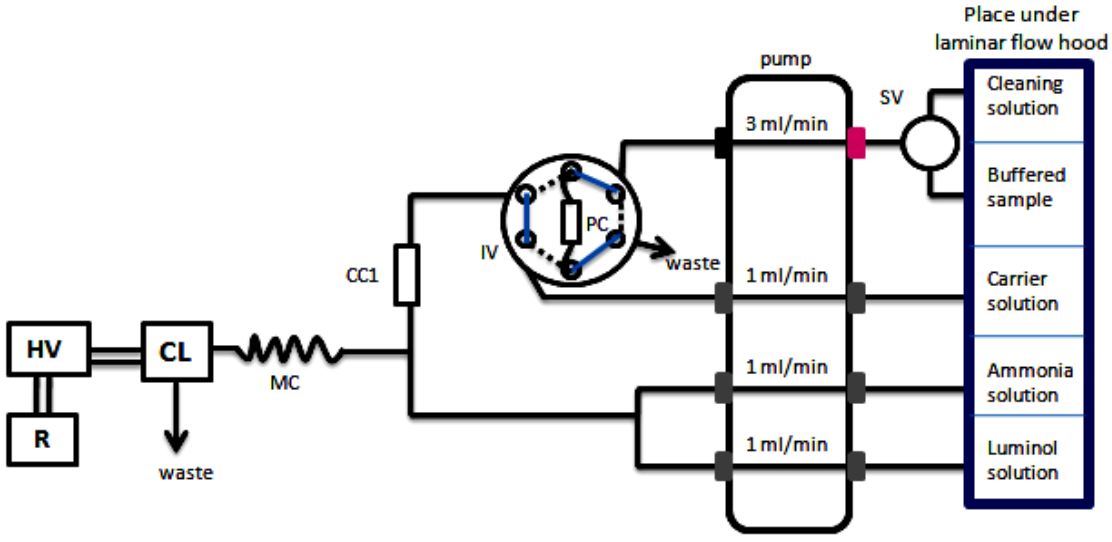

Figure III20. One solenoid valve (SV) was removed from the system to reduce air bubbles due to valve position changed.

Variations in the volume delivered by the pump with time were monitored. The peristaltic pump tubings were checked regularly to avoid becoming flattened after a long used, and

thus reducing the volume intakes. Variability in the pH of formic eluent, waste, and standard/sample would change the efficiency of the CL reaction. However, measurements of the pHs showed that there was no variation in the pH between replicate peaks during the detection step. These modifications did not result in any obvious improvement and negative peak was still appeared (data not shown).

Negative peaks that were obtained before the CL signal peak were due to changes in reaction pH particularly for samples/standards with low concentrations of Mn(II). A small volume of rinse solution (< 80 µL) was remained in the pre-concentration column after the rinsing step and was tranported downstream in front of the formic eluent, producing an area of higher pH in the sample stream. The localised zone of higher pH was above the optimal pH for the CL reation and produces a depression in the baseline signal prior to peak formation. However, when higher concentrations of Mn(II) sample was analysed, this signal depression was not significant as it was obscured by the shoulder of the CL peak. In other FI methods, this pH different has been overcame by increasing the acidity of the rinse solution with a weak acid for example acetic acid (Lohan *et al.,* 2005), but this was not a good option for this method, as acidic rinse solution would strip manganese off the pre-concentration resin column (Aguilar-Islas *et al.,* 2006). This signal depression (negative peak) might be minimised by reducing the baseline level (possibly closer to 0 V), and CL peak signal can be shifted upward.

The electronic noise and software crash during the analysis could enhance the baseline noises. To reduce the noise, the NI DAQ-MX card was frequently checked to ensure the electronic wirings were properly connected. The USB cable that connects the NI DAQ-MX card with the laptop was appropriately plugged. The unstable power supplied to the FIA instrument could stop the analyser which then automatically reset to the rinsing step. Therefore, the Earth wire and the electronic filter were attached to the power supply of the PMT to stabilise the power. However, these modifications did not completely solve the baseline noise problem. This problem seemed to reflect high power uses by other electrical appliances, such as refrigerator, freezer, and laminar flow system, which were plugged in series with the FIA instrument. Removing these appliances to other places solved the unstable power supply problem, thus reducing the baseline noises.

Given that most of the above experiments showed little improvement on CL peak signal, it was hypothesised that poor reproducibility was due to the shorter mixing coil length. Too little mixing reagent resulted in higher baseline level and noise, as observed by Chapin *et al.* (1991). This problem was investigated further as described in the next sections.

5.3.3 Problem c: Poor calibration

An additional problem was identified when attempting to calibrate the analyser, which seemed related to the issues of reproducibility and precision. Several calibrations using standard additions to different batches of acidified filtered seawater were carried out in the range of 0.5 to 4 nM. The problem was that calibration curves did not show positive curvature as expected (Figure III21). In almost all cases, the highest concentration of standard typically gave a lower signal than expected, resulting in a negative curvature curve.

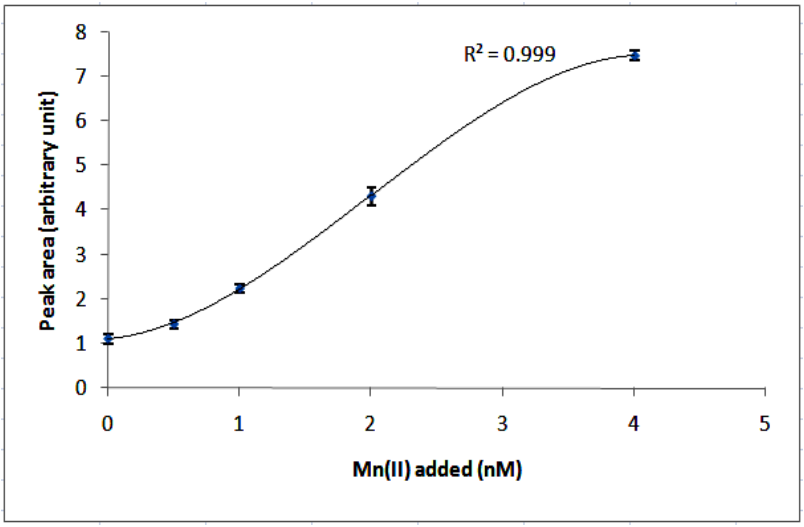

Figure III21. Calibration curve using standard additions of Mn(II) to acidified filtered deep (2000 m) seawater from the Tropical North-Eastern Atlantic Ocean ([Mn] = 0.6 nM). CL pH = 10.2, pre-concentration pH = 8.5 (pH of seawater was adjusted by using ~300 µL borate buffer), elution pH = 2.9. Values were not blank corrected. Curve fitted with a third degree polynomial trendline. Precision ranged between 1.3 – 9.0 % RSD (n = 3-5, average 5.3% RSD). The reagent blank (MQ water) value is 0.05±0.02 nM, lower that the detection limit (estimated at 0.06 nM, detection limit is three times of standard deviation of the blank).

Subsequent work was thus focussed on identifying the factor(s) leading to poor calibration of the analyser. Working reagents (luminol solution, formic eluent, ammonia solution) were checked to be as clean as possible, to avoid any contamination during reagents preparation and analysis. The response of the analyser to different Mn(II) concentration ranges was checked, and several parameters that influenced the response of the analyser during calibrations were tested (Table III4).

Table III4. Summary of the experiments carried out to investigate on the poor response of the Mn(II) FIA-CL during calibrations.

Calibrations with …	Slope of the linear fit (average)	n
Mn(II) standards range 0.5 – 4 nM	1.2 – 4.13 (2.52)	21
Concentrated standards range 5 – 40 nM	0.162 – 0.165 (0.163)	7

In order to test the response of the analyser at relatively high concentrations, several calibrations in the range 5 – 40 nM were carried out with acidified (pH~1.7) filtered (0.2 µm). The CL pH and loading pH were checked and adjusted to the optimum pHs of 10.2 and ~8.5, respectively. These curves were linear, with a precision for each point ranging from 0.6% rsd (relative standard deviation) for a 40 nM standard, and up to 22% rsd for seawater alone (Table III5).

Table III5. Figures of merit of four calibrations by Mn(II) standard additions in the range 5 to 40 nM to acidified filtered seawater collected during the *D326* cruise ([Mn(II)] ~ 0.6 nM). BDL = Below detection limit. Calibration were using a linear fitting curve.

Correlation for linear trendline (R^2)	Precision rsd (*n=4*) (average)	Detection Limit (nM)	Blank (nM) (n=4)
0.984	0.6 – 19% (7.9%)	0.06	0.09
0.993	0.5 – 22% (8.7%)	0.03	0.06
0.990	0.6 – 16% (6.9%)	0.09	BDL
0.976	0.6 – 22% (8.4%)	0.09	0.13

The response of the analyser at high Mn(II) concentrations were much more better over a wide range of Mn(II) concentrations (0 - 40 nM), with only a couple of the calibration did showing a slight of negative curvature at lower concentrations. These results suggest that at high concentrations the system is responding satisfactorily, and that the problem only affects low levels of manganese.

More calibration experiments were done where Mn(II) standards in the range of 0.5 – 4 nM (prepared by standard additions to acidified filtered seawater with ~300 µL of borate buffer as used before) were analysed in random order rather than in order of increasing manganese concentration as performed before, to test whether the negative curvature of the calibration was due to a technical feature of the system. The results showed negative curvatures were observed in all calibrations, infer that the negative curvature was not from the system, but may originated from a parameter likely not related to the standards.

Further experiments were carried out to investigate the effect that the quality of the borate buffer solution may have had on calibrations, to find out wether it may have been responsible for the negative curvature of calibration curves with the Mn(II) technique. Reagents were prepared as they were set up in their last stage of development (see Section 5.2) and two sets of standard additions (0.5 – 4 nM) to filtered seawaters were prepared: one set by using the borate buffer (~300 µL, as before) to adjust the pH to ~8.5, and the other set were prepared by using the 20 µM ammonia solution (≤30 µL) to adjust the pH to ~8.5; the pH was adjusted only when it was ready to analyse (~30 minutes before analysis). All conditions (*i.e.* reagents and standards concentrations, pHs, flow rates) were kept as

similar as possible between experiments, which were both performed in a single day. Calibration curves were slightly different as the calibration curve without borate buffer was linear while the calibration curve with borate buffer had a negative curvature (Figure III22). The signal for non-spiked seawater and +4nM Mn(II) in seawater were about similar for both experiments and then differed for additions of ≥0.5 nM. These results suggested that using ammonia solution to adjust the pH of the spiked seawaters was better than using borate buffer. More borate buffer added into the spiked seawater might also introduce contaminations into the spiked seawaters, and might have diluted the most concentrated standard.

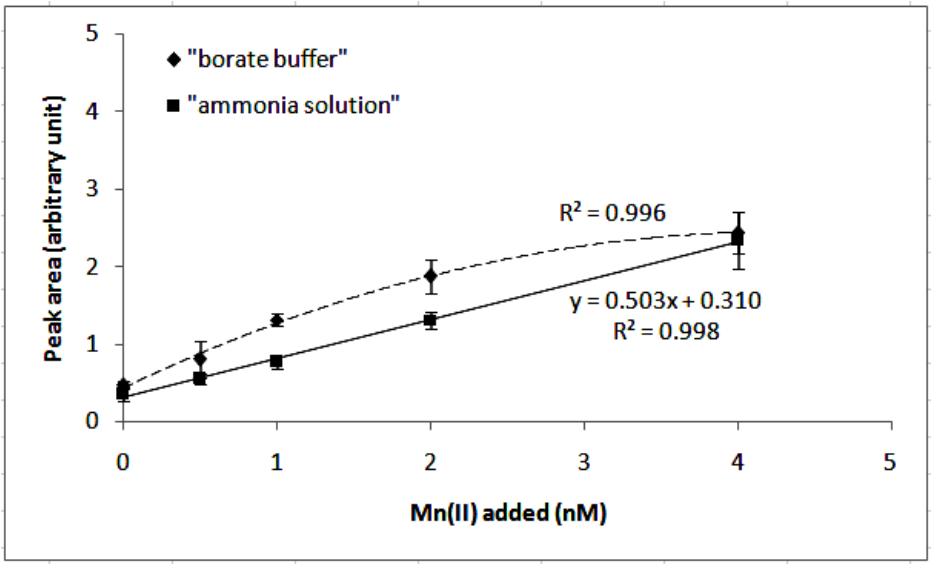

Figure III22. Comparison of calibrations carried out with the "borate buffer" or "ammonia solution" to adjust pH of standards. "Borate buffer" calibration fitted with a second-degree polynomial regression, while “ammonia solution” calibration fitted with a linear regression.

Based on these experiments, although borate buffer was used in the earlier tests to adjust the pH, it was not applied in the next analysis, because it required more borate buffer (≥300µL per 25 mL sample) to bring the pH of the acidified spiked seawaters up to~8.5. On the other hand, the earlier tests were done with MQ water, which only required 25 µL of borate buffer per 25 mL sample. Hence, it was easier to adjust the pH of acidified seawaters by using ammonia solution, as it only needed ~30 µL to get the pH~8.5, and it also could reduce the potential contamination from the buffer, particularly for the low concentrations standards. Additionally, the increases in CL peak signals in these experiments may also due to some manganese leaching from the vial walls as standards with “ammonia solution” were analysed first before standards with “borate buffer”. The most concentrated Mn(II) standard might also have been oxidised to Mn(III) before the analysis hence reducing their CL peak signals.

6. Standard Calibration

All calibrations were performed daily by standard additions from a 1000 mg/L manganese standard solution (ASSURANCE certified reference material) to 2000 m (0.2 μm filtered) Tropical North-Eastern Atlantic acidified (pH~1.7) seawater. A 5 point calibration line (0, +0.5, +1.0, +2.0, and +4.0 nM of Mn(II) standard additions) were made. The CL pH was checked at 10.2 and loading pH at 8.5. The concentrations of manganese in the seawater were calculated from the slope of the daily calibration curve obtained. The calibration gave linear curves in this range with varying sensitivity (Figure III23), depending on the loading time, ageing of the luminol reagent, and the quality of MQ water.

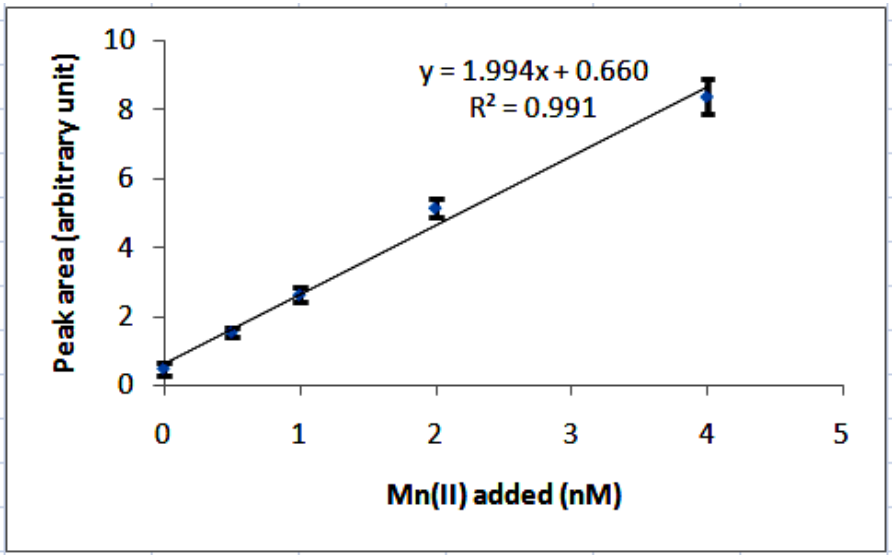

Figure III23. Example of calibration curve by standard additions to acidified (pH ~ 1.7) filtered (< 0.2 μm) surface seawater from the Atlantic Ocean ([DMn] = ~0.6 nM).

The loading time was modified from 120s to 200s in order to increase the sensitivity when low concentrations were expected for some samples. Precision of measurements of standards ranged from 0.05% to 15.75% rsd, averaging 4.15% rsd (n= 17) with a replicates of 3-4 peaks per standard. Precision averaged 4.15% rsd for a total of 180 samples analysed (n = 2-4 (depending on the CL signal peak)).

7. Figures of merit

The accuracy of this analyser was first tested by analysing certified reference material (CRM) obtained from National Research Council of Canada, CASS-4 standard. However, CASS-4 concentration was relatively high compared to the concentrations found during the analysis of seawater samples from the Tropical North-Eastern Atlantic in this study. Therefore, new reference seawater from a recent inter-comparison exercise for iron (Sampling and Analysis of Fe (SAFe)) were used. However, only the surface water sample (S 256) was detectable and deep water value was not. The reagent blank was determined by

measuring acidified (pH~1.7: the MQ water was acidified with ~5 µL 1M HCl (SpA Romil Pure Chemistry) approximately 30 minutes before the analysis) MQ water. The pH of acidified MQ water then was adjusted to pH~8.5 (with ~30 µL of 20 µM ammonia solution), like others standard additions in acidified seawaters, before been analysed as a blank. This blank represents potential manganese contamination from the reagents, column-conditioning solution, as well as the system manifold (tubing and valves). The average blank value for this analyser is 0.08 nM with a standard deviation of ± 0.02 nM, and hence gave a detection limit of 0.06 nM (three times of the standard deviation of the blank), which was higher than that reported by Doi *et al.* (2004). Figures of merit of these calibrations are summarised as ranges in Table III6.

Table III6. Ranges of figures of merit of 17 calibration curves. Calibrations were fitted with a linear trendline. *rsd* = relative standard deviation (*n* = 3-4). Detection limit (DL) defined as three times the standard deviation of the blank. BDL = below detection limit. Certified value of CASS-4 for Mn : 50.55 ± 3.45 nM. Consensus value of SAFe S 256 for Mn: 0.825± 0.079 nM.

Correlation, R^2 (mean)	Slope (mean)	Precision, *rsd* (mean)	Blank (nM) (mean)	DL (nM) (mean)	CRM±S.D (mean)
0.984 – 0.999 (0.993)	0.668 – 3.783 (1.926)	0.05 – 15.05% (4.15%)	BDL – 0.13 (0.08)	0.02 – 0.17 (0.06)	**CASS-4** 48.75 ± 0.17 51.39 ± 0.14 47.98 ± 0.19 (49.37 ± 0.16) **SAFe S256** 0.80 ± 0.08 0.81 ± 0.06 0.77 ± 0.05 (0.79 ± 0.06)

The sensitivity slightly fluctuated most probably because of changes in analytical conditions such as the small variations in the ageing of the luminol reagent. Values of the blank, detection limit, CASS-4 certified seawater material and SAFe seawater (http://es.ucsc.edu/~kbruland/GeotracesSaFe/SAFe%20ReferenceSample-Mn.pdf) were often a bit low, and may have been under-estimated because of poorer quality of MQ water and/or baseline instability. However, the agreement between results obtained from this study and certified and consensus values were still good and acceptable.

The Mn(II)-FIA-CL analyser system with a 1m mixing coil was subsequently used to analyse surface (~1m) samples collected from the Tropical North-Eastern Atlantic Ocean. Data on Mn(II) analysed with this technique are reported in Appendix 3, and further discussed in Chapter V. Analyses having poor quality CL peaks and/or high and unstable baselines were repeated with freshly prepared reagents.

As an important aim of this project was to analyse samples collected during the CROZEX cruises in the Southern Ocean [SO], the developed technique was initially applied to several of these SO samples. However it proved difficult to get a measurable CL peak signal due to the extremely low Mn(II) concentration, and simply increasing the column collection time did not seem to help of the overall quality of data. It was therefore decided to move on by further modifying the Mn(II)-FIA-CL technique to make it appropriate for these SO samples.

8. Development of a high sensitivity automated Mn(II)-FIA-CL analyser to detect Mn(II) concentrations in seawater

8.1 Description and optimisation of the modified automated analyser

The modified system was based on the instrument described above. One innovation was the inclusion of an automated sampler system. The analyser was able to analyse 8 individual samples/standards solutions automatically through a computer control system. An 8-port single output valve was placed before the pump to switch between the individual samples/standards (Figure III24). The use of the auto-sampler reduced the sample handling times and the potential of contamination during handling.

Reagents - Reagents essentially as used in the previous version. The only differences were the used of high purity ammonia (see *Monthly Preparation* below for the preparation of the ammonia solution)).

Daily preparation - The carrier solution (formic eluent) was prepared by mixing 38.46 mL 0.1 M formic acid with 10 mL 0.1 M H_2O_2 and 13 mL 12 mM aqueous ammonia (pH 2.9), and made up until 1 L with MQ water. 0.06 mM of luminol solution was daily made by diluting 600 μL luminol stock solution and 10 μL TETA in 1L MQ water (see Section 5.2.1). A 208 mL of 0.7 mM aqueous ammonia solution was diluted to 1L with MQ water to adjust the CL reaction pH to 10.2. MQ water (pH~7) was used as the cleaning solution to remove the residual sea-salt on column.

Weekly preparation - The luminol stock solution was made by diluting 500mg of 0.32M Na_2CO_3 in 15 mL MQ water, then 270mg of 0.1M luminol diluted in the Na_2CO_3 solution. 86.20 mL 1M hydrochloric acid was made up until 1L with MQ water to flush and remove any manganese residue in the FIA system every day before and after the analyses.

Monthly preparation - High purity ammonia solution was made by bubbling high purity ammonia gas through sub-boiling distilled water (S.B) / MQ water as described in Appendix 1 (courtesy of Prof. Peter Statham and Mr. Brian Dickie).

Procedure - The luminol reagent and the 0.7M ammonia solution were continuously pumped through the analyser and were mixed with the formic eluent just before the PMT flow cell. When the injection valve was in loading position (position A, Figure III26 and Table III7), the buffered standard/sample was first loaded onto the preconcentration resin column. The solenoid valve was switched to allow the resin to be rinsed with MQ water. The injection valve was then switched to the elution position (position B) to allow the formic eluent to go through the preconcentration column and eluted manganese which was carried to the flow cell where it reacted with the luminol reagent. At the end of the elution step, the injection valve was switched back to position A to allow the preconcentration column to be rinsed with MQ water to remove any remaining acid. The solenoid valve was then switched to Position 1 to allow the buffered standard/sample to be loaded onto the column for a new cycle.

Table III7. Timing sequence of ~9 minutes used with the Mn-FIA-CL analyser. Solenoid valves: Position 1 =sample (or standard); Position 2=Cleaning solution (MQ water). Injection Valve: Position A=Loading step; Position B =Eluting step.

Time	Solenoid valve position	Injection valve position	Process
200s	1	A	Loading Mn(II) onto the Toyopearl resin
60s	2	A	Rinsing column with MQ water
200s	2	B	Eluting Mn(II) from the Toyopearl resin
60s	2	A	Rinsing column with MQ water

8.1.1 Baseline level

In the previous analysis, the baseline level was reduced significantly when the NTA resin column was added as a cleaning resin column in the system, thus lowering the blank and detection limits. The effect of the cleaning resin addition was shown in Figure III14 of the previous Section, where the baseline level reduced from ~0.30 to ~0.15 V. This infers that the formic eluent, which contained formic acid, H_2O_2, ammonia solution, and MQ water, has the largest contribution to the baseline level. However, the baseline level of ~0.15V was still relatively higher particularly for relatively lower concentrations of Mn(II) samples. Therefore, when another cleaning resin of the 8-HQ resin column was placed in the system after the luminol reagent solution (luminol+TETA+Na_2CO_3, pH~8.8) (Figure III24), the baseline level was further reduced to ≤0.10V (Figure III25).

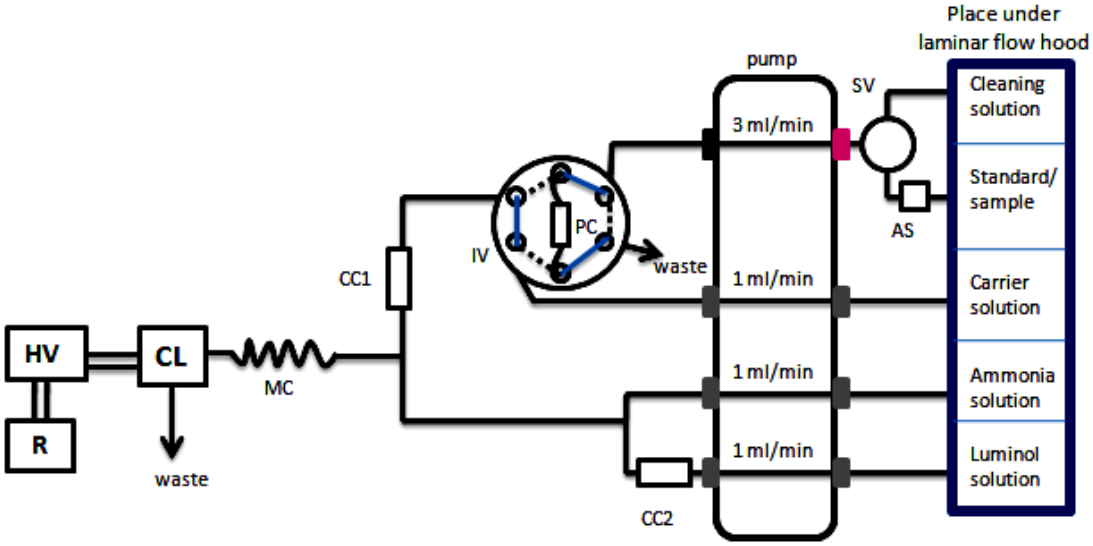

Figure III24. Schematic diagram of Mn(II)-FIA-CL with preconcentration step and two cleaning resin columns. All reagents were placed under the laminar flow hood to prevent additional contamination from the airborne particles during the anaylysis. PC: preconcentration Toyopearl resin column; CC1: first cleaning resin column (NTA resin); CC2: second cleaning resin column (8-HQ resin); SV: solenoid valve; AS: auto-sampler; IV: injection valve; CL: a built-in flow cell and PMT, HV: power supply; R: recorder (laptop). Blue line is Position A (loading step) and dot line is Position B (eluting step).

This second cleaning resin column (CC2) removed other trace metals from the impurities of the TETA, which was not guaranteed to be a clean solution (Nakayama *et al.*, 1989; Doi *et al.*, 2004). In the literature, TETA was recrystallized from a solution of methanol and HCl before been used in the analysis (Nakayama *et al.,* 1989; Doi *et al.,* 2004; Middag *et al.,* 2011a, b). However, Nedelec (2006) was purified the luminol reagent through Chelex-100 resin and 8-HQ resin columns to remove other trace metals, resulted in lower baseline level. This second cleaning resin column could also remove any undissolved particles of Na_2CO_3 that was used to prepare the luminol reagent solution. However, the undissolved particles of Na_2CO_3 could cause backpressure problems. To avoid backpressure problems, the second cleaning resin column was filled half-full, and was turned upside-down and flushed with HCl to remove any clogged particles, before and after the daily analysis.

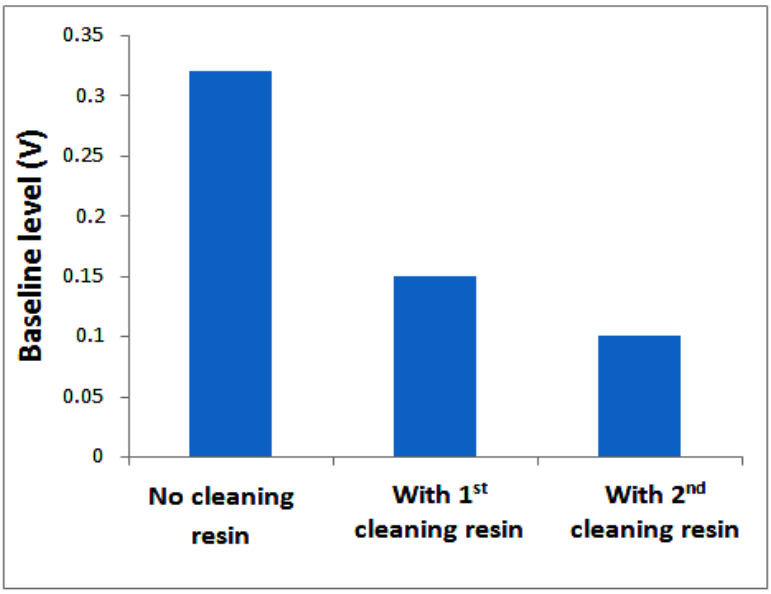

Figure III25. Baseline level was reduced from ~0.30 to ~0.15 V when the first cleaning resin column (NTA resin) was placed after the preconcentration Toyopearl resin column. When the second 8-HQ resin column was placed in the system, the baseline level was further reduced to ~0.10V.

8.1.2 Mixing coil

As discussed in the previous Section, it is very important to get the correct length of mixing coil, due to its influence on the formation of the CL signal. Although a short mixing coil length is believed to be good in controlling the physical dispersion, it is also important to ensure that the chemical reaction (*i.e.* CL reaction with H_2O_2) is also completed. The CL reaction with H_2O_2 is kinectically slow, and become even slower when there is a lack of Mn(II) ion as a catalyst. In the previous Section, a 1m mixing coil was used in the analyser to measure the relatively high concentrations of Mn(II) in surface seawater samples from Tropical North-Eastern Atlantic Ocean, and measurable CL peak signals were produced. However, the length may have been insufficient to ensure a complete CL reaction with H_2O_2, with a lack of Mn(II) ions to act as catalyst in certain seawater samples especially from the CROZEX cruises. Most work in the literatures used more than 1m mixing coil length (*e.g.* Doi *et al.*, 2004; Du *et al.,* 2001; Nedelec *et al.,* 2006, Middag *et al.,* 2011a, b). In addition, Chapin *et al.* (1991) stated that too little mixing resulted in higher baseline signal and noises probably due to insufficient reagent mixing. Therefore, further experiments were carried out to examine the relationship between the length of mixing coil and the CL peak signal. Four lengths (5 cm (straight and unknotted coil), 1m, 3m, and 4m) of the mixing coils were examined for peak area and peak height by using 1 nM Mn(II) standard addition in acidified seawater, by using the system set up in Figure III24. Reagents and experimental procedures were followed as in Section 6.1.

In order to test the response of the analyser for these experiments, calibrations in a range of 0.5 – 4 nM (prepared by standard additions to acidified filtered seawater with ~30 µL of 20 µM ammonia solution to adjust the pH to be around 8.5) were carried out for each

mixing coil length, before 1 nM Mn(II) standard addition in acidified seawater was later analysed. The CL pH was checked and adjusted to the optimum pH of 10.2. Reagents were prepared as they were set up previously (see Section 5.2). All other conditions (*i.e.* reagents and standards concentrations, pHs, flow rates) were kept as similar as possible between experiments, which were performed in a single day. Figures of merit for these calibrations with 1m, 3m, and 4m mixing coils were summarised in Table III8.

Table III8. Figures of merit of calibrations by Mn(II) standard additions in the range of 0.5 – 4.0 nM to acidified filtered seawaters ([Mn(II)] = ~0.6 nM) with 1m, 3m, and 4m mixing coils. BDL = Below detection limit. S.D.: standard deviation. D.L.: detection limit (3x of the S.D. of the blank). Calibrations were using a linear fitting curve.

Standard addition	**Precision, % rsd (mean)**		
	1m	3m	4m
Seawater	1.3 – 12.3 (8.4)	1.0 – 4.1 (3.1)	0.9 – 3.5 (2.6)
Seawater+0.5 nM	3.5 – 22.2 (14.7)	0.7 – 5.5 (3.0)	0.2 – 7.7 (5.2)
Seawater+1.0 nM	0.3 – 12.9 (8.6)	0.6 – 9.5 (5.1)	0.5 – 7.3 (2.8)
Seawater+2.0 nM	0.8 – 11.0 (3.9)	0.9 – 8.6 (4.9)	2.1 – 8.7 (6.5)
Seawater+4.0 nM	0.9 – 12.4 (4.1)	0.6 – 12.5 (4.0)	1.3 – 5.6 (2.8)
Correlation, R^2 (mean) n=4	0.981 – 0.991 (0.988)	0.993 – 0.999 (0.997)	0.981 – 0.997 (0.990)
Average blank±S.D. nM n=4	0.088 (BDL) ± 0.03	0.143 ± 0.024	0.31 ± 0.10
Average D.L. nM	0.09	0.07	0.30

The peak height increased from 1m to 3m knotted mixing coils, and after reaching its steady state (the steady state was reached when there was no more peak height increase after the steady state; 3m was assumed as a steady state), no further increase was observed with 4m knotted mixing coil (Figure III26). The baseline levels for 3m and 4m coil were reasonably low. However, there was no CL signal peak and higher baseline level recorded for the shortest coil (5 cm) (data not presented), suggesting too little or almost no H_2O_2 oxidation reaction occurred due to the shorter length and lack of chemical mixing.

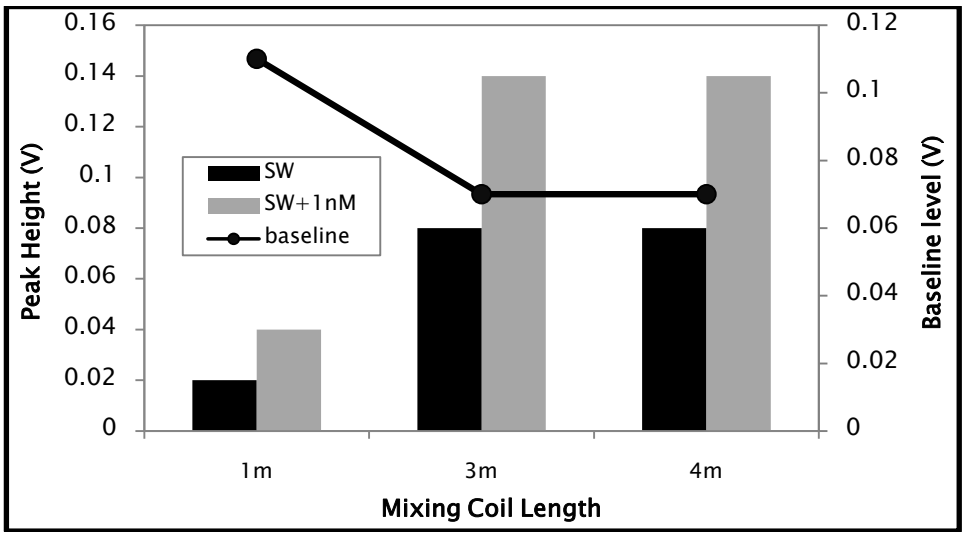

Figure III26. Effects of the length of mixing coil on the peak height and on the baseline level for seawater with no standard addition and seawater+1nM Mn (II) standard solution. The black close circle and line is the baseline level for both seawater and seawater+1nM Mn(II).

However, regarding the peak area value, it was observed that the 4 m coil signal was enhanced significantly compared to the 3 m coil (Figure III27). In other words, the analytical peaks produced from the 4m coil technique became broader as the dispersion coefficient increased. As a result, the peak area values were also increased. Another possible reason for the increasing peak area was the interference of other trace metals, which could emit light after a longer mixing period.

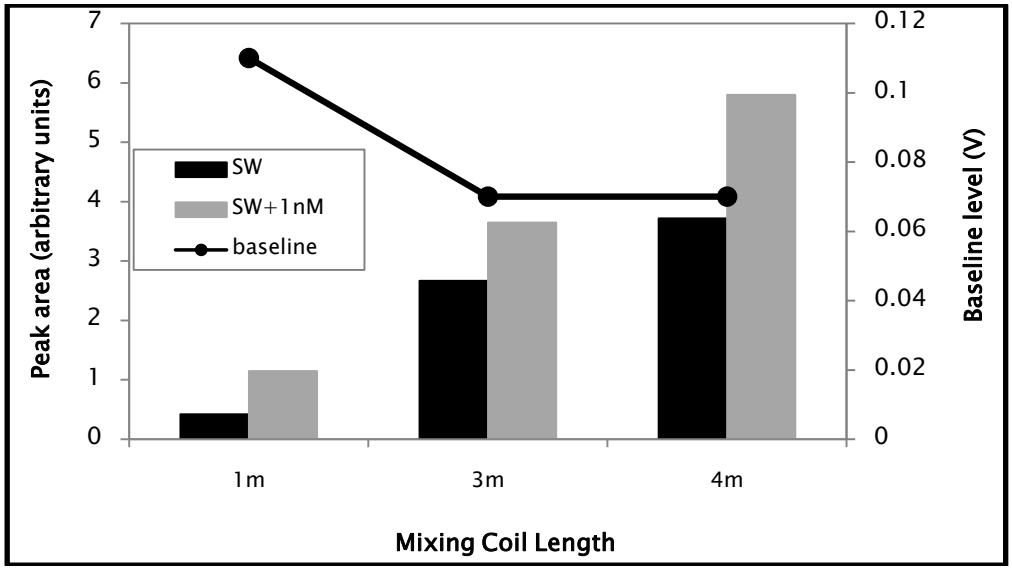

Figure III27. Effects of the length of mixing coil on the peak area and on the baseline level for seawater with no standard addition and seawater + 1 nM Mn (II) standard solution. The black close circle and line is the baseline level for both seawater and seawater+1nM Mn(II).

In addition, the signal depression (negative CL signal peak) obtained with 1m mixing coil was minimised as the baseline level was further reduced in the longer mixing coils, which the CL signal peak then was shifted upward and produced a better CL signal peak, as

shown in Figure III28. These advantages were overall reflected in increased CL sensitivity. Therefore, a 3m mixing coil was presumed to be the optimum mixing coil length in this study and thus was applied in the analysis of Mn(II) in seawater from around the Crozet Islands of the Southern Ocean.

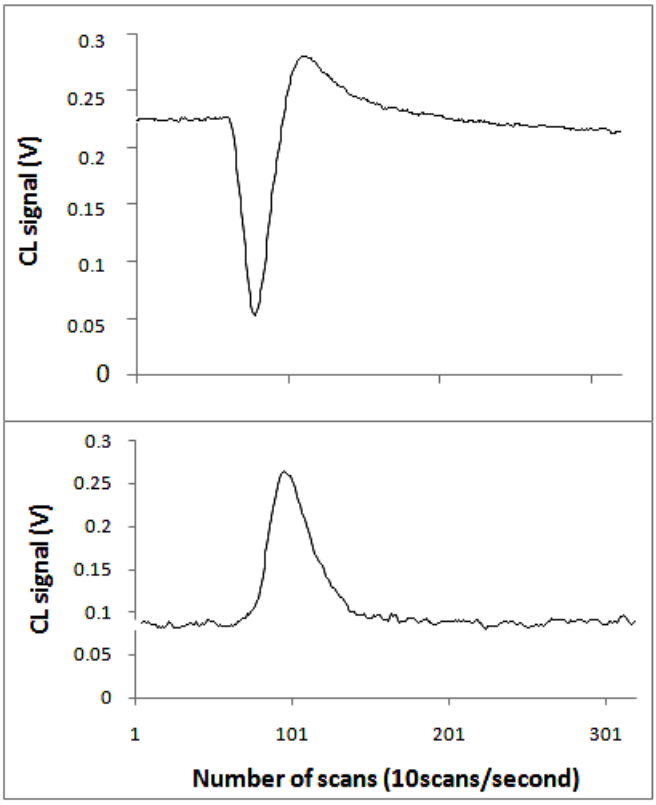

Figure III28. The effects of the mixing coil length of **(above)** 1m and **(down)** 3m on the peak height, negative peak, and baseline level. The higher baseline level in the experiment using 1m mixing coil was minimised when 3m mixing coil was used in the experiment, and thus shifted upward the CL signal peak, producing a better CL signal peak with no negative peak.

Apart from the mixing coil length, other variables, for examples H_2O_2 concentration, TETA concentration, and pre-concentration time, was also tested to investigate their effects on the CL signal peaks.

8.1.3 H_2O_2 concentration

An increase in H_2O_2 concentration theoretically leads to an increase of the CL signal. In order to test this, the concentration (0.1M) of H_2O_2 used in preparing the daily reagent that was originally used by Doi *et al.* (2004), which was applied in this study, was doubled up (to 0.2M). Other variables such as 3m mixing coil, luminol solution, pHs, pump rate and speed, remained unchanged (Figure III24), following the procedures (reagents preparations and experimental procedures) explained in Section 6.1. Later, acidified (pH~2) MQ water, acidified (pH~1.7) seawater, and acidified seawater+1 nM Mn(II) standard addition were analysed in this experiment. But, before the experiment started, all pHs for MQ water,

seawater, and seawater+1 nM Mn(II), were adjusted to pH~8.5 (the optimum pH for pre-concentration of Mn(II) onto the Toyopearl resin).

Based on this experiment, the higher and narrower CL signal peaks were observed for seawater and seawater+1 nM Mn(II) standard addition (Figure III29) compared to the results obtained in Section 8.1.2 (with 3m mixing coil), and no positive peak was observed for MQ water. The higher CL signal peaks obtained here is as a result of increased the existence of the radical ·OH from the H_2O_2 decomposition. More ·OH then enhanced more oxidation of luminol with manganese acting as a catalyst to speed up the reaction. More amount of 3-aminophthalate produced in the excited states which then emitted more light when going to the ground states. However, as H_2O_2 was added in the carrier solution (formic eluent), which was continuously mixed with ammonia and luminol solutions to produce the baseline, it also increased the baseline level, due to any metal contaminants that passed through the flow cell and PMT could also acted as a catalyst in the oxidation of luminol process, particularly if the MQ waters used in the preparation of the reagents were not of good quality.

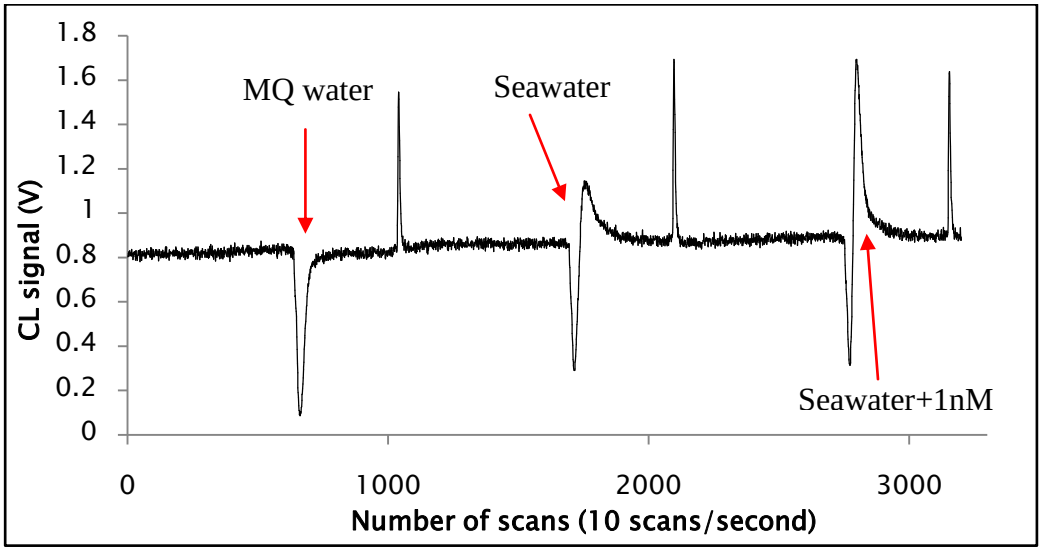

Figure III29. Elution profile for a MQ water, seawater, and seawater+1nM Mn(II) standard addition with 0.2 M concentration of H_2O_2. The peaks were enhanced, as well as the baseline level. The second peak appeared during the washing step was bigger than the CL peak signal.

Increasing the concentration of H_2O_2 in this experiment produced negative peaks (Figure III29), which appeared before the CL signal, due to the huge differences in viscosity or chemical composition between samples and carrier solution. The positive and negative peaks ratio for seawater is 0.6, and for seawater+1nM Mn(II) is 1.6. Surprisingly, there was a second peak that appeared uniformly during the rinsing step with no specific reason. Due to the time constraint, it was not possible to investigate the reason(s) for the second and the huge negative peaks that appeared in this experiment. Therefore, the

concentration of H_2O_2 was decided to remain unchanged (0.1M), as been used in Doi *et al.* (2004) work.

8.1.4 TETA concentration

TETA was added into the luminol solution which then mixed with formic eluent that carried Mn(II) ions and afterwards emitted light. Decomposition of H_2O_2 is more efficient with added TETA, as explained earlier in this Chapter. Several experiments were carried out to investigate the effect of TETA on the CL signal. The concentration of TETA was doubled up (from 0.06 mM (Doi *et al.,* 2004) to 0.12 mM). Other variables (*e.g.* 3m mixing coil, preparation of reagents, pHs, pump rate and speed) were remained unchanged as been explained in Section 8.1 of this Chapter. Two sets of daily standard addition into the seawater solutions (range between 0.5 and 4.0 nM, pH adjusted to ~8.5) were analysed with **(1)** luminol solution containing 0.06mM TETA, and with **(2)** luminol solution containing 0.12 mM TETA. Based on these experiments, increasing the concentration of TETA solution to 0.12 mM did not result in any increased sensitivity (data not shown), so it was decided to maintain the use of the lower concentration (0.06 mM). However, TETA must not be added together with solution containing H_2O_2 because decomposition of H_2O_2 would occur extremely rapid by before it mixed with luminol and Mn(II) ions. Added TETA in the reagent solution containing H_2O_2 gave worse background noises and the baseline level was increased erratically, hence made the analysis of Mn(II) impossible (Figure III30). Therefore, TETA was best to be added into the luminol solution, and the concentration of TETA was kept to a minimum (0.06 mM) to reduce the background noise whilst still maintaining sufficient sensitivity.

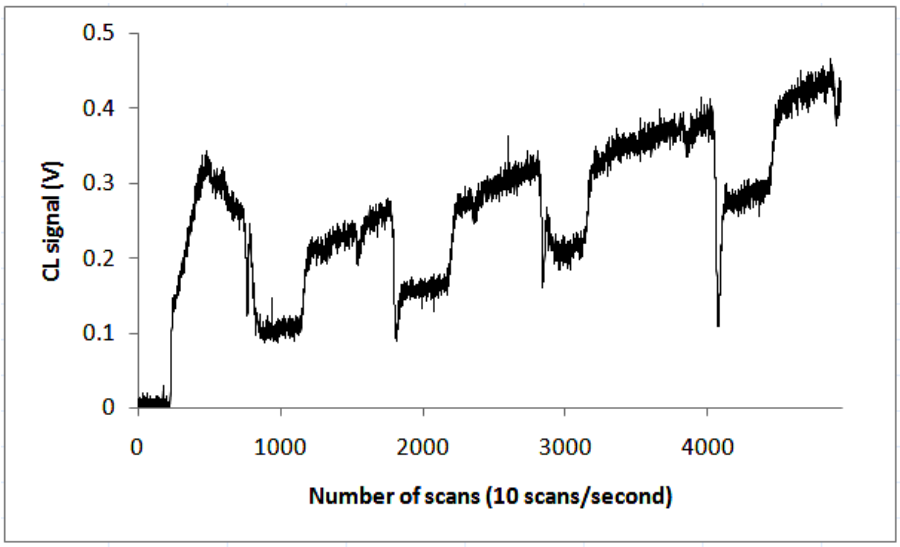

Figure III30. The effect on the Mn analysis when TETA was added in the reagent solution containing H_2O_2. The baseline level was increased erratically with worse background noises made the analysis of Mn(II) was not possible.

8.1.5 Pre-concentration time

The other way to increase the sensitivty of the CL signal peaks is to increase the pre-concentration time, which allowed more Mn(II) ions to be retained on to the Toyopearl resin, thus, provided more Mn(II) ions to catalyse the oxidation of luminol and subsequently increased the rate of the photon emission. In order to test the response of CL signal peak with longer pre-concentration time, an experiment was carried out. The instrument was set up as in Figure III24 with 3m mixing coil, following the procedures (the preparation of reagents and experimental procedures) explained in Section 8.1. Seawater+1 nM Mn(II) standard addition solutions were analysed with 200 s and 400 s of the pre-concentration times. When the pre-concentration times increased, the CL signal peaks were also increased (Figure III31). However, longer pre-concentration times were increased the uptake of standard/sample solutions and reagents solutions, hence, time consuming and wasting the chemicals. As 200s pre-concentration time could obtain a measurable CL signal peaks, thus it remained unchanged.

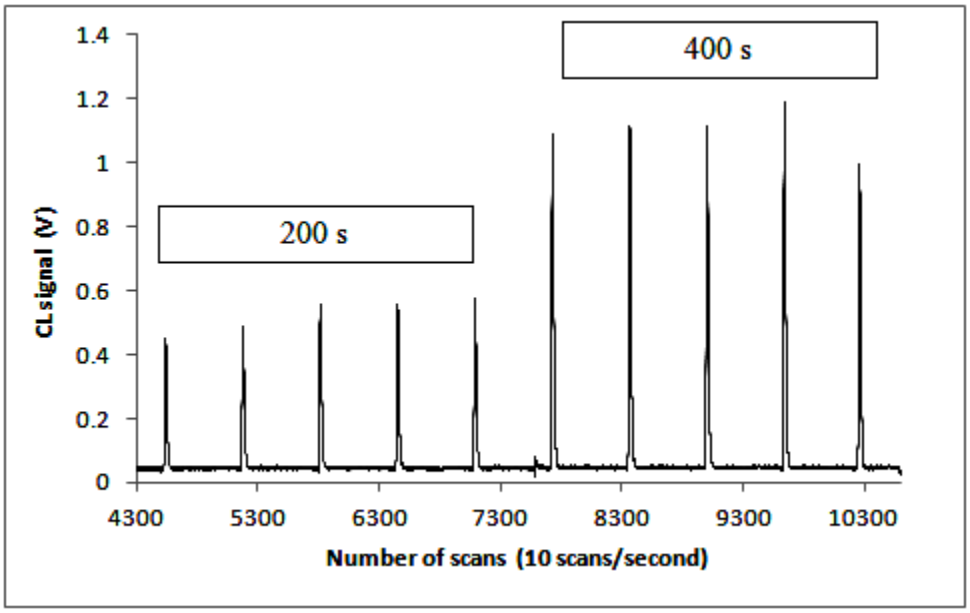

Figure III31. The CL signal peaks for 200s and 400s pre-concentration times. The peaks were doubled up as the pre-concentration times doubled up.

8.2 Stripping of Mn(II) from seawater

The large volume of filtered seawater (0.2 µm) used to prepare standards solutions for daily calibration in this study that was collected from the Tropical North-Eastern Atlantic Ocean were almost run out at this stage of study. Therefore, prior to availability, it was changed with filtered seawaters (0.2 µm) from the European continent/ocean margins in the North Atlantic collected during the Ocean Margin EXchange (OMEX) cruise. However, the concentrations of Mn(II) in OMEX seawaters were relatively high with an average of ~1.7nM (calculated from the slope of the calibration of the day). Thus, Mn(II) was needed to

be stripped from the seawater before it could be used to prepared daily standards calibration for this Mn(II)-FIA-CL system.

Some experiments were carried out in order to strip the Mn(II) from the seawater. A 50mL of acidified (pH~2) OMEX seawater was passed through the preconcentration resin column (Toyopearl AF-Chelate 650M) and was collected in a clean bottle, where the pH of acidified OMEX seawater was adjusted to pH~8.5 before the analysis. It was analysed afterwards using the Mn(II)-FIA-CL system and approximately 60% from the ~1.7 nM of Mn(II) ions were removed resulting in a concentration of ~0.6 nM (Figure III32). However, there was still Mn(II) residue in the seawater and the same experiment was repeated another two times until a low and consistent concentration of Mn(II) was obtained in the seawater (~0.07 nM) (Figure III32). This value remained constant after the experiment was repeated for the third time, suggesting it was the background signal. This Mn-stripped seawater was then used in preparation of daily standard solutions for daily calibration, to replace the low Mn seawater North-Eastern Atlantic.

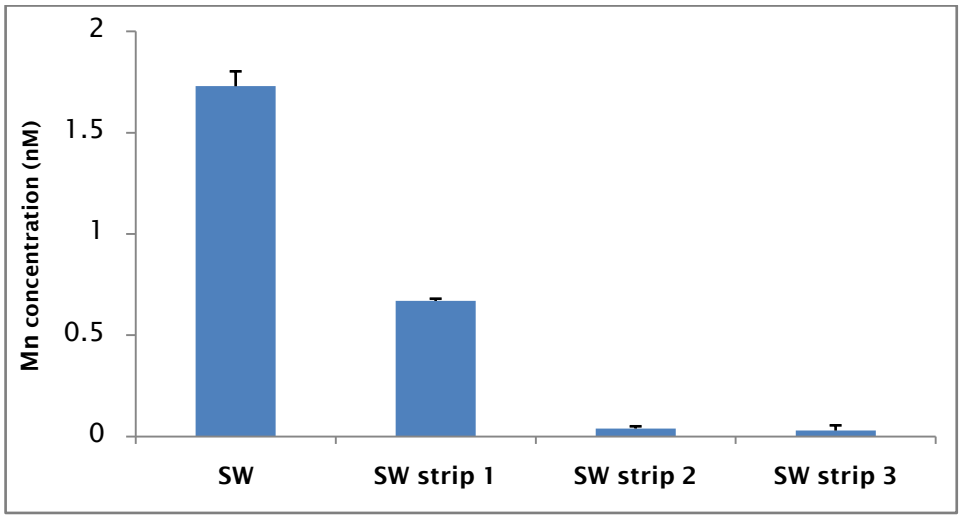

Figure III32. The concentration of Mn(II) in the seawater before and after passing over the preconcentration. Only 60% of Mn(II) concentration was stripped of the seawater in a first experiment. The Mn(II) concentrations were then constant after the experiment was repeated for a couple of times, resulting in a concentration of ~0.07 nM, which was assumed as the background signal.

In order to test the response of the analyser with this Mn-stripped seawaters, several calibrations in a range of 0.5 – 4 nM (prepared by standard addtions to acidified filtered Mn-stripped seawater with ~30 µL of 20 µM ammonia solution to adjust the pH to be around 8.5) were carried out before further modifications and/optimisations were done. The CL pH was checked and adjusted to the optimum pH of 10.2. Reagents were prepared as they were set up previously (see Section 8.1). All other conditions (*i.e.* reagents and standards concentrations, pHs, flow rates) were kept as similar as possible between experiments, which were performed in a single day. The calibration curves were linear (R^2 =

0.998) (Figure III33). Precision for each point ranging from 2.9% *rsd* for +2nM standard, and up to 23.5% *rsd* for seawater alone, with an average of 12% *rsd* (n=3). The reagent blank (MQ water) value is 0.04±0.01 nM, and the detection limit estimated at 0.03 nM (detection limit is three times of standard deviation of the blank).

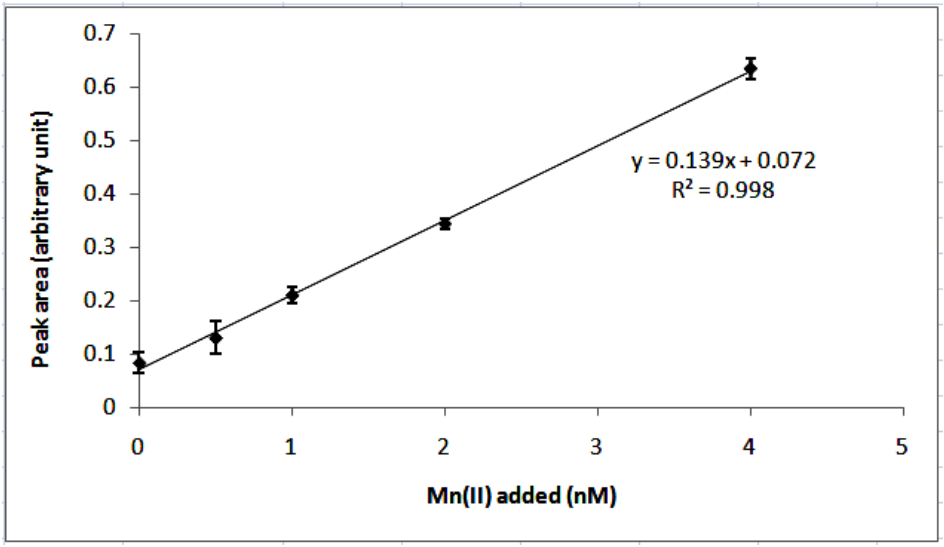

Figure III33. Calibration curve using standard additions of Mn(II) to acidified filtered OMEX seawater ([Mn] = ~0.07 nM). CL pH = 10.2, pre-concentration pH = ~8.5 (pH of seawater was adjusted by using ~30 µL of 20 µM ammonia solution), elution pH = 2.9. Curve fitted with a linear trendline. Precision ranged between 2.9 – 23.5 % *rsd* (n = 3, average 12% *rsd*). The reagent blank (MQ water) value is 0.04±0.01 nM, the detection limit estimated at 0.03 nM (detection limit is three times of standard deviation of the blank).

9. Interference

When some deeper samples from the Crozet region that had previously been analysed with the 1m mixing coil, were re-analysed using a 3m mixing coil, the values were increased approximately threefold. Several reasons were considered for the enhancement including : **(1)** the longer coil allowed more chemical reactions during the analysis, thus giving higher results, **(2)** the longer coil allowed interferences from other trace metals that also could be a catalyst in luminol oxidation processes. A number of studies have shown that several trace metals including Ni(II), Co(II), Cu(II), Zn(II), Cd(II), and particularly Fe(II and III), can interfere in Mn(II) analysis, particularly with a longer mixing coil (Nakayama *et al.,* 1989; Okamura *et al.,* 1998; Doi *et al.,* 2004).

9.1 Fe ion interference

Fe (II and III) ions appeared to have the biggest potential contribution in interfering with the Mn(II) analysis with CL detection, as Fe and Mn showed the highest catalytic activity for decomposition of H_2O_2 in the presence of TETA (Nakayama *et al.,* 1989). Concentrations of Fe in oceanic waters generally are in a range of 0.02 – 2.00 nM, with an average of 0.5 nM (Bruland and Lohan, 2003). In the vicinity of the Crozet Islands, Southern Ocean, the range

is 0.086 – 2.48 nM (Planquette *et al.,* 2007). In the previous modifications, the cleaning resin column (NTA) was added in the system to remove the Fe ions from the formic reagent and standard/sample solutions (see Figure III27), because the Fe ions would bind onto the NTA resin at pH≤3.0 (Table III9). The NTA resin was used because Mn ion was unable to be retained onto the NTA resin (Sohrin *et al.,* 2008). In addition, Cu ion also could be retained onto the NTA resin at pH≤3.0.

Table III9. The optimum pHs for uptake of several trace elements (Mn, Ni, Co, Cu, Zn, Al, Cd, and Fe) onto the Toyopearl Chelate-AF 650M, the NTA and the 8-HQ resins, as reported in the literatures.

Trace metal	Toyopearl Chelate AF 650M	NTA	8-HQ
Mn	8.5 (Willie *et al.*,2001) 8.0-9.0 (Aguilar-Islas *et al.*,2006) 8.8 (Warnken *et al.*, 2000) 9.0 (Beck *et al.*, 2002) 8.1 (Milne *et al.,* 2010)	Difficulty in retaining Mn onto the resin (Sohrin *et al.*, 2008)	>8.0 (Obata *et al.,* 1993) >8.0 (Weeks and Bruland, 2002) ~8.5 (Chapin *et al.,* 1990; Mallini and Shiller, 1993; Doi *et al.,* 2004; Hirata *et al.,* 2003; de Jong *et al.,* 2000)
Ni	5.3 (Willie *et al.*, 2001) 5.6 (Beck *et al.,* 2002) 6.4 (Milne *et al.,* 2010) >9.0 (Warnken *et al.*, 2000)	6.5 (Lohan *et al.* 2005)	6.5 (Hirata *et al.,* 2003) >8.0 (Obata *et al.,* 1993) 5.5 (Okamura *et al.*, 1998) >8.0 (Askun *et al.,* 2008)
Co	5.3 (Willie *et al.,* 2001) 6.2-6.4, (Milne *et al.*, 2010) 5.0-6.0 (Shelley *et al.,* 2010) 5.5 (Cannizzaro *et al.,* 2000)	6.0 (Lohan *et al.,* 2005)	7.5-8.5 (Sakamoto-Arnold and Johnson, 1987) 6.5 (Hirata *et al.,* 2003) >8.0 (Askun *et al.,* 2008)
Cu	5.3 (Willie *et al.,* 2001) 5.6 (Beck *et al.,* 2002) 8.8 (Warnken *et al.,* 2000) 5.1-6.0 (Milne *et al.,* 2010)	≥3.0 (Lohan *et al.,* 2005)	~3.0 (Hirata *et al.,* 2003) 5.5 (Okamura *et al.*, 1998) 5.4 (Weeks and Bruland, 2002)
Zn	5.3 (Willie *et al.,* 2001) 5.6 (Beck *et al.*, 2002) 5.1-6.0 (Milne *et al.*, 2010)	6.0 (Lohan *et al.,* 2005)	4.5-5.0 (Hirata *et al.,* 2003) 5.5 (Okamura *et al.,* 1998)
Cd	5.6 (Beck *et al.,* 2002) 8.8 (Warnken *et al.,* 2000) >6.0 (Milne *et al.,* 2010)	5.5 (Lohan *et al.,* 2005)	>7.0 (Hirata *et al.,* 2003) 6.0-7.0 (Li *et al.,* 2006) ~6.0 (Askun *et al.,* 2008)
Fe		≥2.0 (Lohan *et al.,* 2005)	3 (III) (Obata *et al.,* 1993) 5.5 (both II and III) (Okamura *et al.*, 1998) 3.0 (III) and 5.2 (II) (Weeks and Bruland 2002)

9.2 Interferences on Mn separation of other trace metals

A range of metals (*i.e.* Ni, Co, Pb, Cd, Cu, Fe, and Zn) were also expected to be removed by the NTA resin that was used in this study as a cleaning resin. However, based on the relationship between pH and recovery of trace metals from seawater onto the NTA chelating resin column (Table III9, Lohan *et al.,* 2005), only Fe (100%) and Cu (90%) would be expected to be removed by the NTA resin at pH ≤3. Other metals thus proned to interfere in the manganese analysis. Therefore, several experiments were carried out to investigate to what extent other trace metals would interfere with the determination of manganese.

9.2.1 Interference experiments

The mean oceanic values for trace metals (*i.e.* Ni, Co, Cd, Cu, Fe, Zn) and their tenfold value were showed in Table III10. The elements are typically present at picomolar to nanomolar levels in oceanic seawater with 2-300 pM (average of 150 pM) for Co (Bruland and Lohan, 2003; Ellwood, 2008; Shelley *et al*., 2010); 1-1000 pM (an average of 500 pM) for Cd (Bruland and Lohan, 2003); and around 0.5-4.5 nM with an average of 1.5 nM for Cu (Bruland and Lohan, 2003). Concentrations of Fe in oceanic waters generally are in a range of 0.02 – 2.00 nM, with an average of 0.5 nM (Bruland and Lohan, 2003). Ni concentrations however, are high in oceanic waters, from 2 to 12 nM (Bruland and Lohan, 2003), depending on the ocean regions. In the Southern Ocean, the concentrations of Ni were between 3 and 7 nM, with an average of 5 nM (Loscher *et al*., 1999; Ellwood, 2008) (Southern Ocean average value was used in this experiment because this method would subsequently used to analyse seawater samples from the Crozet Islands surrounding waters of the Southern Ocean).

Table III10. The mean oceanic values of Mn, Ni, Co, Cu, Zn, Cd, Fe and their values of 10 times higher than the mean oceanic values, taken from Bruland and Lohan (2003); and Ni from Loscher *et al*. (1999) and Ellwood (2008). All values are in nM.

Trace metal	Mean oceanic value (nM)	10x higher than mean oceanic value (nM)
Mn	0.3	3
Ni	5.0	50
Co	0.021	0.21
Cu	2.4	24
Zn	5.5	55
Cd	0.5	5
Fe	0.5	5

Based on Table III10, Ni, Cu, and Cd were chosen due to their potential to be retained on the Toyopearl resin at pH between 8 and 9 (Warnken *et al.,* 2000), and Co was chosen due to its significant interference reported in the literatures (Nakayama *et al.,* 1989; Doi *et al.,* 2004). Fe and Zn were chosen as they could interfere in the CL analysis.

In order to investigate the influence of seawater on the CL signal, Mn-stripped seawater (OMEX) was used. Each of the metal ions (Table III10) was added in 10 times higher than the mean oceanic values (Table III10), to get more pronounced values. Other variables, for example the pumping rate and speed, pre-concentration time (200s), mixing coil length (3m), pH of the standards (adjusted to pH~8.6) and the reagents were kept constant and as used in the daily Mn analysis (refer Section 8.1 in this Chapter for details of reagents

preparation and experiment procedures) and all values were blank corrected. The apparent Mn concentrations for these elements were divided by 10 to get the estimated apparent Mn concentrations at the mean oceanic concentrations of each element, and were plotted as shown in Figure III34. All metal ions except Ni hardly catalysed the luminol-H_2O_2 CL reaction, particularly when the NTA cleaning resin column was placed after the pre-concentration column of Toyopearl resin.

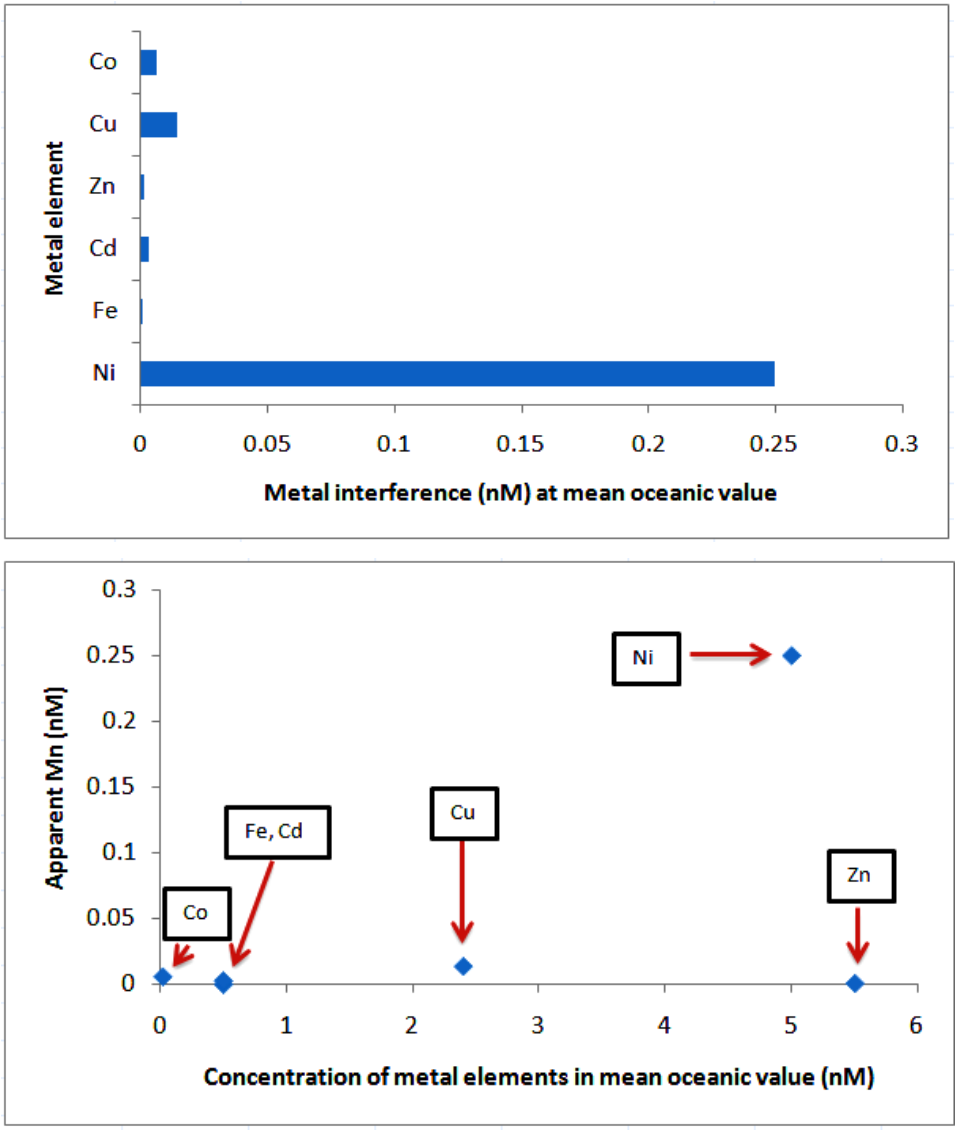

Figure III34. The estimated apparent Mn values for the interfering elements at their mean oceanic values showed that all metal ions were hardly catalysed luminol-H_2O_2 CL, except Ni. Ni gave the highest interference (~0.25 nM) to the Mn analysis, when NTA resin was applied as a cleaning resin (CC1).

At the pH of the formic eluent solution, pH 2.9), the interfering metal elements (*i.e.* Co, Fe, Cd, Cu, and Zn) were retained on the NTA resin. However, as shown in Figure III34, Ni was not fully retained on the NTA resin, and thus gave interference in the Mn analysis. The total metals interference value (as an apparent Mn concentration) presented here is ~0.25 nM.

The metal interference values obtained here were lower than those reported in Doi *et al.* (2004) and Nakayama *et al*. (1989), except for Ni. These differences were really dependent on the details of how the experiments were carried out; for example, Doi *et al.* (2004) added metals to the carrier solution (formic eluent), but here in this study, the standard metal solutions were spiked into the Mn-stripped seawater. In addition, Doi *et al.* (2004) was used the Kelex-100 resin (8-HQ derivative resin) as a cleaning resin, whilst here the NTA resin was used.

9.2.2 Ni interference experiments

Based on the interference experiments above, Ni seemed to be a main interfering element for this study. Before further modification was made, it was very important to investigate the interference of Ni for analyser with 1m mixing coil, as analyses of the surface seawater samples from the tropical North-Eastern Atlantic Ocean were performed using the analyser with 1m mixing coil. Therefore, an experiment to investigate the interference of Ni when using a 1m mixing coil was performed.

A series of 5 and 10 nM of Ni standard solutions were spiked into the Mn-stripped seawater, they were then analysed using a 1m and 3m mixing coils with NTA resin as a cleaning resin. Other variables (*e.g.* the pump rate and speed, the pHs, pre-concentration time, *etc.*) were kept constant as used in the previous interference analysis (*see* Section 9.2.1). All values were blank corrected. The apparent Mn (nM) values were then plotted against the concentrations of Ni added (nM) to the seawater (Figure III35). At Ni mean oceanic values (5nM), the apparent Mn is <0.05 nM for the analyser with 1m mixing coil. From the literatures, the (dissolved) Ni concentrations in the surface water (<6 m depth) of the tropical North-Eastern Atlantic Ocean were in a range of 2 – 3 nM (Kremling and Pohl, 1989; Sunda, 2012; Aparicio-Gonzalez *et al.,* 2012). Therefore, from this experiment as shown in Figure III35, the apparent Mn is < 0.03 nM at a range of 2-3 nM concentrations of dissolved Ni at surface seawater of the tropical North-Eastern Atlantic Ocean. Thus, Ni interference was not critical in the Mn analysis using a 1 m mixing coil.

Ni interference at a range of 2-3nM Mn(II) concentrations in the surface seawater of the tropical North-Eastern Atlantic Ocean is ~0.16nM, when longer mixing coil (3m) was used in the analysis (Figure III35). As previously explained, several reasons were considered to cause the enhance of CL peak signal when longer mixing coil (3m) was used in the analysis, such as: **(1)** the longer coil allowed more chemical reactions during the analysis, thus giving better results, **(2)** the longer coil allowed interferences from other trace metals that also could be a catalyst in luminol oxidation process.

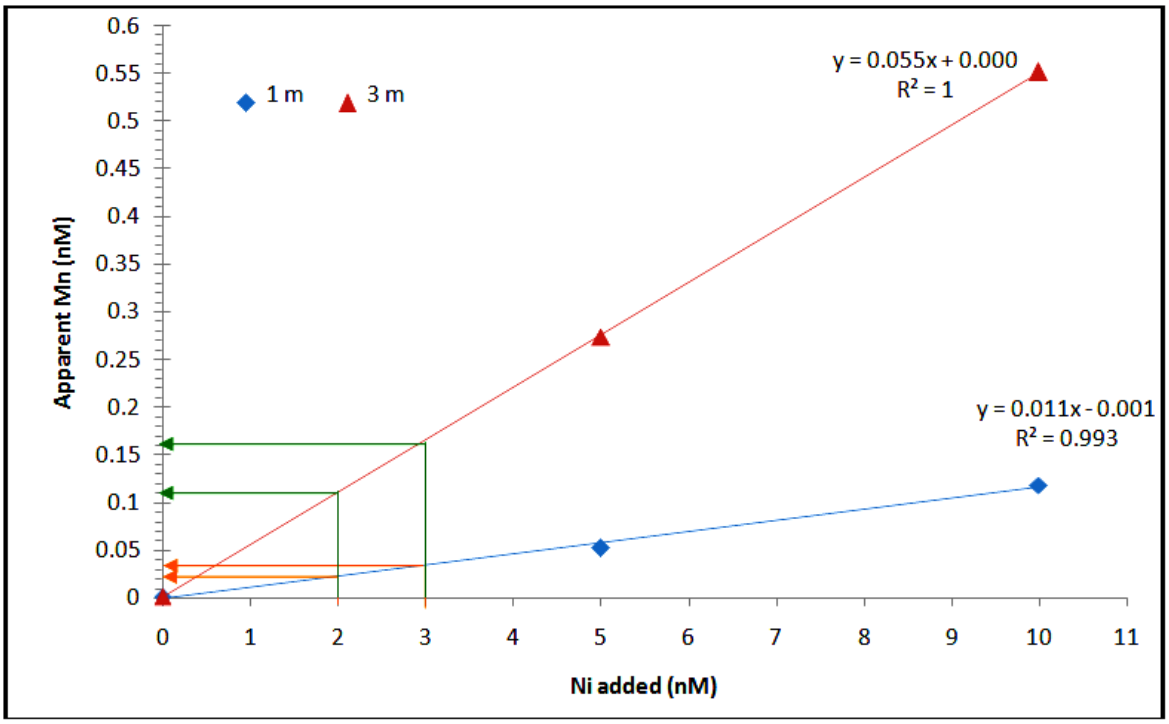

Figure III35. The apparent Mn (nM) of Ni interference with 1m and 3m mixing coils were plotted. The Ni interference in the experiment with 1m mixing coil was considerably low, with <0.03 nM of 2-3 nM Mn(II) in the surface seawater of the tropical North-Eastern Atlantic Ocean, while the Ni interference in the experiment with 3m mixing coil is <0.16nM of 2-3 nM Mn(II) in the surface seawater of the tropical North-Eastern Atlantic Ocean.

As there was a considerably significant interference from Ni when 3 m mixing coil was used in the system, it was therefore, very important to find the best solution on how to remove this problem and hence, make this system specific only to determine Mn(II) concentration.

10. Comparison with the Mn-FIA-CL-Toyopearl technique used by Rob Middag from Royal Netherlands Institute for Sea Research (NIOZ)

A recent Mn(II)-FIA-CL-Toyopearl technique used by Rob Middag and co-workers from NIOZ (Middag *et al.,* 2011a,b) have not mentioned any interference from Ni in their work. Therefore, before the end of this project, some experiments were performed to investigate the efficiency of other ways of removing trace metals interferences, particularly Ni. They were used 8-HQ resin (instead of NTA resin) to remove metal interferences. From their results, it seemed that the 8-HQ resin had taken out almost all of those elements and left only the manganese, and so a comparison study between the NTA and 8-HQ resins was done and discussed here.

Before starting the experiment, it was very important to know the relationship between pH and percent recovery of trace metals from seawater on the 8-HQ (and its derivatives) chelating resin. Sohrin and co-workers (1998) used 8-HQ immobilized on fluorinated metal alkoxide glass (MAF-8HQ) to determine trace metal elements in seawater and observed that the elements were quantitatively retained on the MAF-8HQ resin in the pH range from weakly acidic to neutral (pH 1-7), as concluded in Figure III36. The complexing group (oxine) is the same between MAF-8HQ and 8-HQ, but, the support resin materials are different. Hence, it is expected that the behaviour of both MAF-8HQ and 8-HQ would be similar (Statham, personal communication), thus Figure III36 should give a reasonable estimation of the behaviour of the 8-HQ resin too. From Figure III36, it showed that at pH~2.9, the 8-HQ resin should remove ~100% of the Fe, Ni, Cu, Zn, Co and Cd that can potentially interfer in the CL reaction and not remove Mn.

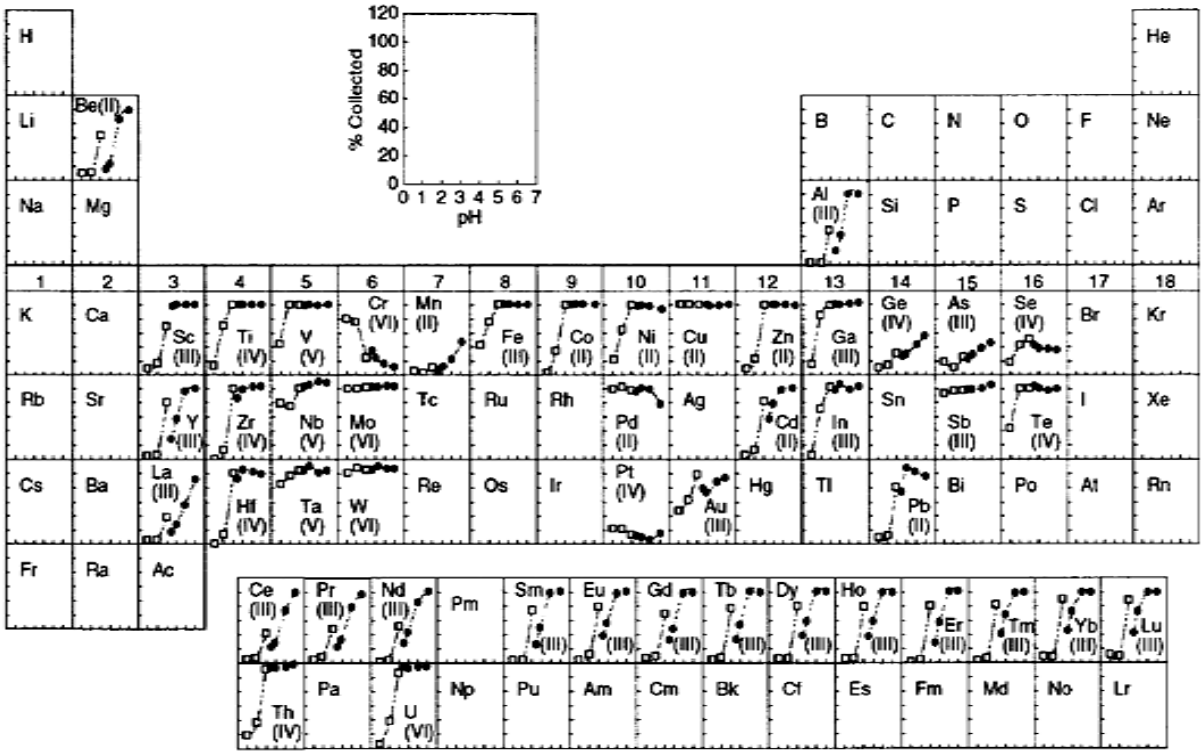

Figure III36. The effect of pH on the recovery of trace metals percentages in seawater on the 8-HQ (and its derivatives) chelating resin column (taken from Sohrin *et al*., 1998).

Therefore, experiments to compare between the NTA and 8-HQ resins were carried out. All procedures for reagents preparation and for the analysis of Mn(II) were set as explained earlier in Section 8.1 in this Chapter with 3m mixing coil. Specific changes in these experiments were explained below with its appropriate reason.

The first cleaning resin column (CC1: NTA resin) was changed to the 8-HQ resin column. Due to insufficient time, the 8-HQ resin that was synthesized previously been used in this

experiment and special thanks are owed to Professor Christopher Measures (University of Hawai'i) for the preparation and supply of the 8-HQ resin used in this study. Before applying the 8-HQ resin in this study, high concentration (5µM) of Mn(II) was initially analysed without the pre-concentration resin column (Toyopearl). High concentration (5µM) of Mn(II) standard addition was added into the Mn-stripped seawater and the pH was adjusted with 20 µM ammonia solution (≤30 µL) to pH~8.5. This high concentration was used to enhance the CL peak signals obtained as the pre-concentration resin column (Toyopearl) was removed in this experiment. The reason to remove the pre-concentration resin (Toyopearl) column was to observe the efficiency of 8-HQ resin on retaining interfering metals at formic eluent pH (2.9), without retaining Mn. As previously explained in Table III9, Mn is very difficult to be retained on the NTA resin (Sohrin *et al*., 2008) at any pH, and Mn can be retained on the 8-HQ resin at the pH>8.0 (Obata *et al.,* 1993; Weeks and Bruland, 2002; Chapin *et al.,* 1990; Mallini and Shiller, 1993; Doi *et al.,* 2004; Hirata *et al.,* 2003; de Jong *et al.,* 2000).

A 1200 mm coil with 0.8 mm i.d. (unknotted coil) with a dead volume of ~600µL was used to replace the Toyopearl resin (Figure III37). The dead volume was calculated using Equation 1 below:

$$\text{Volume} = \text{base area} \cdot \text{length of coil} \qquad \text{(Equation 1)}$$
$$= \pi r^2 \cdot l$$
$$= 22/7 \cdot (0.4\ \text{mm})^2 \cdot 1200\text{mm}$$
$$= 603.43\ \text{mm}^3 = 603.43\ \mu\text{L (rounded to 600 µL)}$$

As the sample pump rate was set at 3.0 mL/min., the dead volume (~600µL) divided by the pump rate (3.0 mL/min), will give the time needed to fill the loop, which was 12s. The loading time then was set up at 30s; long enough to remove any wash MQ water in the loop. The washing and rinsing step were reduced to 15s. The longer eluting time (200s) was needed to ensure all Mn ions were removed from the coil, and to avoid several small peaks obtained before and after the CL peak, possibly due to pH changes with MQ water during rinsing and washing steps.

Two conditions were applied (Figure III37): **(1)** with 8-HQ resin as a cleaning resin, and **(2)** without 8-HQ resin as a cleaning resin. If there was no uptake by the 8-HQ resin, the peak area (peak area was used to measure the CL signal) would be same for both conditions (1 and 2). However, if there was uptake by the 8-HQ resin, the peak area would be less than the peak area without the 8-HQ resin column. Table III11 shows the average peak areas for both conditions, and indicates the peak area with the 8-HQ resin column was about the same as without the 8-HQ resin column, which infers that the 8-HQ resin did not retain Mn at pH~2.9.

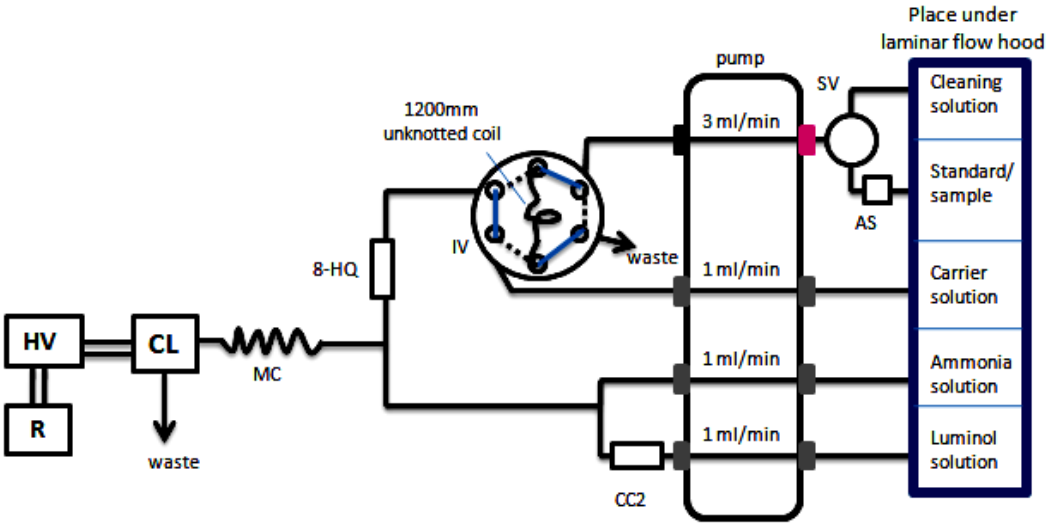

Figure III37. The schematic diagram of the FIA-CL system used to determine the efficiency of removal of Mn ions at pH~2.9 by the 8-HQ resin. 1200mm unknotted coil was replaced the pre-concentration resin (Toyopearl resin) and high concentration (5µM) of Mn(II) standard was analysed. The loading time was 30s, the rinsing and washing step time was 15s, and the eluting time was 200s. Two experiment conditions were applied: (1) with 8-HQ resin column as shown above, and (2) without 8-HQ resin column.

Table III11. The average values of peak area of 5µM Mn(II) for condition 1 (with 8-HQ resin column) and condition 2 (without 8-HQ resin column). Peak areas for both conditions were about the same, inferring that the 8-HQ resin would not adsorb any Mn ion at the formic eluent pH of ~2.9. Values are in arbitrary unit.

Condition 1: With 8-HQ resin column	Condition 2: Without 8-HQ resin column
4.93 ± 0.36 (n=17)	4.96 ± 0.62 (n=18)

When it was confirmed that the 8-HQ resin column would not retain any Mn ions at pH~2.9, the resin was then tested on several trace metal elements (*i.e.* Ni, Cu, Co and Cd) to check the efficiency of the 8-HQ resin of removal of these metals. 5µM standard solutions of Ni, Cu, Co and Cd were prepared Mn-stripped seawater were analysed for 5-6 replicates for each elements, following the above procedure.

Table III12 showed the peak areas of every element for both conditions (with and without 8-HQ resin column). Peak areas in Conditions 2 (without 8-HQ resin) were higher than in Condition 1 (with 8-HQ resin), suggesting that the 8-HQ resin column could retain >80% of these elements at pH~2.9. However, the concentrations of these elements (5µM) that was used were very much higher than their mean oceanic concentrations. Therefore, estimated calculation were made base on values in Table III12 to give the estimation of the mean concentrations of the interference elements in the average oceanic values, as showed in Table III13. The estimated values obtained here were extremely low, this suggested that 8-HQ resin was a better cleaning resin for this Mn(II)-analyser.

Table III12. The average values of Mn equivalent peak area of 5µM Ni, Cu, Co, and Cd, for condition 1 (with 8-HQ resin column) and condition 2 (without 8-HQ resin column). Peak areas in Condition 2 were higher than in Conditions 2, suggesting that 8-HQ resin column adsorbed these metals at pH~2.9. Values are in arbitrary area units.

Trace metal elements	Condition 1: With 8-HQ resin column	Condition 2: Without 8-HQ resin column
Ni	0.80 ± 0.09 (n=5)	4.09 ± 0.29 (n=6)
Cu	0.84 ± 0.08 (n=5)	4.27 ± 0.27 (n=6)
Co	0.63 ± 0.07 (n=5)	4.04 ± 0.06 (n=6)
Cd	0.67 ± 0.06 (n=5)	4.02 ± 0.05 (n=6)

Table III13. The estimated average values of Mn equivalent peak area of Ni, Cu, Co, and Cd when present at the mean oceanic concentrations for condition 1 (with 8-HQ resin column) and condition 2 (without 8-HQ resin column). Peak areas were extremely low, thus suggesting that 8-HQ resin was a better resin to remove these elements in the Mn analysis than NTA. Values are in arbitrary area units.

Trace metal elements	Condition 1: With 8-HQ resin column	Condition 2: Without 8-HQ resin column
Ni	0.0008 ± 0.0001 (n=5)	0.0041 ± 0.0003 (n=6)
Cu	0.0004 ± 0.000037 (n=5)	0.0021 ± 0.00013 (n=6)
Co	0.000003 ± 0.0000003 (n=5)	0.00002 ± 0.0000001 (n=6)
Cd	0.00007 ± 0.000006 (n=5)	0.0004 ± 0.000005 (n=6)

Another experiment were carried out to compare the efficiency between the 8-HQ resin and the NTA resin to remove Ni as a major interference element in this study. Three conditions of the Mn(II)-analyser were set up to analyse a set of standard additions (0, 1, 2, 4, 5, 10 nM) of Ni into the Mn-stripped seawaters: (1) with NTA resin as a first cleaning resin column (CC1), (2) with 8-HQ resin as a CC1, and (3) without a CC1. Results were plotted as in Figure III38, which showed that calibration using the 8-HQ resin as a CC1 was giving the lowest values for all Ni concentrations. An increase of 80 to 90% with an average of ~ 85% was recorded for the results in an experiment with NTA resin as resin cleaning (compared to the results obtained from the experiment with the 8-HQ resin column as a CC1). In addition, experiment without a CC1 was carried out to prove that without any CC1, the Ni interference was even worst, with an average of ~80% increment compared to values for NTA resin.

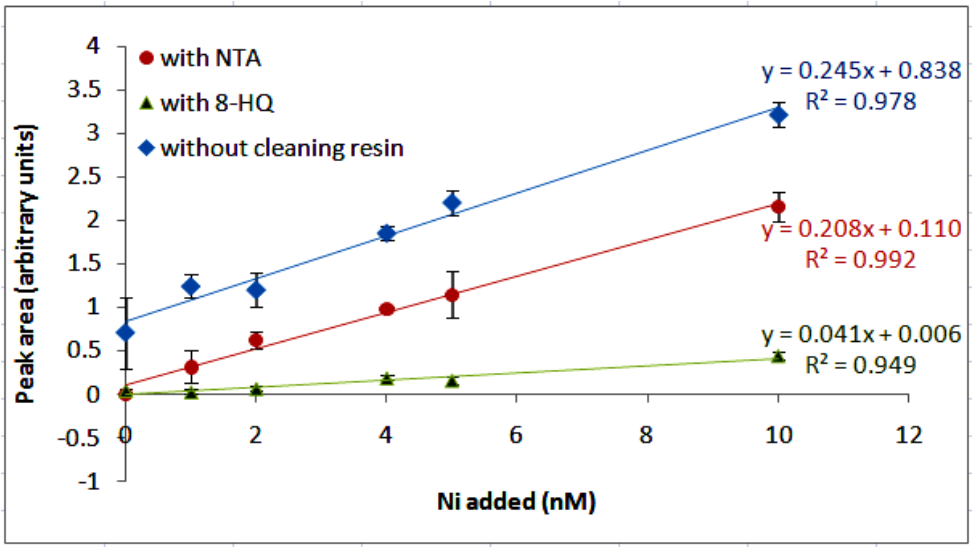

Figure III38. Calibration of Ni standard additions (0-10 nM) into Mn-stripped seawater with three different conditions: (1) with NTA resin as a first cleaning resin column (CC1), (2) with 8-HQ resin as a CC1, and (3) without CC1. Calibration with 8-HQ resin as CC1 gave the lowest peak areas infer that most of the Ni ions were retained onto the 8-HQ resin.

Later, the same experiment in Section 9.2.1 was repeated, but by replacing the CC1 with the 8-HQ resin column, to investigate the total interference values with the 8-HQ resin column as a CC1.

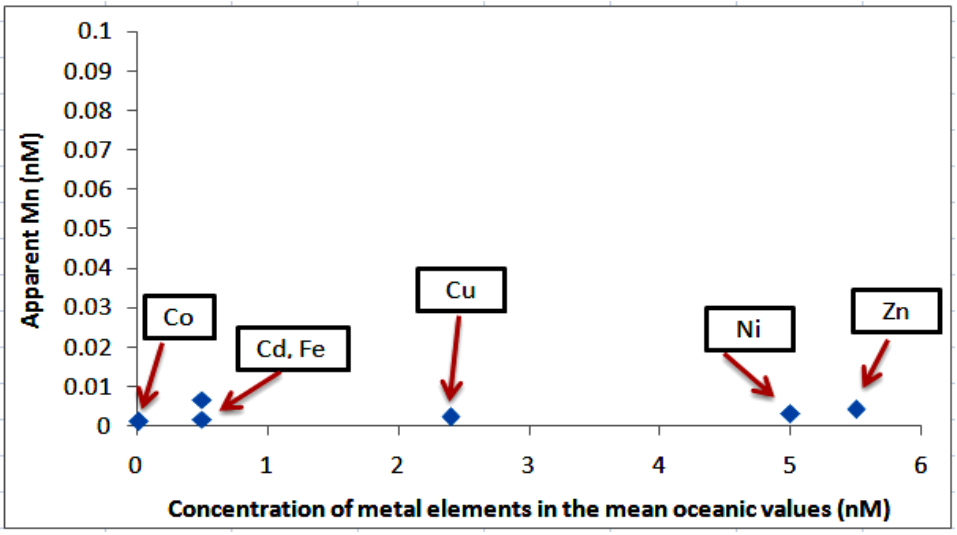

Figure III39. The estimated apparent Mn values for the interfering elements at their mean oceanic values showed that lower values for all metal ions were hardly catalysed luminol-H_2O_2 CL, as the metal ions were strongly retained onto the 8-HQ resin at pH2.9. Ni, which was the greatest interference element in the previous experiment showed a significant reduction (to <0.003 nM) to the Mn analysis, when 8-HQ resin was applied as a CC1.

Figure III41 showed the estimated results of the average oceanic values for respective metal elements (Co, Cd, Fe, Cu, Ni and Zn) for this repeated experiment with apparent Mn values for Ni interference was significantly reduced (98.8% reduction from value in Section 7.2.1) to approximately 0.003 nM (in this experiment). Total interference values (for all elements analysed) are <0.02 nM. Hence, based on these interference experiments, the 8-

HQ resin appears to be a better resin to remove the interfering metal elements, including Ni in the Mn(II)-FIA-CL analyser developed here.

11. Correction of Mn(II) concentrations

Previously, all samples (Tropical NE Atlantic and Crozet seawater samples) were analysed using the NTA resin as a CC1. However, Tropical NE Atlantic samples which were analysed by using 1 m mixing coil, were not affected with Ni interference. Only Crozet samples, which were analysed by using 3 m mixing coil were affected with Ni interference. Therefore, these values needed to be corrected in order to obtain the accurate values. Correction of these values, however, was not easy. To ensure that the Mn concentrations obtained in this study using the current Mn(II)-FIA-CL-Toyopearl technique developed here were of a good quality, samples were needed to be re-analysed using the latest modification, as shown in Figure III40.

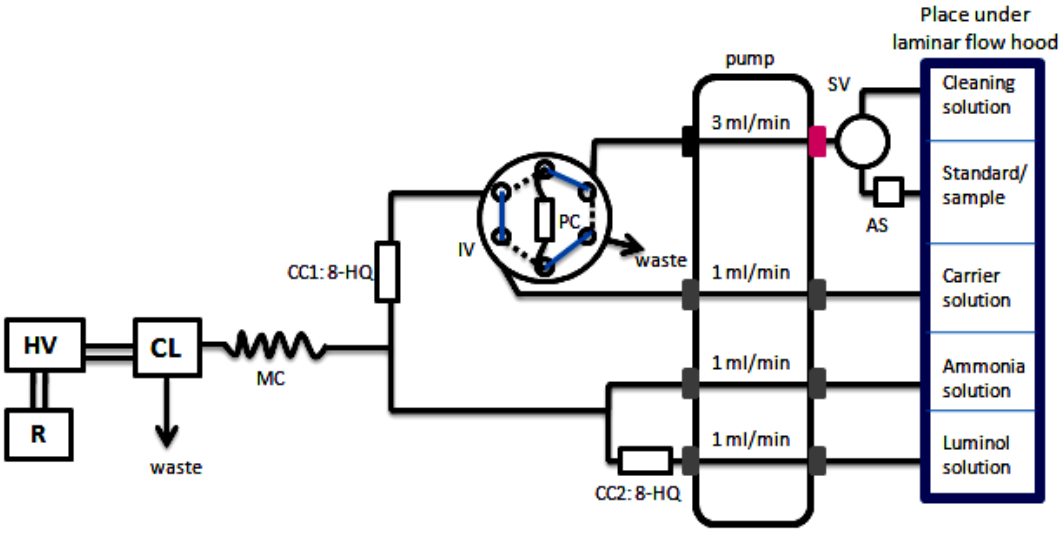

Figure III40. Schematic diagram of final modification of Mn(II)-FIA-CL with preconcentration step and two cleaning resin columns. All reagents were placed under the laminar flow hood to prevent additional contamination from the airborne particles during the anaylysis. PC: preconcentration Toyopearl resin column; CC1: first cleaning resin column (8-HQ resin); CC2: second cleaning resin column (8-HQ resin); SV: solenoid valve; AS: auto-sampler; IV: injection valve; MC: mixing coil (3 m); CL: a built-in flow cell and PMT, HV: power supply; R: recorder (laptop). Blue line is Position A (loading step) and dot line is Position B (eluting step).

Depth profiles of Station M3 (496), Station M2 (502), Station BA (567), Station BA+1 (568), and Station BA+2 (569)) were all re-analysed using the analyser as in Figure III40. The results obtained then were compared with the previous results, which were plotted in Figure III41 and III42.

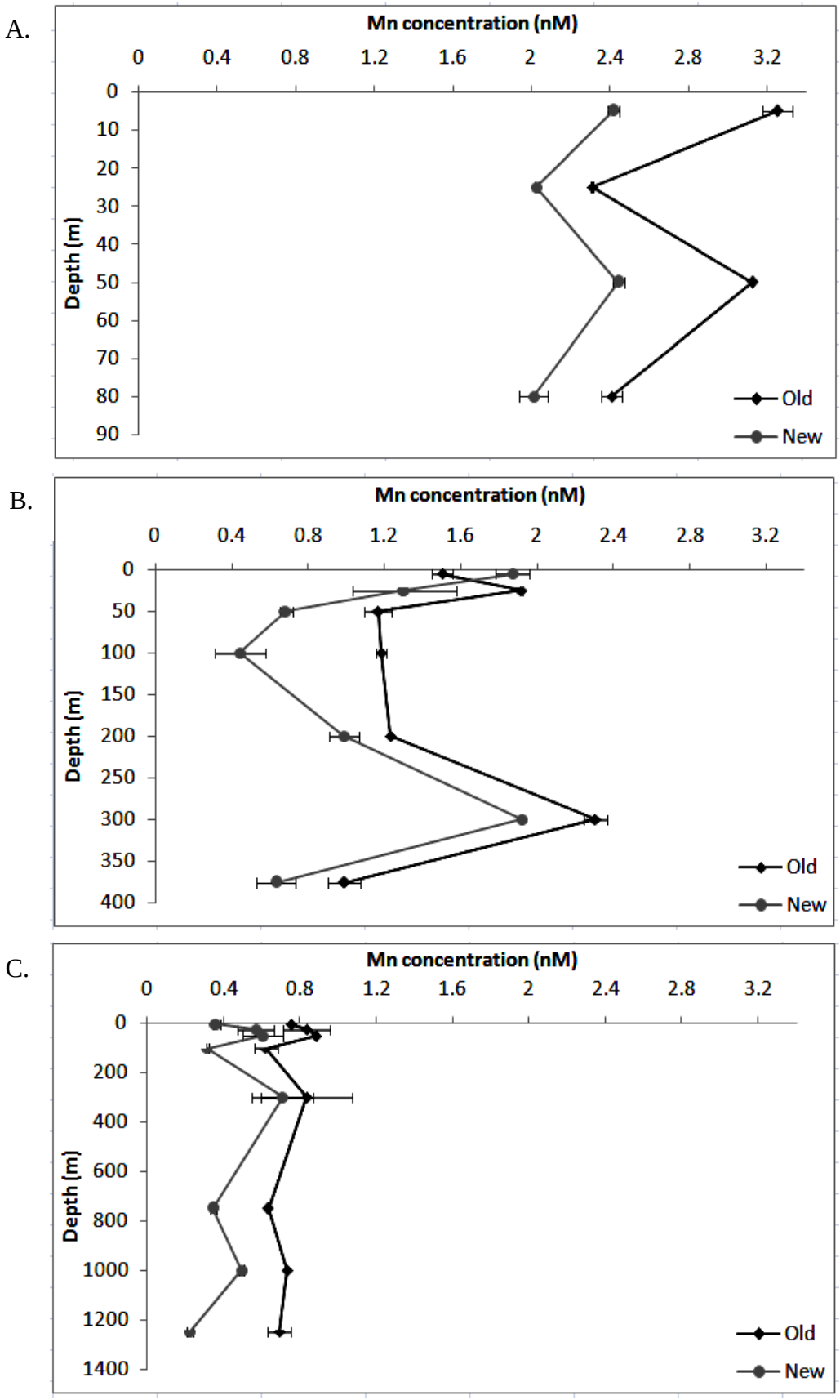

Figure III41. Depth profiles for Stations (A) BA 567, (B) BA+1 568, (C) BA+2 569 were re-analysed (indicate by grey closed round and line) by using the latest modification method, in comparison with the old values (indicate by black closed diamond and line) which were analysed with NTA as a CC1 in the analyser.

A.

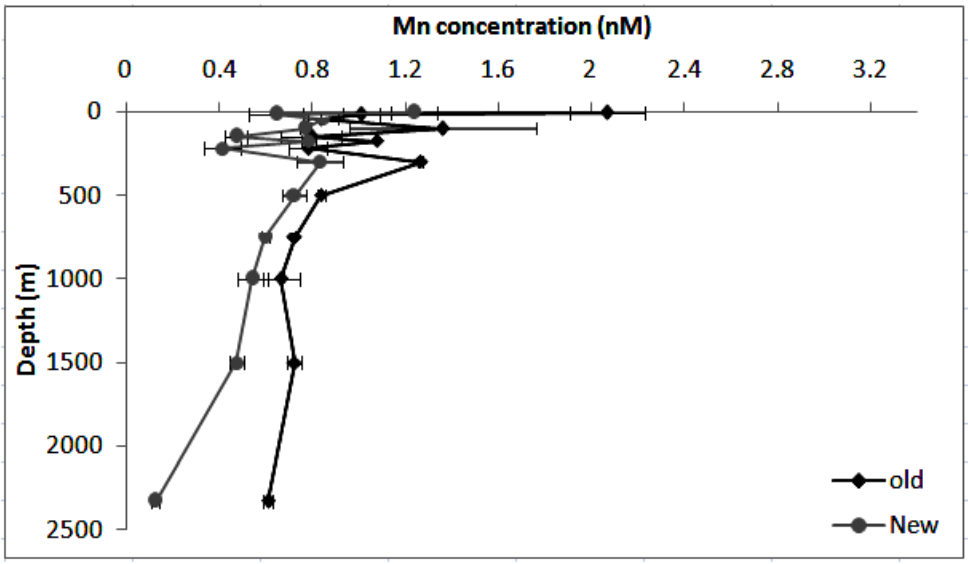

B.

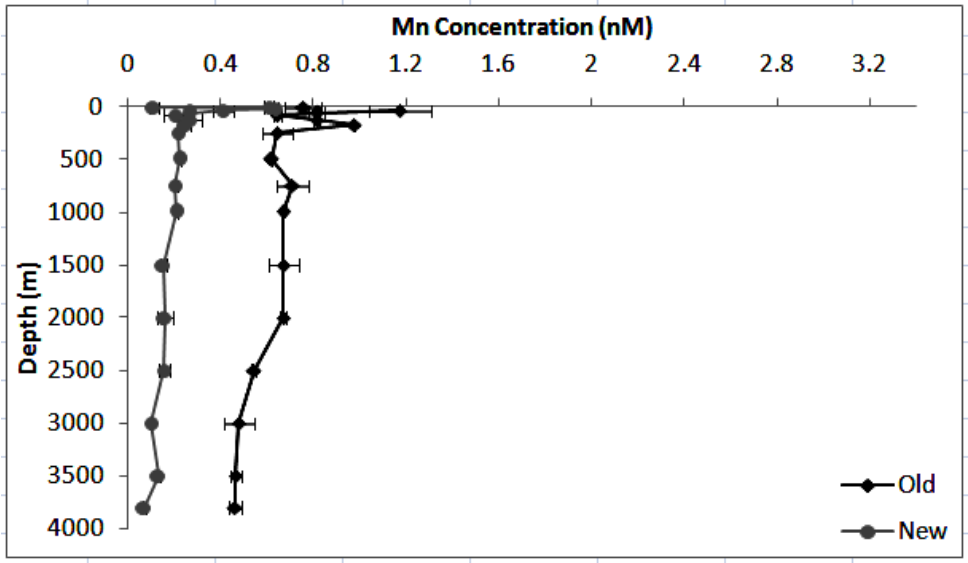

Figure III42. Depth profiles for Stations (A) M3 496, and (B) M2 502 were re-analysed (indicate by grey closed round and line) by using the latest modification method, in comparison with the old values (indicate by black closed diamond and line) which were analysed with NTA as a CC1 in the analyser.

The different between the new and the old data were calculated and showed in Table III14 to estimated their different, that caused by the metals interference, particularly Ni. The average different in percentage for Stations BA (567) is 55%, BA+1 (568) is 35%, BA+2 (569) is 30%, M3 (496) is 33%, M2 (502) is 37% to give an average of 38% reduction of Mn(II) concentrations of the new values. Details explanation on the distributions of the Mn(II) concentrations would be discussed in Chapter IV.

Table III14. Seawater samples from Stations BA (567), BA+1 (568), BA+2 (569), M3 (469) and M2 (502) were re-analysed using the newly modified Mn(II)-FIA-CL analyser. The new concentrations of Mn(II) were reduced approximately 38% (average value) from the old values.

Station	Depth (m)	new (with 8-HQ) (nM)	old (with NTA) (nM)	Average different (%)
BA (567)	5	2.42±0.03	3.25±0.08	55
	25	2.03±0.01	2.31±0.01	
	50	2.44±0.03	3.13±0.00	
	80	2.01±0.07	2.41±0.05	
BA+1 (568)	5	1.87±0.09	1.50±0.05	35
	25	1.30±0.27	1.92±0.07	
	50	0.69±0.03	1.17±0.07	
	100	0.45±0.13	1.18±0.03	
	200	0.99±0.08	1.23±0.01	
	300	1.92±0.01	2.31±0.06	
	376	0.63±0.10	0.99±0.08	
BA+2 (569)	5	0.36±0.02	0.75±0.00	30
	25	0.57±0.10	0.83±0.12	
	50	0.60±0.11	0.89±0.01	
	100	0.31±0.01	0.62±0.06	
	300	0.71±0.16	0.83±0.24	
	750	0.34±0.02	0.63±0.00	
	1000	0.49±0.03	0.73±0.01	
	1250	0.22±0.02	0.69±0.06	
M3(496)	5	1.24±0.10	2.07±0.16	33
	15	0.64±0.12	1.01±0.08	
	42	0.85±0.06	0.84±0.01	
	100	0.77±0.03	1.36±0.40	
	150	0.47±0.05	0.80±0.13	
	175	0.78±0.03	1.08±0.01	
	218	0.41±0.08	0.78±0.08	
	300	0.83±0.10	1.27±0.01	
	500	0.72±0.05	0.84±0.02	
	750	0.60±0.02	0.72±0.00	
	1000	0.54±0.07	0.67±0.08	
	1500	0.47±0.03	0.72±0.03	
	2200	0.13±0.02	0.61±0.02	
M2 (502)	5	0.61±0.02	0.76±0.08	37
	10	0.11±0.02	1.17±0.13	
	20	0.64±0.01	0.81±0.04	
	40	0.41±0.05	0.65±0.02	
	60	0.27±0.05	0.81±0.02	
	80	0.21±0.03	0.98±0.01	
	125	0.27±0.05	0.65±0.07	
	175	0.25±0.02	0.62±0.00	
	250	0.22±0.02	0.71±0.07	
	500	0.22±0.01	0.67±0.01	
	750	0.21±0.01	0.67±0.01	
		0.21±0.01	0.67±0.07	

	1000 1500 2000 2500 3000 3500 3800	0.15±0.02 0.16±0.02 0.16±0.03 0.10±0.01 0.13±0.02 0.07±0.01	0.67±0.03 0.54±0.09 0.48±0.07 0.47±0.02 0.46±0.03	

However due to time constraints further analysis of the remaining samples from other Stations were not possible. The values however, were estimated to reduce approximately 38% than the old values, assumed that they would follow on the trend showed by the samples that were re-analysed (see Table III14). The calculations were showed in Table III15 below for new values of the remaining samples from Southern Ocean samples of Stations M1(491), M7 (524), M10 (563), M3 (572), M3 (622), M2 (511) and M6 (598). Details explanation on these Mn(II) concentrations would be further discussed in Chapter IV.

Table III15. Seawater samples from Stations M1(491), M7 (524), M10 (563), M3 (572), M3 (622), M2 (511) and M2 (598) were estimated to be reduced approximately 38% from the old values.

Station	Depth (m)	new (with 8-HQ) (nM)	old (with NTA) (nM)
M1 (491)	5	0.64±0.09	1.04±0.13
	10	0.27±0.01	0.43±0.02
	15	0.43±0.03	0.69±0.05
	25	0.12±0.01	0.31±0.02
	35	0.33±0.03	0.53±0.04
	55	0.26±0.01	0.42±0.01
	75	0.31±0.02	0.50±0.03
	100	0.10±0.04	0.16±0.06
	125	0.33±0.06	0.53±0.09
	150	0.21±0.02	0.34±0.04
	200	0.11±0.02	0.17±0.04
	300	0.30±0.01	0.49±0.01
	500	0.27±0.04	0.44±0.07
M7 (524)	5	0.72±0.04	1.16±0.07
	10	0.73±0.06	1.17±0.09
	15	0.39±0.03	0.63±0.05
	25	0.65±0.06	1.04±0.10
	35	-	-
	55	0.42±0.04	0.68±0.07
	75	-	-
	125	-	-
	200	0.19±0.02	0.31±0.03
	500	0.20±0.01	0.32±0.02

	1000	0.17±0.04	0.27±0.07
	1500	0.23±0.04	0.37±0.07
	2000	0.14±0.07	0.23±0.12
	2500	0.20±0.02	0.32±0.03
	3000	0.14±0.05	0.23±0.08
M10 (563)	5	0.14±0.05	0.23±0.08
	10	0.29±0.05	0.46±0.08
	20	-	-
	40	0.38±0.17	0.61±0.12
	60	0.32±0.03	0.51±0.05
	80	0.22±0.01	0.35±0.01
	125	0.22±0.04	0.35±0.07
	175	0.23±0.06	0.37±0.09
	250	0.20±0.04	0.32±0.07
	500	0.19±0.04	0.31±0.07
	750	0.21±0.04	0.33±0.06
	1000	0.19±0.03	0.31±0.05
	1500	0.16±0.04	0.25±0.07
	2000	0.15±0.01	0.24±0.01
	2500	0.11±0.04	0.18±0.06
	3000	0.10±0.04	0.17±0.07
	3500	0.09±0.03	0.16±0.05
	3800	0.09±0.02	0.16±0.03
M3(572)	5	1.31±0.06	2.12±0.09
	10	-	(10.11±0.31)a
	15	1.23±0.02	1.99±0.03
	25	0.84±0.01	1.35±0.02
	35	0.65±0.11	1.04±0.17
	75	0.72±0.04	1.16±0.06
	175	0.46±0.04	0.74±0.07
	500	-	-
M3 (622)	5	-	-
	10	0.37±0.03	0.59±0.04
	20	-	-
	50	-	-
	100	0.55±0.04	0.88±0.07
	200	0.40±0.01	0.64±0.01
	400	0.24±0.07	0.39±0.12
	500	(0.45±0.13)a	(0.73±0.21)a
	1000	0.23±0.14	0.37±0.23
	1250	0.17±0.07	0.27±0.11
	1500	0.12±0.07	0.20±0.11
	2000	0.06±0.01	0.09±0.03
M6 (511)	5	0.31±0.03	0.50±0.04

	10	0.21±0.01	0.34±0.01
	20	0.24±0.05	0.38±0.08
	40	0.36±0.04	0.58±0.06
	60	0.13±0.03	0.33±0.04
	80	-	-
	250	-	-
	750	0.24±0.06	0.39±0.09
	1000	0.16±0.03	0.25±0.05
	1250	0.25±0.03	0.40±0.05
	1750	0.13±0.04	0.21±0.07
	2500	0.09±0.01	0.14±0.02
	3000	-	-
	3500	0.13±0.02	0.21±0.03
	4000	0.12±0.03	0.19±0.05
	4273	0.19±0.03	0.31±0.05
M6 (598)	5	0.19±0.03	0.30±0.05
	10	0.13±0.02	0.21±0.03
	40	0.16±0.03	0.25±0.05
	60	0.13±0.05	0.21±0.08
	80	0.33±0.02	0.53±0.02
	100	0.14±0.02	0.23±0.03
	160	0.11±0.03	0.18±0.04
	255	0.24±0.08	0.38±0.12
	750	0.10±0.02	0.16±0.04
	1500	0.07±0.02	0.11±0.03
	2000	0.03±0.03	0.05±0.04
	3000	0.09±0.01	0.14±0.02
	4000	0.09±0.06	0.15±0.09
	4168	(0.42±0.12)a	(0.68±0.19)a

12. Recovery test with ICP-MS technique

To further validate the response and selectivity of the CL method for Mn(II) analysis, it was compared to an Inductively Coupled Plasma Mass Spectrometer (ICP-MS) 7500ce (Agilent) method, which is highly selective (mass specific detection) method for trace metals. The objectives here were to compare the CL detection system with an independent determination step (ICP-MS), and also to examine the recovery of the Mn using the Toyopearl resin. An inter-comparison experiment was performed using Mn-stripped OMEX (North Eastern Atlantic Ocean) seawater with a range of standard additions of Mn(II) (0, 90, 180, 300 and 360 nM) to calibrate ICP-MS. As formic solution (0.1M formic acid+H_2O_2+12mM NH_4OH) was used to elute Mn from the resin in FIA-CL analysis, thus, it was also used in this ICP-MS analysis as well. The calibration of the ICP-MS method was

excellent with R^2 = 0.992, a slope of 0.021 and an intercept of 0.042 (Figure III43) for counts per second against added Mn(II) concentrations.

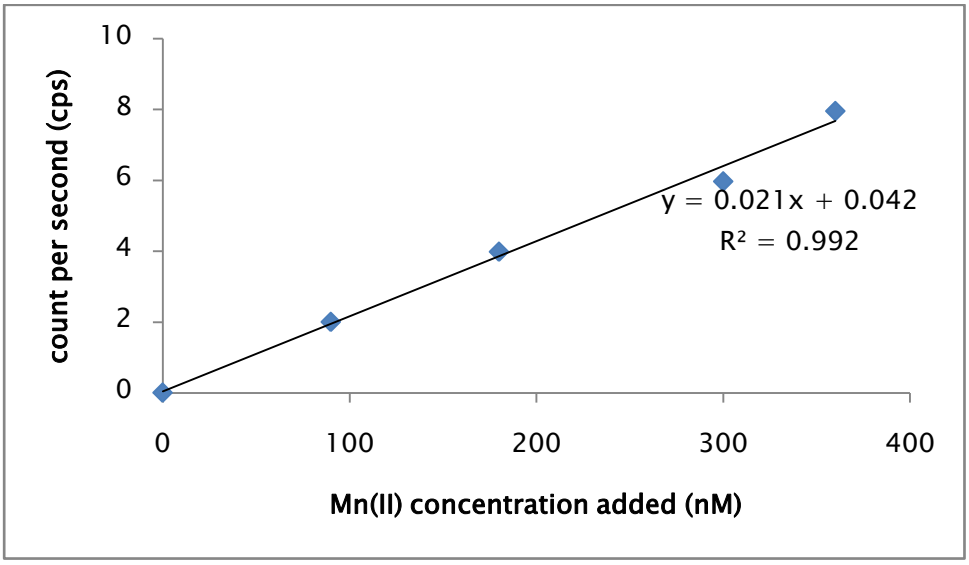

Figure III43. Standard calibration of Mn(II) for ICP-MS method (with pre-concentration step) showed a good linear relationship.

Recovery of the Mn-FIA-CL-Toyopearl Chelate 650M was determined by adding 20 nM Mn(II) into the 50 mL of Mn-stripped seawater and pre-concentrating it onto the Toyopearl Chelate AF 650M resin for 15 minutes, with the pump speed of 3.0 mL/minute. The reason of using high concentration of Mn(II) was to make it easier to get a profound result to fit in the calibration curve showed in Figure III43. Later, the pre-concentrated Mn was eluted using the formic eluent for 1.11 minutes (times for formic eluent to completely flush the pre-concentrated Mn(II) from the Toyopearl resin into the acid-cleaned collecting bottle) at the same pump speed. Seawater without any standard addition was also examined in order to check the concentration of Mn(II) that was already in the seawater. Three replicates of both seawater and seawater+20 nM Mn(II) addition were analysed using the ICP-MS (7500ce, Agilent) at the University of Portsmouth with the help from Dr. Gary Fones.

In theory, all the Mn in 50 mL of seawater or seawater+20 nM Mn(II) addition should be pre-concentrated onto the Toyopearl column, and after eluting for 1.11 minutes at the same pump speed, ~3.33 mL of formic acid solution should be collected for analysis by ICP-MS. By calculation, approximately 270 nM of Mn should be present in this ~3.33 mL solution. However, the experimental values were more or less than the theoretical values, and the calculation of seawater and seawater+20 nM Mn(II) addition volumes and concentrations are shown in Table III15, which was then used to calculate the percentage recovery value of Mn.

Table III16. Theoretical and experimental values for recovery test using ICP-MS technique. (1) is replicate 1, (2) is replicate 2, and (3) is replicate 3; sw is Mn-stripped seawater.

	Theoretical value	Experimental value
Volume of sw+20 nM Mn pre-concentrated onto the Toyopearl resin column	50 mL	49.34 mL (1) 49.62 mL (2) 49.94 mL (3) Average = 49.63 mL
Volume of the formic eluent passing through the Toyopearl resin column	3.33 mL	3.41 mL (1) 4.18 mL (2) 3.53 mL (3) Average = 3.71 mL
The concentration of Mn (II) in sw+20 nM Mn(II) addition	270 nM	(values from ICP-MS) 276 nM (1) 237 nM (2) 259 nM (3) Average = 268 nM
The concentration of Mn(II) in sw		(values from ICP-MS) 0.60 nM (1) 1.57 nM (2) 0.60 nM (3) Average = 0.92 nM
True Mn concentration value		275.40 nM (1) 235.43 nM (2) 258.40 nM (3) Average = 256.41 nM

A percentage recovery value was calculated by dividing the average value of the true Mn concentration value (Table III16) with the theoretical value of the concentration of Mn(II) in sw+20 nM Mn standard addition to give around 95 % as showed below:

(256.41 / 270)*100% = **94.97 %**

13. Figures of merit

All calibrations were performed daily by standard addition from a 1000 mg/L manganese standard solution (ASSURANCE certified reference material) to Mn-stripped OMEX seawaters. A 5 point calibration line (0, 0.5, 1.0, 2.0, and 4.0 nM Mn standard additions) and blank determination were made (Figure III44). The average dissolved Mn concentration in the seawater used to prepare the standard calibration was calculated from the intercept of the calibration knowing the blank of the system (Figure III44). The concentrations of Mn in the seawater samples were calculated from the slope of the daily calibration curve obtained. Precision of measurements were summarized in Table III17 and Table III18.

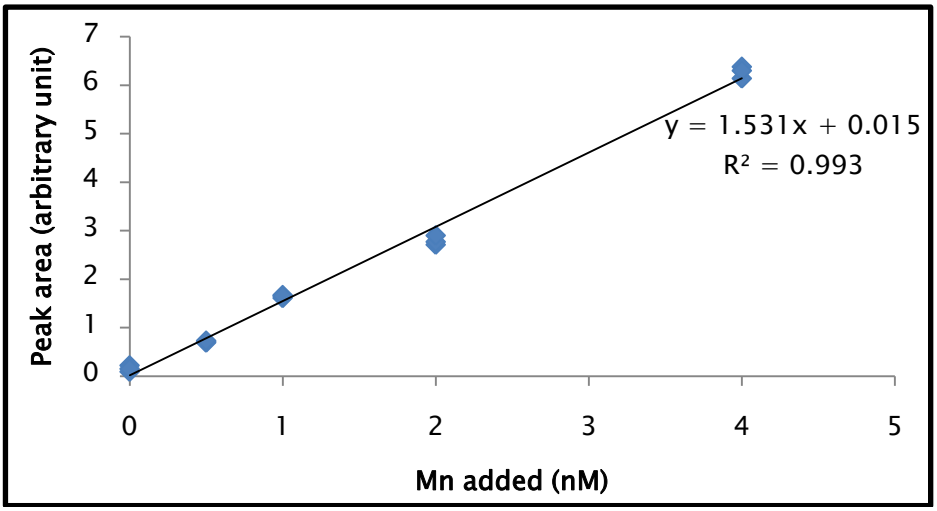

Figure III44. Example of calibration curves by standard additions to acidified (pH~1.7) filtered (<0.2 µm) seawater from tropical North-Eastern Atlantic+OMEX for 3m mixing coil. Mn(II) in the seawaters were stripped off before used. Five point calibration line (0, 0.5, 1, 2, 4 nM) were made.

Table III17 showed ranges of figures of merit for Mn(II)-FIA-CL analyser calibrations with 3 m and the NTA resin column as CC1. The instrument blank was determined by measuring MQ water through a standard addition method. This blank takes into account any potential Mn contamination from the reagent, column-conditioning solution as well as the system manifold (tubing, valves, etc.). A series of replicate analyses (n=5) of MQ water blank with the pH were adjusted to pH~8.5 gave an average blank value of 0.13 nM, a standard deviation of ±0.033 nM, and hence, a detection limit of 0.10 nM. Detection limit is three times of the standard deviation. The precision (rsd) is in a range of 0.09 – 4.22%, with an average of 1.83%.

Table III17. Ranges of figures of merit of 5 calibration curves with the NTA resin column as CC1. Calibrations were fitted with a linear trendline. *rsd* = relative standard deviation (*n* = 3-4). Detection limit (DL) defined as three times the standard deviation of the blank. BDL = below detection limit.

Correlation, R^2	Slope	Precision, *rsd (%)*	Blank (nM)	DL (nM)
0.988	2.484	0.09 – 1.50	0.30±0.10	0.30
0.833	2.142	0.30 – 3.45	0.03±0.02 (BDL)	0.06
0.997	2.571	1.05 3.55	0.11±0.01	0.03
0.991	1.921	0.30 – 4.22	0.17±0.02	0.06
0.981	3.208	0.19 – 3.57	0.06±0.02	0.06
range: 0.833 – 0.997 (mean:0.960)	range: 1.921 – 3.208 (mean:2.465)	range: 0.09 – 4.22 % (mean: 1.83%)	range: BDL – 0.30 nM (mean: 0.130±0.033 nM)	range: 0.03 – 0.30 (mean: 0.099 nM)

However, when the 8-HQ resin was replaced the NTA resin as a CC1, the blank was further reduced to 0.06 nM, a standard deviation of ±0.026 nM and thus, a limit of detection of 0.077 nM. The precision (rsd) is in a range of 2.00 – 12.00%, with an average of 5.50%.

Table III18. Ranges of figures of merit of 3 calibration curves with the 8-HQ resin column as CC1. Calibrations were fitted with a linear trendline. *rsd* = relative standard deviation (*n* = 3-4). Detection limit (DL) defined as three times the standard deviation of the blank. BDL = below detection limit.

Correlation, R^2	Slope	Precision, *rsd (%)*	Blank (nM)	DL (nM)
0.993	1.582	3.61 – 3.18	0.09±0.06 (BDL)	0.18
0.996	1.589	2.00 – 12.00	0.16±0.01	0.03
0.953	2.838	3.58 – 8.63	0.03±0.007	0.021
range: 0.953 – 0.996 (mean:0.981)	range: 1.582 – 2.838 (mean:2.003)	range: 2.00 – 12.00 % (mean: 5.50%)	range: BDL – 0.16 nM (mean: 0.060±0.026 nM)	range: 0.03 – 0.30 (mean: 0.077 nM)

The accuracy of this Mn(II)-FIA-CL-Toyopearl method with 3m mixing coil was tested by analysing certified reference materials (CRMs) obtained from the National Research Council of Canada, NASS-5 standards and with SAFe samples (SAFe S (surface water), and SAFe D2 (deep water)). The method conditions were kept as in sub-Section 8.2, and Section 11 with Figure III44, earlier in this Chapter (*i.e.* the use of the Toyopearl resin to pre-concentrate Mn, the NTA resin as CC1 (*see* sub-Section 8.2), the 8-HQ resin as CC1 (*see* Section 11), loading and eluting time was kept at 200 s, and with the used of the same reagents solution). Prior to analysis the pH of the CRM samples were adjusted with ammonia solution (Romil UpA) to pH ~8.5. All values were blank corrected and the values were in the range of the given certified values. Thus, the agreement between results obtained from this study and certified value are very good (Table III19).

Table III19. The NASS-5 values (nM) for the analyser with the NTA resin column as a CC1 was not good and has a significant different with the certified value, but the NASS-5 values (nM) for the analyser with the 8-HQ resin column as a CC1 obtained in this study showed a good consistency with the certified values (nM) given (National Research Council, Canada).

CRM	Certified value (nM)	This study value (nM)
NASS-5	16.73 ± 1.04	20.63 ± 0.69 (n=4) (with 3 m mixing coil, NTA resin as cleaning resin) 16.53 ± 0.60 (n=4) (with 3 m mixing coil, 8-HQ resin as cleaning resin)

Analysis of SAFe samples with 3 m coils was showed in Table III20. SAFe S value with NTA resin is 1.27±0.07 nM, and with 8-HQ resin 0.77± 0.07 nM. Value for 8-HQ resin is about the same with the value obtained by Middag *et al.* (2011a,b), which was also used 8-HQ resin as a cleaning resin in their analyser. Values of SAFe D2 with NTA is 0.43±0.04 nM and with 8-HQ is 0.27 ± 0.04 nM. These differences were related to the interference issues which were resolved in Sections 9 and 10 of this Chapter. This value is also shows good agreement with the 'consensus value' (http://es.ucsc.edu/~kbruland/GeotracesSaFe/SAFe%20ReferenceSample-Mn.pdf) of 11 participating laboratories which are 0.825±0.079 nM for SAFe S and 0.371±0.070 nM for SAFe D2. All SAFe S and D2 values were blank corrected.

Table III20. The SAFe values between the consensus values, 3 m coil with two conditions were applied: with NTA and 8-HQ resins as a cleaning resin (CC1).

SAFe sample	Consensus value (nM)	3 m coil value (nM) (NTA)	3 m coil value (nM) (8-HQ)
SAFe S 256	0.825±0.079	1.27±0.07	0.77 ± 0.07
SAFe D2 233	0.371±0.070	0.43±0.03	0.27 ± 0.04

14. Summary

Development of a manual Mn(II)-FIA-CL analyser to detect Mn(II) concentrations in seawater

The Mn(II)-FIA-CL-Toyopearl technique set up here was initially based on the system of Doi *et al*. (2004). This technique was chosen because it is simple, used relatively low cost equipment, the closed system reduced the risk of airborne contamination, and it allowed near real-time determination of Mn(II) with a small volume of seawater. Development of the method however, proved difficult. The main problems were with the pre-concentration step, mixing coil length, CL reaction and interferences. Initially, a 1m mixing coil length was used based on the assumption that a longer mixing coil would waste the reagents. Moreover, a 1m mixing coil gave a good measurable CL signal for high Mn(II) concentrations. The commercially available Toyopearl AF-Chelate 650M resin that was used to pre-concentrate Mn(II) in seawater was packed in a Perspex column, and Mn(II) in seawater was quantitatively collected onto the resin at the pH ~8.5.

However, the seawater matrix is complex and may create interferences during the detection step and enhance the baseline level. Thus a MQ washing step was needed to

remove sea-salts present in the dead volume of the Toyopearl column. The cleaning resin of the NTA Superflow resin column was placed in series with the Toyopearl resin column, to remove the interference of Fe and Cu ions. Adding the NTA resin as a cleaning resin reduced the baseline level and the blank. When 'old' luminol stock solution was used in the analysis the baseline level increased and made the CL peak shorter and broader, thus, the luminol stock solution was freshly made every week, and luminol+TETA solution was made every day to ensure a low baseline.

However, there were analytical challenges occurred during the processes of improving and optimising the performance of the system: (1) problem with pH conditions on adsorption and desorption of Mn(II) onto/from the Toyopearl resin, and on the CL reaction; (2) problem of poor reproducibility and double peak for low Mn(II) concentration samples; and (3) poor calibration. Extensive works were carried out in order to find the sources of the problems and to solve them as they arouse. (1) The resin uptake/release and the CL reaction were pH depended. It was very important to ensure that standard/sample and reagents to be in the correct pHs to perform a good analysis. Therefore, the optimum pH of ~8.5 to adsorb and pH of 2.9 to desorb Mn(II) from the Toyopearl resin, and the optimum pH of 10.2 for the CL reaction to occur were chosen after testing with a range of pH conditions. (2) There were several limitations in this system that caused problem with poor reproducibility when low concentrations of Mn(II) (≤0.5 nM) were analysed: very small or no CL peak signal obtained, negative peak formed before the CL peak, second peak appeared during the rinsing step, and higher and bigger baseline level and noises. Several components and parameters (*i.e.* tubing system, valves, peristaltic pump, NI DAQ-MX card, and power supply) of the system were tested to investigate their influences on the reproducibility. However, only little improvement was showed *i.e.* second peak appeared during the rinsing step was vanished. Given that most of the above experiments showed little improvement on CL peak signal, it was hypothesised that poor reproducibility was due to other factor, such as the shorther mixing coil length, as too little reagent mixing resulted in higher baseline level and noises, as observed by Chapin *et al.* (1991). This problem was investigated. (3)The calibration curves of standard additions of Mn(II) to acidified filtered seawaters did not showed positive curvature as expected. In almost all cases, calibrations showed the highest concentration (4nM standard addition) typically gave a lower signal, resulting in a negative curvature curve. From the extensive works carried out, it was found borate buffer that was used to adjust the pH of the standard solutions introduced contaminations into the spiked seawaters and also might have diluted the most concentrated standard. Therefore, the borate buffer was replaced with the 20 µM ammonia solution, as only small amounts (~30µL) of ammonia solution were needed to bring the pH to~8.5 and gave linear calibration, compared to borate buffer which required ~300 µL per 25 mL standard/sample solution.

Standard calibrations (with the ammonia solution used to adjust the pH of the standard solutions) were performed daily with 5 points calibration line (0, +0.5, +1.0, +2.0, +4.0). The precision of the standards ranged from 0.05% to 15.75% rsd (n=17) with replicates of 3-4 peaks per standard, and the average precision of total 180 samples from surface seawater of the tropical North-Eastern Atlantic Ocean analysed is 4.15% rsd (n=3-4), depending on the quality of the CL peak signal. The average reagent blank is 0.08 nM with the detection limit of 0.06 nM. However, when CROZEX samples were analysed, it was difficult to get a measurable CL peak signal due to low Mn(II) concentration, higher and instability of the baseline level, and probably lack of chemical mixing because of shorter mixing coil length.

As one of the aims of this project was to analyse seawater samples collected during the D326 (surface Tropical North-Eastern Atlantic Ocean) and CROZEX (around the Crozet Islands of the Southern Ocean) cruises, it was decided to further modify this Mn(II) technique to solve the problems with the method used here.

Development of an automated Mn(II)-FIA-CL analyser to detect Mn(II) concentrations in seawater

The Mn(II)–FIA-CL–Toyopearl technique set up here was a further modifications of the method used in the previous Section. Given the extensive experience gained through working on this Mn(II) technique, the development and optimisation of this modified version to determine lower concentrations of Mn(II) in seawater was relatively rapid. Problems highlighted at the end of the section were successfully resolved by changing the mixing/reaction coil to the longer one (3m). Further optimisations and modifications were done and the FIA-CL system eventually gave better calibration, lower baseline level, enhanced sensitivity and accuracy at low concentrations. However, the interferences with other trace metals were detected in the longer mixing coil. The NTA resin which was initially used as the first cleaning resin column (CC1) in the system to remove the interference of other metals, particularly Fe and Cu, could not retain all of the interfering elements at the pH2.9 of the formic eluent. When an 8-HQ resin replaced the NTA resin, the interferences were subsequently eliminated after a number of experiments were carried out to investigate the efficiency of removing the metals interferences by using the 8-HQ resin. The 8-HQ resin column was also used as a second cleaning resin column (CC2), which was placed after the luminol solution in the system to remove impurities in the TETA and luminol solutions.

Most importantly, these modifications reduced the total interference of other trace metal elements values, from ~0.25 to <0.01 nM Mn(II) equivalent. In addition, these further modifications also removed problems encountered with the negative peak formed before

the CL peak. These further modifications resulted in a low blank value for (1) with 8-HQ resin is 0.06 nM and detection limit is 0.077 nM compared to (2) with NTA resin is 0.13 nM and detection limit is 0.099 nM. Standard calibrations were performed daily with 5 points calibration line (0, +0.5, +1.0, +2.0, +4.0 nM of Mn(II)). The precision of the standards ranged from 0.09% to 4.22% rsd with an average of 1.83% (with NTA resin), and from 2% to 12% with an average of 5.50% (with 8-HQ resin), with replicates of 3-4 peaks per standard, depending on the quality CL peak signal. The NASS-5 manganese was found to be slightly higher (20.63±0.69 nM) than the certified value, when the NTA resin was used as a cleaning resin. The most likely reason was Ni interference or/and random contamination during handling. However, the NASS-5 manganese value was in a good agreement (16.53±0.60 nM) with the certified value, when the 8-HQ resin was used in replaced of the NTA resin. The SAFe values of SAFe S 256 and SAFe D2 233 when the NTA resin column was used as a CC1in the system were 1.27±0.07 nM and 0.43±0.03 nM, respectively. Whilst the SAFe values for S 256 (0.77±0.07 nM) and D2 233 (0.27±0.04 nM) was reduced when the 8-HQ resin column was used, which showed an exceptionally good agreement with the '*consensus values*'.

Therefore, this newly optimised method was then applied to the re-analysis of selected full depth profiles (BA 567, BA+1 568, BA+2 569, M3 496, M2 502) of seawater samples from around the Crozet Islands in the Southern Ocean. The different between the new (with 8-HQ resin as CC1) and the old (with NTA resin as CC1) data were calculated in a range of 55, 35, 30, 33 and 37% to give an average of 38% reduction of Mn(II) concentrations of the new values. However, due to time constraints, further analyses of the remaining samples from other Stations were not possible. The values however, were estimated to reduce approximately 38% than the old values, assumed that they would follow on the trend showed for re-analysed samples. Further discussion of these data is given in the next Chapter.

Chapter IV: Dissolved Manganese around the Crozet Islands, Southern Ocean

1 Introduction

The Southern Ocean is considered to be the largest High Nutrient Low Chlorophyll (HNLC) ocean (de Baar *et al.,* 1995), plays a key role in climate regulation and is the most sensitive oceanic region to climate change (Sarmiento *et al.*, 1998). Across most of the Southern Ocean, despite the abundance of the macro-nutrient content of surface waters transported by the easterly flowing Antarctic Circumpolar Current (ACC), chlorophyll a (Chl-*a*) concentrations generally remain low and do not exceed 0.5 mg m^{-3} (Comiso *et al.*, 1993; Moore and Abbott, 2002). However, there are areas in the Southern Ocean where there are regular annual phytoplankton blooms (*see* Chapter I) (Pollard *et al.* 2007a), *i.e.* South Georgia Islands, Kerguelen Islands, and Crozet Islands, where annual phytoplankton blooms were hypothesized to be initiated by a natural source of iron supplied from the islands or shallow sediments (Pollard *et al.*, 2007a; Planquette *et al.* 2007).

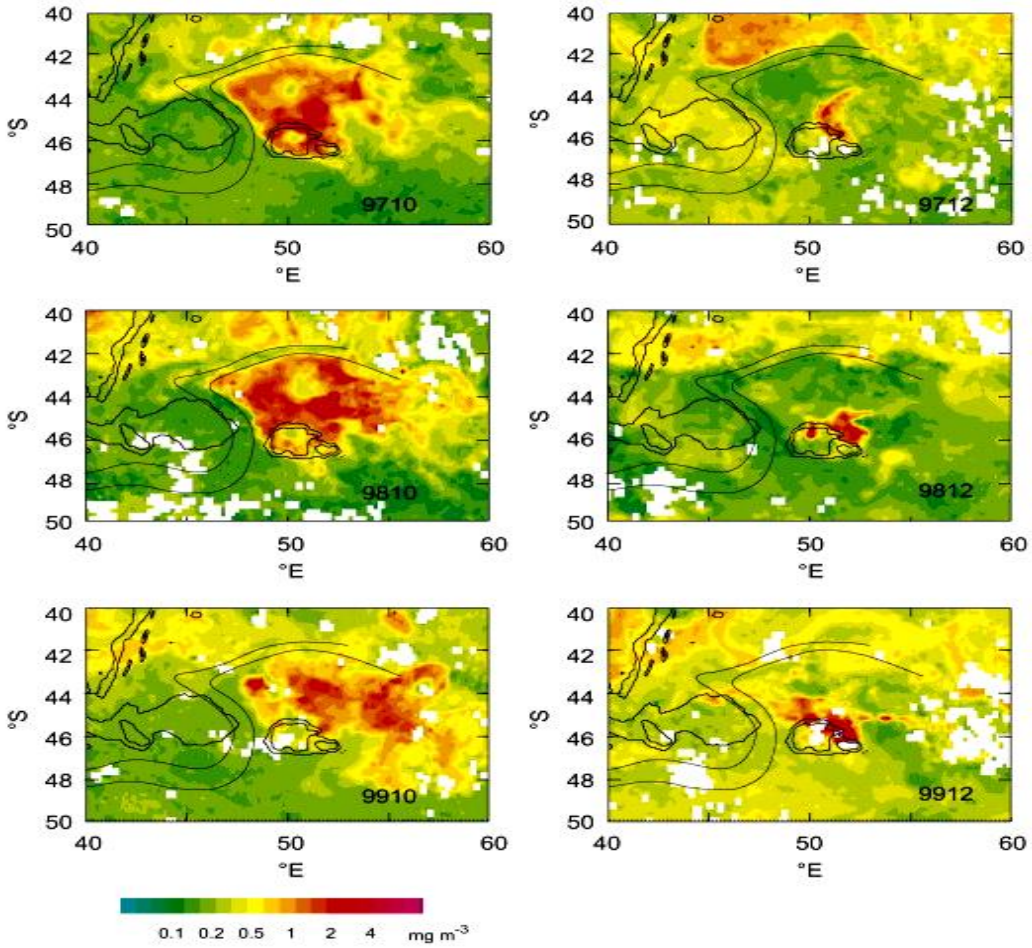

Figure IV1. The SeaWiFS chlorophyll images for the annual phytoplankton blooms occur to the north of the Crozet Plateau in October and December of 1997, 1998, and 1999. Satellite images were taken from Pollard *et al.* (2007a).

SeaWiFS images around Crozet in 1997, 1998 and 1999 (Figure IV1) showed an annual bloom with a rather well defined spatial distribution. The bloom is constrained to the west and north by the Sub-Antarctic Front (SAF) (Pollard and Read, 2001). The surface flow that contacts the Crozet Plateau and Islands was weak and moving to the north (Pollard *et al.,* 2007a). For these reasons, the area around the Crozet (Islands and Plateau) was chosen to examine a natural occurring phytoplankton bloom in the Southern Ocean, particularly around Crozet.

It has been shown that iron is the primary limiting factor for primary production (PP) in the Southern Ocean through a number of artificial iron enrichment experiments both *in situ* and in bottles (De Baar, 1994; de Baar *et al.,* 2005; Boyd *et al.,*2007). A range of other bioactive trace metals are also vital for biological productivity as they are often involved in enzymatic activity or become part of proteins (Morel *et al*., 2003), and these metals may be co-limiting when at low concentrations or toxic at elevated concentrations; their bioavailability strongly depends on complexation with organic ligands (Morel *et al*., 2003). For example, dissolved Mn has been proposed to be a co-limiting factor (Martin *et al.,* 1990), as it has been inferred from lab experiments (Peers and Price, 2004) and in some field experiments (Buma *et al.,* 1991; Coale, 1991). However, the effectiveness of experiments at sea is often disputed because the response of a phytoplankton bloom could not be observed clearly (Buma *et al.,* 1991; Scharek *et al.,* 1997; Sedwick *et al.,* 2000), suggesting that in some parts of the Southern Ocean the ambient concentrations of dissolved Mn are in sufficient supply (*i.e.* not limiting).

Mn is an important micronutrient which is required in enzymes for various biological processes in cells (see Chapter 1), particularly in the Photosystem II (PS II). (*e.g.* Sunda and Huntsman, 1983). Thus the availability of Mn is crucial, especially under Fe deficient conditions.

The multidisciplinary and complex CROZet natural iron bloom and EXport experiment (CROZEX) was carried out to examine the causes and consequences of the annual bloom that forms at the north of the Crozet Plateau in the Southwest Indian Ocean sector of the Southern Ocean. The CROZEX project, confirmed that Fe released from the Crozet Islands and Plateau (Planquette *et al.,* 2007) supports an annual bloom and leads to an increase of the C export (Pollard *et al.,* 2009). Meso-scale circulation constrains the phytoplankton bloom to the north of the islands, providing an ideal location to compare the behaviour of manganese in the naturally induced bloom with HNLC conditions south of the archipelago.

Therefore, seawater samples that were collected during CROZEX were analysed for dissolved manganese. This provided an excellent opportunity to study how any natural source of dissolved manganese (either directly from the islands or from the shallow

surrounding sediments) that may be released from the islands could possibly enhance the growth of phytoplankton. This is the first report of dissolved (<0.2 µm) manganese concentrations in this area and in this chapter, these new data are presented. Sampling, sample processing and study sites are briefly described before presenting the results in detail and discussing the data.

2 Study area and sampling sites

Crozet (46°S, 52°E) is located in the western Indian Sector of the Southern Ocean, approximately 2500 km southeast of South Africa. It consists of a shallow plateau, and has two main islands, Île de la Possession and Île de l'Est (Figures IV2 and IV3).

Samples were collected for dissolved manganese analysis during the CROZEX cruises (D285 and D286) on board *RRS Discovery.* RRS Discovery cruise 285 departed from Cape Town, South Africa on 3 November 2004, docking at Port Elizabeth 37 days later on 10 December. Leg 2, RRS Discovery cruise 286 departed on 13 December and docked at Durban 39 days later on 21 Jan 2005. Nine major hydrographic (M1 – M10) Stations around the Îles Crozet were sampled (Figures IV2 and IV3), and in some cases there were repeat visits. These islands are the surface projections of the Crozet Plateau (~1220 km x ~600 km), and the islands were hypothesized to provide a direct input of trace metals (and especially iron) to surrounding waters (Bucciarelli *et al.,* 2001; Planquette *et al.,* 2007, 2009).

The main stations for water sampling and other physical observations were established at the strategic locations shown in Figures IV2 and IV3 and are:

(1) The Central Sites: Stations M3 (casts [note that from here onwards individual three figure numbers refer to specific casts at a Station] 496, 572, 622),
(2) The Island Sites: Baie Americaine (BA) Sites (near the main island Île de la Possession): Stations BA (567), BA+1 (568), BA+2 (569); cast 567 was closest to the island and cast 569 furthest away
(3) The Southern Sites: Stations M6 (598, 511) and M2
(4) The Northern Sites : Stations M1, M7, and M10

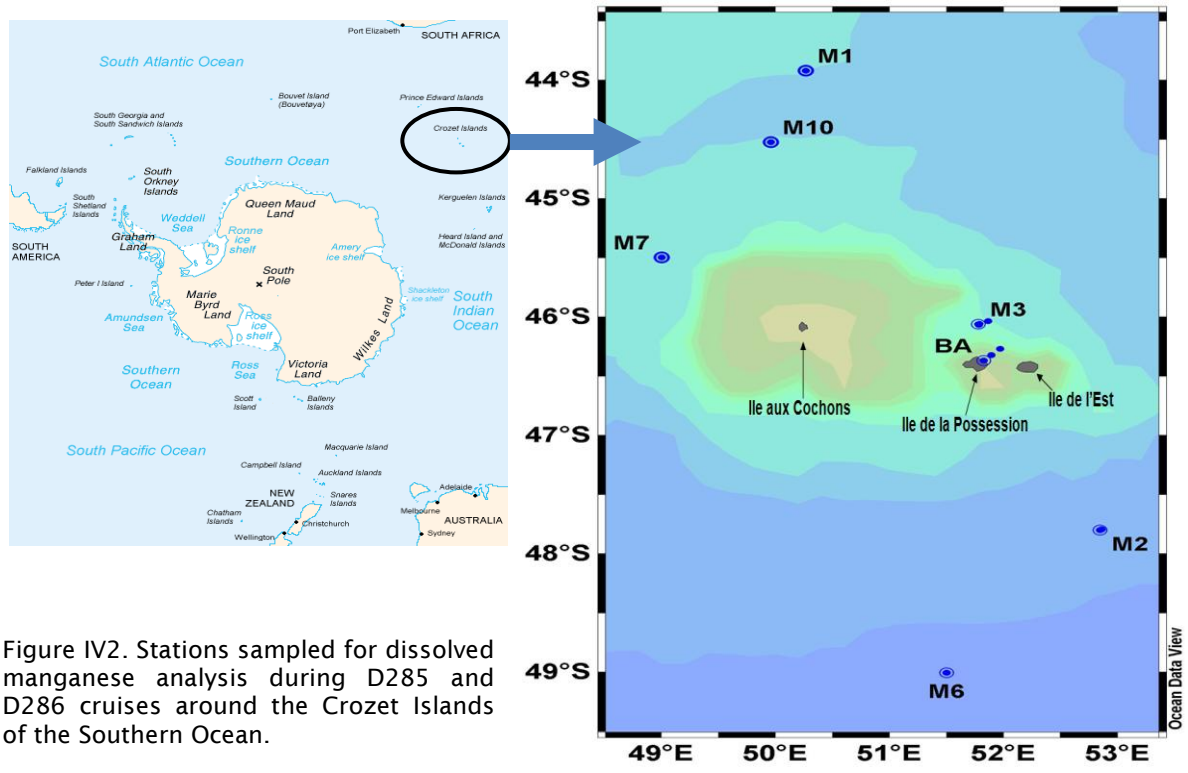

Figure IV2. Stations sampled for dissolved manganese analysis during D285 and D286 cruises around the Crozet Islands of the Southern Ocean.

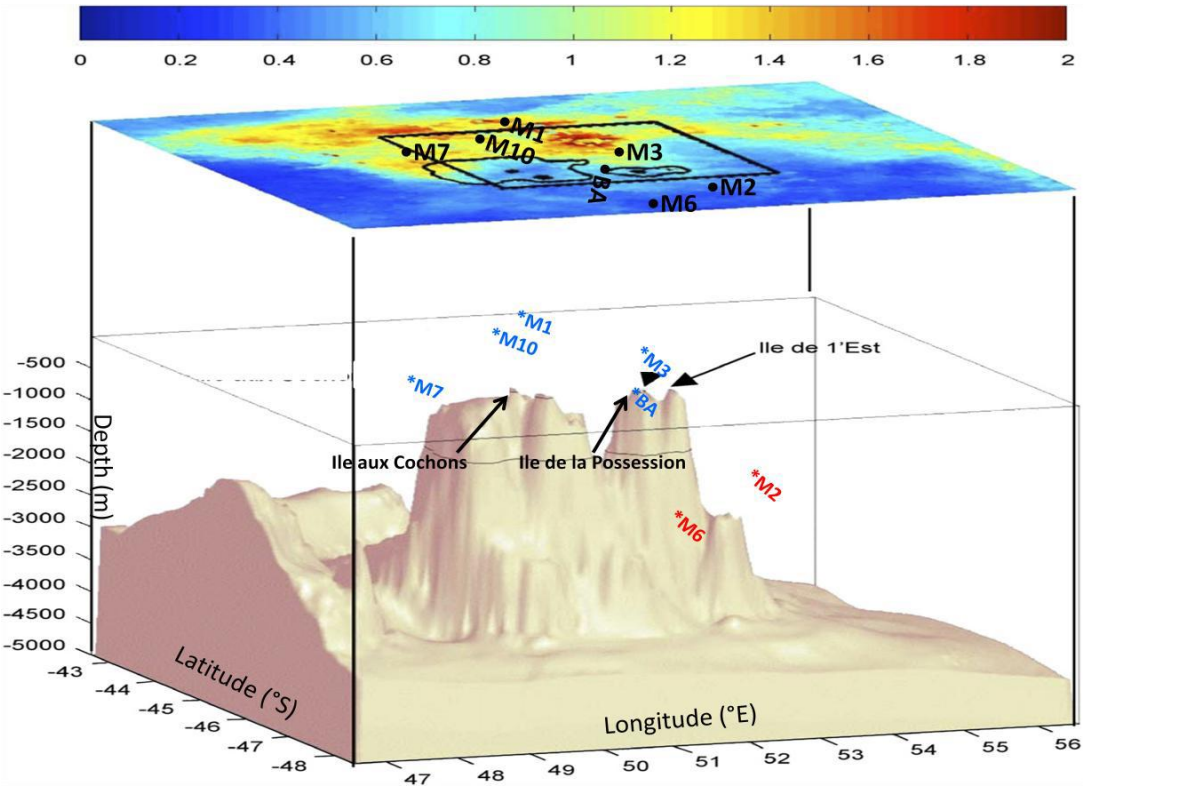

Figure IV3. Crozet Islands topography combined with stations sites and SeaWIFS Chl-*a* concentrations averaged image over the austral summer 2004-2005. Stations located at or near the bloom area are in blue. Stations far from the bloom area are in red. BA stands for the 3 stations occupied in Baie Americaine on Ile de la Possession. Station M3 was occupied several times during the cruises.

3 Sampling and Sample Processing

Clean techniques for seawater sampling, sample processing and sample acidification have been thoroughly explained in Chapter II.

4 Dissolved Manganese Analysis

Analysis of dissolved manganese concentrations were performed after the cruise with the FIA-CL method originally developed by Doi *et al*. (2004) with the significant development and modifications described in Chapter III (*see* Section 13) by using the low level optimised method using the 8-HQ resin to remove interference with other metals (*e.g.* Ni, Fe and Cu). All data presented in this chapter and in the figures have been made using the modified method in which Ni interferences have been removed.

5 Results

5.1. Hydrography

The hydrography and the mesoscale circulation (Figure IV4) of the Crozet Islands have been fully described by Pollard *et al.* (2007b) and Read *et al*. (2007). Briefly, the topography of the Crozet Plateau (including Del Caño Rise) forms the most important feature that influences the surroundings flow. The strongest flow through the area is the Agulhas Return Current (ARC) adjacent to the Subtropical Front (STF), which flows from west to east with strong meanders as it crosses the Southwest Indian Ridge, and then slowly turns to the southeast to cross 60 °E at 44 °S. Further south, the SubAntarctic Front (SAF) constrains the Antarctic Circumpolar Current (ACC) that brings the HNLC waters from west to east, and they turn north throughout the gap between the Rise and the Crozet Plateau (Figure IV4). Central, Northern and Western Sites are bounded to the west and north sides of the Rise by the SAF, thus they received little influence from subtropical waters. However, there is evidence of eddies penetrating from the SAF (Pollard *et al.,* 2007b; Read *et al.,* 2007) causing the bloom patchiness (seen as variable high Chl-*a*) observed in the satellite imagery for up to 2 months (Venables *et al.,* 2007).

Waters in the bloom area (around Stations M1, M7, and M10) have been in contact with the volcanic sediments of Crozet (Planquette *et al*., 2007). Surface waters (Salinity (S) < 34.0) had similar features to those found in a nearby station by Read *et al.* (2007) and were related to Sub-Antarctic Surface Water (SASW) (Figure IV5). The upper 300 m of the water column at the Central Sites (Stations M3 (496, 572, 622) and BA (567, 568, 569)) were also identified as SASW by Charette *et al*. (2007) based on radium (Ra) isotopes (*i.e.* ^{226}Ra activities). Attributions of intermediate and deep waters at the Central Sites are rather difficult and it was suggested they are a mixture of Antarctic Intermediate Water (AAIW)

and Circumpolar Deep Water (CDW) (Charette *et al.,* 2007), which is commonly subdivided between Upper Circumpolar Deep Water (UCDW) and Lower Circumpolar Deep Water (LCDW). The UCDW has a relative temperature maximum induced by the colder overlying AAIW. The LCDW has a salinity maximum due the influence of the relatively warm and saline water from the north.

Southern Stations (Stations M6 and M2) were chosen as controls and are representative of typical HNLC conditions, although Argo floats show that water from the islands or the plateau may occasionally reach this site (*i.e.* M2) (Pollard *et al.,* 2007b). Surface waters of the Southern Sites (Figure IV5) showed a subsurface minimum in the potential temperature (θ) (<2.1ºC) typical of Antarctic Surface Waters (AASW) of the Antarctic Zone (AAZ) which confirms that the Southern Sites are immediately south of the Polar Front (PF). This is consistent with a detailed description of water masses around the Crozet Plateau and Basin reported by Read *et al.* (2007) and Park *et al.* (1993). Intermediate waters from about 300 m to 1000 m were assumed to be AAIW in agreement with the water mass classification adopted in a nearby station (Charette *et al.*, 2007). The water mass from 1000 m to ~2000 m probably corresponds to CDW. More saline (S > 34.77) waters of the underlying water mass possibly correspond to LCDW centred at 2000 m. Waters below 3500 m are colder and fresher (θ< 0.2 and S < 34.71) and correspond to Antarctic Bottom Water (AABW). It was reported that AABW passes close to the Crozet Plateau on its way to the Indian Ocean (Park *et al.,* 1993).

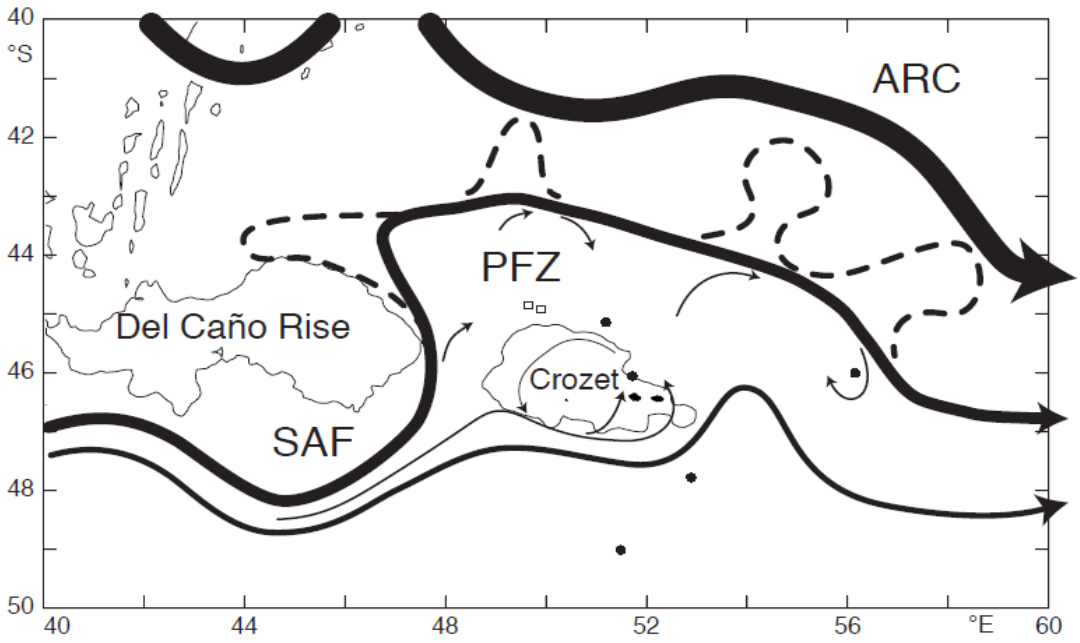

Figure IV4. The circulations in the vicinity of the Crozet Plateau of the Southern Ocean. ARC: Agulhas Return Current; PFZ: Polar Frontal Zone; SAF: SubAntarctic Front (After Pollard *et al.* (2007b)).

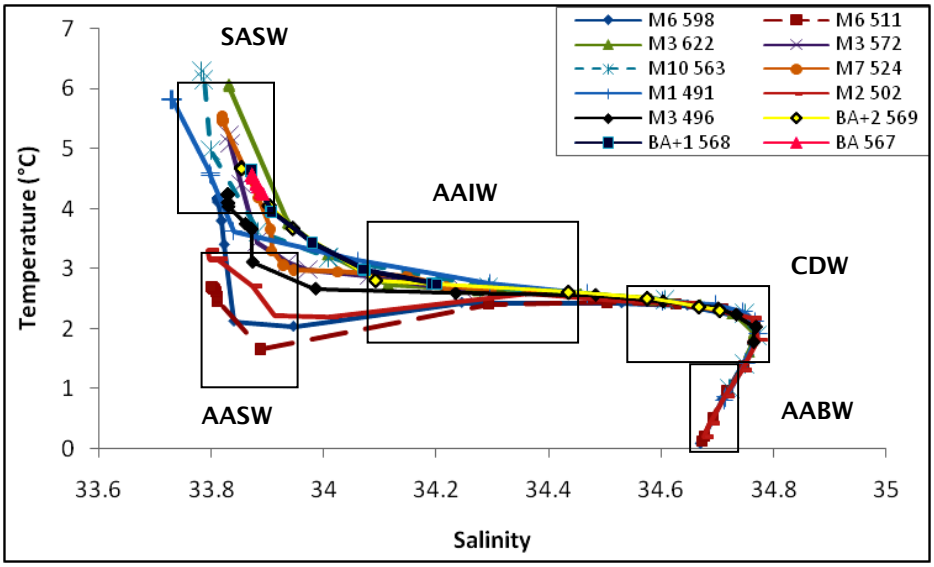

Figure IV5. Diagrams of potential temperature (°C) versus salinity in the whole water columnat the stations sampled for trace metals determination (*i.e.* Northern, Central, Western and Southern Sites). SASW: Sub-Antarctic Surface Water. AASW: Antarctic Surface Waters. AAIW: Antarctic Intermediate Water. CDW: Circumpolar Deep Water. AABW: Antarctic Bottom Water.

5.2 Chl-*a*, dissolved Mn, and macronutrients in the water column upper layer

An annual phytoplankton bloom occurs north of the Crozet Plateau, starting in mid-September and continuing to January, as is seen in satellite Chl-*a* images, (Venables *et al.,* 2007). The peak bloom occurred before the sampling period in November, with Chl-*a* concentrations reaching a local maximum of about 8 mg/m^{3}in early November and the bloom then declined in late November (Venables *et al.,* 2007, Figure IV6), and the lowest Chl-*a* concentration was approximately 0.6 mg/m^3. At the end of January, a smaller secondary bloom was observed to the north of the islands. There is a well-defined but low Chl-*a* peak observed at the end of November and at the beginning of December 2004, prior to maximum light availability, indicating that the Southern Sites are not light limited at the time of peak Chl-*a* concentrations (Venebles *et al.,* 2007). After this, the chl-*a* concentrations are low, similar to background Southern Ocean levels (Venables *et al.*, 2007).

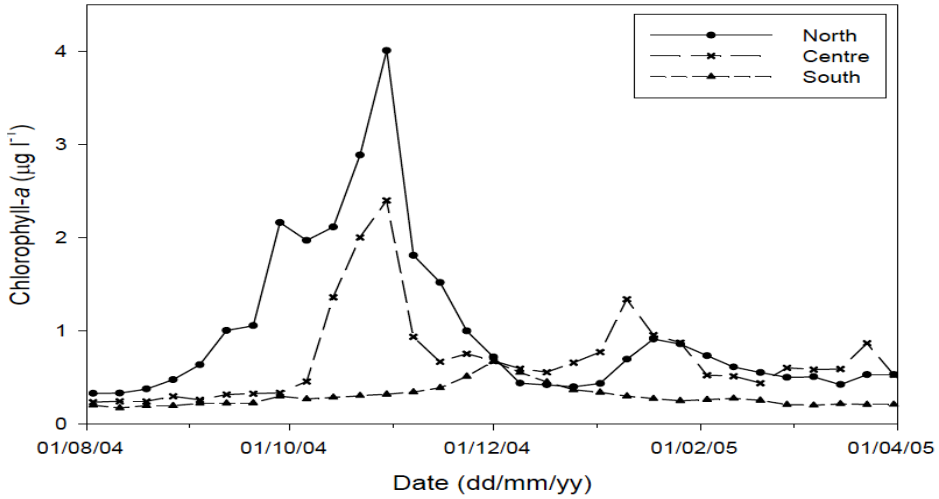

Figure IV6. Remotely sensed temporal progression of chl-*a* in the north, centre and south. Data taken from Venables *et al.* (2007).

Figure IV7-IV17 shows the comparison of Chl-*a,* macronutrients (phosphate, dissolved silicon, and nitrate), and surface concentrations of dissolved manganese during the sampling period, and these data can be examined to investigate possible organism-Mn interactions.

The concentration of dissolved manganese in the upper surface layer (SASW and AASW) to the north and west of the Crozet Islands in the PFZ are generally below 0.75 nM (Figure IV7-IV9). These Northern and Western Sites (*i.e.* Stations M1, M10 and M7) were occupied after the main annual bloom event (Venables *et al.*, 2007), consequently, surface Chl-*a* concentrations were lower than earlier in the year at these Sites. The concentrations of dissolved manganese at the Station M1 (491) and M7 (524) show typical scavenged vertical profiles where the concentrations were highest at the surface and decreased with depth as dissolved manganese was adsorbed onto sinking particles. These surface maximums coincided with lower biomass values. However, concentrations of dissolved silicon were already limiting at M7 as dissolved silicon was fully stripped from the water column in this Northern Site, at which the annual bloom occurred. At Station M10 (563), the concentrations of dissolved manganese showed a nutrient-like profile in the surface layer, with moderate correlation with nitrate, phosphate and dissolved silicon. The Mn subsurface maximum at this station coincided with a gradient in the potential density anomaly (σ_0) where the σ_0 of the surface water was relatively constant to a depth of 15 m before a steep increase in σ_0 with depth was observed.

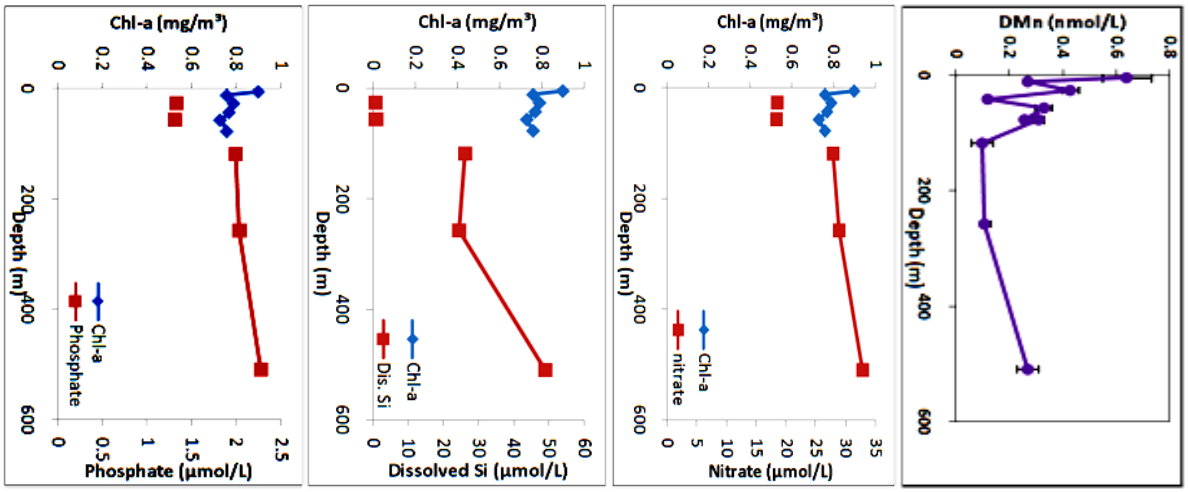

Figure IV7. Chl-a (mg/m³), macronutrients (phosphate, dissolved silicon, nitrate (µM)) and dissolved manganese (nM) at Station M1 (491).

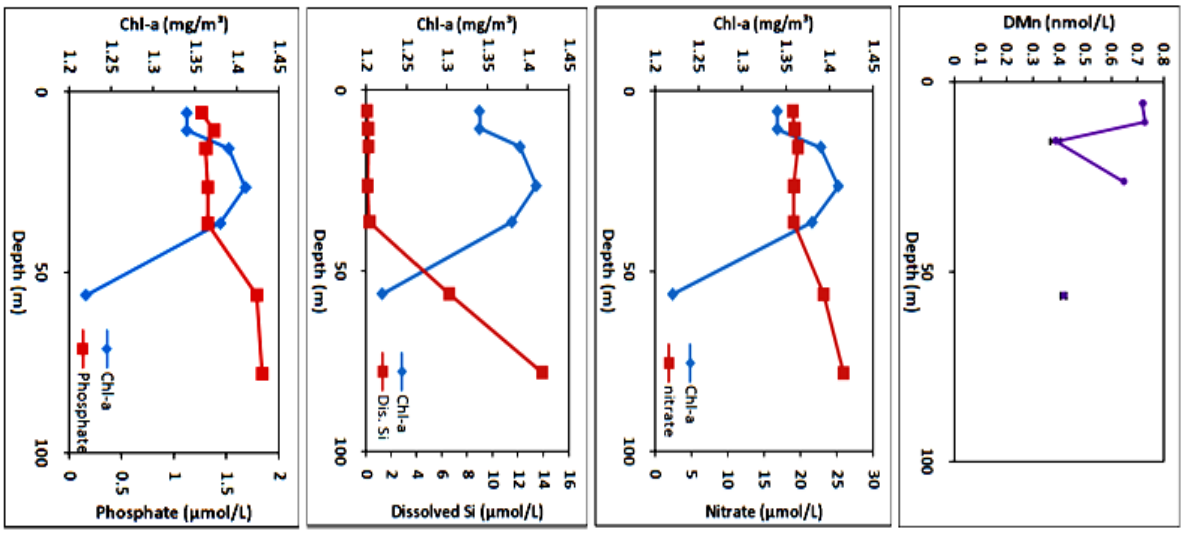

Figure IV8. Chl-a (mg/m³), macronutrients (phosphate, dissolved silicon, nitrate (µM)) and dissolved manganese (nM) at Station M7 (524).

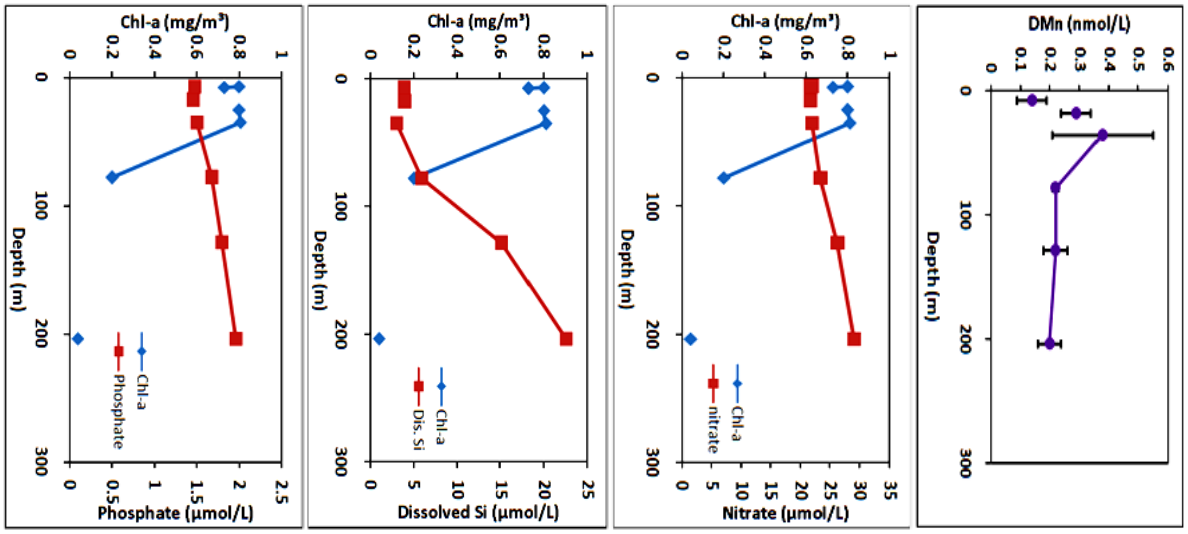

Figure IV9. Chl-a (mg/m³), macronutrients (phosphate, dissolved silicon, nitrate (µM)) and dissolved manganese (nM) at Station M10 (563).

Areas to the south of the plateau were not directly fertilized by the island source of iron as water flow was to the north. Thus the highest nitrate and dissolved silicon were observed around stations M2 and M6 in the HNLC waters with > 25 µmol L^{-1} nitrate and up to19 µmol L^{-1} dissolved silicon, which are well away from the bloom areas (Figure IV10 – IV11). A small bloom was observed around Station M2 that was linked to water that had circulated anti-cyclonically around the Crozet Plateau collecting Fe, and reached Station M2 (Pollard *et al.*, 2007b). This water had been in contact with the plateau and may have had enhanced manganese concentrations. Consequently, the concentrations of dissolved manganese at Station M2, which is located northeast of Station M6, were higher than at M6 where there was no similar water input from the north.

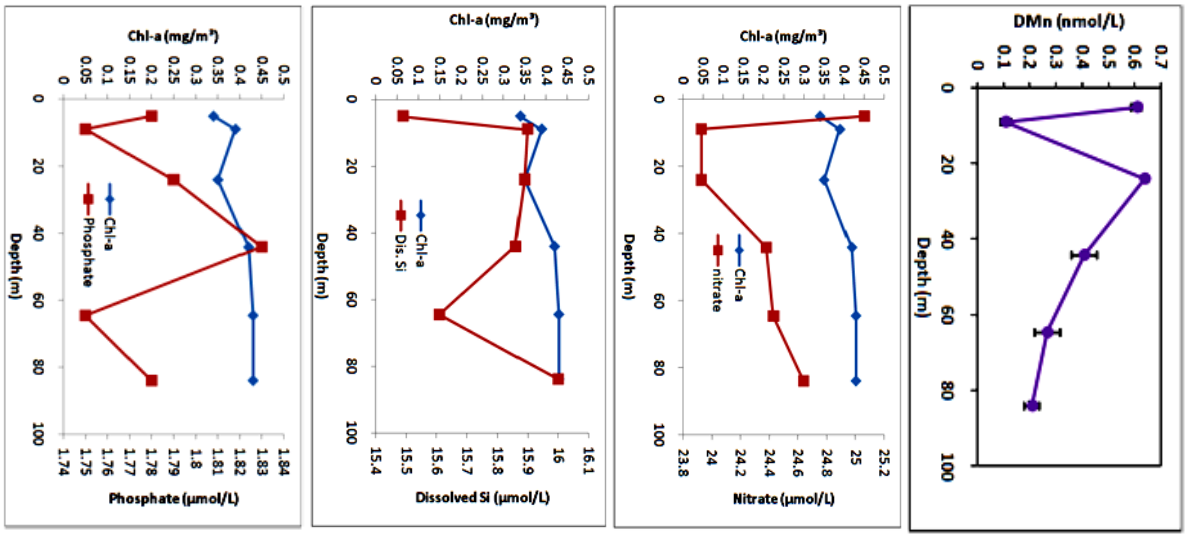

Figure IV10. Chl-a (mg/m³), macronutrients (phosphate, nitrate, dissolved silicon (µM)) and dissolved manganese (nM) at Station M2 (502).

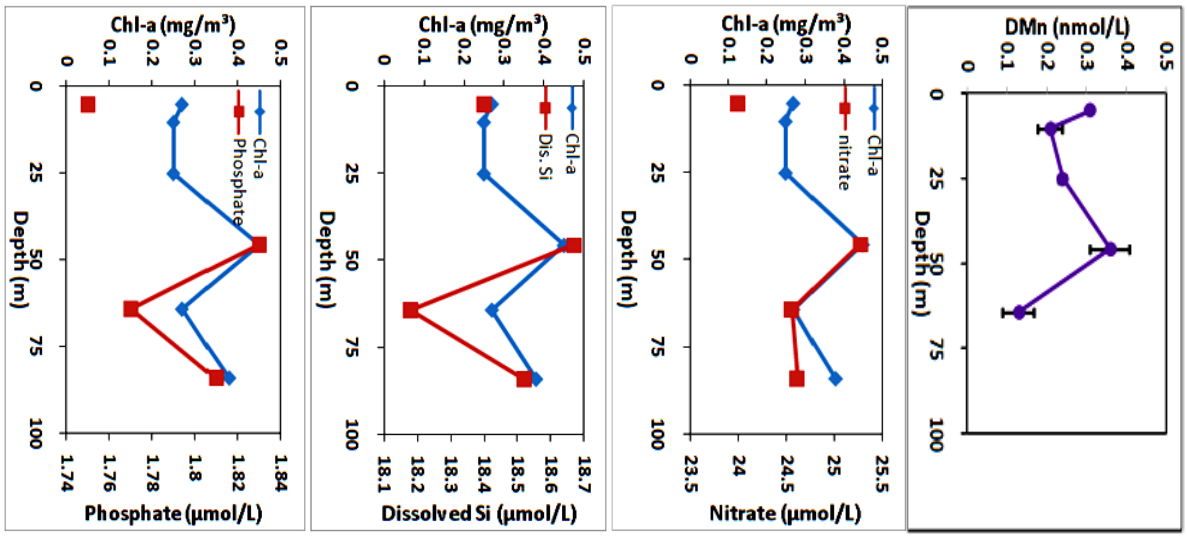

Figure IV11. Chl-a (mg/m³), macronutrients (phosphate, nitrate, dissolved silicon (µM)) and dissolved manganese (nM) at Station M6 (511).

Central and Island Sites (*i.e.* Stations M3 and Baie Americaine) were located in the bloom area that are in close proximity to the Crozet plateau where it was hypothesized there would be a direct input of trace metals (*e.g.* iron and aluminium) from the islands (Planquette *et al.*, 2007, 2009). During the sampling period, the main bloom event has just finished and thus relatively low surface Chl-*a* concentrations were observed at M3 (496 and 572) (Figure IV12-IV13), with the maximum value of ~1.00 mg/m^3. Nitrate was pulled down to ~23 µmol L^{-1} and dissolved silicon and phosphate declined to 0.4 µmol L^{-1} at both Stations. The lowest values of nitrate are found in the SAF in the area around the bloom (Pollard *et al.,* 2007a). The concentrations of dissolved manganese at Station M3 (for cast 496) above the mixed layer depth decreased from high surface concentration, 1.24 nM, to approximately 0.50 nM at the mixed layer with a mean value of 0.80 nM above the mixed layer depth. At Station M3 (cast 572), the concentrations of manganese were higher at the surface, approximately 1.30 nM, with an average of 1.00 nM within the mixed layer depth. The last occupation of Station M3 (622) was in January 2005 during the secondary bloom event, when the highest Chl-*a* concentrations were measured in the Crozet area for this study, with a maximum of ~5 mg/m^3 in the surface water, and the dissolved silicon concentrations were almost fully stripped from the water column. The dissolved manganese concentrations were low in surface water at <0.40 nM, and slightly increased at the depth where the Chl-*a* values were low (Figure IV14).

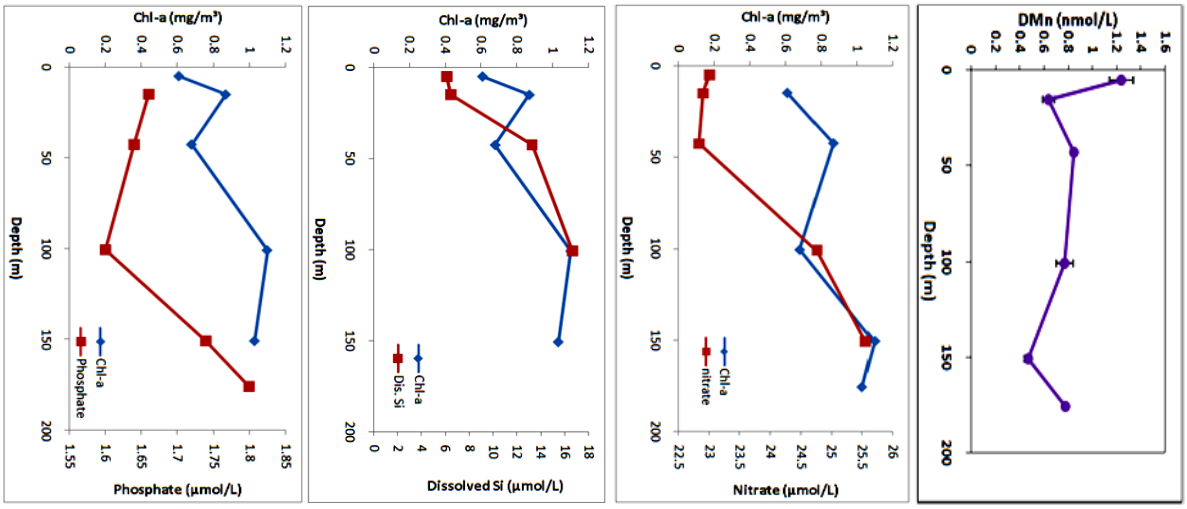

Figure IV12. Chl-a (mg/m^3), macronutrients (phosphate, nitrate, dissolved silicon (µM)) and dissolved manganese (nM) at Station M3 (496).

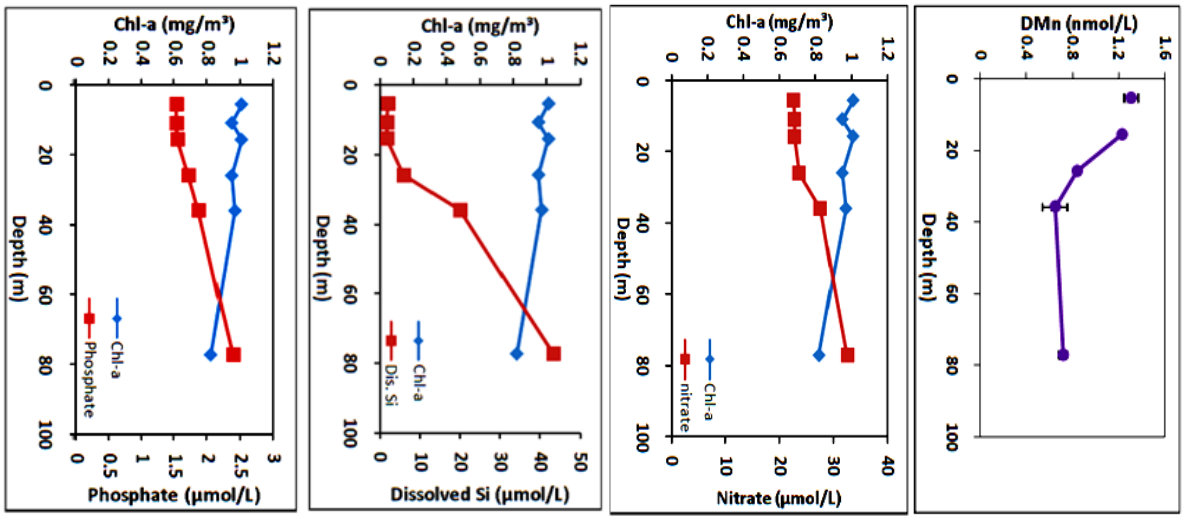

Figure IV13. Chl-a (mg/m³), macronutrients (phosphate, nitrate, dissolved silicon (µM)) and dissolved manganese (nM) at Station M3 (572).

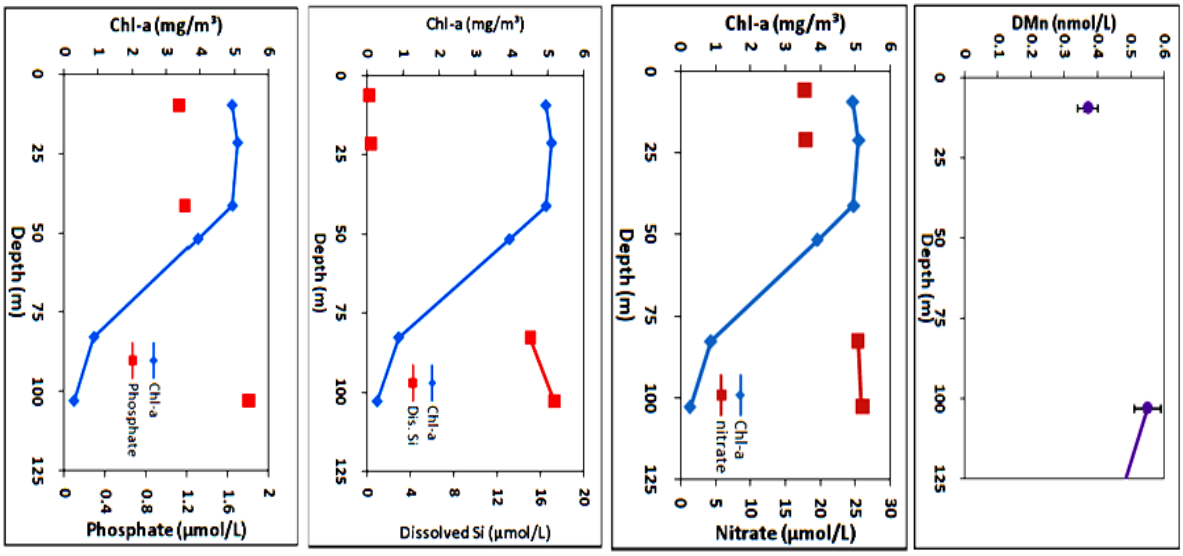

Figure IV14. Chl-a (mg/m³), macronutrients (phosphate, nitrate, dissolved silicon (µM)) and dissolved manganese (nM) at Station M3 (622).

Baie Americaine (BA) island Stations were located close to Ile de la Possession. Data from these Stations were very important to test if the islands were a major source of manganese to the water column. The first Station, BA (567) was sampled in shallow waters (80m) about 1km from the shore. In these shallow waters, Chl-*a* concentrations were low with a mean value of 0.56 mg/m³ that were possibly due to light limitation in these turbid water near-shore waters. Dissolved manganese concentrations were exceptionally high at this Station with a maximum of 2.50 nM in surface water (Figure IV15). The second BA station, BA+1 (568) was approximately 8km from the shore, northeast of the Station BA (567). Chl-*a* values were fairly constant within the mixed layer depth with an average value of ~0.56 mg/m³. Dissolved manganese concentrations were high at the surface (< 2.00 nM) and then decreased to 0.50 nM at 100m. There was an increase in dissolved manganese concentrations to 1.0 nM at 200m then 2 nM at 300 m, which corresponded with AAIW,

and a lower value of 0.5nM near the bottom (376 m) was observed (Figure IV16). The last BA Station was BA+2 (569), and was located around 16km from the shore. Elevated near surface dissolved manganese concentrations were also observed for this Station with 0.36 nM at the surface, to 0.60 nM at the bottom of the mixed layer (50m). Below the mixed layer, dissolved manganese concentrations decreased to 0.31 nM, and increased again to 0.71 nM at 300m due to the apparentinfluence of the island shelf. A similar peak was also observed in dissolved iron concentration (Planquette *et al.,* 2007). Surface Chl-*a* concentrations were higher at Station BA+2 (569) than stations nearer shore, with up to ~1.00 mg/m^3 that corresponded to a drop in dissolved manganese concentrations (Figure IV17). Between 350 and ~1200m at 569 Mn concentrations were <0.5 nM.

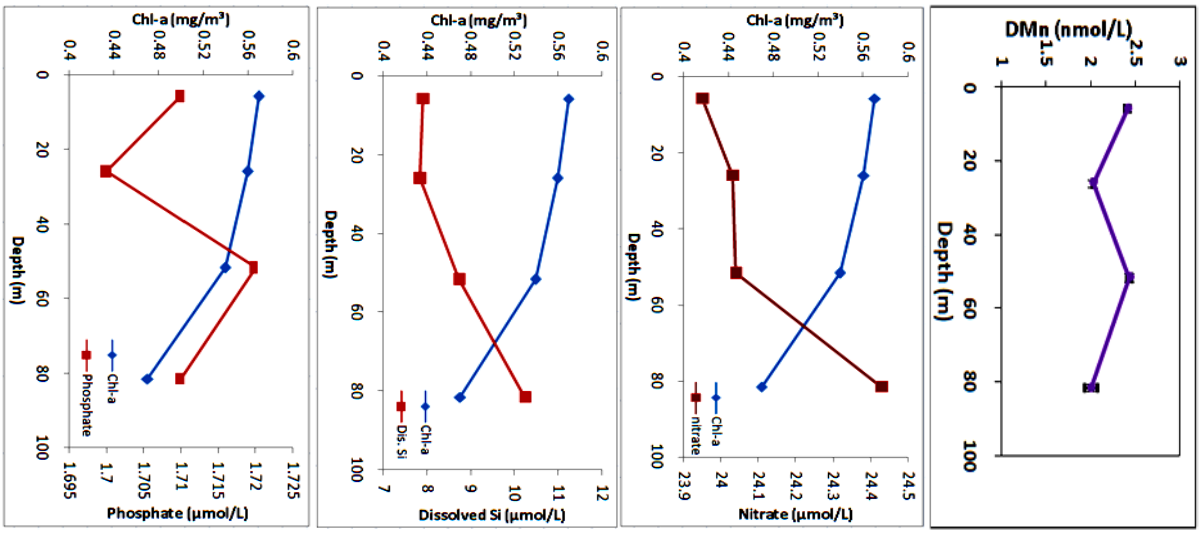

Figure IV15. Chl-a (mg/m^3), macronutrients (phosphate, nitrate, dissolved silicon (µM)) and dissolved manganese (nM) at Station BA (567).

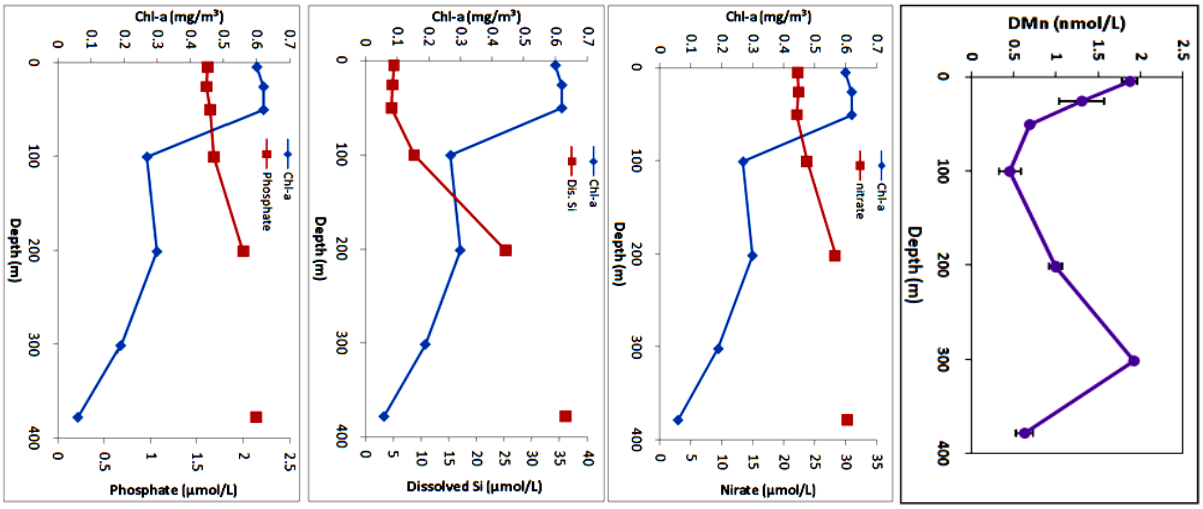

Figure IV16. Chl-a (mg/m^3), macronutrients (phosphate, nitrate, dissolved silicon (µM)) and dissolved manganese (nM) at Station BA+1 (568).

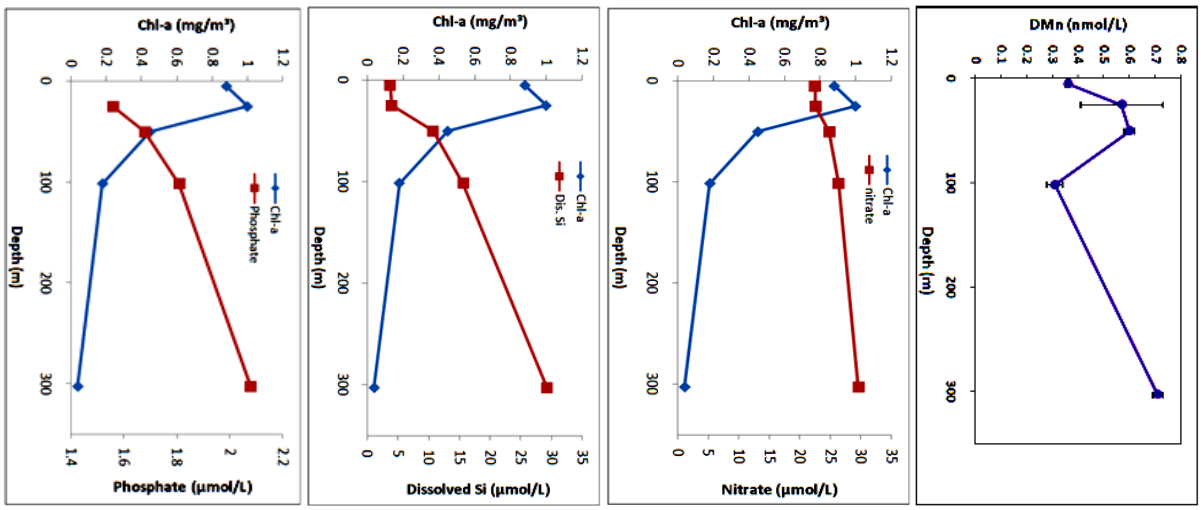

Figure IV17. Chl-a (mg/m³), macronutrients (phosphate, nitrate, dissolved silicon (µM)) and dissolved manganese (nM) at Station BA+2 (569).

5.3 Full water column profile of dissolved manganese

The full water column stations were grouped around four main locations: at the bloom area close to the Ile de la Possession island (Central Sites: Stations M3 and BA), at the productive area northwards of the islands (Northern Sites: Stations M1, M7 and M10), and at the oligotrophic area southwards of the islands (Southern Sites: Stations M2 and M6).

5.3.1 The Central Sites (Stations M3)

The Station M3 was sampled five times but samples from only three casts (496, 572 and 622) were available for dissolved manganese analysis. Full depth profiles of dissolved manganese in the water column are plotted in Figure IV18(a).

The first occupation of M3 (cast 496) was in mid November 2004 when southern HNLC water (Pollard *et al.,* 2007b) mixed with the water around the M3 Stations. The main bloom event had finished and thus lower surface Chl-*a* values (*see* Section 5.2) were observed. A surface maximum of manganese (1.24 nM) was observed for cast 496 and below this concentrations were relatively invariant (0.4-0.8 nM) down to 500m. Deeper in the water column the concentrations of manganese decreased through the AASW to approximately 0.55 nM at 1000 m depth. The concentration of manganese remained in the range 0.50 – 0.55 nM in the AAIW up to 1500 m depth, and below this manganese decreased to around 0.13 nM at approximately 2300 m depth within the CDW.

Station M3 (572), the second M3 occupation, was sampled in late December 2004 after the main bloom event but before the secondary bloom event. The water column was only sampled to 175m and showed elevated concentrations of manganese in the surface layer

(0.84 - ~1.30 nM) with no distinct subsurface maximum. Below the surface layer the concentrations of manganese generally decreased into AASW to values of around 0.4 nM.

Cast 622, the third occupation of M3 was sampled in January 2005 during the secondary bloom event. Surface concentrations of Mn were the lowest measured at M3, and in the SASW above the subsurface maximum, the concentrations of manganese were around 0.4 nM. A slight subsurface maximum of manganese was observed around 100 m depth and below this the concentrations of manganese decreased with increasing depth to a mid-depth minimum (below 0.25 nM) at approximately 400 m depth. Below the mid-depth minimum, the concentrations increased to around 0.45 nM in the deeper layer within the AAIW, before decreasing to approximately 0.06 nM at the greatest sampled depth of 2000 m.

All M3 Stations showed variability in the concentrations of dissolved manganese in the upper water column (between surfaces to ~500 m) that will reflect changes in inputs, cycling and biological activity, as discussed in section 5.2.

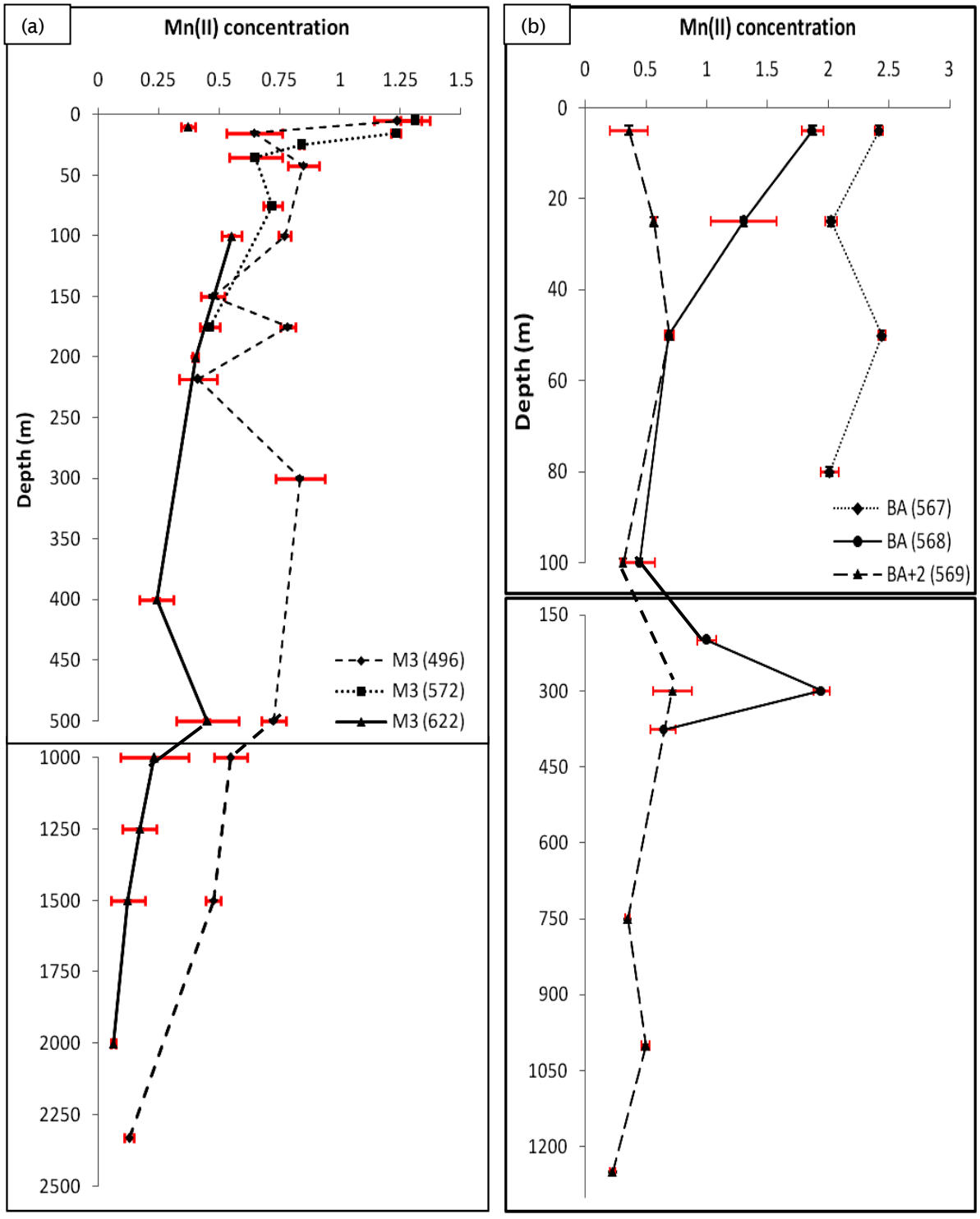

Figure IV18. Full depth profile of dissolved manganese concentrations with standard deviation at **(a)** Stations M3 (496, 572, 622), and at **(b)** Stations BA (567, 568, 569).

5.3.2 The Island Sites (Stations BA)

The three BA Stations were occupied at locations from near shore to further away from the coast. These Stations were in shallow waters and results have been presented in Section 5.2. Full depth profiles of dissolved manganese in the water column are plotted in Figure

IV18(b). Only cast 569 sampled below 350m and here concentrations of manganese decreased to ~ 0.22 nM at 1200m near to bottom within the UCDW.

5.3.3 The Southern Sites

Stations to the south in HNLC waters (M2 and M6) and located to the south of the Ile de la Possession and Ile de l'Est Islands were not significantly influenced by the Crozet plateau (Pollard *et al.,* 2007b).

Surface manganese concentration for both M6 casts (511 and 598) were low compared to other Crozet Stations, at approximately 0.2 nM and 0.3 nM for Stations M6 (598) and M6 (511), respectively (Figure IV19a). Below the surface layer for both M6 casts, the concentrations of manganese decreased with increasing depth. A subsurface maximum was observed at 40 m depth for cast 511 (0.36 nM), coincided with an increased in σ_0 within the AASW. A subsurface manganese maximum was also observed for cast 598 at 80 m depth (0.33 nM) within the AASW. The concentrations of Mn were depleted within the AAIW for both M6 casts between about 750 m and 1250 m depth. At 1250 m depth, the manganese concentration for cast 511 was slightly increased due to the introduction of the UCDW. The manganese concentrations below this depth for cast 511 decreased with increasing depth within the UCDW. Cast 598 also showed a decreasing trend in manganese concentrations within the UCDW until approximately 2300 m depth. Deeper, manganese concentrations were slightly increased within the LCDW. The concentration of manganese for cast 598 was constant in near bottom water in the AABW, but there was a slight increase observed close to the bottom for cast 511.

Station M2 (cast 502) was the other Southern Site and was northeast of Station M6. In this water column, the concentrations of manganese were relatively elevated in the surface (Figure IV19a) with a subsurface maximum at approximately 20 m depth (0.64 nM) that coincided with low Chl-*a* concentrations. Below the subsurface maximum the concentrations of manganese decreased to a value of around 0.25 nM through the AASW until approximately 500 m depth. Deeper, the concentrations of manganese were in a range of 0.2 – 0.22 nM within the AAIW until ~1250 m depth. Below this depth, the manganese concentrations decreased into the CDW to values of around 0.15 nM and stayed relatively constant throughout the UCDW until about 2500 m depth. Deeper, the concentration of manganese further decreased to a value around 0.1 nM in the LCDW until approximately 3000 m depth. Below 3000 m the concentration of manganese increased again to a value of around 0.13 nM in the AABW. Close to the sediments, the concentrations of manganese decreased to around 0.07 nM at the maximum sampled depth.

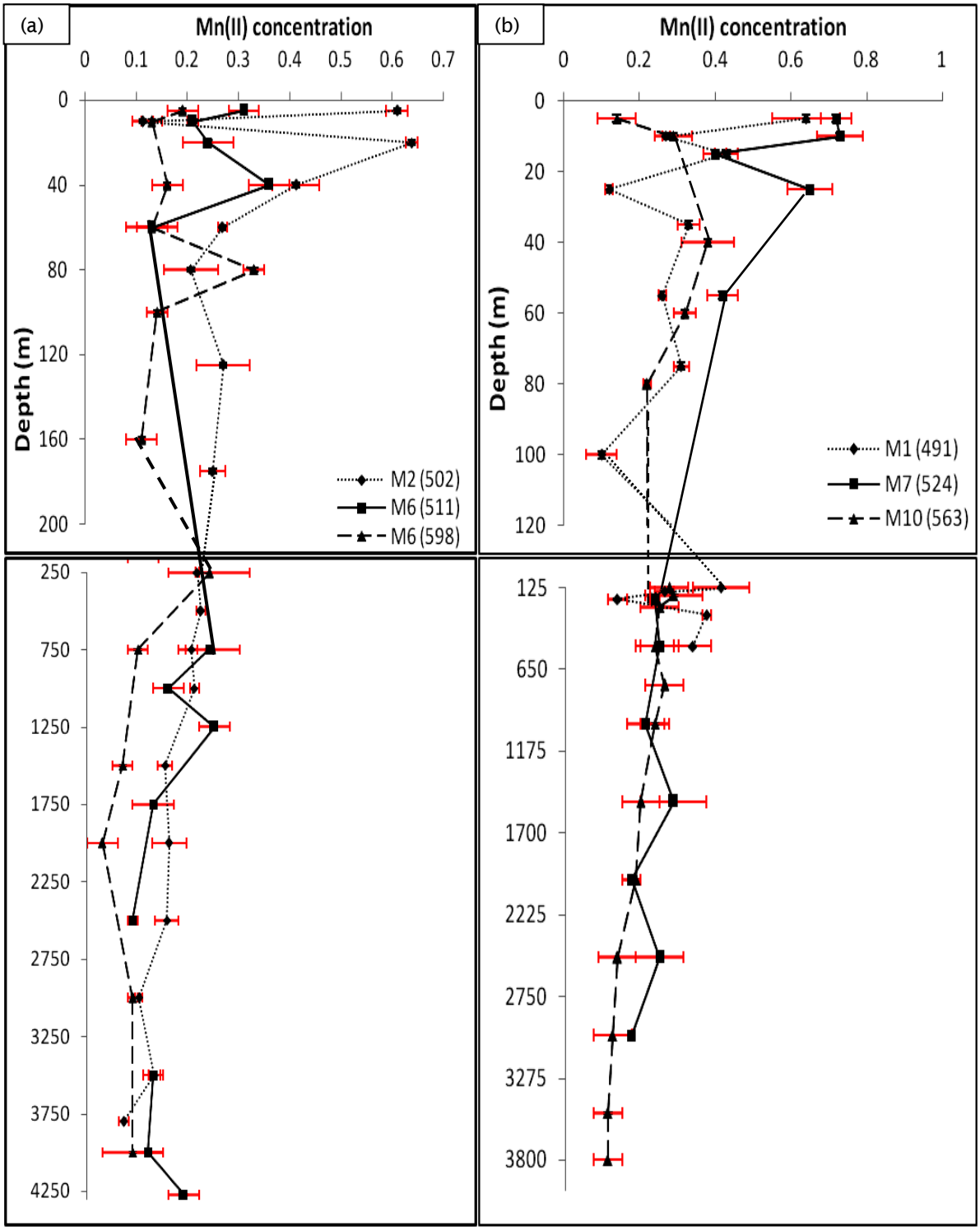

Figure IV19. Depth profile of dissolved manganese at: **(a)** Southern Site (Station M2(502), Station M6(511), and Station M6(598)). **(b)** Northern Sites (Station M1(491), Station M7(524), and Station M10(563)).

5.3.4 The NorthernSites

Stations M1 (491) and M10 (563) were situated to the north of the Crozet Plateau, and Station M7 (524) was situated slightly west and north of the Crozet Plateau; in the region where the bloom event occurred (Pollard *et al.,* 2007a). Stations M1 and M7 were occupied

just after the main bloom in November 2004 where the concentrations of Chl-*a* were still fairly high (>0.9 mg/m³) for both Stations, but considerably lower than the concentrations of Chl-*a* during the bloom event (early November) which can reach up to 8 mg/m³. At the most northerly Crozet Stations (*i.e.* Station M1(491)) a surface maximum of Mn was observed (Figure IV19b). High surface manganese concentrations were also observed at Station M7(524) (Figure IV19b); these coincided with relatively low Chl-*a* values during the sampling period in both Stations. A subsurface maximum was observed at Station M7 at 25 m depth with a concentration of 0.65 nM, coincided with a steep increase in σ_0 with increasing depth. Below the subsurface maximum the concentrations of manganese decreased through the SASW and AASW to values below 0.2 nM. A subsurface maximum (0.33 nM) was also observed at Station M1 at 35 m depth. Deeper, the concentration of manganese dropped to a value 0.26 nM and increased again to approximately 0.30 nM at 75 m depth within the SASW. This increase in manganese coincided with a steep increase of σ_0. Below this depth, the manganese concentration was decreased further to 0.1 nM at 100 m depth before increased again to a value around 0.30 nM at 125 m depth. Deeper the concentration of manganese increased into the AAIW to values around 0.30 nM.

Below 500 m at Station M7, the concentrations of manganese were between ~0.15 and 0.2 nM. Station M10 (563) was sampled late December 2004 before the second bloom and the Chl-*a* concentrations were slightly lower (0.8 mg/m³) than both M1 and M7 Stations. A subsurface maximum of manganese (approximately 0.4 nM) was observed around 40 m depth and below this maximum the concentrations of manganese decreased with increasing depth, coincided with depleted Chl-*a* values. In the SASW above the subsurface maximum, the concentrations of manganese were below 0.30 nM. Below the surface waters the concentrations of manganese remained constant at approximately 0.22 nM until 125 m depth. Deeper, the concentrations of manganese decreased to about 0.15 nM in the CDW and remained constant until close to the sediments at about 3800 m depth.

Overall, there is an increase of approximately 0.4 nM from the dissolved manganese background values (*i.e.* Southern Site dissolved manganese values) at these Northern Sites.

6 Discussion

6.1 Comparison with previously reported dissolved manganese data in the Southern Ocean

The dissolved manganese and associated data presented here are the first comprehensive dataset for dissolved manganese in the vicinity of the Crozet Islands of the Southern Ocean. The near-surface concentrations of manganese in the AASW open ocean water were <0.65 nM with the lowest concentration of 0.11 nM being measured at the Southern Sites

(Stations M2 (502), M6 (511), M6 (598)), and these values are comparable to those higher values determined by Bucciarelli *et al.* (2001) in surface waters (AASW) in the wake of Kerguelen Islands (ranging from 0.46 - < 1.3 nM). However, values obtained in the present study were similar to or greater than the concentrations (0.08 – 0.26 nM) reported by Martin *et al.* (1990) in open ocean surface waters of the Drake Passage (Southern Ocean) and by Middag *et al*. (2011a) in the AASW surface layer of the Bouvet region (~0.3 nM), and close to the values reported in the AASW (~0.61 nM) of the Ross Sea (Corami *et al.,* 2005).

Coastal waters (Central Sites) manganese values in this study were up to 2.44 nM near shore. These values were lower than those of Bucciarelli *et al*. (2001), probably because of the bigger surface area (7000 km^2) of the Kerguelen islands which is 20 times bigger than Crozet (350 km^2); thus the magnitude of natural manganese release was less in our study area. The data of Bucciarelli *et al.* (2001) showed considerable enrichment in dissolved manganese in coastal waters of the Kerguelen Islands of up to 8.5 nM, which are ~4 times higher than Baie Americaine near shore values of 2.44 nM. Further away from the shore, their surface values were in a range of 1.4 – 2.88 nM, higher than northern and M3 Stations presented here (0.3 – 1.25 nM). However, the values obtained in the study presented here were consistently greater than the concentrations (0.08 – 0.83 nM) reported by Sedwick *et al.* (2000), and (0.35 – 0.90 nM) (Corami *et al*., 2005) in the shallow waters of the Ross Sea.

Surface concentrations (~0.7 nM) of dissolved manganese at the Northern Sites in this study were higher than values obtained by Sedwick *et al.* (1997) in the Australian sub Antarctic region east and southeast of Tasmania (~0.33 nM), and by Middag *et al.* (2011a) in the Atlantic sector of the Southern Ocean (~0.2 nM). However, in the present study the surface concentrations to the north of the islands may be impacted by island inputs.

6.2 Atmospheric inputs

The annual phytoplankton blooms observed in the waters around the Crozet Islands (Pollard *et al.,* 2007a), have been hypothesized to reflect natural iron fertilization from the islands (Planquette *et al*., 2007). However, as manganese is essential to phytoplankton (*see* Chapter I); it is also important to understand the various sources that added manganese to these fertilized Crozet seawaters. There are three possible main inputs of manganese into seawaters around Crozet: (1) atmospheric inputs (dry and wet); (2) vertical transport of dissolved manganese to surface water; and (3) lateral inputs of dissolved manganese from the islands. Using the data available, these various sources of manganese can be estimated, and then the average concentration of dissolved manganese before the main bloom event can be calculated following the approach of Planquette *et al*. (2007). In addition to these potential inputs, there were several other processes that could also influence the distributions of dissolved manganese in this region, and these will be discussed later in this Section.

Atmospheric inputs are one of the crucial sources of manganese into the ocean. Manganese can enter the ocean through atmospheric inputs by rain (wet) or/and by dust (dry) deposition.

6.2.1 Dry deposition

During the water column sample collection, aerosol samples were collected but not for trace metals analysis (Planquette *et al.*, 2007). Therefore, as suggested by Planquette and co-workers (2007), the atmospheric dust deposition flux (F_{dust}) was estimated in two ways: (1) excess (non-sea-salt) aerosol calcium (nss Ca) and (2) using the estimated aerosol soluble Si.

Firstly, the $F_{dust/year}$ was calculated by multiplying the flux of the nss Ca ($F_{nss\ Ca}$) with the relative atomic mass (RAM) of Ca, and dividing this by crustal dust Ca content, (A_{Ca}; 1.6 wt%), with the assumption that excess Ca is 100% soluble, as shown below:

$$F_{dust\ /year} = \frac{F_{nssCa}\ RAM_{Ca}}{A_{Ca}}\ x\ 365.25 \qquad (1)$$

From the Crozet atmospheric concentrations (Table IV1, Planquette *et al.,* 2007), dry atmospheric deposition fluxes (F) were calculated. By applying the flux of nss Ca^{2+} value from Table IV1 in equation (1) where A_{Ca}; 1.6 wt% = 0.016 g g^{-1}, gives an $F_{dust/year}$ value of **0.16 g m^{-2} yr^{-1}**, as shown below:

$$F_{dust\ /year} = \frac{F_{nss\ Ca} RAM_{Ca}}{A_{Ca}}\ x\ 365.25$$

= ((172 nmol m^{-2} d^{-1} x 40.08 g mol^{-1}) / (0.016 g g^{-1})) x 365.25 = **0.16 g m^{-2} yr^{-1}**

Deposition fluxes (F) in Table IV1 were calculated from atmospheric concentrations by assuming excess Ca and silicate are associated with coarse-mode aerosol, with deposition velocities of 0.1cms^{-1} (Baker *et al.,* 2003).

Table IV1. Estimated terrestrial dust fluxes to the Crozet region (adapted from Planquette *et al.,* 2007).

Analyte	Concentration (nmol m^{-3})	Deposition flux (F) (nmol m^{-2} d^{-1})
nss Ca^{2+}	0.1 ± 0.2* 0.55 ± 1	172*
Sol_{Si}	0.016 ± 0.004* 0.027 ± 0.027	28*

*n = 6 except *n = 5*

Secondly, the $F_{dust/year}$ was calculated using an estimation of aerosol soluble Si (assumed to be totally of terrestrial origin) with a Si solubility (Sol_{Si}) of 0.3%, (Baker *et al.,* 2006) and assuming the abundance of Si (A_{Si}) in dust is 30wt%:

$$F_{dust\,/year} = \frac{F_{Si}\,RAM_{Si}}{A_{Si}\,Sol_{Si}}\,x\,365.25 \quad (2)$$

By using the flux of Sol_{Si} value in Table IV1 in equation (2) by considering an estimated Si solubility (Sol_{Si}) was 0.3% (Baker *et al.,* 2006) and the abundance of Si (A_{Si}) in dust as 30 wt%, gives the $F_{dust/year}$ value of **0.32g m^{-2} yr^{-1}**, as calculated below:

$$F_{dust\,/year} = \frac{F_{Si}\,RAM_{Si}}{A_{Si}\,Sol_{Si}}\,x\,365.25$$

= ((28 nmol m^{-2} d^{-1} x 28.09 g mol^{-1}) / (0.30 x 0.003 g g^{-1})) x 365.25

= **0.32g m^{-2} yr^{-1}**

These two approaches gave estimated F_{dust} values varying between 0.16 and 0.32 g m^{-2} yr^{-1} with and an average value of **0.24g m^{-2} yr^{-1}.** An estimation of dry deposition flux of manganese can be calculated from this value using equation (3) below (de Jong *et al.*, 2007):

$$F_{atm,\,TMn} = (D\,A_{Mn}) / M_{Mn} \quad (3)$$

where $F_{atm,\,TMn}$ is the total dry deposition atmospheric flux (µmol m^{-2} yr^{-1}) of manganese, D is dust input (g m^{-2} yr^{-1}), A_{Mn} is manganese abundance in dust, M_{Mn} is atomic weight of manganese. D value is 0.24 g m^{-2} yr^{-1} (from the equation (1) and (2)). Nakayama *et al.* (1995) and Taylor and McLennan (1985) estimated the A_{Mn} to be 0.07 wt% and 0.14 wt%, respectively to give an average A_{Mn} value of ~0.1 wt% and this average was therefore used as an A_{Mn} value, the total atmospheric dry flux of manganese to Crozet waters is thus about 4.37 µmols m $^{-2}$ yr $^{-1}$, as calculated below:

$F_{atm,\,TMn}$ = (0.24 g/m^2/yr **x** 0.1 % g/g) **/** (54.94 g/mol)

= **4.37 µmol m $^{-2}$ yr $^{-1}$**

6.2.2 Wet deposition

Manganese concentrations in the rainwater samples (Table IV2) were analysed by Dr. Alex Baker, from the University of East Anglia and details of the method are described in Planquette *et al.* (2007) and references therein. Clean atmospheric sampling was performed at the highest place on the ship, above the bridge when wind and ship movements give no contamination from the ship. The sampling areas were located truly in remote Southern Ocean air where the rain and aerosol samples had contact only with the Antarctic land mass over approximately 5 days prior to collection, based on the air parcel

back-trajectories (Draxler and Rolph, 2003). However, data for CRO-R9 was excluded from later interpretation due to a contamination issue and this value was considered invalid.

Table IV2. Manganese concentrations obtained from the rain samples collected during cruise D285.

Sample	Start Date	Start Latitude (°S)	Start Longitude (°E)	Rain Volume (mL)	Mn concentration (nM)
CRO-R2	08/11/2004	40.63	41.98	60	21.2
CRO-R3	08/11/2004	40.95	43.37	100	10.7
CRO-R4	08/11/2004	41.25	44.69	540	3.4
CRO-R5	18/11/2004	46.06	51.79	230	1.6
CRO-R6	22/11/2004	49.00	51.50	200	2.0
CRO-R7	30/11/2004	44.95	49.94	130	3.6
*CRO-R9	**03/12/2004**	**43.12**	**47.19**	**130**	**74.1**

* *contaminated*

Using $\mathbf{M_w = C \cdot P}$, the wet deposition of manganese was estimated, where M_w is the wet deposition of manganese, C is the total volume weighted mean concentration of manganese, where $\mathbf{C = \Sigma\, C}i\, \mathbf{V}i\, \mathbf{/\ \Sigma\, V}i$, where C*i* is manganese concentration and V*i* is the sample volume (Table IV2) (C=7.1 nmol). P is the precipitation rate for the Crozet region. However, there are no data for the Crozet precipitation rate. Therefore, data from the nearby Kerguelen Islands (1140 mm yr^{-1}); Marion Island (2499 mm yr^{-1}); and Prince Edward Island (2557 mm yr^{-1}), were used to estimate the level of precipitation for Crozet, with an average of 2065 mm yr^{-1}. Some precipitation might fall as snow and might possibly carry dust differently from rain, but because no quantitative information was available that could be used to address this, the value above was used for this rate of precipitation. A wet deposition rate for manganese around the Crozet Islands is **14.66 (rounded to 15) µmol m^{-2} yr^{-1}.** The total manganese deposition (dry+wet) is thus calculated at **19.03 (rounded to 19) µmol m^{-2} yr^{-1}** with 77 % of this existing as wet deposition. From this value, estimation of the soluble manganese inputs is calculated using equation (4) below as used in de Jong *et al.* (2007).

$$F_{atm,\,dMn} = S_{Mn} \cdot F_{atm,\,TMn} \qquad (4)$$

where $F_{atm,\,dMn}$ is dissolved atmospheric flux (µmol/m^2/yr) of manganese, $F_{atm,\,TMn}$ is the total atmospheric flux of manganese (µmol/m^2/yr), S_{Mn} is the solubility of non-Saharan dust (13 - 28 % with median of 20.5 % (Baker *et al.,* 2006) for dry deposition and 40 % for wet deposition (Jickells *et al.,* 1994). A soluble manganese input of 6.24 µmol m^{-2} yr^{-1}, is then derived which is equivalent to a dissolved manganese flux ($F_{atm,dMn}$) of 17.08 (rounded to 17) nmol m^{-2} d^{-1} , as calculated below:

$$F_{atm,\,dMn\,(dry)} = 0.205 \cdot 4.37\ \mu mol/m^2/yr = 0.90\ \mu mol\ m^{-2}\,yr^{-1}$$

$$F_{atm,\,dMn\,(wet)} = 0.4 \cdot 15\ \mu mol/m^2/yr = 5.86\ \mu mol\ m^{-2}\,yr^{-1}$$

$$F_{atm,\,dMn\,(dry+wet)}\ 0.90+5.86\ (\mu mol\ m^{-2}\,yr^{-1}) = \mathbf{6.76\ \mu mol\ m^{-2}\,yr^{-1}}$$

The $F_{atm, dMn (dry+wet)}$ per day can be calculated as followed:

6.76 µmol m^{-2} yr^{-1}/365.25 =**18.50 nmol m^{-2} d^{-1}**.

6.3 Estimation of the vertical transport of dissolved manganese fromsurface waters

Manganese can be delivered to surface waters from below, by both advective transport and turbulent diffusive fluxes (eddy-diffusion). Here, the contribution of both processes were estimated by using the same approach as Charette *et al.* (2007) for Stations closer to the islands.

Short-lived radium (Ra) isotopes are natural radio-tracers that are a powerful tool to trace island and deep water sources of manganese, and its dispersion and mixing with adjacent waters. The use of ratios of natural existing radium isotopes with respective half-lives: $t_{1/2}$ ^{223}Ra = 11.4 days, $t_{1/2}$ ^{224}Ra = 3.66 days, $t_{1/2}$ ^{226}Ra = 1600 years, and $t_{1/2}$ ^{228}Ra = 5.75 years, have been used for decades to estimate their lateral mixing processes between shelf waters and the open ocean **(**Moore *et al*., 1995**;** Key*et al*., 1985**;** Moore, 2000). Ra -228 is particularly useful for estimating vertical mixing rates. The Ra isotopes are produced by radio-decomposition of particles which contain bound thorium (Th) isotopes in the sediments, and they are consistently added to shelf waters across the sediment water boundary by advective and diffusive processes. Ra isotopes are normally found around the coastal region as well as at any sediment water interface, and only mixing and decay processes affect their distributions (Charette *et al.,* 2007). Therefore, using Ra isotopes with the manganese concentrations is the best way to evaluate the manganese inputs from the islands into the surface waters. Charette *et al.* (2007) used a simple one-dimensional diffusive model (Equation 4) with the vertical profile of ^{228}Ra at Station M3 along with dissolved iron concentrations (Planquette *et al*., 2007) data across the same depth range to quantify possible sources of dissolved iron to the bloom region northwards of the Crozet Plateau. Therefore, it was also possible to quantify the manganese sources by applying manganese data obtained in this study into this one-dimensional diffusive model (Charette *et al.,* 2007). Two mixing scenarios were used here, as the degree of mixing is variable across the entire depth range: (1) a slow mixing between 300 and 1000 m depth (K_z = 1.5cm^2s^{-1}), and (2) a fast mixing between surface and 300 m depth (K_z = 11cm^2s^{-1}) (details of this model are fully described in Charette *et al.,* 2007):

$$A_z = A_0 \exp\left(-z\sqrt{\frac{\lambda}{Kz}}\right) \qquad (4)$$

where A_z is the activity of ^{228}Ra at a depth of z from the surface, A_0 is the activity at the surface, **λ** is the decay constant and K_z is the vertical eddy diffusion coefficient. Dissolved manganese data (from Station M3(496)) combined with ^{228}Ra data were shown in Figure IV20. The corresponding dissolved manganese gradient between surface and 300 m was calculated using 1.24 nM at surface and 0.83 nM at 300 m depth, leading to a gradient of -

0.0014 nM m^{-1} or -1.40 nmol m^{-3} m^{-1}. A very important point here was that deep waters have lower concentrations than surface water and thus any mixing would reduce surface concentration. The negative value here indicates that any manganese flux was into deep waters.

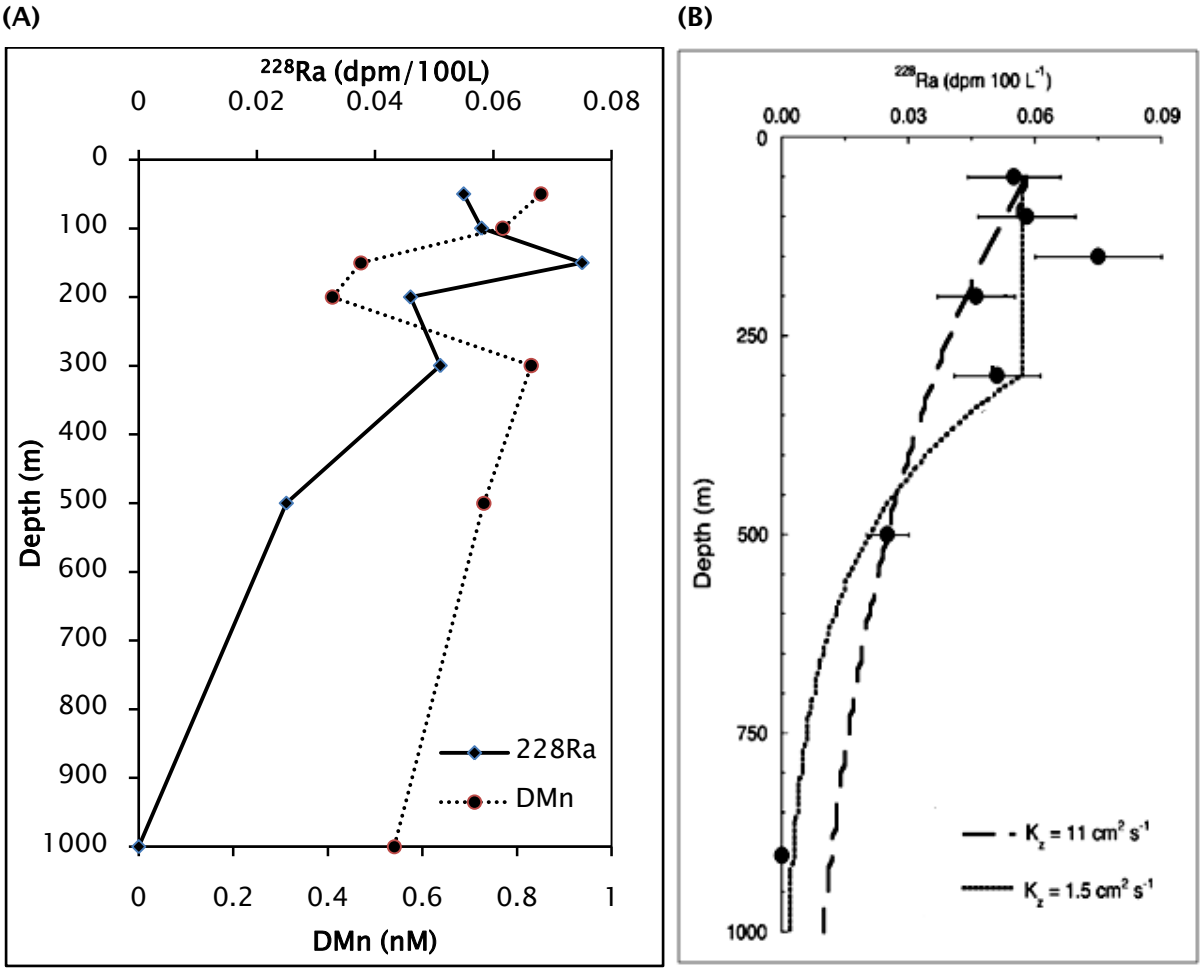

Figure IV20. **(A)** Depth profiles of ^{228}Ra and dissolved manganese concentrations at Station M3(496). **(B)** Model estimates of K_z fitted to the ^{228}Ra profile at stations M3 (adapted from Charette *et al.*, 2007).

The maximum vertical input of dissolved manganese, DMn_v was possible to estimate by combining this dissolved manganese gradient with the vertical coefficient, K_z, at the upper 300 m depth (Equation 5):

$$DMn_{vmax} = DMn_{gradient} \cdot K_z \qquad (5)$$

, where $DMn_{gradient}$ is the vertical dissolved manganese gradient (-1.40 nmol m^{-3} m^{-1}), K_z is the vertical diffusion coefficient (11 cm^2 s^{-1} (Charette *et al.*, 2007)):

$$DMn_{vmax} = -1.40 \text{ nmol } m^{-3} \text{ } m^{-1} \cdot 0.11 \times 10^{-4} \text{ } m^2 \text{ } s^{-1} \cdot 3600 \text{ s} \cdot 24$$
$$= \mathbf{-133 \text{ nmol } m^{-2} \text{ } d^{-1}}$$

The dissolved manganese gradient between 300 and 1000 m was calculated using 0.83 nM at 300 m and 0.54 nM at 1000 m depth leading to a gradient of -0.0004 nM m^{-1} or -0.40 nmol m^{-3} m^{-1}. The minimum vertical mixing rate of dissolved manganese was estimated using the smaller mixing rate coefficient (1.5 cm^2 s^{-1} (Charette *et al.,* 2007)):

$$DMn_{vmin} = -0.40 \text{ nmol } m^{-3}\ m^{-1} \cdot 0.15 \times 10^{-5}\ m^2\ s^{-1} \cdot 3600\ s \cdot 24$$
$$= \mathbf{-5.2 \text{ nmol } m^{-2}\ d^{-1}}$$

Klunder *et al.* (2010) reported an average K_z of 0.3 $cm^2 s^{-1}$ over the Atlantic Sector of the Southern Ocean, larger than the faster K_z value around the Crozet Islands, due to strong eddy-diffusion during the austral winter period. Combining this value (0.3 cm^2 s^{-1}) with the reported dissolved manganese data during GEOTRACES at the same region (Middag *et al.,* 2011a), gave a vertical dissolved manganese flux of -104 nmol m^{-2} d^{-1}, slightly lower than the maximum vertical flux reported here (-133 nmol m^{-2} d^{-1}) due to the lower deep manganese concentrations reported in Middag *et al.* (2011a). van Beek *et al.* (2008) reported a K_z of 1.5 cm^2 s^{-1} and Blain *et al.* (2007) reported a K_z of 3.3 cm^2 s^{-1} , to give an average of 2.4 cm^2 s^{-1} over the Kerguelen Plateau, leading to a massive vertical input of 3733 nmol m^{-2} $d^{-1}$when combined with the previously reported higher concentrations of dissolved manganese during the ANTARES 3/JGOFS cruise (Bucciarelli *et al.*, 2001). The vertical flux estimated here is in the range of -5–(-133) nmol $m^{-2}d^{-1}$, which is lower than previously reported values in the Kerguelen Plateau, suggesting that the vertical manganese flux from deep waters around the Crozet Plateau was not a significant natural source of manganese into the surrounding surface waters, and was in fact a sink for the surface layer Mn.

6.4 Lateral sources of dissolved manganese from the Crozet system

Dissolved manganese was potentially transported horizontally from the islands to the surrounding waters, in a manner similar to dissolved iron. The concentrations of dissolved manganese in the water column of the BA transects showed a clear decreasing trend from near shore to further offshore (Figure IV21) during this study. In addition to the BA transect, Station M3 (622) was chosen as an offshore Station (~35 km from shore) and was plotted together in this figure because this Station was occupied after the BA transects. This clear decreasing concentration trend (Figure IV23) obtained in this study showed that the island system was a major potential manganese source to waters surrounding the Crozet region.

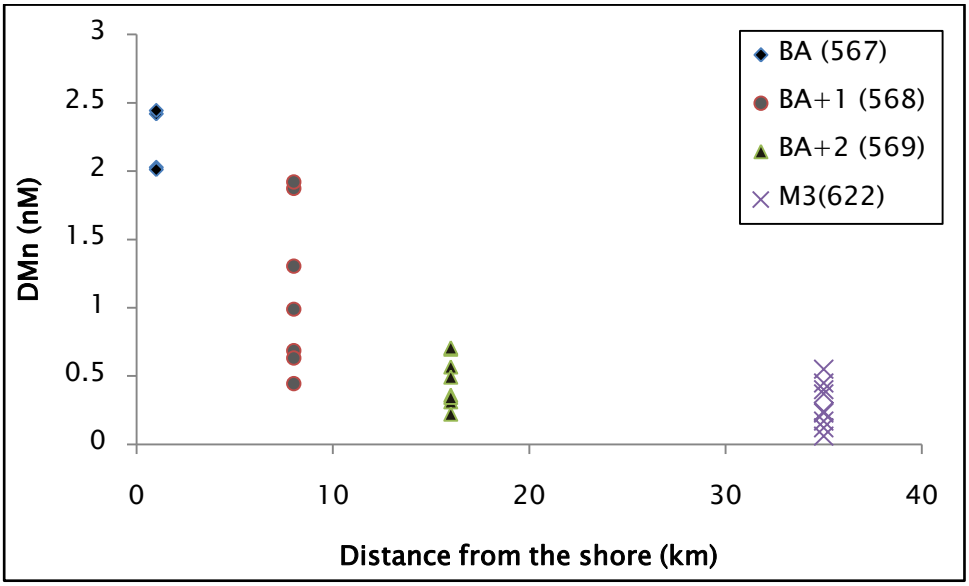

Figure IV21. Dissolved manganese concentrations at all depths in BA Stations and associated Station M3 (622) (at all depths) on moving offshore.

Charette and co-workers (2007) investigated the activities of the radium isotopes in a series of stations with increasing distance from the island, which were then used to study whether the Crozet Islands were an important source of iron to the bloom area or not. These radium isotopic activities can also be used to investigate the lateral source of manganese from the Crozet Islands. Short lived radium isotopes ^{223}Ra and ^{224}Ra were used on the BA transects (Stations 567, 568 and 569) to estimate the island-derived manganese source; DMn_h.

Details for radium sampling and analysis are given in Charette *et al.* (2007).^{223}Ra and ^{224}Ra were used to examine the lateral mixing because their half-lives were short enough relative to seasonal changes in their input functions to assure the constant boundary condition assumption, which means the activities only depends on the distance, as their coastline inputs were in steady-state (Moore, 2000). Variations of activity of these two short-lived Ra isotopes were followed using the equation:

$$A_x = A_0 \exp\left(-x\sqrt{\frac{\lambda}{Kh}}\right) \qquad (6)$$

where A_x is the activity at a distance x from the shore, A_0 is the activity at distance 0 from the coast, λ is the decay constant and Kh is the horizontal eddy dispersion coefficient.

Using Equation (6), the gradient of the ^{224}Ra was used to estimate the maximum horizontal mixing coefficient, Kh of -39 m^2 s^{-1}. The minimum horizontal diffusion coefficient Kh estimated using ^{223}Ra gave a value of -6.6 m^2 s^{-1}. The slope of the ln-transformed ^{224}Ra data (Charette *et al.*, 2007) was compared with the slope of the ln-transformed dissolved manganese data for the Baie Americaine transects (Stations 567 (~1 km distance from the

island), 568 (~8 km distance from the island), 569 (~16 km distance from the island), as shown in Figure IV22. From Figure IV22, the gradient of ln-transformed dissolved manganese concentrations of surface waters (0-50 m) of the BA transects (Stations 567, 568, 569), and the distance from the island could be calculated to give –0.096 nM km^{-1} or -0.096 nmol m^{-3} m^{-1}. Negative values obtained here showed that the concentrations of dissolved manganese were decreasing with increasing distance from the island. Okubo (1971) demonstrated that Kh increased with increasing scale length of the island. Looking at the upper 50 m, the scale length for Crozet was 25 km, which is very much smaller than 151 km of the scale length estimated by Bucciarelli *et al.* (2001) in the vicinity of Kerguelen Islands. This difference may be explained by the different surface areas of the islands. The Kerguelen Islands have a surface area of 7000 km^2 and the Crozet Islands have only 350 km^2, thus the magnitude of natural manganese fertilisation should be less at Crozet.

Combining the maximum and minimum estimates of these lateral diffusion coefficients, Kh, with the dissolved manganese gradient, leads to the estimation of the maximum and minimum lateral fluxes of dissolved manganese Mn_{hmax} and Mn_{hmin}, (Equation 7 below):

$$DMn_h = DMn_{gradient} \cdot Kh \qquad (7)$$

where DMn_h is the lateral flux of dissolved manganese, $DMn_{gradient}$ is the horizontal dissolved manganese gradient (-0.096 nmol m^{-3} m^{-1}), Kh is the horizontal diffusion coefficient (-39 m^2 s^{-1} for maximum, and -6.6 m^2 s^{-1} minimum).

$$DMn_{hmax} = -0.096 \text{ nmol } m^{-3}\, m^{-1} \cdot -39 \text{ } m^2 \text{ } s^{-1} \cdot 3600 \text{ s} \cdot 24 = 323 \text{ µmol } m^{-2} \text{ } d^{-1}$$

$$DMn_{hmin} = -0.096 \text{ nmol } m^{-3}\, m^{-1} \cdot -6.6 \text{ } m^2 \text{ } s^{-1} \cdot 3600 \text{ s} \cdot 24 = 55 \text{ µmol } m^{-2} \text{ } d^{-1}$$

These DMn_{hmax} and DMn_{hmin} can now be used to estimate the cumulative effect of the lateral manganese flux ($F_{DMn.ch}$) to the bloom area. However, before estimating the $F_{DMn.ch}$, the following assumptions should be recognised:

(1) The dissolved manganese gradient was assumed to be representative of the entire plateau, as Giret *et al.* (2002) reported that the mantle geochemical composition was homogeneous in this zone.

(2) It is assumed that a) the Mn release process was occurring over the total 600 km perimeter of the shelf system (Charette *et al.,* 2007), b) the bloom area was about 90,000 km^2 (Venables *et al.,* 2007), c) the deep winter mixing could reach a mixed layer depth of 250 m, and d) that the released manganese was uniformly mixed into these waters.

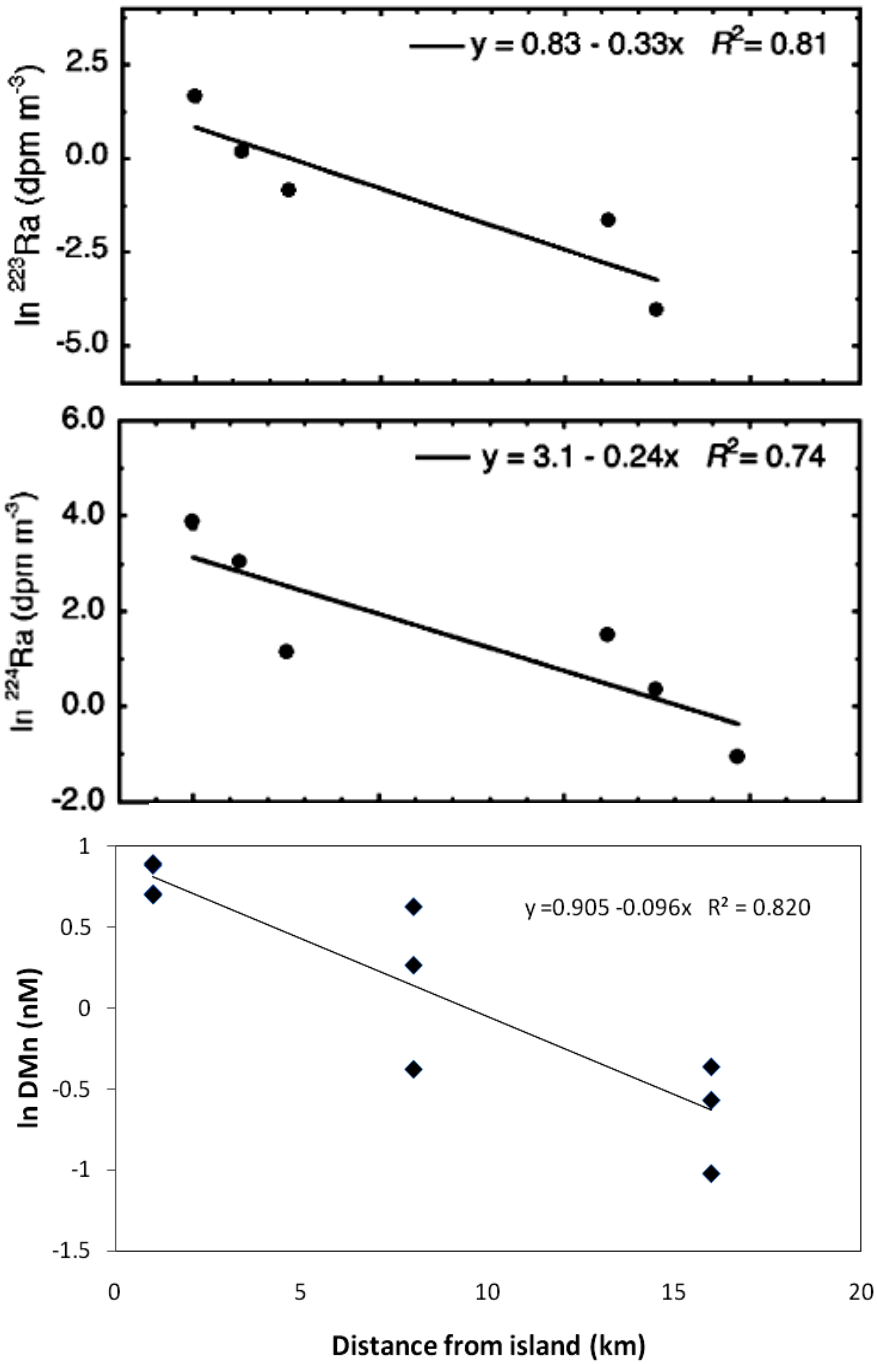

Figure IV22. Ln-transformed ^{223}Ra and ^{224}Ra with slope used to estimate Kh **(top two)** and dissolved manganese data **(below)** of the Baie Americaine transects (BA (567): ~1km distance from island; BA+1 (568): ~8km distance from island; BA+2 (569): ~16km distance from island) in the upper 50 m (^{223}Ra and ^{224}Ra data were taken from Charette *et al.*, 2007).

By using a 600 km shelf-line and a bloom area of 90 000 km^2 (Charette *et al.,* 2007), the $F_{DMn.ch}$ over the fertilised area could be estimated using Equation 8:

$$F_{DMn.ch} = \frac{Mn\,h \bullet C \bullet MLD}{A} \qquad (8)$$

where Mn_h is the lateral flux of dissolved manganese, C is the length of the Plateau, MLD is the winter mixed layer depth and A is the bloom area. Therefore, the maximum and minimum of the cumulative effect of the manganese flux around the Crozet were:

$$DMn_{hmax} = (323\ \mu mol\ m^{-2}\ d^{-1} \cdot 600x10^{3}\ m \cdot 250m) / (90000x10^{6}m) = \mathbf{538\ nmol\ m^{-2}\ d^{-1}}$$

$$DMn_{hmin} = (55\ \mu mol\ m^{-2}\ d^{-1} \cdot 600x10^{3}\ m \cdot 250m) / (90000x10^{6}m) = \mathbf{92\ nmol\ m^{-2}\ d^{-1}}$$

The $F_{DMn.ch}$ were estimated to be up to 538 nmol m^{-2} d^{-1}, which is by far the largest process adding dissolved manganese to the waters surrounding Crozet, followed by the atmospheric and then removal via the vertical exchange (Figure IV24). However, the lateral gradient of dissolved manganese was calculated in the upper 50 m near the shore and thus excludes the deeper waters of the plateau itself because these deeper waters have lower concentrations than surface waters, and thus any vertical mixing would reduce surface concentrations of manganese. This makes the lateral flux of manganese even more important in the Crozet region.

A positive and significant (values obtained were within the 95% confidence level) (R^2= 0.587, $p<0.05$) relationship between dissolved manganese and dissolved iron concentrations at the BA stations was evidence for dissolved manganese and dissolved iron coming from the same source (*i.e.* from the island system) (Figure IV23).

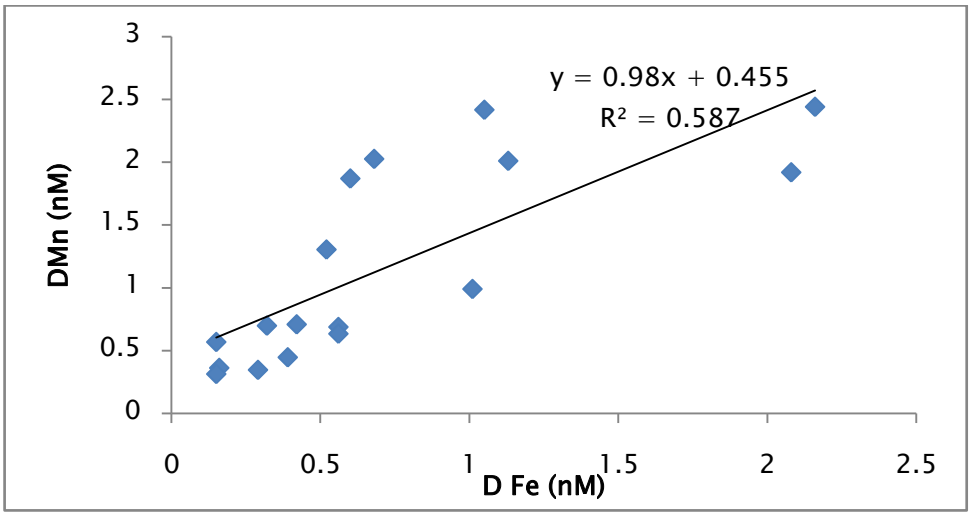

Figure IV23. A positive relationship with R^2=0.59 obtained between dissolved manganese and dissolved iron at BA transect, suggesting that both metals came from a similar local source: the islands themself.

At the BA stations that were in close proximity of the Crozet Islands the concentrations of manganese in surface waters were thus high because of the island source, and with low Chl-*a* values, significant uptake by phytoplankton is not evident. In these turbid waters removal to particles may occur but the source term still seems large enough to mask any such removal. As iron can easily be oxidised to the solid (particulate) phase, the

concentrations of dissolved iron at the stations closest to the shore (turbid water) were low relative to dissolved manganese, which is oxidized and removed more slowly. Overall, the concentrations of dissolved iron were elevated at all BA stations (Figure IV23), and this information was used in proving that lateral advection was very important in relieving HNLC conditions to the north of the islands (Planquette *et al*., 2007).

6.5 Budget summary of dissolved manganese concentrations before the bloom event

Using the available data on the concentrations of dissolved manganese, where samples were collected during the end of the austral spring bloom (Figure IV24), the concentration of dissolved manganese that accumulated during the austral winter (before the beginning of the bloom events) could be estimated.

The Crozet Plateau, which is strongly influenced by the islands effect, received three main inputs that could be considered in this study: atmospheric, vertical and lateral fluxes. The combination of these three fluxes over the winter period of 100 days divided by the depth of the winter mixed layer of 100 m (Equation 9), gives an increase in concentration of 0.10 nM (minimum estimate) and 0.42 nM (maximum estimate) of dissolved manganese prior to the bloom, as calculated below:

$$((Mn_{atm} + Mn_{vertical} + Mn_{lateral} (nmol\ m^{-2}\ d^{-1})) \cdot 100\ d / 100\ m \quad (9)$$

$$(18.5\text{-}5.2\text{+}92) \cdot 100) / 100) = \mathbf{105.3\ nmol\ m^{-3} = 0.10\ nM\ (minimum)}$$

$$(18.5\text{-}133\text{+}532) \cdot 100) / 100) = \mathbf{417.5\ nmol\ m^{-3} = 0.42\ nM\ (maximum)}$$

where Mn_{atm} is the atmospheric input, $Mn_{vertical}$ is the vertical input, $Mn_{;lateral}$ is the lateral input of total dissolved manganese.

An increase in dissolved manganese of about 0.4 nM (*see* Figure IV19) at the Northern Sites due to lateral and other inputs is consistent with the difference in surface dissolved manganese between the north and the south stations.

Light limits PP over the winter period; the concentration of dissolved manganese is therefore estimated to increase by up to 0.42 nM in waters to the north of the islands. As light levels increase gradually over the spring and summer, relatively high dissolved manganese concentrations are expected in surface seawaters due to photoinhibition of Mn(II) oxidation by bacteria (Tankere *etal.,* 2000; Sunda and Huntsman, 1988) and high rates of Mn oxide reductive dissolution (Tankere e*t al.,* 2000). Moreover, Sunda and Huntsman (1998) found that sunlight increased the dissolution rate of manganese oxides in seawater 6-70 times that in the dark. Previous studies showed that the lack of manganese oxide particles (particulate manganese) near the surface waters result in low

manganese removal rates by aggregation and sinking of manganese oxide particles (Sunda and Huntsman, 1988; Sunda and Huntsman, 1998; Tankere *et al.,* 2000). These low scavenging rates and photo-inhibition of the bacteria, in turn, increase the residence time of dissolved manganese in surface seawater and thereby contributed to surface maxima in dissolved manganese concentrations.

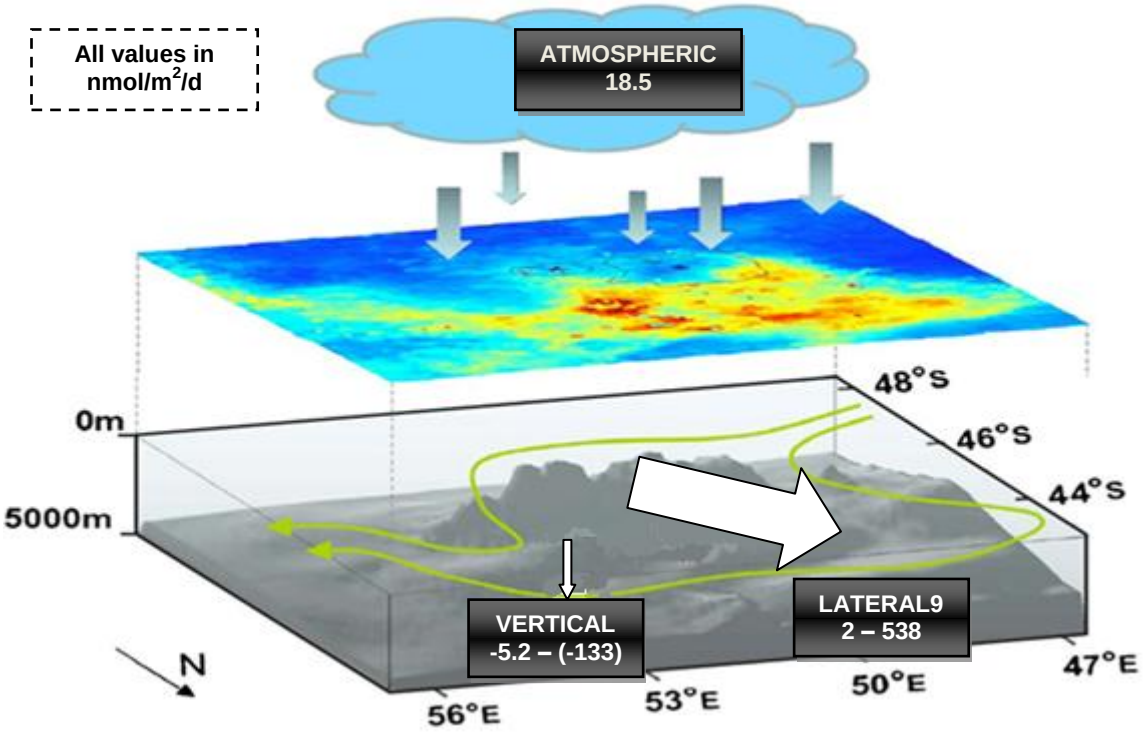

Figure IV24. Major dissolved manganese inputs into the bloom area around the Crozet Islands during austral summer 2004-2005, combined with the main circulation paths (green lines), topography and a SeaWIFS chlorophyll image. All dissolved manganese values are in nmol/m^2/d. *Note: negative values for vertical input indicated the direction of the flux (i.e. into the deep waters)*. Chart and circulation paths adapted from Planquette (2008)).

6.6 Removal and cycling processes of manganese

6.6.1 Biomass uptake

Manganese plays an important role in biological processes of phytoplankton, mainly in the metabolic and PSII processes. However, there are a variety of factors to take into account before one can simply say that manganese provides a big influence on the phytoplankton bloom; these include: (1) variable inputs (e.g. dust and island) which may lead to varying manganese concentrations in the water column, (2) when the phytoplankton need the manganese, and (3) how much manganese is needed by the phytoplankton.

The uptake of dissolved manganese is at maximum during the growth of phytoplankton, and depends on the species. Phytoplankton growth is stopped at some stage, may be due to lack of macronutrients (*e.g.* phosphate, nitrate+nitrite, dissolved silicon) in the upper water column. During this stationary phase of the phytoplankton life cycle, dissolved manganese is adsorbed onto the outer layer of phytoplankton cells. Biogenic material, which is the main component of particle flux, then increases after the bloom event as dead phytoplankton sink down through the water column into the deep ocean, thus losing the dissolved manganese from the upper ocean. The sinking manganese is then released back into the water column by recycling processes and the vertical mixing (*e.g.* upwelling) brings the dissolved manganese back into the upper water column. Some fraction of the particulate manganese will be removed from the water column and deposited into the sediment.

However, only small amount of manganese is required by phytoplankton to get function for the growth. From the extended Redfield ratio show in Chapter I, the amount of manganese needed by phytoplankton can be calculated. By assuming all organic carbon (C) are phytoplankton, therefore at approximately 0.6 µg Chl-*a*/L, 1.0 µM C (Moore *et al.*, 2007) is produced. Based on the extended Redfield ratio, the ratio of C:Mn is 41300:1, which shows only tiny fraction of manganese (~25 pM) relative to the manganese concentration is needed by the phytoplankton to support their growth. This is explained the scattering and not significant (values obtained were not within the 95% confidence level) plots in DMn-Chl-*a* relationship (R^2=0.008, p>0.05) (Figure IV25). Thus, the distribution of dissolved manganese is largely driven by the inputs term and the biogenic sinking flux of the water column.

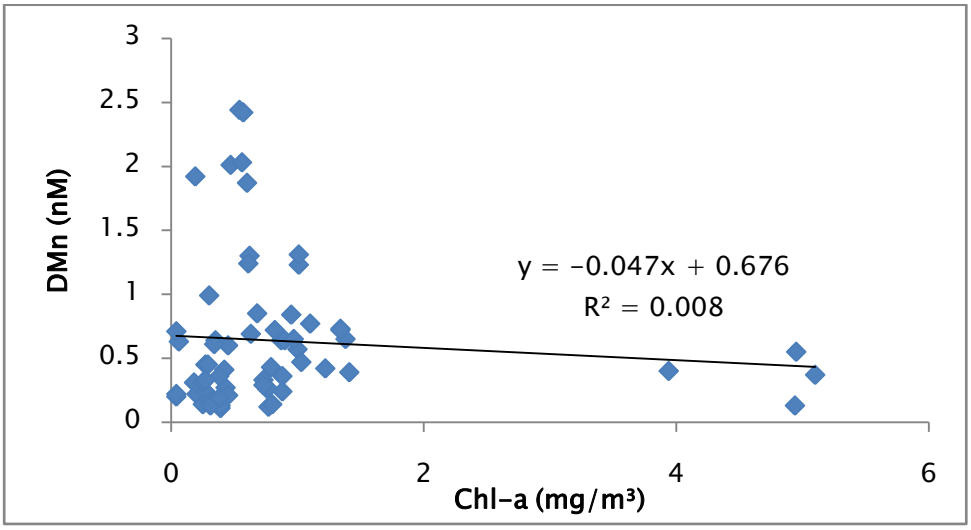

Figure IV25. The relationship between dissolved manganese and Chl-*a* around the Crozet Islands.

6.6.2 Residence time of dissolved manganese around the Crozet Islands

Estimation of the residence times of dissolved manganese around the Crozet Islands is important in order to calculate the average amount of time that dissolved manganese spends in these waters. An important assumption is that the average of the manganese inputs are equal tothe manganese removal terms i.e. the system is in steady state. For stations away from the islands residence times were obtained by dividing the inventory of dissolved manganese in the mixed layer by the dissolved manganese atmospheric flux into the mixed layer (Equation 10; de Jong *et al.,* 2007):

$$\tau_{DMn} = ([DMn]_{obs} \cdot Z_{mix}) / F_{atm,\ dMn} \quad (10)$$

whereτ_{DMn} is the residence time for a dissolved manganese, $[DMn]_{obs}$ is the measured average dissolved manganese concentration at the surface, Z_{mix} is the mixed layer depth, and $F_{atm,\ dMn}$ is the dissolved manganese atmospheric flux (**6.24 µmols m^{-2} yr^{-1}**; seedetails inSection 6.1). However, for BA and M3 stations, the dissolved manganese lateral flux **(average value of 315 µmols m^{-2} yr^{-1}**) must be included into Equation 10 since the island/plateau fluxes are orders of magnitude higher than the atmospheric fluxes. These higher fluxes will bring down the residence time dramatically, and these inputs would be balanced with biological uptake/adsorptionand particle loss during the bloom. The detailed results were shown in the Table IV3.

Table IV3. Dissolved manganese residence time at all stations with the mixed layer depth (MLD) and the average of surface dissolved manganese concentrations.

Station	MLD (m)	Average surface dissolved Mn (nmol/m^3)	Residence time (years)
M3 (496)	108	1240	0.4
M3 (572)	75	1310	0.3
M3 (622)	150	550	0.3
BA (567)	50	2420	0.4
BA+1 (568)	60	1870	0.4
BA+2 (569)	55	500	0.1
M1 (491)	95	640	10
M7 (524)	85	720	10
M10 (563)	75	140	2
M2 (502)	10	610	1
M6 (511)	60	310	3
M6 (598)	85	190	3

The residence times of manganese varied from approximately 3 months to 10 years with an average of: 0.3 years at the Central Sites which received direct influence from the island system, 7 years at the Northern Sites where the annual bloom event occurred, 2 years at

the Southern Site which received less/no influence from the island. However, there are several limitations to the residence times estimated here, including:

1. residence times estimated are based on a single manganese value at a particular point in a year. However, dissolved manganese will likely vary over the year and produce different manganese masses in the water column that will give different residence time to those estimated here.
2. there was a clear evidence of manganese build up over the winter time at the Northern Sites where the bloom occurred, but the residence times of manganese given at these Sites maybe overestimated as the lateral flux from the islands were not including in the calculation. The lateral fluxes estimated in this study were in very close proximity to the island system, and as it was not known how these could be attenuated during transit offshore to the distant Northern Sites they could not be readily used.

Overall, the average manganese residence time calculated here was lower than the reported values in the literature in different oceanic waters; for example, 50 years in the Pacific Ocean (Landing and Bruland, 1980), and 20 years in the middle of the North Atlantic Ocean (Sunda and Huntsman, 1988). The residence times presented here are also lower than the residence time given by Shiller (1997) and Middag *et al.* (2011a) who estimated residence times in a range of 4-20 years in the Southern Atlantic Ocean.

6.6.3 Manganese adsorption onto organic particles

Manganese can became associated with biogenic material through:

1. being an intra cellular component for cell functioning
2. non-specific adsorption onto organic debris and particles

Since dissolved manganese removal via internal sequestration is small (*see* Section 6.6.1), , non-specific adsorption onto the organic particles was expected to be significant. The adsorption of manganese onto organic particles might be modelled by using a traditional tracer of particle export such as the disequilibrium between thorium-234 and uranium-238 ($^{234}Th/^{238}U$). The $^{234}Th/^{238}U$ ratio is known to equal 1 at secular equilibrium. A $^{234}Th/^{238}U$ ratio of <1 in a given parcel of water indicates particle export of settling biogenic particles from this parcel. A $^{234}Th/^{238}U$ ratio of >1 indicates particle accumulation and perhaps remineralisation (Morris, 2008 and references therein). The half-life of the soluble ^{238}U is $4.47x10^9$ years, which decays to form the very particle reactive ^{234}Th with a half-life of only 24.1 days. The resulting disequilibrium between the parent ^{238}U and the daughter ^{234}Th activity reflects the net rate of particle export from the upper ocean on timescales of days to weeks (Middag *et al.*, 2011a).

Details of sample collection and sample processing of the soluble parent ^{238}U and the measured daughter ^{234}Th activity are given in Morris (2008). Dissolved manganese concentrations obtained in this study were plotted against the $^{234}Th/^{238}U$ ratio, as shown in Figure IV26. From this figure, modest and significant relationships (values obtained were within the 95% confidence level) were observed between dissolved manganese concentrations (nM) and $^{234}Th/^{238}U$ ratios at all sampling Sites (*i.e.* Northern (R^2=0.565, $p<0.05$), Central (R^2=0.561, $p<0.05$), and Southern (R^2=0.186, $p<0.05$)). All Sites showed positive correlations which indicated more particle export (ratio <1) corresponded to less dissolved manganese (removal of manganese from the water column) and more remineralisation (ratio ≥1) correspond to high dissolved manganese concentrations (recycling of manganese into the water column).

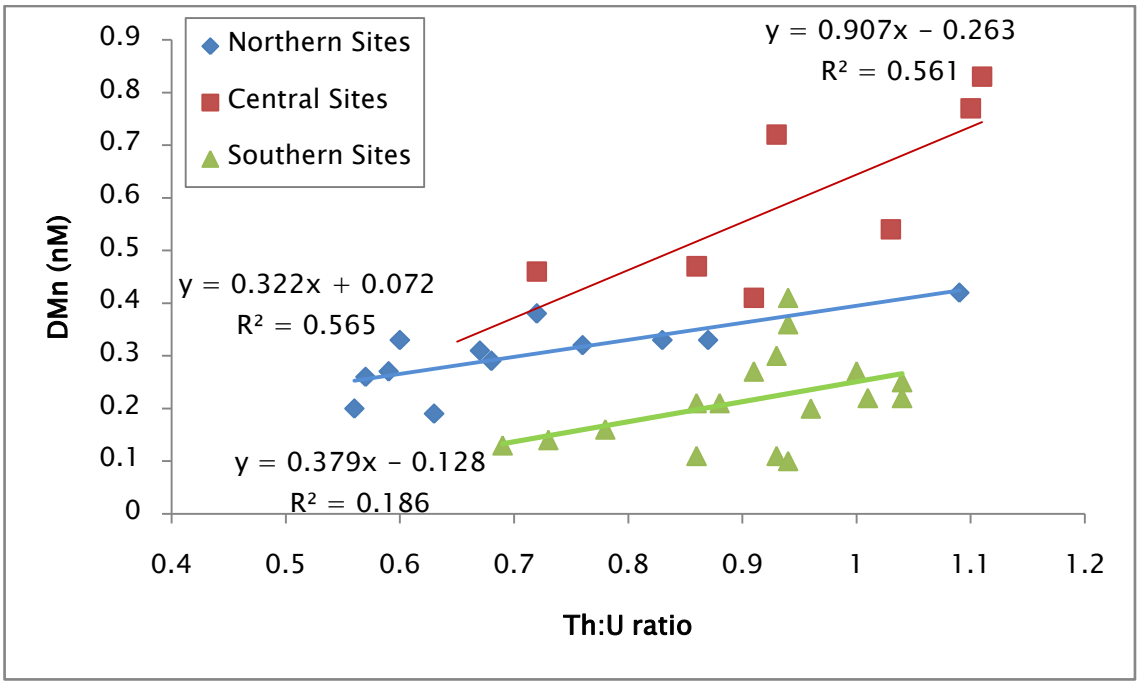

Figure IV26. Relationship between dissolved manganese (DMn) and the $^{234}Th/^{238}U$ ratio at Northern Sites (blue), Central Sites (red) and Southern Sites (green). Data for Th and U were taken from Morris (2008).

In addition to manganese removal by adsorption onto organic particles, Morel *et al.* (2003) suggested manganese might replace iron in some of the enzymes used by the phytoplankton in PSII, and this was supported by Peers and Price (2004) finding that showed diatoms under iron deplete conditions require more manganese than diatoms under iron-replete conditions. When looking at the concentrations of dissolved iron in the surface layer from our north (bloom region) and south (HNLC region) stations (Planquette *et al.,* 2007) the concentrations of iron were lower in the part of the south station compared to the northen part. Typical HNLC diatoms species *i.e. Corethron Antarctica* and *Fragilariopsis kergulensis* were the dominant taxa (>48%) inthe south (Poulton *et al.,*

2007). Here thelow iron concentrations could potentially have been offset by use of Mn. The low concentrations of manganese in the surface layer reported in this study, in combination with low concentrations of iron may have been stressful for phytoplankton particularly diatoms.

7 Summary

The first comprehensive dataset for dissolved manganese in waters surrounding the Crozet islands presented here is internally consistent and generally in agreement with concentrations previously reported for the Southern Ocean. The exceptionally good quality of the data has allowed new insights into the sources, biological uptake and cycling of manganese in the Southern Ocean around the Crozet Islands.

Highest upper water column concentrations of manganese were observed at the BA Stations close to the islands (ranging up to 2.44 nM). Elevated manganese concentrations at these nearshore stations were due to the lateral advection of manganese from the Crozet Plateau in combination with meso-scale circulation. Lateral fluxes from the Crozet plateau were the major source of manganese to the surrounding Crozet waters, especially in the constrained regions to the north of the islands which are influenced by the circulation. The lateral manganese fluxes were calculated using the short-lived Ra isotopes to obtain the minimum and maximum cumulative effect of manganese fluxes around the Crozet of 92 and 538 nmol/m^2/d, respectively.

The manganese concentrations in the deep oceanic waters were low and quite uniform at around 0.1-0.2 nM. By using short-lived Ra isotopes to estimate deep water exchanges of manganese, it can be calculated that any net Mn flux will be into the deep water. A very important point here that deep waters have lower concentration than surface and thus any vertical flux (from deep to surface waters) would reduce surface manganese concentrations. The negative fluxes from the vertical mixing estimated in this study are in a range of -5.2 – -133 nmol/m^2/d.

Another manganese source is the atmospheric input. The atmospheric manganese fluxes by rain (wet) and by dust (dry) depositions were estimated. The total atmospheric dry manganese flux in the Crozet region was calculated to be around 0.4 µmol/m^2/yr, and the estimated wet atmospheric manganese flux was calculated to be around 5.90 µmol/m^2/yr. Combining these dry and wet atmospheric fluxes gives an estimated value of dissolved atmospheric flux of manganese to surface waters of approximately 17 nmol/m^2/d. An increase in dissolved manganese concentrations of ~0.4 nM at the Northern Sites due to lateral and other inputs are consistent with the different of dissolved manganese concentrations between Northern and Southern Sites.

Removal of manganese from the water column can be by association with biogenic material through: (1) as an intra-cellular component for cell functioning, and (2) non-specific adsorption onto organic particles. Manganese removal via internal sequestration is small as only tiny fraction of manganese (~25 pM) relative to the manganese concentration is needed by the phytoplankton to support their growth. Thus, the distribution of dissolved manganese is largely driven by the inputs term and the biogenic sinking flux of the water column. The adsorption of manganese onto the organic particles can be seen by using $^{234}Th/^{238}U$ ratios (Morris, 2008). Positive correlations were observed between dissolved manganese concentrations and the $^{234}Th/^{238}U$ ratio at all sampling Sites (*i.e.* Northern, Central, and Southern Sites) indicating that more particle export corresponds to less dissolved manganese concentrations and the remineralisation process corresponds to high dissolved manganese concentrations in the water column. These high particle exports also correspond very well with lower residence times estimated in this study, except for the Northern Sites where there are several limitations that made the residence times estimation here overestimates.

In addition to manganese removal by adsorption onto organic particles, it was suggested that manganese might replace iron in some of the enzymes used by the phytoplankton when iron was limiting (*e.g.* at the Southern Sites). This is indicative of potential co-limitation by iron and manganese for phytoplankton growth in the Southern Ocean, but more detailed ship incubation studies are required to prove this is so.

Chapter V: Distributions of Dissolved Manganese in the Surface Waters of the Tropical North-Eastern Atlantic Ocean

1 Introduction

The distributions of dissolved manganese in the water column strongly reflect local sources, removal, and recycling processes. In remote ocean regions where there are low manganese inputs, the distribution of dissolved manganese are reported to be a scavenged type where the concentrations are depleted at depth relative to surface values. However, manganese distributions can be significantly modified when there are major atmospheric inputs (de Jong *et al*., 2007; Spokes *et al.,* 2001; Statham and Burton, 1986), sedimentary inputs from shelf and island systems (Chase *et al.,* 2005; Bucciarelli *et al*., 2001; Gordon *et al.,* 1998), and local biological activity may remove Mn. Photochemical reactions can also enhance the concentrations of dissolved manganese in surface waters when this particulate manganese and manganese oxides are brought to the surface during upwelling or/and vertical mixing, or atmospheric inputs may be photo-reduced to the dissolved form, which can be measured using FIA methods (Chase *et al.,* 2005).

Removal of dissolved manganese may occur by (1) uptake by the biota (Luengen *et al.,* 2007); (2) precipitation (Mendez *et al.,* 2010); and (3) scavenging removal of manganese from dissolved to particulate phases (Statham *et al.,* 1998). Therefore, in productive oceanic systems with high inputs from the atmosphere, shelf, and islands, there are a series of complex interacting processes that influence the biogeochemical cycles of dissolved manganese.

In the present study dissolved manganese was determined in seawater samples collected across the Tropical NE Atlantic Ocean which receives episodic atmospheric dust inputs from the Sahara Desert. Moreover, these oceanic waters also contain islands (*i.e*. Cape Verde and Canary) which can also supply manganese from benthic sources in shallow waters (see previous chapter). Therefore, this study aims to investigate the input of manganese from islands as well as from atmospheric sources. The work presented here describes dissolved manganese concentrations in the surface water, and the data are used to study processes affecting dissolved manganese, including island inputs, that provide a conceptual framework for discussing dissolved manganese distributions for such a system.

2 Study area and sampling sites

The tropical NE Atlantic Ocean region receives about a third of global oceanic dust inputs, and NE Atlantic inputs are estimated to range between 400 and 1000 x 10^{12} g y^{-1} (Jickells and Spokes, 2001), and most originate from the Sahara Desert. Thus, high concentrations of dissolved manganese are expected (Xylouri, 2009) to be observed in this region, particularly in the surface water due to these dust inputs. Therefore, 189 Underway surface seawater samples were collected for dissolved manganese analysis during the UK SOLAS project cruise (D326) in the tropical NE Atlantic Ocean on board *RRS Discovery* between 5 January and 5 February 2008, that started and finished at Santa Cruz, Tenerife (Canary Islands) and covered an oceanic area between 12– 27 ˚N and 17– 36 ˚W (see Appendix 3). There were two dust events during the sampling period, as shown in Figure V1.

The Underway stations were divided into three regions based on the locations of the dust events, islands, and water masses in the study region as shown in Figure V1:

- Tropical NE Atlantic (TNEA) (north of ~20 ˚N)
- Cape Verde (CV) (~14 – 20 ˚N)
- Equatorial (EQ) (below ~14 ˚N)

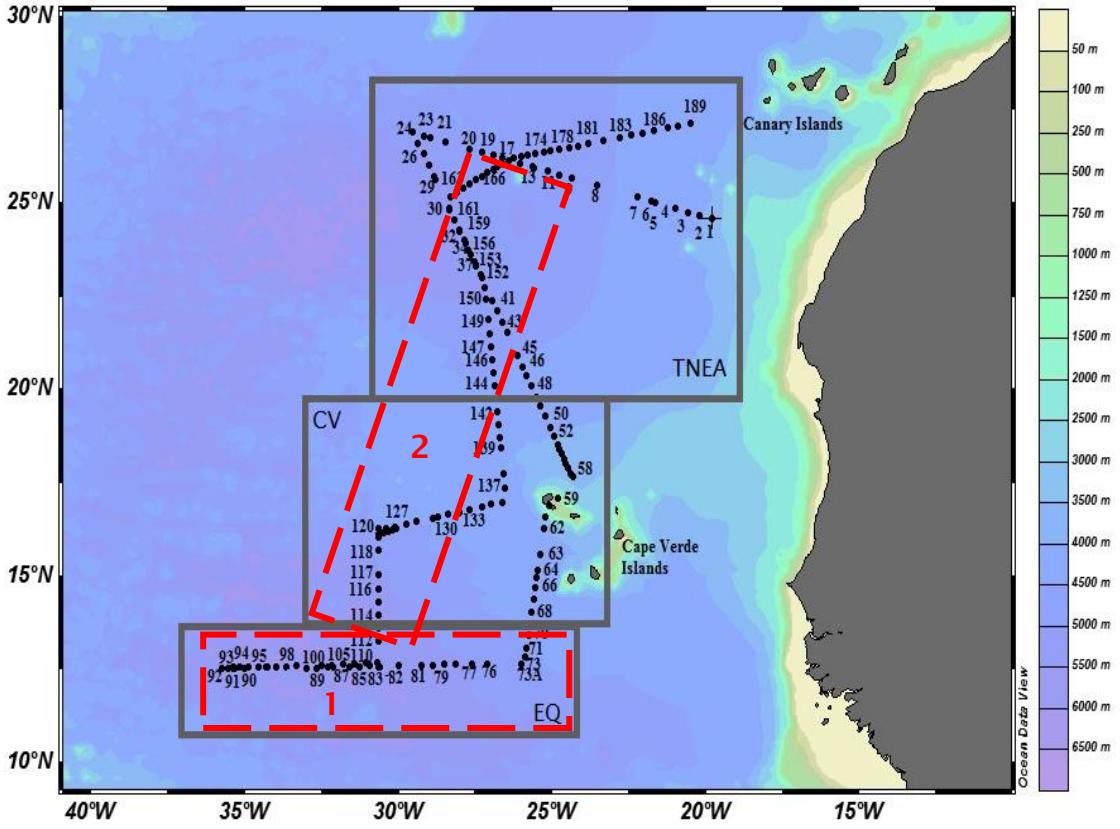

Figure V1: Map of the Underway stations sampled for dissolved manganese analysis during D326 in the Tropical NE Atlantic Ocean. The stations were divided into three regions as marked in grey boxes. Red dash lines show the two regions where there were dust events during the sampling (1: the first event was in the EQ region and, 2: the second event was in the TNEA and CV regions). TNEA: Tropical NE Atlantic; CV: Cape Verde; and EQ: Equatorial.

3 Dissolved Manganese Analysis

Seawater sampling and sample processing were discussed in Chapter II. Analysis of dissolved manganese concentrations were performed after the cruise with the FIA-CL method as described in Chapter III (*see* Section 7) which the Ni interferences were not significant.

4 Results

4.1. Hydrography

Between 27 °N (north of Canary Islands) and 12 °N (south of Cape Verde Islands), the Canary Current flows southward along the African coast at 10-30 cms^{-1}, and about 1000 km wide and ~500 m deep (Batten *et al.,* 2000; Zhou *et al.,* 2000). To the north of the Cape Verde Islands (north of 13 °N), there is the North Equatorial Current (NEC) and Canary Current (CC) (Stramma *et al.,* 2005) characterized by lower temperatures and higher Chl-*a* concentrations due to the North West African Upwelling (Sarthou *et al.,* 2003). A distinct oxygen minimum zone is positioned south of the NEC and north of the North Equatorial Counter-current (nNECC). In the region of 15 °N, the current diverges westward under the influence of the Equatorial Counter-current (Peterson *et al.,* 1996). The northern region at 30 °N is in the subtropical gyre and is characterized by oligotrophic conditions with a deep pycnocline and lower atmospheric dust inputs than the stations close to 10 °N. The 10 °N site is on the edge of the subtropical gyre and equatorial system, and has a shallow pycnocline and higher dust inputs (Bergquist and Boyle, 2006). The hydrography around the Canary Islands and Cape Verde Islands themselves are additionally influenced by coastal upwelling, filaments and eddies (Johnson and Stevens, 2000) (Figure V2).

Temperature-salinity diagrams for all stations indicated three distinct regions, which have been termed as the TNEA, CV, and EQ regions (Figure V3). The TNEA region had mixed layer depth between 100 and 150 m, with a moderate temperature gradient between upper and lower layers (Hill, 2010). Warm waters with shallow mixed layers of 35 to 70 m were evident in the EQ region. A complex surface temperature-salinity pattern was shown in the vicinity of the CV, particularly in the CVFC, (Figure V3) where waters around the CV region received influences from the topography of the Cape Verde Islands (Hill, 2010).

Based on these water masses, station numbers 1 – 48 and 144 – 189 correspond to TNEA, station numbers 49 – 68 and 114 – 143 correspond to CV, and station numbers 69 – 113 correspond to EQ (Figure V3).

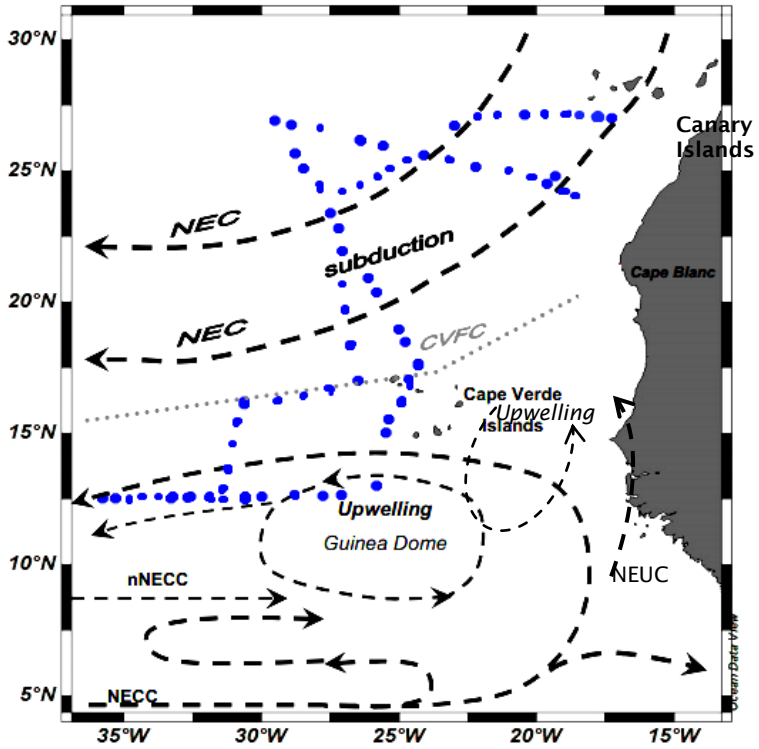

Figure V2. Map of the study area with the cruise track of the *RRS Discovery 326* sailed in January-February 2008. The cruise track is shown in the map with dots together with the large scale near-surface flow field described by black-dashed arrows (Stramma *et al.*, 2005). NEC: North Equatorial Current; nNECC: the return flow of the northern North Equatorial Counter-current; NECC: the north flowing part of the North Equatorial Counter-current which is connected to the NEUC; NEUC: North Equatorial Undercurrent; CVFC: Cape Verde Frontal Zone; and the upwelling regions around the Guinea Dome and Cape Verde Islands.

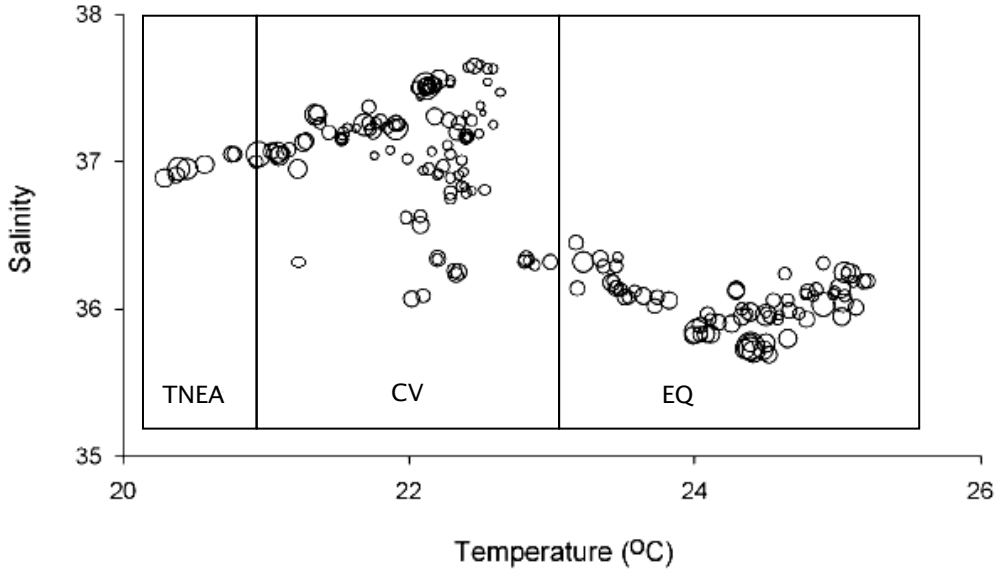

Figure V3: Temperature-salinity plots during the D326 cruise. T-S plots were divided according to three regions: TNEA (Tropical NE Atlantic), CV (Cape Verde), and EQ (Equatorial) regions (adapted from Rijkenberg *et al.*, 2012).

4.2 Dissolved Mn, Chl-*a* , and macronutrients

(Chl-*a* data courtesy of Dr. Duncan Purdie and nutrients data adapted from Dr. Matt Patey of NOCS).

The highest Chl-*a* concentration occurred in the TNEA region to the south of the Canary Islands, with the maximum of ~0.8 µg/L close to the islands (Figure V5).

The concentrations of dissolved manganese in the surface layer of the TNEA region (Figure V4) were generally below 2 nM, with the exceptions of station 1 and Station 146 where the concentrations of dissolved manganese were above 3 nM. Higher dissolved manganese concentrations that were observed close to the Canary Islands coincided with higher phosphate concentrations (~100 nM). However, concentrations of nitrate+nitrite (Figure V7) and Chl-*a* were also elevated at this station with ~50 nM and ~0.8 µg/L, respectively. These elevated concentrations showed that there were additional inputs of nutrients and manganese from the Canary Islands and possibly also the African coast, which subsequently increased the Chl-*a* concentrations. The minimum concentration of the surface Chl-*a* (~0.02 µg/L) was observed in the TNEA region (Station 21) at some distance from the Canary Islands, during the second dust event (Figure V5). During the second dust event, the concentrations of dissolved manganese were not uniform due to sporadic inputs from the atmosphere. In areas where there were assumed to have been high dust inputs recently (containing high soluble manganese), increased concentrations of dissolved manganese (*e.g.* at station 146 (~ 3 nM)) were observed. When the cruise approached the Cape Verde Islands, elevated dissolved manganese concentrations were observed, coinciding with the increased concentrations of phosphate.

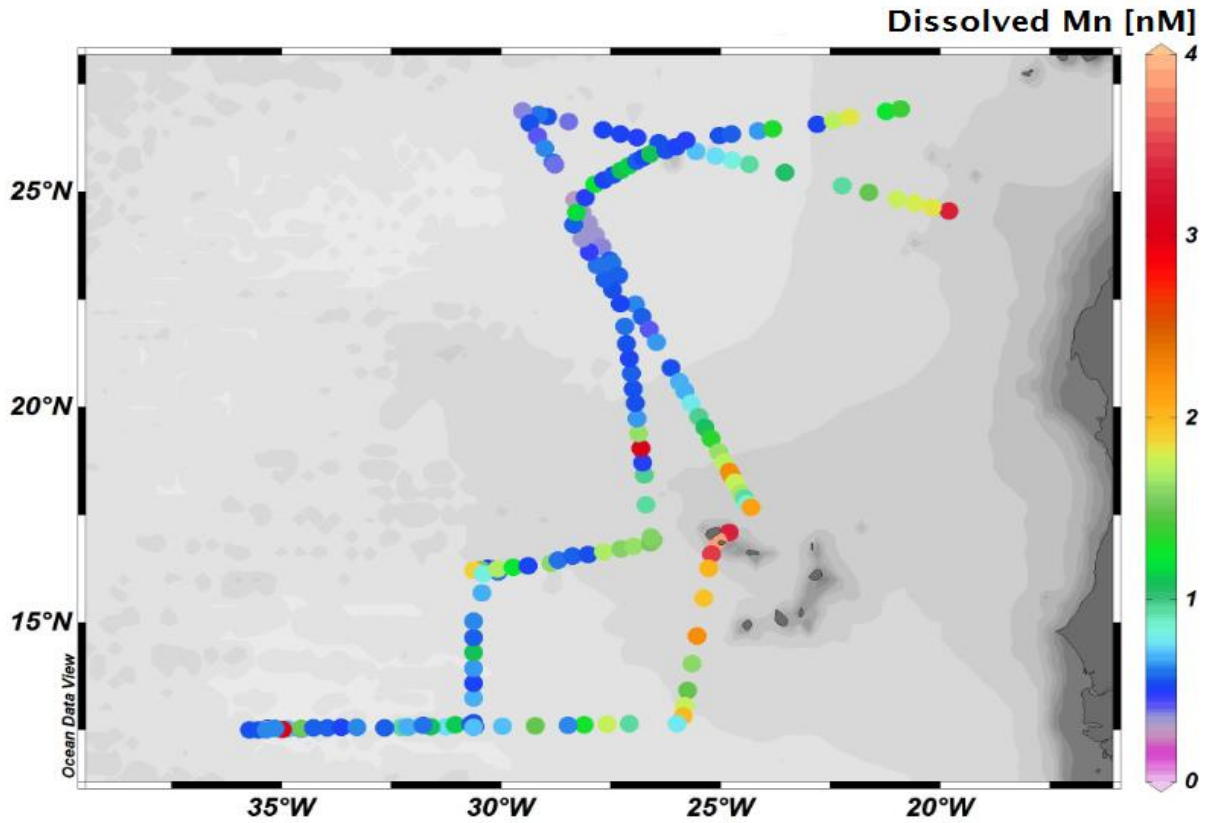

Figure V4. Distributions of surface dissolved manganese (nM) observed during the UK SOLAS Discovery (cruise D326) in the tropical NE Atlantic Ocean.

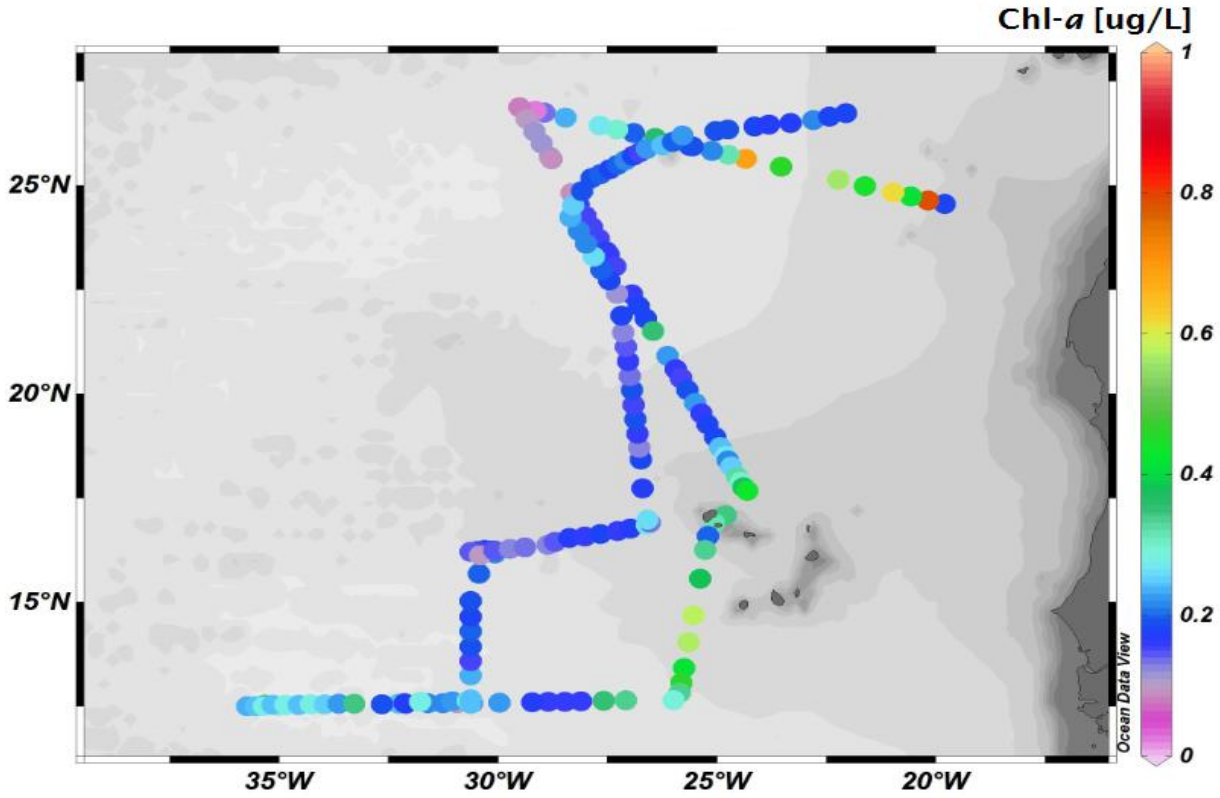

Figure V5. Distributions of surface Chl-*a* concentrations (µg/L), observed during the UK SOLAS Discovery (cruise D326) in the tropical NE Atlantic Ocean.

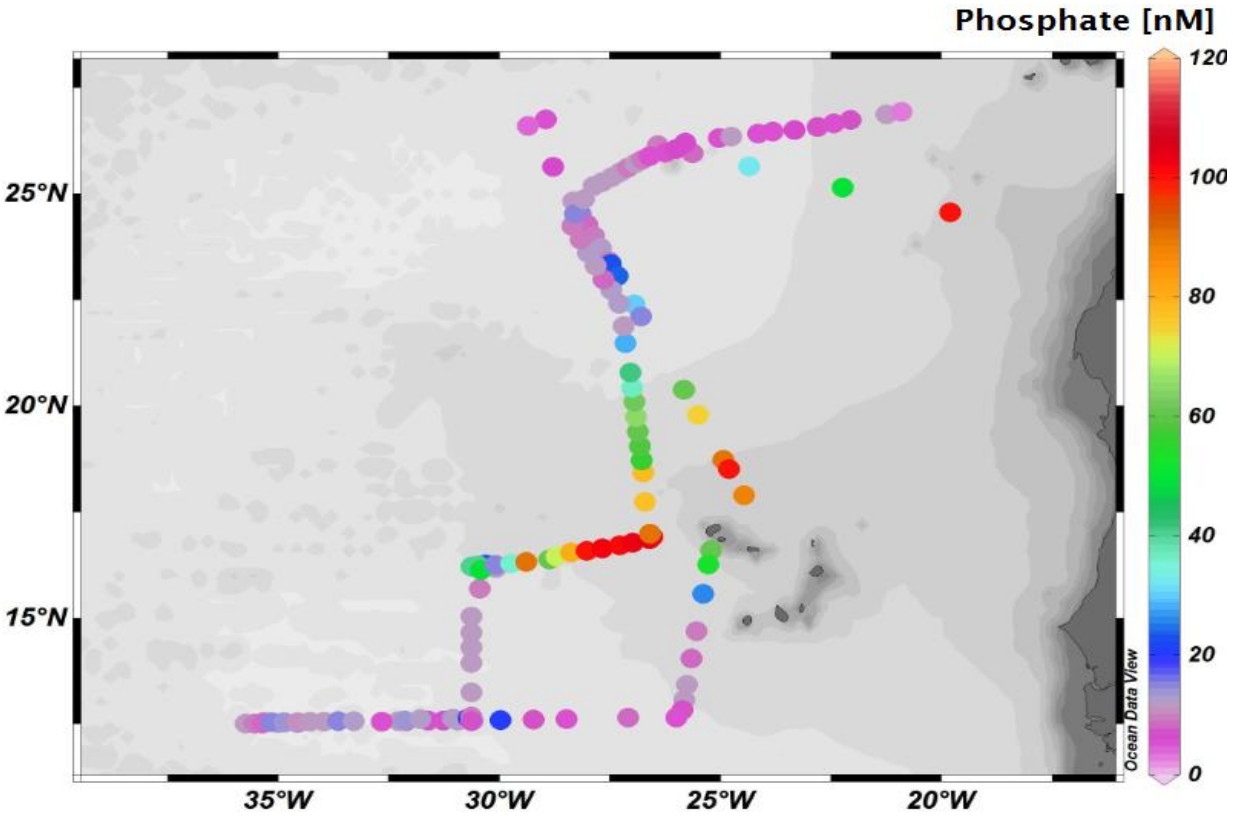

Figure V6. Distributions of surface phosphate concentrations (nM), observed during the UK SOLAS Discovery (cruise D326) in the tropical NE Atlantic Ocean.

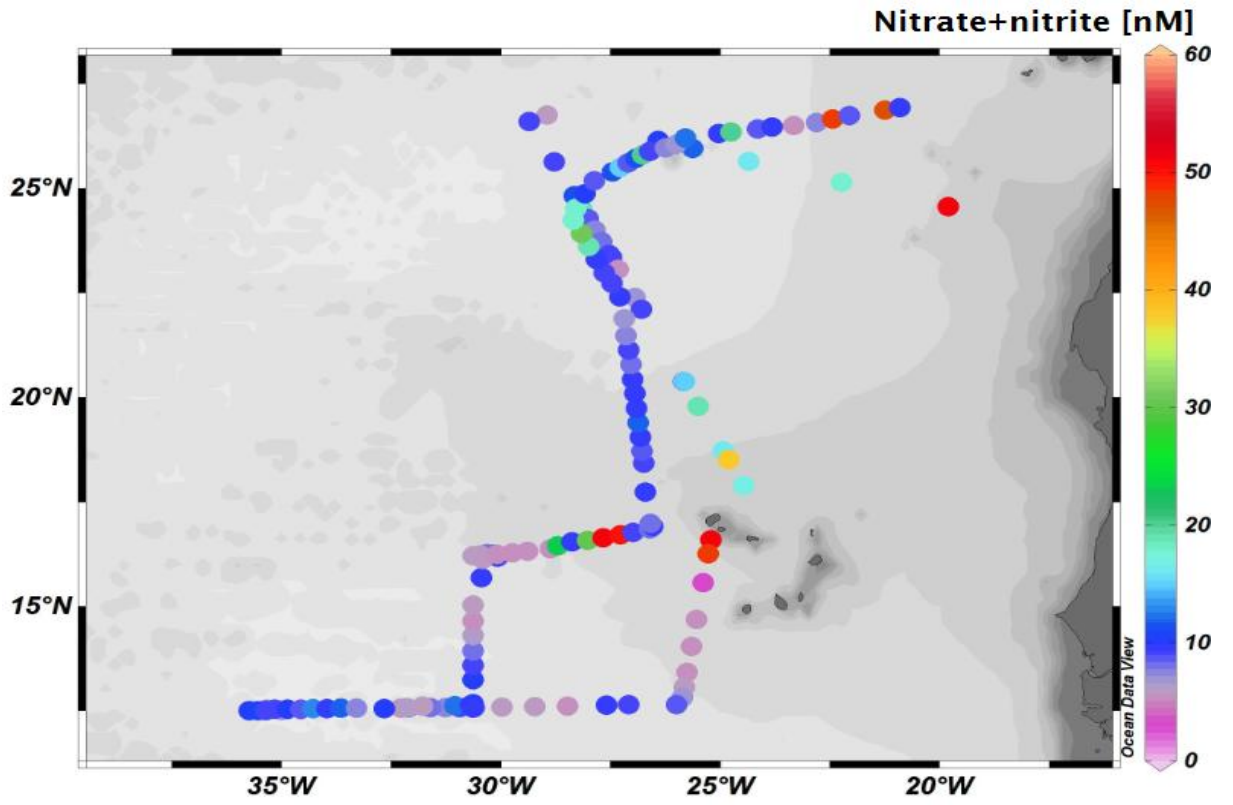

Figure V7. Distributions of surface nitrate+nitrite concentrations (nM), observed during the UK SOLAS Discovery (cruise D326) in the tropical NE Atlantic Ocean.

In the CV region, the concentrations of Chl-*a* were increased up to ~0.6 µg/L (Figure V5) particularly around the Cape Verde Islands. However, the concentrations of Chl-*a* decreased (until ~0.1 µg/L) during the sampling periods (when the cruise sailed back to the Canary Islands) of the second dust event occurred. The surface concentrations of dissolved manganese around the Cape Verde Islands ranged between approximately 0.5 nM and 3.87 nM, with an average of 1.41±0.78 nM (Figure V4). The observed high dissolved manganese concentrations in this region coincided with a complex temperature-salinity pattern in the vicinity of the CVFZ (Figure V3). The dissolved manganese concentrations increased significantly (up to 3.87 nM) in the shallow water (<250 m) depth of the Cape Verde Islands, coinciding with low Chl-*a* and nitrate concentrations. In addition to upwelling, there was also input from the atmosphere at this location. Chiapello *et al*. (1995) observed that the Cape Verde Islands receive maximum dust inputs between November and April as winds direction which transport dusts from the African continent in the trade-wind layer affects only the tropical NE Atlantic Ocean. At station 68, where the highest Chl-*a* concentration (~0.6 µg/L) of this region was recorded, both major nutrients (phosphate and nitrate+nitrite) concentrations were at minimum (Figures V6-V7), and the concentration of dissolved manganese was also significantly decreased to approximately 1.6 nM. When the second dust storm started (on 25th January 2008), dissolved manganese concentrations were reduced to ~1.09 nM before gradually increasing to approximately 1.90 nM. The phosphate concentrations also following a similar trend, but with significant increases. Enhanced phosphate concentrations during the dust events have been observed in the Mediterranean Sea, where aerosols form a crucial source of phosphate to oligotrophic oceans (Rijkenberg *et al.,* 2012 and references therein).

In the EQ region, there were variable concentrations of Chl-*a* during the first dust event that occurred, with highest and lowest concentrations of ~0.6 µg/L and ~0.1 µg/L respectively, to give an average concentration of ~0.26 µg/L (Figure V5). The concentration of Chl-*a* was at a maximum at station 69, coinciding with low phosphate and dissolved manganese concentrations. When the concentrations of Chl-*a* gradually decreased along the underway stations the phosphate and dissolved manganese concentrations showed an inverse pattern. Phosphate concentrations were enhanced significantly (~20 nM) during the first dust event at station 82 and at station 93 to approximately 24 nM, corresponding with elevated dissolved manganese concentrations at both stations (Figure V4). However, nitrate+nitrite and Chl-*a* concentrations were low during the first dust event, with an exception at station 90 where the Chl-*a* concentration was elevated, when both nitrate and phosphate concentrations were low. Apart from the dust event, these variable concentrations of dissolved manganese, Chl-*a*, and major nutrients observed at this region were also influenced by the large scale near-surface currents (Figure V2) flow across this

EQ region, such as the NECC, the nNECC and the upwelling around the Guinea Dome. Chl-*a* and macronutrients are variable depending on bloom development.

Overall, dissolved manganese concentrations obtained in this study were about double the concentrations observed by de Jong *et al.* (2007) who found an average value of approximately 0.50±0.08 nM. However, our values were lower than the values determined by Bergquist and Boyle (2006) further offshore in the Tropical and Subtropical Atlantic Ocean, who found an average concentration of 2.60±0.36 nM. Our values are in the range of values obtained by Statham *et al.* (1998) within the range of 0.90-2.12 nM in the North-eastern Atlantic Ocean.

5 Discussion

Dissolved manganese and associated data (*e.g.* chl-*a* concentration, macronutrients, temperature, and salinity) were used to study the biogeochemistry of dissolved manganese in the surface Tropical NE Atlantic Ocean. Firstly the sources of dissolved manganese in near-surface waters across the study area are identified. The distribution of low dissolved manganese concentrations were then examined particularly during the dust events, focusing on upper water column transport. Finally, dissolved manganese distributions were studied in relation to the biology.

5.1 Atmospheric dust as a potential dissolved manganese source

Distributions of manganese in seawater are controlled by a combination of several important factors, but particularly the sources of manganese. Atmospheric input is the most important source of manganese in the open ocean. Modifications of biogeochemical fluxes in surface waters mainly depend on atmospheric inputs, plus photo-reduction and physical processes. However, tracing individual sources of manganese to specific regions is complicated by several factors and really depends on the physical and chemical properties of the waters at the stations. During the research cruise, two significant dust events were noticeable. The first dust event was encountered between 17 and 22 January 2008 (EQ area) and the second dust event (further north) was longer, from 25 January to 1 February 2008.

Dissolved aluminium data have been used as a proxy of atmospheric dust deposition in the ocean (Measures and Vink, 2000). From Al data obtained from this cruise, estimated atmospheric fluxes of soluble manganese to the Tropical NE Atlantic Ocean can be calculated. (Special thanks to Dr. Sebastian Steigenberger from NOCS for providing dissolved aluminium data).

Atmospheric deposition occurs by dry (dust) and wet (rain) deposition. However, in this thesis it is not possible to calculate wet deposition fluxes as there were no rain samples collected during the sampling period. In addition, dry dusts originating from the arid regions of western Africa are associated with very little rainfall, thus it make dry deposition the dominant atmospheric mode of input (Baker *et al*., 2007). The dust input D (**8.55 g/m^2/yr**), was estimated using the Equation 1 below, as described by Measures and Vink (2000) and de Jong *et al*. (2007):

$$D = ([DAl]_{sw} M_{Al} z_{mix} / \tau_{DAl}) / (S_{Al} A_{Al}) \qquad (1)$$

,where $[DAl]_{sw}$ is the average concentration of dissolved aluminium in surface seawater (27.53 nmol/m^3, (Patey, 2010)), M_{Al} is the atomic weight of aluminium (26.98 g/mol), z_{mix} is the mixed layer depth (90 m), τ_{DAl} is upper ocean residence time of dissolved aluminium (4 year), S_{Al} is the Al solubility of Saharan dust (3.0 %) from Baker *et al*. (2006), A_{Al} is the abundance of Al in Saharan dust (6.51 % by weight (Guieu *et al*., 2002)).

From the calculated atmospheric dust flux above, the atmospheric flux of manganese was calculated using the Equation 3 in Chapter IV:

$$F_{atm, TMn} = (D A_{Mn}) / M_{Mn}$$

where $F_{atm, TMn}$ is the total atmospheric flux (**111 µmol/m^2/yr**) of manganese, D is dust input (8.55 g/m^2/yr), A_{Mn} is manganese abundance in Saharan dust (0.0712%, Wedepohl, 1995), M_{Mn} is atomic weight of manganese (54.94 g/mol).

From the $F_{atm, TMn}$ value, the dissolved manganese flux ($F_{atm, DMn}$ = **61.10 µmol/m^2/yr**) was calculated after the equation of de Jong *et al.* (2007):

$$F_{atm, DMn} = (S_{Mn}) \cdot (F_{atm, TMn}) \qquad (2)$$

,where S_{Mn} is solubility for median particle size values for Saharan dust from Baker *et al*. (2006): Mn 55% (range 50-64%).

Therefore, the atmospheric dust deposition flux for soluble manganese in the study region is **0.17 µmol/m^2/d**. This value is low compared to iron and aluminium values which are approximately 3870 µmol/m^2/d and approximately 140 µmol/m^2/d, respectively (Patey, 2010).

5.2 Residence time of dissolved manganese

Estimation of the residence time of dissolved manganese around the study region gives the average time that dissolved manganese spends in the surafce waters. As explained in Section 6.4.1 of Chapter IV, the residence time of dissolved manganese at a steady state can be calculated by using the equation below:

$$\tau_{DMn} = ([DMn]_{obs} \cdot Z_{mix}) / F_{atm,\ dMn}$$

where τ_{DMn} is the residence time for dissolved manganese, $[DMn]_{obs}$ is the measured surface average of dissolved manganese concentration (this is assumed to be constant throughout the mixed layer), Z_{mix} is the mixed layer depth (90 m), and $F_{atm,\ dMn}$ is the dissolved manganese atmospheric flux (**61.1 µmol m^{-2} yr^{-1}** or **170 nmol/m^2/d**). The residence times for individual stations are shown in Appendix 3, and results are summarized in Table V1.

Table V1. Average of dissolved manganese residence times for different regions. The mixed layer depth (MLD) is 90 m, and the atmospheric flux of dissolved manganese is 61.10 µmol m^{-2} yr^{-1}.

Station	Residence time (years)
	Average (year)
TNEA region	0.66
CV region	1.14
EQ region	0.75

Overall, average residence time of dissolved manganese at these study regions were approximately 1 year and the residence times obtained in this study were slightly shorter than previously estimated, for example, de Jong *et al.* (2007) estimated a range of 1.0 – 3.8 years, with an average of 1.9 year in the NE Atlantic Ocean. However, their atmospheric input was low compared to the atmospheric input during this study. The surface concentrations of dissolved manganese in this study are also higher than de Jong *et al.* (2007) values. Therefore, the dissolved manganese distributions at the tropical NE Atlantic Ocean and atmospheric sources are more temporally variable than previously thought.

On the repeat transect along the EQ section, the concentrations of dissolved manganese were lower than on the outbound leg. However, the concentrations of dissolved aluminium and dissolved iron (Rijkenberg *et al.*, 2012) were elevated in the surface layer, indicating an atmospheric source of trace metals at these stations. The expected dissolved manganese concentrations enrichment in a cubic meter of seawater due to atmospheric inputs can be calculated by using Equation 3:

$$\text{DMn enrichment} = F_{atm,\ DMn} / \text{MLD} \qquad (3)$$

where $F_{atm,\ DMn}$ is the atmospheric dust deposition flux for soluble manganese, (170 nmol/m^2/d) and MLD is mixed layer depth (90 m). By putting these values into Equation 3, the concentrations of dissolved manganese per 1 m^3 (1000L) input around the dust event regions is **0.002 nmol/L/d**, to give approximately **0.73 nmol/L/yr,** which is consistent with the data obtained here (given typical concentration values and a residence time of about 1 year) . These values thus supported the low average residence time calculated in dust event regions of around 1 year.

The reason for the observed low Mn values compared to high Al and Fe is most likely the large inputs of Al and Fe relative to Mn in this zone.

5.3 Islands and coastal mainland systems as potential sources of dissolved manganese

The relationship between concentrations of dissolved manganese adjacent to the African continent, and the distance from the African continent (in km) were examined in order to investigate the source of dissolved manganese in the surface layer ocean (adapted from Rijkenberg *et al*. (2012)). The distribution of dissolved manganese in the TNEA region decreased exponentially with increasing distance from the African continent (R^2 = 0.897, [DMn] (nM) = $2.812e^{-(x)}$, where x is the distance in km) (Figure V8). However it must be remembered that a part of this signal may originate from the upstream Canary Islands, as well as the African coast.

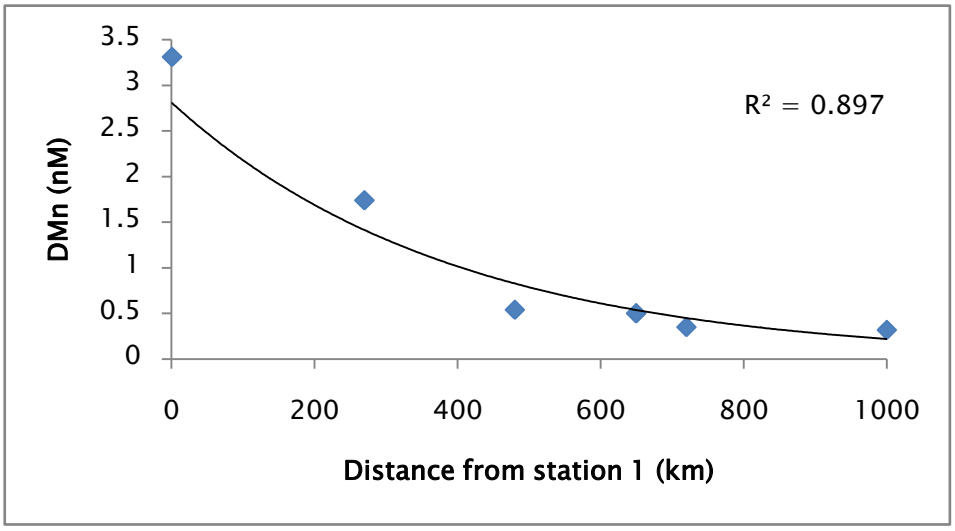

Figure V8. The dissolved manganese concentration in the surface layer for stations influenced by Canary Islands and the African continent inputs, and the offshore stations. Station 1 is the closest to the African continental shelf and its x-position is set to 0 km.

The horizontal flux of dissolved manganese (F_{DMn}) was calculated using Equation 4:

$$F_{DMn} = C_0 e^{-x/D} \qquad (4)$$

where C_0 is the concentration at station 1, x is the distance (km) from station 1, and D is the scale length (451 km, Rijkenberg *et al*. (2012)). The exponential fit was [DMn] = $2.812e^{-x/451}$ (Figure V.7). Then, the parameterization to estimate lateral diffusion coefficient (K_h, m^2/s) can be calculated by using Equation 5 to give a value of **1.83 m^2/s**:

$$K_h = 7.3x10^{-4}D^{0.15} \qquad (5)$$

Combining this estimated lateral diffusion coefficient, K_h, with the dissolved manganese gradient from near shore to further offshore ($DMn_{gradient}$), gives a lateral flux of dissolved manganese (DMn_h) of **47.4 µmol m^{-2} d^{-1}** or **17.3 mmol m^{-2} yr^{-1}** (dependent on the coastline length), as calculated in Equation 6:

$$DMn_h = DMn_{gradient} \cdot K_h \qquad (6)$$

$$DMn_h = 0.003 \text{ nmol } m^{-3}\, m^{-1} \cdot 1.83 \text{ m}^2\, s^{-1} \cdot 3600 \text{ s} \cdot 24 = 47.4 \text{ µmol } m^{-2}\, d^{-1}$$

The decrease in dissolved manganese coincided with an increase in dissolved aluminium (Rijkenberg *et al.,* 2012). Therefore, a continental source of waters rich in dissolved manganese but not dissolved aluminium appears to have influenced the dissolved manganese distribution. The source of dissolved manganese may either be anoxic shelf sediments (Chase *et al.,* 2005) or the upwelling of deep waters along the continental shelf which may have collected Mn from the shelf on its trajectory. Elevated concentrations of dissolved manganese in bottom waters may be due to the release of dissolved forms of manganese from re-suspended particles and the diffusion from pore waters (Laes *et al.,* 2007). Sediment on the continental shelf may be high in dissolved and particulate manganese including manganese oxides (MnO_x).. Particulate manganese from the sediment can be brought back to the surface water during the upwelling and strong sunlight in the tropical NE Atlantic Ocean can enhance the photo-reduction process which changes the particulate form of manganese to the dissolved form (Sunda and Huntsman, 1983; Chase *et al*., 2005).

Hence, from our observation, it suggests that the shelf and sediments are major sources of dissolved manganese for this area and not the dust input alone. As the atmospheric inputs estimated for this study are small (0.17 µmol m^{-2} d^{-1}), this makes the shelf+sediment sources the most important dissolved manganese sources in the seawater close to the islands and mainland. Further offshore atmospheric inputs are expected to dominate.

There is a potential to gain much more biogeochemistry knowledge of the system if the manganese data presented here were interpreted in combination with the corresponding iron and aluminium data. This could be a target for future work.

7 Summary

The Tropical NE Atlantic Ocean receives dust inputs mostly originating from the Saharan Desert. There were two dust events that occurred during the sampling period. The first dust event was from 17 until 22 January 2008, and the second was longer than the first event and occurred between 25 January and 2 February 2008.

However, relatively low concentrations of dissolved manganese were observed during both dust events, suggesting only small inputs. Dust inputs will be episodic, but an estimation of the annual atmospheric flux of dissolved manganese was calculated and gave a value of approximately 61 μmol/m^2/yr or about 0.17 μmol/m^2/d, which was low compared to the atmospheric fluxes of dissolved iron and dissolved aluminium (Patey, 2010). The residence times obtained from this study were approximately 1 year which was slightly shorter than previously estimated, thus suggesting that the dissolved manganese distribution in the Tropical NE Atlantic Ocean are more temporally variable than previously thought. Furthermore, dissolved manganese enrichments of 0.002 nmol/L/d or 0.73 nmol/L/yr were estimated in the seawater around the dust events, which is consistent with the background concentrations of dissolved manganese obtained here.

Higher surface concentrations of dissolved manganese were observed at stations in close proximity of the islands and coastal mainland sources (*e.g.* the Canary Islands, the Cape Verde Islands, and the African continent), up to ~3.90 nM. To investigate the source of dissolved manganese in the surface layer ocean at these regions, the relationship between dissolved manganese concentrations and the distance of the stations from the closest station (Station 1) to the African continent were studied. The distribution of dissolved manganese decreased with increasing distance away from the land sources (*i.e.* TNEA region). The lateral dissolved manganese flux was calculated to give a value of approximately 47 μmol/m^2/d or ~17.3 mmol/m^2/yr. However, the atmospheric input estimated for this study were small (0.17 μmol m^{-2} d^{-1}), thus making the shelf+sediment the most prominent dissolved manganese sources in the seawater close to the islands and mainland. Further offshore, the atmospheric inputs dominate.

Chapter VI: Conclusions and Future Work

1 Overview

The aim of this project was to improve our understanding of the marine manganese cycle by investigating the processes influencing the dissolved manganese distributions in two different regions. The two main objectives were: **(1)** to develop a working analyser for measuring down to picomolar concentrations of dissolved manganese, and to ensure the data obtained were in good quality; and **(2)** to apply this method to determine dissolved manganese in seawater samples collected in two different regions: the Crozet Islands in the Southern Ocean, and the tropical NE Atlantic Ocean.

The implementation of the analytical method using recently published methods proved difficult. Given the difficulties in optimizing the initial method chosen (*see* Chapter III), an alternative technique was developed, which also proved difficult, but with a few modifications to remove interferences, it was finally used successfully (*see* Chapter III). The data quality was high and data for CRMs were in a good agreement with accepted values. A summary of major findings from this analytical work and suggestions on the future work are given in Section 2.

Seawater samples from the two study regions were collected using clean trace metal techniques to avoid any risk of contamination. Initially, seawater samples collected during the UK SOLAS project cruise (D326) in the tropical NE Atlantic Ocean were analysed using the newly developed method for dissolved manganese (the flow injection analysis technique with chemiluminescence technique) as described in Chapter III. Then, samples collected during the CROZEX cruises (D285 and D286) on board *RRS Discovery* around the Crozet Islands on the edge of the Southern Ocean were also analysed using the same technique but with further modifications, as described towards the end of Chapter III.

The concentrations of dissolved manganese in these regions were generally in agreement with other studies (see Chapter IV and V), and the data was interpreted in terms of processes (inputs, removal, and transport/cycling) that influence the distributions of dissolved manganese in the Southern Ocean – Crozet Islands, and in the Tropical NE Atlantic Ocean. These data were used in association with additional information to give a conceptual framework for future studies in these environments (see Chapter IV and V). A summary of main findings from the study of the Crozet Islands samples and suggestions for future work are given in Section 3.1, and the findings from the study of the Tropical NE Atlantic Ocean samples and suggestions for future work are given in Section 3.2.

2 Objective 1: Analysis of dissolved manganese

The flow injection analysis (FIA) method developed in this study was chosen on the basis of several important criteria such as offering the possibility of low detection limits, requiring very little samples, reagents and analysis time, and reducing the risk of contamination during analysis. FIA with the chemiluminescence (CL) reaction with luminol were chosen for analysing dissolved manganese in this study (*see* Chapter III).

2.1 Implementation of a manual Mn(II)-FIA-CL analyser to detect Mn(II) concentrations in seawater

Chemiluminescence (CL) is the emission of light during the oxidation of luminal by H_2O_2 in the presence of Mn(II) as catalyst. The Mn(II)-FIA-CL detection system was relatively simple and quick to assemble; however development of the method proved difficult. The main problems were with the pre-concentration step, mixing coil length, CL reaction and interferences. However, this CL reaction was not actually detecting Mn(II) alone, and several secondary reactions were occuring simultaneously. Thus, optimisation of resins used and chemical reactions involved during the analysis were needed to make determination of Mn(II) possible. The commercially available Toyopearl AF-Chelate 650M resin was used in this study to pre-concentrate Mn(II) in seawater at pH~8.5.

However, the seawater matrix is complex and may create interferences during the detection step and enhance the baseline level. Thus a washing step with MQ water was needed to remove seasalts present in the dead volume of the Toyopearl column. The cleaning resin of the NTA Superflow resin column was placed in series with the Toyopearl resin column, to remove the inteference of other trace metals *e.g*. iron and copper ions. Adding the NTA resin as a cleaning resin reduced the baseline level and the blank. When 'old' luminol stock solution was used in the analysis the baseline level increased and made the CL peak shorter and broader, thus, the luminol stock solution was needed to freshly prepare every week, and luminol+TETA solution was made every day to ensure a low baseline level.

There were still other analytical challenges that occurred during the processes of improving and optimising the performance of the system: (1) problem with pH conditions on adsorption and desorption of Mn(II) onto/from the Toyopearl resin, and on the CL reaction; (2) problem of poor reproducibility and double peak for low Mn(II) concentration samples; and (3) poor calibration. Extensive works were carried out in order to find the sources of the problems and to solve them as they arouse. (1) The resin uptake/release and the CL reaction were pH depended. It was very important to ensure that standard/sample and reagents to be in the correct pHs to perform a good analysis. Therefore, the optimum pH of ~8.5 to adsorb and pH of 2.9 to desorb Mn(II) from the

Toyopearl resin, and the optimum pH of 10.2 for the CL reaction to occur were chosen after testing with a range of pH conditions. (2) There were several limitations in this system that caused problem with poor reproducibility when low concentrations of Mn(II) (≤0.5 nM) were analysed: very small or no CL peak signal obtained, negative peak formed before the CL peak, second peak appeared during the rinsing step, and higher and bigger baseline level and noises. Several components and parameters (*i.e.* tubing system, valves, peristaltic pump, NI DAQ-MX card, and power supply) of the system were tested to investigate their influences on the reproducibility. However, only little improvement was shown *i.e.* second peak appeared during the rinsing step vanished. Given that most of the above experiments showed little improvement on CL peak signal, it was hypothesised that poor reproducibility was due to other factor, such as the shorther mixing coil length, as too little reagent mixing resulted in higher baseline level and noises, as observed by Chapin *et al.* (1991). This problem was investigated further as detailed in the next sections. (3)The calibration curves of standard additions of Mn(II) to acidified filtered seawaters were not showing positive curvature as expected. In almost all cases, calibrations showed the highest concentration (4nM standard addition) typically gave a lower signal, resulting in a negative curvature curve. From the extensive works carried out, it was found borate buffer that was used to adjust the pH of the standard solutions introduced contaminations into the spiked seawaters and also might have diluted the most concentrated standard. Therefore, the borate buffer was replaced with the 20 µM ammonia solution, as only small amounts (~30µL) of ammonia solution were needed to bring the pH to~8.5 and were given linear calibration, compared to borate buffer which required ~300 µL per 25 mL standard/sample solution.

Standard calibrations (with the ammonia solution used to adjust the pH of the standard solutions) were performed daily with 5 points calibration line (0, +0.5, +1.0, +2.0, +4.0 nM of Mn(II)). The precision of the standards ranged from 0.05% to 15.75% rsd (n=17) with replicates of 3-4 peaks per standard, and the average precision of total 180 samples from surface seawater of the tropical NE Atlantic Ocean analysed is 4.15% rsd (n=3-4), depending on the quality of the CL peak signal. The average reagent blank is 0.08 nM with the detection limit of 0.06 nM. However, when CROZEX samples were analysed, it was difficult to get a measurable CL peak signal due to low Mn(II) concentration, higher and unstable baseline level, and probably lack of chemical mixing because of shorter mixing coil length.

As one of the aims of this project was to analyse seawater samples collected during the D326 (surface Tropical NE Atlantic Ocean) and CROZEX (around the Crozet Islands of the Southern Ocean) cruises, it was decided to further modify this Mn(II) technique to solve the problems with the method used here.

2.2 Implementation of an modified automated Mn(II)-FIA-CL analyser to detect Mn(II) concentrations in seawater

The Mn(II)-FIA-CL-Toyopearl technique set up here was a further modifications of the method used in the previous Section. Given the extensive experience gained through working on this Mn(II) technique, the development and optimisation of this modified version to determine lower concentrations of Mn(II) in seawater was relatively rapid. Problems highlighted in the previous section were successfully resolved by changing the mixing/reaction coil to the longer one (3m). Further optimisations and modifications were done and the FIA-CL system eventually gave better calibration, lower baseline level, enhanced sensitivity and accuracy at low concentrations. However, the interferences with other trace metals were detected in the longer mixing coil. The NTA resin which was initially used as the first cleaning resin column (CC1) in the system to remove the interference of other metals, particularly Fe and Cu, could not retain all of the interfering elements at pH2.9 of the formic eluent. When an 8-HQ resin replaced the NTA resin, the interferences were subsequently eliminated after a number of experiments were carried out to investigate the efficiency of removing the metals interferences by using the 8-HQ resin. The 8-HQ resin column was also used as a second cleaning resin column (CC2), which was placed after the luminol solution in the system to remove impurities in the TETA and luminol solutions.

Most importantly, these modifications reduced the total interference of other trace metal elements values, from ~0.25 to <0.01 nM Mn(II) equivalent. In addition, these further modifications also removed problems encountered with the negative peak formed before the CL peak. These further modifications resulted in a low blank value for (1) with 8-HQ resin is 0.06 nM and detection limit is 0.077 nM compared to (2) with NTA resin is 0.13 nM and detection limit is 0.099 nM. Standard calibrations were performed daily with 5 points calibration line (0, +0.5, +1.0, +2.0, +4.0 nM of Mn(II)). The precision of the standards ranged from 0.09% to 4.22% rsd with an average of 1.83% (with NTA resin), and from 2% to 12% with an average of 5.50% (with 8-HQ resin), with replicates of 3-4 peaks per standard, depending on the quality CL peak signal. The NASS-5 manganese was found to be slightly higher (20.63±0.69 nM) than the certified value, when the NTA resin was used as a cleaning resin. The most likely reason was Ni interference or/and random contamination during handling. However, the NASS-5 manganese value was in a good agreement (16.53±0.60 nM) with the certified value, when the 8-HQ resin was used in replaced of the NTA resin. The SAFe values of SAFe S 256 and SAFe D2 233 when the NTA resin column was used as a CC1in the system were 1.27±0.07 nM and 0.43±0.03 nM, respectively. Whilst the SAFe values for S 256 (0.77±0.07 nM) and D2 233 (0.27±0.04 nM) was reduced when the 8-HQ resin column was used, which showed an exceptionally good agreement with the '*consensus values*'.

Therefore, this newly optimised method was then applied to the re-analysis of selected full water column profiles (*i.e.* BA 567, BA+1 568, BA+2 569, M3 496, M2 502) of seawater samples from around the Crozet Islands in the Southern Ocean. The different between the new (with 8-HQ resin as CC1) and the old (with NTA resin as CC1) data were calculated in a range of 55, 35, 30, 33 and 37% to give an average of 38% reduction of Mn(II) concentrations of the new values. However, due to time constraints, further re-analyses of the remaining samples from other Stations were not possible. The values however, were reduced 38% from the old values, assumed that they would follow on the trend showed for these re-analysed samples.

2.3 Future analytical work

Looking further ahead, the main aim is at a fully automated FIA instrument with no contamination during the analysis that can also produce a reliable calibration. However, there will be significant challenges to overcome before this target is reached. To ensure contamination would not happen during the analysis, it is suggested to put more attention on the '*cleanliness*' of the reagents and on the removal of the interfering trace elements.

A possible solution to these difficulties may be using the new commercially available resin, Nobias Chelate – PA1 resin (Sohrin *et al.,* 2008, Biller and Bruland, 2012) which is widely used by Japanese scientists in trace metal studies (personal communications with Professor Kenneth Bruland, Professor Hajime Obata, and Professor Yoshiki Sohrin during IUPAC International Congress on Analytical Sciences 2011 (ICAS2011)). This resin has shown good recovery for Fe(III) (100%), Cu (100%), Ni (100%), Cr (100%), Zn (100%), Cd (100%) at pH~3.0 (Sohrin *et al.,* 2008). On top of that, recovery of Mn(II) at pH~3.0 is very bad (<1%). This resin therefore gives many advantages in the CL system described here, such as: **(1)** varying quality of the resin would be avoided; **(2)** interference with other trace elements could be easily removed; **(3)** potentially lowering the blank and producing reliable calibration. Most of all, the main advantages are that this commercial available resin would avoid troubles associated with the preparation of the resin, and can potentially allow better inter-comparison of manganese data if is used by a number of laboratories.

3 Objective 2: Dissolved manganese distribution at the Southern Ocean (around the Crozet Islands) and at the tropical NE Atlantic Ocean

3.1 Dissolved manganese around the Crozet Islands, Southern Ocean

Seawater samples were collected at nine Stations around the Crozet Islands of the Southern Ocean, at up to sixteen depths. The first comprehensive dataset for dissolved manganese

in waters surrounding the Crozet islands presented here is internally consistent and generally in agreement with concentrations previously reported for the Southern Ocean. The exceptionally good quality of the data has allowed new insights into the sources, biological uptake and cycling of manganese in the Southern Ocean around the Crozet Islands.

Highest upper water column concentrations of manganese were observed at the BA Stations close to the islands (ranging up to 2.44 nM). These manganese concentrations fell completely outside the ranges of the correlations between manganese and the nutrients at northern and southern stations. Elevated manganese concentrations at these nearshore stations were due to the lateral advection of manganese from the Crozet Plateau in combination with meso-scale circulation. Lateral fluxes from the Crozet plateau were the major source of manganese to the surrounding Crozet waters, especially in the constrained regions to the north of the islands which are influenced by the larger circulation. The lateral manganese fluxes were calculated using the short-lived Ra isotopes to obtain the minimum and maximum cumulative effect of manganese fluxes around the Crozet of 92 and 538 nmol/m^2/d, respectively.

The manganese concentrations in the deep oceanic waters were low and quite uniform at around 0.1-0.2 nM. By using short-lived Ra isotopes to estimate deep water exchanges of manganese, it can be calculated that any net Mn flux will be into the deep water. A very important point here that deep waters have lower concentration than surface and thus any vertical flux (from deep to surface waters) would reduce surface manganese concentrations.

Another manganese source is the atmospheric input. The atmospheric manganese fluxes by rain (wet) and by dust (dry) depositions were estimated. The total atmospheric dry manganese flux in the Crozet region was calculated to be around 0.4 µmol/m^2/yr, and the estimated wet atmospheric manganese flux was calculated to be around 5.90 µmol/m^2/yr. Combining these dry and wet atmospheric fluxes gave an estimated value of dissolved atmospheric flux of manganese to surface waters of approximately 17 nmol/m^2/d.

Removal of manganese from the water column can be by association with biogenic material through: (1) as an intra-cellular component for cell functioning, and (2) non-specific adsorption onto organic particles. Manganese removal via internal sequestration is small as only tiny fraction of manganese (~25 pM) relative to the manganese concentration is needed by the phytoplankton to support their growth. Thus, the distribution of dissolved manganese is largely driven by the inputs term and the biogenic sinking flux of the water column. The adsorption of manganese onto the organic particles can be seen by using $^{234}Th/^{238}U$ ratios (Morris, 2008). Positive correlations were observed between dissolved manganese concentrations and the $^{234}Th/^{238}U$ ratio at all sampling Sites (*i.e.* Northern,

Central, and Southern Sites) indicating that more particle export corresponds to less dissolved manganese concentrations and the remineralisation process corresponds to high dissolved manganese concentrations in the water column. These high particle exports also correspond very well with lower residence times estimated in this study, except for the Northern Sites where there are several limitations that made the residence times estimation here overestimates.

3.2 Dissolved manganese in the surface waters of the Tropical NE Atlantic Ocean

189 the underway surface seawater samples were collected during the UK SOLAS project cruise (D326) in the tropical NE Atlantic Ocean. The Tropical NE Atlantic Ocean receives dust inputs mostly originated from the Saharan Desert. There were two dust events occurred during the sampling period. The first dust event was occurred from 17 until 22 January 2008, and the second dust event was longer than the first event occurred between 25 January and 2 February 2008.

However, low concentrations of dissolved manganese were observed during both of dust events. The atmospheric flux of dissolved manganese was calculated to give a value of approximately 61 μmol/m^2/yr or about 0.17 μmol/m^2/d, which was lower compared to the atmospheric fluxes of dissolved iron and dissolved aluminium (Patey, 2010). The residence times obtained from this study were slightly shorter (ranging from 0.3 until 3.2 years) than previously estimated, with an average of ~1.15 year, thus suggested that the dissolved manganese distribution at the Tropical NE Atlantic Ocean were more temporally variable than previously thought. Furthermore, low dissolved manganese enrichment of 0.002 pmol//L/d or 0.73 nmol/L/yr was estimated in the seawater around the dust events, which is consistent with the background concentrations of dissolved manganese obtained in this study.

Higher surface concentrations of dissolved manganese were observed at stations closer proximity of the land sources (*e.g.* the Canary Islands and the Cape Verde Islands), up to ~3.90 nM. To investigate the source of dissolved manganese in the surface layer ocean in these regions, the relationship between dissolved manganese concentrations and the distance of the stations from the African continent were studied. The distribution of dissolved manganese decreased with increasing distance away from the land sources (*e.g.* TNEA region). The lateral dissolved manganese flux was calculated to give a value of approximately 47 μmol/m^2/d or ~17.3 mmol/m^2/yr. However, the atmospheric input estimated for this study were small (0.17 μmol m^{-2} d^{-1}), thus making the shelf+sediment the most prominent dissolved manganese sources in the seawater close to the islands and mainland. Further offshore, the atmospheric inputs dominate.

Based on both study regions (Crozet Islands, Southern Ocean, and Tropical NE Atlantic Ocean), the "islands/lands mass effect" is considered to be a major source of dissolved manganese, in association with other sources (*i.e.* atmospheric inputs) and internal processes.

3.3 Future work on aspects of manganese biogeochemistry

The aim of this work was to test the hypothesis that the source of manganese in the study regions (*i.e.* around the Crozet Islands of the Southern Ocean, and tropical NE Atlantic Ocean) originated from/or are associated with the islands/lands. Several aspects of the manganese cycle in these systems could not be covered in the span of this study, and these provide a basis for future work.

In order to better understand the "islands mass effect" around the study regions particularly around the Crozet Islands (Southern Ocean) and the Cape Verde Islands (Tropical NE Atlantic Ocean), good process studies are essential to improve our understanding of the biogeochemistry of manganese, in terms of input, removal, and transport/cycling processes of dissolved manganese from seawater and sediments to the ocean. Furthermore, the geochemistry of manganese in the upper oceanic water is generally much more complex than in the deeper waters due to the diversity of processes than can affect the surface distributions. Future studies should focus on the release of manganese from the sediments and the balance of input and removal of manganese. Determining total dissolvable manganese (including both dissolved and particulate manganese) is also important to explain how high dissolved manganese concentrations are maintained in these waters that can probably be transported further offshore and vertically transported to the surface. Bottom nepheloid layers can possibly be the transport mechanism for dissolved manganese to the oceanic waters; hence there is a need to investigate them. Another further important element to study is surface biology, as apart from other factors, it is the major factor that influences the distributions of manganese in seawater and also the major carbon supplier to the sediments. As more than 700,000 Cells/mL of bacteria were found in the study areas (*i.e.* Tropical NE Atlantic Ocean), therefore, it is necessary to include bacterial incubation experiments on the ship to study the uptake of manganese.

In addition to manganese removal by adsorption onto organic particles, it was suggested that manganese might replace iron in some of the enzymes used by the phytoplankton when iron was limiting (*e.g.* at the Southern Sites of the Crozet). This is indicative of potential co-limitation by iron and manganese for phytoplankton growth in the Southern Ocean, but more detailed ship incubation studies are required to prove this is so.

References

Aballea, M., J. Radford-Knoery, P. Appriou, H. Bougault, J. L. Charlou, J. P. Donval, J. Etoubleau, Y. Fouquet, C. R. German & M. Miranda (1998) Manganese distribution in the water column near the Azores Triple Junction along the Mid-Atlantic Ridge and in the Azores domain. *Deep-Sea Research Part I-Oceanographic Research Papers,* 45**,** 1319-1338.

Aguilar-Islas, A. M. & K. W. Bruland (2006) Dissolved manganese and silicic acid in the Columbia River plume: A major source to the California current and coastal waters off Washington and Oregon. *Marine Chemistry* 101, 233–247.

Aguilar-Islas, A. M., J. A. Resing & K. W. Bruland (2006) Catalytically enhanced spectrophotometric determination of manganese in seawater by flow-injection analysis with a commercially available resin for on-line preconcentration. *Limnology and Oceanography-Methods,* 4**,** 105-113.

Albrecht, H.O. (1928) Chemiluminescence of aminophthalic hydrazide. Z. *Physical Chemistry*, 136, 321.

Alkan, N., & M. Tufekci (2009) Distributions of dissolved forms of manganese and iron in the water column of the Southeastern Black Sea. *Turkish Journal of Fisheries and Aquatic Sciences*, 9, 159-164.

Anschutz, P., K. Dedieu, F. Desmazes & G. Chaillou (2005) Speciation, oxidation state, and reactivity of particulate manganese in marine sediments. *Chemical Geology*, 218, 265-279.

Arslan, Z. & A. J. Paulson (2003) Solid phase extraction for analysis of biogenic carbonates by electrothermal vaporization inductively coupled plasma mass spectrometry (ETV-ICP-MS): an investigation of rare earth element signatures in otolith microchemistry. *Analytica Chimica Acta,* 476**,** 1-13.

Askun, H., B. Gulbakan, O. Celikbicak, C. Uzun, G. Guven & B. Salih (2008) Preconcentration and matrix elimination for the determination of Pb(II), Cd(II), Ni(II), and Co(II) by 8-hydroxyquinoline anchored poly(styrene-divinylbenzene) microbeads. *Journal of Applied Polymer Science,* 107**,** 2714-2722.

Baker, A. R., T. D. Jickells, M. Witt & K. L. Linge (2006) Trends in the solubility of iron, aluminium, manganese and phosphorus in aerosol collected over the Atlantic Ocean. *Marine Chemistry,* 98**,** 43-58.

Baker, A. R., K.Weston, S. D. Kelly, M. Voss, P. S. Streu, J. N. Cape (2007) Dry and wet deposition of nutrients from the tropical Atlantic atmosphere: Links to primary productivity and nitrogen fixation. *Deep Sea Research Part I: Oceanographic Research Papers* 54(10): 1704-1720.

Batten, M.L., J.R. Martinez, D.W. Bryan, and E.J. Buch (2000) A modeling study of the coastal eastern boundary current system off Iberia and Morocco. Journal of Geophysical Research, 105, 14173-14195.

Beck, N. G., K. W. Bruland & E. L. Rue (2002a) Short-term biogeochemical influence of a diatom bloom on the nutrient and trace metal concentrations in South San Francisco bay microcosm experiments. *Estuaries,* 25**,** 1063-1076.

Beck, N. G., R. P. Franks & K. W. Bruland (2002b) Analysis for Cd, Cu, Ni, Zn, and Mn in estuarine water by inductively coupled plasma mass spectrometry coupled with an automated flow injection system. *Analytica Chimica Acta,* 455**,** 11-22.

Bergquist, B. A. & E. A. Boyle (2006) Dissolved iron in the tropical and subtropical Atlantic Ocean. *Global Biogeochemical Cycles,* 20.

Biller, D.V. & K. W. Bruland (2012) Analysis of Mn, Fe, Co, Ni, Cu, Zn, Cd, and Pb in seawater using the Nobias-chelate PA1 resin and magnetic sector inductively coupled plasma mass spectrometry (ICP-MS). *Marine Chemistry* 130-131 (2012) 12–20.

Blain, S., P. Treguer, S. Belviso, E. Bucciarelli, M. Denis, S. Desabre, M. Fiala, V. M. Jezequel, J. Le Fevre, P. Mayzaud, J. C. Marty, S. Razouls (2001). A biogeochemical study of the island mass e!ect in the context of the iron hypothesis: Kerguelen Islands, Southern Ocean. *Deep-Sea Research I* 48(1): 163-187.

Boyd, P., T. Jickells, C.S. Law, S. Blain, E.A. Boyle, K.O Buessler,K.H. Coale, J.J. Cullen, H.J.W. de Baar, M. Follows, M.C. Harvey, C. Lancelot, M. Levasseur, R. Pollard, R.B. Rivkin, J.L. Sarmiento, V. Schoemann, V. Smetacek, S. Takeda, A. Tsuda,S. Turner, and A.J. Watson (2007) Mesoscale iron enrichment experiments 1993-2005: synthesis and future directions. *Science*, 315, (5812), 612-617.

Brown, M. T. & K. W. Bruland (2008) An improved flow-injection analysis method for the determination of dissolved aluminum in seawater. *Limnology and Oceanography-Methods,* 6**,** 87-95.

Bruland, K. W., R. P. Franks, G. A. Knauer & J. H. Martin (1979) Sampling And Analytical Methods For The Determination Of Copper, Cadmium, Zinc, And Nickel At The Nanogram Per Liter Level In Sea-Water. *Analytica Chimica Acta,* 105**,** 233-245.

Bruland, K. W., J. R. Donat & D. A. Hutchins (1991) Interactive influences of bioactive trace-metals on biological production in oceanic waters. *Limnology and Oceanography,* 36**,** 1555-1577.

Bruland, K. W., K. J. Orians & J. P. Cowen (1994) Reactive trace metals in the stratified central North Pacific. *Geochimica et Cosmochimica Acta*, 58, 3171-3182.

Bruland, K. W. & M. C. Lohan (2003) Controls of trace metals in seawater, pp. 23-48. In *The Oceans and Marine Geochemistry* (ed. H. Elderfield) Vol. 6 *Treatise on Geochemistry* (eds. H.D. and K.K. Turekian), Elsevier-Pergamon, Oxford.

Bucciarelli, E., S. Blain & P. Treguer (2001) Iron and manganese in the wake of the Kerguelen Islands (Southern Ocean). *Marine Chemistry,* 73**,** 21-36.

Buma, A.G. J., H. J. W., De Baar, R.F., Nolting, A.J., Van Bennekom (1991). Metal enrichment experiments in the Weddell-Scotia Seas: effects of iron and manganese on various plankton communities. *Limnology and Oceanography* 36 (8), 1865–1878.

Burton, J.D., M. Althaus, G. E. Millward,A. W. Morris, P. J. Statham, A. D. Tappin, A. Turner (1993) Processes influencing the fate of trace metals in the North Sea. *Philos. Trans. R. Soc. London,* 343A, 557–568.

Burton, J. D. & P. J. Statham (1988) Trace-metals as tracers in the ocean. *Philosophical Transactions of the Royal Society of London Series a-Mathematical Physical and Engineering Sciences,* 325**,** 127-145.

Cannizzaro, V., A. R. Bowie, A. Sax, E. P. Achterberg & P. J. Worsfold (2000) Determination of cobalt and iron in estuarine and coastal waters using flow injection with chemiluminescence detection. *Analyst,* 125**,** 51-57.

Carter, L., I. N. McCave & M. J. M. Williams (2009) Circulation and Water Masses of the Southern Ocean: A Review. In *Developments in Earth & Environmental Sciences, 8,* ed. F. Florindo and M. Siegert, 85-114. Elsevier.

Chapin, T. P., K. S. Johnson & K. H. Coale (1991) Rapid-Determination Of Manganese In Sea-Water By Flow-Injection Analysis With Chemiluminescence Detection. *Analytica Chimica Acta,* 249**,** 469-478.

Charette, M. A., M. E. Gonneea, P. J. Morris, P. Statham, G. Fones, H. Planquette, I. Salter & A. N. Garabato (2007) Radium isotopes as tracers of iron sources fueling a Southern Ocean phytoplankton bloom. *Deep-Sea Research Part II-Topical Studies in Oceanography,* 54**,** 1989-1998.

Chase, Z., K. S. Johnson, V. A. Elrod, J. N. Plant, S. E. Fitzwater, L. Pickell & C. M. Sakamoto (2005) Manganese and iron distributions off central California influenced by upwelling and shelf width. *Marine Chemistry,* 95**,** 235-254.

Chavagnac, V., J.J. Waniek, D. Atkin, J.A. Milton, T. Leipe, D.R.H. Green, R. Bahlo, T.E.F. Hayes, & D.E. Schulz-Bull (2007). Anti-Atlas Moroccan Chain as the source of lithogenic-derived micronutrient fluxes to the deep Northeast Atlantic Ocean. *Geophysical Research Letters,* 34, 5.

Chester, R (2003) The transport of material to the oceans: the river pathway. In *Marine Geochemistry 2nd edition,* 11-26, Blackwell Science Ltd.

Chiapello, I., G. Bergametti, L. Gomes, B. Chatenet, F. Dulac, J. Pimenta & E. S. Suares (1995) An additional low layer transport of Sahelian and Saharan dust over the North-Eastern Tropical Atlantic. *Geophysical Research Letters,* 22**,** 3191-3194.

Chiapello, I., G. Bergametti, B. Chatenet, P. Bousquet, F. Dulac, E.S. Soares (1997). Origins of African dust transported over the northeastern tropical Atlantic. *Journal of Geophysical Research-Atmospheres,* 102, 13701-13709.

Coale, K.H. (1991). Effects of iron, manganese, copper, and zinc enrichments on productivity and biomass in the sub-arctic Pacific. *Limnology and Oceanography* 36 (8), 1851–1864.

Coale, K. H., C. S. Chin, G. J. Massoth, K. S. Johnson & E. T. Baker (1991) Insitu chemical mapping of dissolved iron and manganese in hydrothermal plumes. *Nature,* 352**,** 325-328.

Comiso, J. C., C.R., McClain, C. W., Sullivan, j.P., Ryan, and C.L. Leonard (1993) Coastal Zone Color Scanner Pigment Concentrations in the Southern Ocean and Relationships to Geophysical Surface Features. *Journal of Geophysic Research*, 98, 2419–2451.

Corami, F., G. Capodaglio, C. Turetta, F. Soggia, E. Magi & M. Grotti (2005) Summer distribution of trace metals in the western sector of the Ross Sea, Antarctica. *Journal of Environmental Monitoring,* 7**,** 1256-1264.

Croot, P. L. & K. A. Hunter (1998) Trace metal distributions across the continental shelf near Otago Peninsula, New Zealand. *Marine Chemistry,* 62**,** 185-201.

Cullen, J.T., Z. Chase, K.H. Coale, S.E. Fitzwater, R.M. Sherrell (2003). Effect of iron limitation on the cadmium to phosphorus ratio of natural phytoplankton assemblages from the Southern Ocean. *Limnology and Oceanograph*y 48 (3), 1079–1087.

De, A., S. Khopkar, and R. Chalmers (1970). Solvent extraction of metals. Van Nostrand Reinhold.

De Baar, H.J.W. (1994). von Liebig's law of the minimum and plankton ecology (1899-1991). *Progress In Oceanography* 33 (4), 347-386.

De Baar, H.J.W., J.T.M. De Jong, D.C.E. Bakker, B.M. Loscher, C. Veth, U. Bathmann, V. Smetacek (1995). Importance of Iron for plankton blooms and carbon-dioxide drawdown in the Southern-Ocean. *Nature* 373 (6513), 412-415.

De Baar, H.J.W., M.A. Van Leeuwe, R.A. Scharek, L. Goeyens, K. Bakker, P. Fritsche (1997). Nutrient anomalies in Fragilariopsis kerguelensis blooms, iron deficiency and the nitrate/phosphate ratio (A.C. Redfield) of the Antarctic Ocean. *Deep-Sea Research II,* 44(1-2),229-260.

De Baar, H.J.W., Boyd, P.W., Coale, K.H., Landry, M.R., Tsuda, A., Assmy, P., Bakker, D.C.E., Bozec, Y., Barber, R.T., Brzezinski, M.A., Buesseler, K.O., Boye, M., Croot, P.L., Gervais, F., Gorbunov, M.Y., Harrison, P.J., Hiscock, W.T., Laan, P., Lancelot, C., Law, C.S., Levasseur, M., Marchetti, A., Millero, F.J., Nishioka, J., Nojiri, Y., van Oijen, T., Riebesell, U., Rijkenberg, M.J.A., Saito, H., Takeda, S., Timmermans, K.R., Veldhuis, M.J.W., Waite, A.M., Wong, C.S. (2005). Synthesis of iron fertilization experiments: From the iron age in the age of enlightenment. *Journal of Geophysical Research-Oceans* 110 (C9), C09S16.

De Jong, J. T. M., M. Boye, M. D. Gelado-Caballero, K. R. Timmermans, M. J. W. VeldhuiS, R. F. Nolting, C. M. G. van den Berg & H. J. W. de Baar (2007) Inputs of iron, manganese and aluminium to surface waters of the Northeast Atlantic Ocean and the European continental shelf. *Marine Chemistry,* 107**,** 120-142.

De Schamphelaire, L., K. Rabaey, N. Boon & W. Verstraete (2007) Minireview: The potential of enhanced manganese redox cycling for sediment oxidation. *Geomicrobiology Journal*, 24, 547-558.

Dierssen, H., W. Balzer & W. M. Landing (2001) Simplified synthesis of an 8-hydroxyquinoline chelating resin and a study of trace metal profiles from Jellyfish Lake, Palau. *Marine Chemistry,* 73**,** 173-192.

Doi, T., H. Obata & M. Maruo (2004) Shipboard analysis of picomolar levels of manganese in seawater by chelating resin concentration and chemiluminescence detection. *Analytical and Bioanalytical Chemistry,* 378**,** 1288-1293.

Draxler, R. R. & G. D. Rolph. 2003. HYSPLIT (HYbrid Single-Particle Lagrangian Integrated Trajectory) Model access via NOAA ARL READY Website (http://www.arl.noaa.gov/ready/hysplit4.html). NOAA Air Resources Laboratory, Silver Spring, MD.

Du, J. X., Y. H. Li & J. R. Lu (2001) Determination of trace amounts of sulfide by flow-injection chemiluminescence method. *Chinese Journal of Analytical Chemistry,* 29**,** 189-191.Blain, S., P. Treguer, et al. (2001). A biogeochemical study of the island mass effect in the context of the iron hypothesis: Kerguelen Islands, Southern Ocean. *Deep-Sea Research I* 48(1): 163-187.

Duce, R. A., P. S. Liss, J. T. Merrill, E. L. Atlas, P. Buat-Menard, B. B. Hicks, J. M. Miller, J. M. Prospero, R. Arimoto (1991) The atmospheric input of trace species to the world ocean. *Global Biogeochemical Cycles,* 5**,** 193-260.

Ellwood, M. J. (2008) Wintertime trace metal (Zn, Cu, Ni, Cd, Pb and Co) and nutrient distributions in the Subantarctic Zone between 40-52 degrees S; 155-160 degrees E. *Marine Chemistry,* 112**,** 107-117.

Elrod, V. A., W. M. Berelson, K. H. Coale & K. S. Johnson (2004) The flux of iron from continental shelf sediments: A missing source for global budgets. *Geophysical Research Letters,* 31.

Fahrbach, E., G. Rohardt, M. Schröder, V. Strass (1994) Transport and structure of the Weddell Gyre. *Annales Geophysicae*, 12, 840-855.

Foster, T.D., & E.C. Carmack (1976) Frontal zone mixing and Antarctic Bottom Water formation in the southern Weddell Sea. *Deep-Sea Research,* 23**,** 301-317.

Gao, Y., Y.J. Kaufman, D. Tanre, D. Kolber, & P.G. Falkowski (2001) Seasonal distributions of aeolian iron fluxes to the global ocean. *Geophysical Research Letter*, 28, 29-32.

German, C. R., & K. L. Von Damm (2003). Hydrothermal processes. In *The Oceans and Marine Geochemistry,* ed. H. Elderfield, 181 - 222. Oxford: Elsevier - Pergamon.

Giret, A., S. Tourpin, S. Marc, O. Verdier & J. Y. Cottin (2002) Penguins Island, Crozet archipelago, volcanic evidence for a heterogeneous mantle in the southern Indian Ocean. *Comptes Rendus Geoscience,* 334**,** 481-488.

Gordon, R. M., K. S. Johnson & K. H. Coale (1998) The behaviour of iron and other trace elements during the IronEx-I and PlumEx experiments in the Equatorial Pacific. *Deep-Sea Research Part II-Topical Studies in Oceanography,* 45**,** 995-1041.

Grotti, M., F. Soggia, M. L. Abelmoschi, P. Rivaro, E. Magi & R. Frache (2001) Temporal distribution of trace metals in Antarctic coastal waters. *Marine Chemistry,* 76**,** 189-209.

Guieu, C., R. Duce & R. Arimoto (1994) Dissolved input of manganese to the ocean-aerosol source. *Journal of Geophysical Research-Atmospheres,* 99**,** 18789-18800.

Guieu, C., M.-D. Loÿe-Pilot, C. Ridame, C. Thomas (2002) Chemical characterization of the Saharan dust end-member: some biogeochemical implications for the western Mediterranean Sea. *Journal of Geophysical Research 107 (D15).* doi:10.1029/ 2001JD000582.

Hirano, Y., J. Nakajima, K. Oguma & Y. Terui (2001) Determination of traces of cadmium in natural water samples by flow injection on-line preconcentration-graphite furnace atomic absorption spectrometry. *Analytical Sciences,* 17**,** 1073-1077.

Hirata, S., Y. Ishida, M. Aihara, K. Honda & O. Shikino (2001) Determination of trace metals in seawater by on-line column preconcentration inductively coupled plasma mass spectrometry. *Analytica Chimica Acta,* 438**,** 205-214.

Hirata, S., T. Kajiya, M. Aihara, K. Honda & O. Shikino (2003) Development of determination methods for trace elements in seawater by on-line column preconcentration/ICP-MS. *Bunseki Kagaku,* 52**,** 1091-1104.

Horsburgh, M. J., S. J. Wharton, M. Karavolos & S. J. Foster (2002) Manganese: elemental defence for a life with oxygen? *Trends in Microbiology,* 10**,** 496-501.

Jarnagin, R.C. and J.H. Wang (1958) Further Studies on the Catalytic Decomposition of Hydrogen Peroxide by Triethylenetetramine-Fe (III) Complex and Related Substances. *Journal of the American Chemical Society*, 80 24, 6477-6481.

Jickells, T., T. Church, A. Veron & R. Arimoto (1994) Atmospheric inputs of manganese and aluminium to the Sargasso Sea and their relation to surface-water concentrations. *Marine Chemistry,* 46**,** 283-292.

Jickells, T. D., and L. J. Spokes (2001). Atmospheric iron inputs to the oceans, p. 85-122. In D. R. Turner and K. A. Hunter [eds.], The biogeochemistry of iron in seawater. *IUPAC series on analytical and physical chemistry of environmental systems*. John Wiley & Sons, LTD.

Jickells, T. D., Z. S. An, K. K. Andersen, A. R. Baker, G. Bergametti, N. Brooks, J. J. Cao, P. W. Boyd, R. A. Duce, K. A. Hunter, H. Kawahata, N. Kubilay, J. laRoche, P. S. Liss, N. Mahowald, J. M. Prospero, A. J. Ridgwell, I. Tegen & R. Torres (2005) Global iron

connections between desert dust, ocean biogeochemistry, and climate. *Science,* 308**,** 67-71.

Johnson, J. and I. Stevens (2000) A fine resolution model of the eastern North Atlantic between the Azores, the Canary Islands and the Gibraltar Strait.*Deep-Sea Research*, 47: 875-899.

Kato, Y. & W. Sakamoto (2009) Protein Quality Control in Chloroplasts: A Current Model of D1 Protein Degradation in the Photosystem II Repair Cycle. *Journal of Biochemistry,* 146**,** 463-469.

Kernen, N., M. J. Kidd, J. E. a. Penner-Hahn & H. B. Pakrasi (2002) A light-dependent mechanism for massive accumulation of manganese in the photosynthetic bacterium Synechocytis sp. PCC 6803. *Biochemistry,* 41(50), 15085-15092.

Key, R. M., R. F. Stallard, W. S. Moore & J. L. Sarmiento (1985) Distribution and flux of Ra-226 and Ra-228 in the Amazon River estuary. *Journal of Geophysical Research-Oceans,* 90**,** 6995-7004.

Klinkhammer G. P., C. S. Chin, R. A. Keller, A. Dahlmann, H. Sahling, G. Sarthou, S. Petersen, F. Smith and C. Wilson (2001) Discovery of new hydrothermal vent sites in Bransfield Strait, Antarctica. Earth Planet. Sci. Lett. 193(3–4), 395– 407.

Klunder, M., P. Laan, R. Middag, H. J. W. De Baar & J. V. Ooijen (2010). Dissolved Iron the Southern Ocean (Atlantic Sector). In *Deep-Sea Research II.* doi:10.1016/j.dsr2.2010.10.042.

Korb, R.E. and M. Whitehouse (2004), SeaWiFS in the southern ocean: spatial and temporal variability in phytoplankton biomass around South Georgia, *Deep-Sea Research I*, 51, 721–738.

Konovalov, S., A. Samodurov, T. Oguz & L. Ivanov (2004) Parameterization of iron and manganese cycling in the Black Sea suboxic and anoxic environment. *Deep-Sea Research I,* 51, 2027-2045.

Kremling, K. (1985) The distribution of cadmium, copper, nickel, manganese, and aluminium in surface waters of the open Atlantic and European shelf area. *Deep Sea Research Part A. Oceanographic Research Papers,* 32**,** 531-555.

Laes, A., S. Blain, P. Laan, S. J. Ussher, E. P. Achterberg, P. Treguer & H. J. W. de Baar (2007) Sources and transport of dissolved iron and manganese along the continental margin of the Bay of Biscay. *Biogeosciences,* 4**,** 181-194.

Landing, W. M. & K. W. Bruland (1980) Manganese in the North Pacific. *Earth and Planetary Science Letters,* 49**,** 45-56.

Landing, W. M. & K. W. Bruland (1987) The contrasting biogeochemistry of iron and manganese in the Pacific Ocean. *Geochimica Et Cosmochimica Acta,* 51**,** 29-43.

Le Gall, A. C., P. J. Statham, N. H. Morley, D. J. Hydes & C. H. Hunt (1999) Processes influencing distributions and concentrations of Cd, Cu, Mn and Ni at the North West European shelf break. *Marine Chemistry,* 68**,** 97-115.

Li, L., B. Hu, L. B. Xia & Z. C. Jiang (2006) Determination of trace Cd and Pb in environmental and biological samples by ETV-ICP-MS after single-drop microextraction. *Talanta,* 70**,** 468-473.

Lin, J. M., H. Arakawa & M. Yamada (1998) Flow injection chemiluminescent determination of trace amounts of hydrogen peroxide in snow-water using KIO4-K2CO3 system. *Analytica Chimica Acta,* 371**,** 171-176.

Lohan, M. C., A. M. Aguilar-Islas, R. P. Franks & K. W. Bruland (2005) Determination of iron and copper in seawater at pH 1.7 with a new commercially available chelating resin, NTA Superflow. *Analytica Chimica Acta,* 530**,** 121-129.

Loscher, B. M. (1999) Relationships among Ni, Cu, Zn, and major nutrients in the Southern Ocean. *Marine Chemistry,* 67, 67-102.

Lowman, F. G., T. R. Rice, F. A. Richards (1971) Accumulation and redistribution of radionuclides by marine organisms, pp. 161-199. In *Radioactivity in the marine environment*, National Academic Science, Washington D.C.

Lubbers, G. W., W. W. C. Gieskes, P. del Castilho, W. Salomons, J. Bril (1990) Manganese accumulation in the high pH microenvironment of *Phaeocystis sp*. (Haptophyceae) colonies from the North Sea. *Marine Ecology Progress Series*, 59, 285-293.

Lucas, M., S. Seeyave, R. Sanders, C. M. Moore, R. Williamson, M. Stinchcombe (2007) Nitrogen uptake responses to a naturally Fe-fertilised phytoplankton bloom during the 2004/2005 CROZEX study. *Deep-Sea Research II* 54, 2138–2173.

Luengen, A. C., P. T. Raimondi & A. R. Flegal (2007) Contrasting biogeochemistry of six trace metals during the rise and decay of a spring phytoplankton bloom in San Francisco Bay. *Limnology and Oceanography,* 52**,** 1112-1130.

Mackey, D. J., J. E. O'Sullivan, R. J. Watson & G. Dal Pont (2002) Trace metals in the Western Pacific: temporal and spatial variability in the concentrations of Cd, Cu, Mn and Ni. *Deep-Sea Research Part I-Oceanographic Research Papers,* 49**,** 2241-2259.

Mahowald, N. M., A. R. Baker, G. Bergametti, N. Brooks, R. A. Duce, T. D. Jickells, N. Kubilay, J. M. Prospero & I. Tegen (2005) Atmospheric global dust cycle and iron inputs to the ocean. *Global Biogeochemical Cycles,* 19.

Mallini, L. J. & A. M. Shiller (1993) Determination of dissolved manganese in seawater by flow injection analysis with colorimetric detection. *Limnology and Oceanography,* 38**,** 1290-1295.

Marsh, R., R.A. Mills, D.R.H. Green, I. Salter, S. Taylor (2007) Controls on sediment geochemistry in the Crozet region. *Deep-Sea Research II,* 54, 2260–2274.

Martin, J.H., R.M. Gordon, S.E. Fitzwater, (1990) Iron in Antarctic waters. *Nature*, 345, 156-158.

Martin, J.H., K.H. Coale, K.S. Johnson, S.E. Fitzwater, R.M. Gordon, S.J. Tanner, C.N. Hunter, V.A. Elrod, J.L. Nowiicki, T.L. Coley, R.T. Barber, S. Lindley, A.J. Watson, K. Van Scoy, C.S. Law, M.I. Liddicoat, R. Ling, T. Stanton, J. Stockel, C. Collins, A. Anderson, R. Bidigare, M. Ondrusek, M. Latasa, F.J. Millero, K. Lee, W. Yao, J.Z. Zhang, G. Friederich, C. Sakamoto, F. Chavez, K. Buck, Z. Kolber, R. Greene, P. Falkowski, S.W. Chisholm, F. Hoge, R. Swift, J. Yungel, S. Turner, P. Nightingale, A. Hatton, P. Liss & N.W. Tindale (1994) Testing the iron hypothesis in ecosystems of the equatorial Pacific Ocean. *Nature,* 371**,** 123–129.

Measures, C.I., and S. Vink (2000). On the use of dissolved aluminium in surface waters to estimate dust deposition to the ocean. *Global Biogeochemical Cycles,* 14, 317–327.

Mendez, J., C. Guieu & J. Adkins (2010) Atmospheric input of manganese and iron to the ocean: Seawater dissolution experiments with Saharan and North American dusts. *Marine Chemistry,* 120**,** 34-43.

Middag, R., H. J. W. De Baar, P. Laan, P. H. Chai & J. C. Van Ooijen (2011a) Dissolved manganese in the Atlantic sector of the Southern Ocean. In *Deep–Sea Research II*, 58, 2661-2677.

Middag, R., H. J. W. de Baar, P. Laan & M. B. Klunder (2011b) Fluvial and hydrothermal input of manganese into the Arctic Ocean. *Geochimica et Cosmochimica Acta,* 75**,** 2393-2408.

Millero, F. J. (2003) Physicochemical Controls on Seawater, pp. 1-22. In *The Oceans and Marine Geochemistry* (ed. H. Elderfield) Vol. 6 *Treatise on Geochemistry* (eds. H.D. and K.K. Turekian), Elsevier-Pergamon, Oxford.

Milne, A., W. Landing, M. Bizimis & P. Morton (2010) Determination of Mn, Fe, Co, Ni, Cu, Zn, Cd and Pb in seawater using high resolution magnetic sector inductively coupled mass spectrometry (HR-ICP-MS). *Analytica Chimica Acta,* 665**,** 200-207.

Moore, J.K., & M.R. Abbott (2002) Surface chlorophyll concentrations in relation to the Antarctic Polar Front: seasonal and spatial patterns from satellite observations. *Journal of Marine Systems*, 37, 69–86.

Moore, W. S., H. Astwood & C. Lindstrom (1995) Radium isotopes in coastal waters on the Amazon shelf. *Geochimica Et Cosmochimica Acta,* 59**,** 4285-4298.

Moore, W. S. (2000) Determining coastal mixing rates using radium isotopes. *Continental Shelf Research,* 20**,** 1993-2007.

Morel, F. M. M., A. J. Milligan & M. A. Saito (2003) Marine Bioinorganic Chemistry: The Role of Trace Metals in the Oceanic Cyles of Major Nutrients. In *The Oceans and Marine Geochemistry,* ed. H. Elderfield, 113 - 144. Oxford: Elsevier - Pergamon.

Morris, P. J. (2008) Carbon Export from Natural Iron Fertilisation in the Southern Ocean. *PhD Thesis,* University of Southampton, Southampton.

Morley, N. H., P. J. Statham & J. D. Burton (1993) Dissolved trace metals in the Southwestern Indian Ocean. *Deep-Sea Research Part I-Oceanographic Research Papers,* 40**,** 1043-1062.

Muhs, D. R., J. Budahn, G. Skipp, J. M. Prospero, D.A. Patterson and E. A. Bettis (2010). Geochemical and mineralogical evidence for Sahara and Sahel dust additions to Quaternary soils on Lanzarote, eastern Canary Islands, Spain. *Terra Nova* 22, 399–410.

Murray, J.W., Codispoti, L.A., Friederich, G.E., 1995. Oxidation–reduction environments: the suboxic zone in the Black Sea. In: Huang, C.P., O'Melia, C.R., Morgan, J. J. (Eds.), Aquatic Chemistry: Interfacial and Interspecies Processes. *American Chemical Society, The Black Sea Ecology and Oceanography,* 238pp.

Nakayama, E., K. Isshiki, Y. Sohrin & H. Karatani (1989) Automated-Determination Of Manganese In Seawater By Electrolytic Concentration And Chemi-Luminescence Detection. *Analytical Chemistry,* 61**,** 1392-1396.

Nakayama, E., H. Obata, K. Okamura, K. Isshiki, H. Karatani & T. Kimoto (1995) Iron and Manganese in the Atmosphere and Oceanic Waters. *Biogeochemical Processes and Ocean Flux in the Western Pasific***,** 53-68.

Nedelec, F. 2006. Implementation of a Method to Determine Subnanomolar Concentrations of Iron in Seawater and Its Application to the Study of Marine Iron Biogeochemistry at the Ocean-shelf Interface. PhD Thesis, University of Southampton, Southampton, 150 pp. In *Ocean Biogeochemistry and Ecosystems*, 150. Southampton: University of Southampton.

Neretin, L. V., C. Pohl, G. Jost, T. Leipe & F. Pollehne (2003) Manganese cycling in the Gotland Deep, Baltic Sea. *Marine Chemistry*, 82, 125-143.

Obata, H., H. Karatani & E. Nakayama (1993) Automated-Determination Of Iron In Seawater By Chelating Resin Concentration And Chemiluminescence Detection. *Analytical Chemistry,* 65**,** 1524-1528.

Obata, H., T. Doi, Y. Hongo, D. S. Alibo, H. Minami, Y. Kato & M. Maruo (2007) Manganese, cerium and iron in the Sulu, Celebes and Philippine Seas. *Deep-Sea Research Part Ii-Topical Studies in Oceanography,* 54**,** 38-49.

Obata, H., K. Shitashima, K. Isshik & E. Nakayama (2008) Iron, manganese and aluminum in upper waters of the western South Pacific ocean and its adjacent seas. *Journal of Oceanography,* 64**,** 233-245.

Okamura, K., T. Gamo, H. Obata, E. Nakayama, H. Karatani & Y. Nozaki (1998) Selective and sensitive determination of trace manganese in sea water by flow through technique using luminol hydrogen peroxide chemiluminescence detection. *Analytica Chimica Acta,* 377**,** 125-131.

Okubo, A. (1971) Oceanic diffusion diagrams. *Deep-Sea Research*, 18, 789–802.

Orsi A.H., W.D. Nowlin Jr, T. Whitworth III (1993) On the circulation and stratification of the Weddell Gyre. *Deep-Sea Research I*, 40**,** 169-203.

O'Sullivan, D.W., A.K. Hanson & D.R. Kester (1995) Stopped-Flow Luminol Chemiluminescence Determination Of Fe(Ii) And Reducible Iron In Seawater At Subnanomolar Levels. *Marine Chemistry,* 49**,** 65-77.

Ouddane, B., M. Skiker, J.C. Fischer & M. Wartel (1999) Distribution of iron and manganese in the Seine river estuary: approach with experimental laboratory mixing. *Journal of Environmental Monitor*, 1, 489–496.

Park, Y. H., L. Gamberoni, & E. Charriaud (1993), Frontal structure, water masses, and circulation in the Crozet Basin, *Journal of Geophysical Research-Oceans*, 98(C7), 12361-12385.

Patey, M. (2008) Nanomolar Inorganic Nutrients. *UK SOLAS Cruise Report*, 66-69.

Patey, M.D., M.J.A. Rijkenberg, P.J. Statham, M.C. Stinchcombe, E.P Achterberg, & M. Mowlem (2008) Determination of nitrate and phosphate in seawater at nanomolar concentrations. *Trac-Trends in Analytical Chemistry*, 27(2): 169-182.

Patey, M. D. (2010) Trace metals and nutrients in aerosols over the tropical and subtropical North Atlantic Ocean. *PhD Thesis*, University of Southampton, Southampton, 182 pp.

Peers, G., & N.M., Price (2004). A role for manganese in superoxide dismutases and growth of iron-deficient diatoms. *Limnology and Oceanography* 49 (5), 1774–1783.

Peterson, R.G., L. Stramma, & G. Kortum (1996) Early concepts and charts of ocean circulation. *Progress in Oceanography*, 37: 1-115.

Planquette, H. (2008) Iron biogeochemistry in the waters surrounding the Crozet Islands, Southern Ocean. *PhD Thesis*, University of Southampton, Southampton.

Planquette, H., P. J. Statham, G. R. Fones, M. A. Charette, C. M. Moore, I. Salter, F. H. Nedelec, S. L. Taylor, M. French, A. R. Baker, N. Mahowald & T. D. Jickells (2007) Dissolved iron in the vicinity of the Crozet Islands, Southern Ocean. *Deep-Sea Research Part II-Topical Studies in Oceanography,* 54**,** 1999-2019.

Planquette, H., G. R. Fones, P. J. Statham & P. J. Morris (2009) Origin of iron and aluminium in large particles (>53 μm) in the Crozet region, Southern Ocean. *Marine Chemistry,* 115**,** 31-42.

Pollard, R.T., and J.F. Read (2001). Circulation pathways and transports of the Southern Ocean in the vicinity of the Southwest Indian Ridge. *Journal of Geophysical Research* 106, 2881–2898.

Pollard, R., R. Sanders, M. Lucas & P. Statham (2007a) The crozet natural iron bloom and EXport experiment (CROZEX). *Deep-Sea Research Part II-Topical Studies in Oceanography,* 54**,** 1905-1914.

Pollard, R. T., H. J. Venables, J. F. Read & J. T. Allen (2007b) Large-scale circulation around the Crozet Plateau controls an annual phytoplankton bloom in the Crozet Basin. *Deep-Sea Research Part II-Topical Studies in Oceanography,* 54**,** 1915-1929.

Prospero, J. M., R. A. Glaccum & R. T. Nees (1981) Atmospheric transport of soil dust from Africa to South America. *Nature,* 289**,** 570-572.

Prospero, J. M., K. Barrett, T. Church, F. Dentener, R. A. Duce, J. N. Galloway, H. Levy, J. Moody & P. Quinn (1996) Atmospheric deposition of nutrients to the North Atlantic Basin. *Biogeochemistry,* 35**,** 27-73.

Prospero J.M., I. Olmez, & M. Ames (2001) Al and Fe in PM 2.5 and PM 10 suspended particles in South-Central Florida: The impact of the long range transport of African mineral dust. *Water, Air, and Soil Pollution*, 125, 291-317.

Prospero, J. M. and Lamb, P. J. (2003). African Droughts and Dust Transport to the Caribbean: Climate Change Implications. *Science* 302(5647): 1024-1027.

Read, J. F., R. T. Pollard & J. T. Allen (2007) Sub-mesoscale structure and the development of an eddy in the Subantarctic Front north of the Crozet Islands. *Deep-Sea Research Part II-Topical Studies in Oceanography,* 54**,** 1930-1948.

Recq, M., J. Godin, P. Charvis & S. Operto (1998) Small-scale crustal variability within an intraplate structure: the Crozet Bank (southern Indian Ocean). *Geophysical Journal International*, 134, 145-156.

Redfield, A.C., Ketchum, B.H. and Richards, F.A., (1963) The influence of organisms on the composition of seawater. In: Hill, M.N., Editor, , 1963. *The sea (2)*, Interscience, New York, pp. 26–77.

Resing, J. A. & C. I. Measures (1994) Fluorometric-Determination Of Al In Seawater By Flow-Injection Analysis With In-Line Preconcentration. *Analytical Chemistry,* 66**,** 4105-4111.

Rijkenberg, M.J.A., S. Steigenberger, C.F. Powell, H. van Haren, M. D. Patey, A. R. Baker, & E. Achterberg (2012) Fluxes and distribution of dissolved iron in the eastern (sub-) tropical North Atlantic Ocean. *Global Biogeochemical Cycles,* 26, GB3004.

Roitz, J. S. & K. W. Bruland (1997) Determination of dissolved manganese(II) in coastal and estuarine waters by differential pulse cathodic stripping voltammetry. *Analytica Chimica Acta,* 344**,** 175-180.

Roitz, J. S., A. R. Flegal & K. W. Bruland (2002) The biogeochemical cycling of manganese in San Francisco Bay: Temporal and spatial variations in surface water concentrations. *Estuarine Coastal and Shelf Science,* 54**,** 227-239.

Rose, A. L. & T. D. Waite (2001) Chemiluminescence of luminol in the presence of iron(II) and oxygen: Oxidation mechanism and implications for its analytical use. *Analytical Chemistry,* 73**,** 5909-5920.

Ruzicka, J. & E. H. Hansen (1988). Flow Injection Analysis in Chemical Analysis: A Series of Manographs on Analytical Chemistry and Its Applications. *Flow Injection Analysis, 2nd Edition*, Wiley & Sons Inc., New York, USA.

Saager, P. M., H. J. W. Debaar & P. H. Burkill (1989) Manganese and iron in Indian Ocean waters. *Geochimica Et Cosmochimica Acta,* 53**,** 2259-2267.

Saager, P. M., H. J. W. deBaar, J. T. M. deJong, R. F. Nolting & J. Schijf (1997) Hydrography and local sources of dissolved trace metals Mn, Ni, Cu, and Cd in the northeast Atlantic Ocean. *Marine Chemistry,* 57**,** 195-216.

Sakamotoarnold, C. M. & K. S. Johnson (1987) Determination Of Picomolar Levels Of Cobalt In Seawater By Flow-Injection Analysis With Chemiluminescence Detection. *Analytical Chemistry,* 59**,** 1789-1794.

Sarmiento, J. L., T.M.C. Hughes, R.J. Stouver and S. Manabe (1998). Simulated response of the ocean carbon cycle to anthropogenic climate warming. *Nature,* 393, 245–249.

Sarthou, G., A.R. Baker, S. Blain, E.P. Achterberg, M. Boyé, A.R. Bowie, P. Croot, P. Laan, H.J.W. De Baar, T.D. Jickells, P.J. Worsfold (2003) Atmospheric iron deposition and sea-surface concentrations in the eastern Atlantic Ocean. *Deep-sea Research I,* 50, 1339–1352.

Scharek, R., M.A., Van Leeuwe, H.J.W., De Baar (1997). Reponses of Southern Ocean phytoplankton to the additions of trace metals. *Deep-Sea Research Part II* 44 (1-2), 209–227.

Schoemann, V., H. J. W. de Baar, J. T. M. de Jong, C. Lancelot (1998) Effects of phytoplankton blooms on the cycling of manganese and iron in coastal waters. *Limnology and Oceanography*, 43, 1427– 1441.

Schoemann, V., R. Wollast, L. Chou & C. Lancelot (2001) Effects of photosynthesis on the accumulation of Mn and Fe by Phaeocystis colonies. *Limnology and Oceanography,* 46**,** 1065-1076.

Sedwick, P. N., P. R. Edwards, D. J. Mackey, F. B. Griffiths & J. S. Parslow (1997) Iron and manganese in surface waters of the Australian subantarctic region. *Deep-Sea Research Part I-Oceanographic Research Papers,* 44**,** 1239-1253.

Sedwick, P. N., G. R. DiTullio & D. J. Mackey (2000) Iron and manganese in the Ross Sea, Antarctica: Seasonal iron limitation in Antarctic shelf waters. *Journal of Geophysical Research-Oceans,* 105**,** 11321-11336.

Seeyave, S., M. I. Lucas, C. M. Moore & A. J. Poulton (2007) Phytoplankton productivity and community structure in the vicinity of the Crozet Plateau during austral summer 2004/2005. *Deep-Sea Research Part II-Topical Studies in Oceanography,* 54**,** 2020-2044.

Shelley, U. R., B. Zachhuber, P. N. Sedwick, P. J. Worsfold & M. C. Lohan (2010) Determination of Total Dissolved Cobalt in UV-Irradiated Seawater Using Flow Injection with Chemiluminescence Detection. *Limnol. Oceanogr.: Methods 8, 2010, 352–362***,** 352-362.

Shiller, A. M. (1997) Manganese in surface waters of the Atlantic Ocean. *Geophysical Research Letters,* 24**,** 1495-1498.

Sohrin, Y., S. Iwamoto, S. Akiyama, T. Fujita, T. Kugii, H. Obata, E. Nakayama, S. Gado, Y. Fujishima, H. Hasegawa, K. Ueda, & M. Matsui (1998) Determination of trace elements in seawater by fluorinated metal alkoxide glass-immobilized 8-

hydroxyquinoline concentration and high-resolution inductively coupled plasma mass spectrometry detection. *Analytica Chimica Acta,* 363, 11-19.

Sohrin, Y., S. Urushihara, S. Nakatsuka, T. Kono, E. Higo, T. Minami, K. Norisuye & S. Umetani (2008) Multielemental determination of GEOTRACES key trace metals in seawater by ICPMS after preconcentration using an ethylenediaminetriacetic acid chelating resin. *Analytical Chemistry,* 80**,** 6267-6273.

Spokes, L., T. Jickells & K. Jarvis (2001) Atmospheric inputs of trace metals to the northeast Atlantic Ocean: the importance of southeasterly flow. *Marine Chemistry,* 76**,** 319-330.

Statham, P. J. & J. D. Burton (1986) Dissolved manganese in the North-Atlantic Ocean, 0-35 degrees-N. *Earth and Planetary Science Letters,* 79**,** 55-65.

Statham, P. J. & R. Chester (1988) Dissolution of manganese from marine atmospheric particulates into seawater and rainwater. *Geochimica Et Cosmochimica Acta,* 52**,** 2433-2437.

Statham, P. J., P. A. Yeats & W. M. Landing (1998) Manganese in the eastern Atlantic Ocean: processes influencing deep and surface water distributions. *Marine Chemistry,* 61**,** 55-68.

Stein, C.A. & R.P. Von Herzen (2007) Potential effects of hydrothermal circulation and magmatism on heatflow at hotspot swells. In Foulger, G.R., and Jurdy, D.M., eds., Plates, plumes, and planetary processes: Geological Society of America Special Paper 430, p. 261–274.

Stramma, L., S. Hüttl, and J. Schafstall (2005), Water masses and currents in the upper tropical northeast Atlantic off northwest Africa, *J. Geophys. Res., 110,* C12006, doi:10.1029/2005JC002939.

Stumm,W., J.J. Morgan (1996) Aquatic Chemistry. pp. 1022. Wiley-Interscience, New York.

Sturgeon, R. E., S. S. Berman, S. N. Willie & J. A. H. Desaulniers (1981) Pre-Concentration Of Trace-Elements From Sea-Water With Silica-Immobilized 8-Hydroxyquinoline. *Analytical Chemistry,* 53**,** 2337-2340.

Sunda, W. G. & S. A. Huntsman (1983) Effect of competitive interactions between manganese and copper on cellular manganese and growth in estuarine and oceanic species of the diatom *Thalassiosira*. *Limnology and Oceanography,* 28**,** 924-934.

Sunda, W. G. & S. A. Huntsman (1988) Effect of sunlight on redox cycles manganese in the Southwestern Sargasso Sea. *Deep-Sea Research Part a-Oceanographic Research Papers,* 35**,** 1297-1317.

Sunda, W. G. & S. A. Huntsman (1990) Diel cycles in microbial manganese oxidation and manganese redox speciation in coastal waters of the Bahama Islands. *Limnology and Oceanography,* 35(2), 325-338.

Sunda, W. G. & S. A. Huntsman (1998) Interactive effects of external manganese, the toxic metals copper and zinc, and light in controlling cellular manganese and growth in a coastal diatom. *Limnology and Oceanography,* 43**,** 1467-1475.

Tappin, A. D., D. J. Hydes, J. D. Burton & P. J. Statham (1993) Concentrations, distributions and seasonal variability of dissolved Cd, Co, Cu, Mn, Ni, Pb and Zn in the English-Channel. *Continental Shelf Research,* 13**,** 941-969.

Taylor, S. R. & S. M. McLennan. 1985. *The Continental Crust: Its Composition and Evolution.* Oxford: Blackwell.

Tebo, B. M., H. A. Johnson, J. K. McCarthy & A. S. Templeton (2005) Geomicrobiology of manganese(II) oxidation. *Trend in Microbiology*, 13, 421-428.

Tebo, B. M., K. Geszvain & S. Lee (2010) The molecular geomicrobiology of bacterial manganese(II) oxidation, pp. 285-308. *In Geomicrobiology: Molecular and Environmental Perspective* (eds. L. L. Barton et al.), Springer Science+Business Media, Beaverton.

Tonkin, J. W., L. S. Balistrieri, J. W. Murray (2004) Modeling sorption of divalent metal cations on hydrous manganese oxide using the diffuse double layer model. *Applied Geochemistry*, 19, 29-53.

Turner, D. and K. Hunter (2001) The Biogeochemistry of Iron in Seawater. *Series on Analytical and Physical Chemistry of Environmental Systems*, 396 pp.

Twining, B. S., S. B. Baines & N. S. Fisher (2004) Element stoichiometries of individual plankton cells collected during the Southern Ocean Iron Experiment (SOFeX). *Limnology and Oceanography,* 49**,** 2115-2128.

Usher, C.R., A.E. Michel & V.H. Grassian (2003) Reactions on mineral dust. *Chemical Reviews*, 103, 4883-4939.

van Beek, P., M. Bourquin, J. L. Reyss, M. Souhaut, M. A. Charette & C. Jeandel (2008) Radium isotopes to investigate the water mass pathways on the Kerguelen Plateau (Southern Ocean). *Deep-Sea Research Part II-Topical Studies in Oceanography,* 55**,** 622-637.

Vassileva, E. & N. Furuta (2003) Application of iminodiacetate chelating resin muromac A-1 in on-line preconcentration and inductively coupled plasma optical emission spectroscopy determination of trace elements in natural waters. *Spectrochimica Acta Part B-Atomic Spectroscopy,* 58**,** 1541-1552.

Venables, H. J., R. T. Pollard & E. E. Popova (2007) Physical conditions controlling the development of a regular phytoplankton bloom north of the Crozet Plateau, Southern Ocean. *Deep-Sea Research Part II-Topical Studies in Oceanography,* 54**,** 1949-1965.

Warnken, K. W., D. G. Tang, G. A. Gill & P. H. Santschi (2000) Performance optimization of a commercially available iminodiacetate resin for the determination of Mn, Ni, Cu, Cd and Pb by on-line preconcentration inductively coupled plasma-mass spectrometry. *Analytica Chimica Acta,* 423**,** 265-276.

Webb, S. M., G. J. Dick, J. R. Bargar, & B. M. Tebo (2005) Evidence for the presence of Mn(III) intermediates in the bacterial oxidation of Mn(II). *Proceedings of the National Academy of Sciences of the USA*, 102, 5558 - 5563.

Wedepohl, K.H. (1995). The composition of the continental crust. *Geochimica et Cosmochimica Acta* 59, 1217–1232.

Weeks, D. A. & K. W. Bruland (2002) Improved method for shipboard determination of iron in seawater by flow injection analysis. *Analytica Chimica Acta,* 453**,** 21-32.

Welschmeyer, N.A. (1994). Fluorometric analysis of chlorophyll-a in the presence of chlorophyll-b and pheopigments. *Limnology and Oceanography* 39 (8), 1985–1992.

Willie, S. N., J. W. H. Lam, L. Yang & G. Tao (2001) On-line removal of Ca, Na and Mg from iminodiacetate resin for the determination of trace elements in seawater and fish otoliths by flow injection ICP-MS. *Analytica Chimica Acta,* 447**,** 143-152.

Xiao, C. B., D. W. King, D. A. Palmer & D. J. Wesolowski (2000) Study of enhancement effects in the chemiluminescence method for Cr(III) in the ng 1(-1) range. *Analytica Chimica Acta,* 415**,** 209-219.

Xylouri, A. (2009) Impact of Atmospheric Cycling on the Release of Iron and Manganese into Seawater from Saharan Soil Particles. *PhD Thesis,* University of Leeds, Leeds.

Zagatto, E. A. G., M. A. Z. Arruda, A. O. Jacintho & I. L. Mattos (1990) Compensation Of The Schlieren Effect In Flow-Injection Analysis By Using Dual-Wavelength Spectrophotometry. *Analytica Chimica Acta,* 234**,** 153-160.

Zhou, M., J. D. Paduan, P. P. Niiler (2000). Surface currents in the Canary Basin from drifter observations. J*ournal of Geophysical Research-Oceans* **105**(C9): 21893-21911.

Zubkov, M. V., R. J. Holland, P. H. Burkill, I. W. Croudace & P. E. Warwick (2007) Microbial abundance, activity and iron uptake in vicinity of the Crozet Isles in November 2004-January 2005. *Deep-Sea Research Part II-Topical Studies in Oceanography,* 54**,** 2126-2137.

Appendices

APPENDIX 1:
PROTOCOL FOR THE DETERMINATION OF DISSOLVED MANGANESE WITH FIA-CL-TOYOPEARL ANALYSER

1 Apparatus

The chelating resin pre-concentration column and chemiluminescence (CL) systems are shown in Figure A2-1 in this appendix. The manifold consists of a pre-concentration column made from Perspex packed with ~0.1 g of chelating resin, which is blocked with two pieces of Teflon mesh (170 mesh), a Gilson Minipuls 3: 8-channel peristaltic pump (a four channel equivalent would also be suitable), one 8-port single valve auto-sampler, one 6-port two position valve (VICI Cheminert C22-3186D), one 3-port two position valves (Cole Parmer 01367-72) for selection of sample/MQ water streams, one 1-m/3-m knotted mixing coil, a CL cell which has a built-in flow cell and a photomultiplier tube (PMT), high voltage power supply, and an electrometer. The systems are automatically controlled with interlocking four-step timers of the National Instrument DAQ-MX card. The flow cell is a clear 1.2 mm i.d. Teflon tube coiled on a vortex groove 28 mm in diameter and notched on an aluminium block, which is fixed to a quartz screen facing the PMT. The PMT (Hamamatsu Photonics, H8443) is cooled to 5 °C with an electronic cooler to reduce dark current. The high voltage power supply is generally set at -12 V. The pre-concentration and CL systems are connected with a NTA resin column, which removes interfering iron ions in the carrier solution (eluent). Container for the reagent is put in vacuum pump cylinder to prevent generation of air bubbles in the flow system and to stabilize the CL reaction. All data observed and recorded through the Toshiba Sattelite Pro laptop.

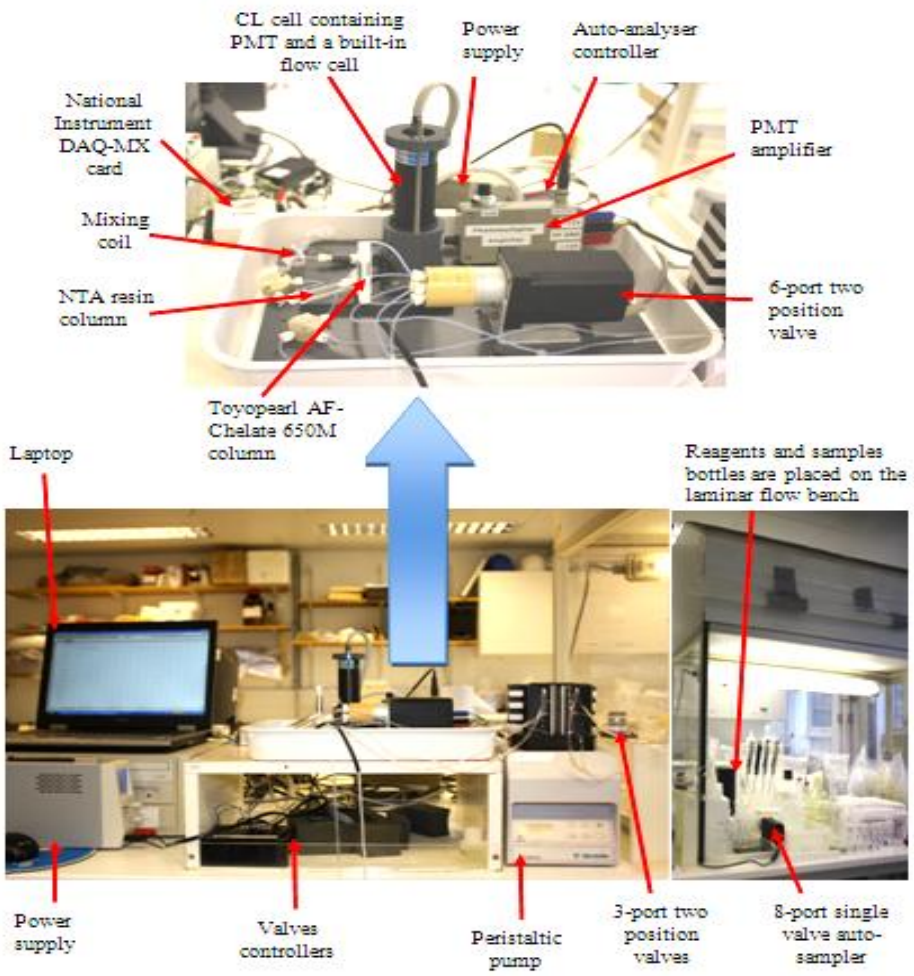

Figure A1-1. Photo image of the FIA-CL-Toyopearl manifold with labels for automatic determination of dissolved manganese in seawater

2 Reagents

All solutions are prepared with deionized water of resistivity 18.2 MΩ cm or greater from a MQ analytical reagent-grade water purification system (MQ Water; Millipore). 3-aminophthalhydrazide (luminol, Fluka), triethylenetetramine (TETA, Aldrich), formic acid (SpS Romil Pure Chemistry), hydrogen peroxide (Fisher Scientific, trace analysis grade), sodium carbonate (Fisher Scientific, analytical reagent grade), hydrochloric acid (SpA Romil Pure Chemistry), and ammonia solution (UpA Romil Pure Chemistry or high purity ammonia (see section 2.3 below for the preparation of the ammonia solution)) are used without further purification.

2.1 Daily preparation:

The carrier solution (eluent) is prepared by mixing 38.46 mL 0.1 M formic acid with 10 mL 0.1 M hydrogen peroxide and 13 mL 12 mM aqueous ammonia (pH 2.9), and make up until 1 L with MQ water. 0.06 mM of luminol solution is daily made by diluting 600 μL luminol

stock solution and 10 μL TETA in 1 L MQ water. A 208 mL 0.7 mM aqueous ammonia solution is making up until 1 L with MQ water to adjust the CL reaction pH to 10.2. MQ water is used as the cleaning solution to remove the residual sea-salt.

2.2 Weekly preparation:

The luminol stock solution is made by diluting 270 mg 0.1 M luminol and 500 mg 0.32 M sodium carbonate in 15 mL MQ water. 86.20 mL 1 M hydrochloric acid is made up until 1 L with MQ water to remove any manganese residue in the FIA system every day before and after the analyses.

2.3 Monthly preparation:

High purity ammonia solution is made by bubbling high ammonia gas in sub-boiling water (S.B) / MQ water as described below (courtesy of Prof. Peter Statham and Mr. Brian Dickie):

Water bottle:

1. Fill 1 L Teflon bottle with no more than 700 mL of sub-boiling water.
2. Double bag the bottle and place it in a 5 L beaker. Pack the beaker with ice and ~250 mL of water.
3. Place the PTFE bubbler tube into the bottle.

Operating instructions:

1. Check the tubing and carefully open main valve quarter of a turn.
2. Adjust second stage pressure regulator to no more than 0.3 bar.
3. Gradually open the delivery valve (attached to tube going to the bubbler).
4. Check by lifting the bottle or tube that there is a steady gentle stream of ammonia bubbles passing through the water in the bottle.
5. Keep bubbling until saturation of the solution occurs (typically about 1 hour).
6. Check the flow rate every 10 minutes (as in 5) and ensure that the bottle does not overflow (due to thermal expansion). If the bottle does 'overflow', remove the PTFE tubing and shut the system down. Replace the ice and re-start when the solution has cooled.

Closing down the system:

1. Carefully remove the PTFE tubing from the bottle. Ensure that there is no liquid inside the tube.
2. Close the main valve on the cylinder.
3. Close the regulator valve.
4. Close the delivery valve.
5. Ensure that there is no liquid in the tubing above the filter.

6. Cap the bottle rinse the outside with MQ water and transfer into a clean (double) bag.
7. Dispose of any other liquids (ice/ice melts) into the drain inside the fume cupboard. Wash out the old bag with tap water and pour away any liquids inside the fume cupboard. When rinsed (and clear of any ammonia) dispose of the bag in the bin. Turn off the cold water.

2.4 Standards preparation:

Take 1 mL of 18.20 mM manganese standard stock solution (ASSURANCE certified reference material) to prepare 182 µM (F1) in 100 mL volumetric flask. From F1, take 1 mL and make up 1820 nM (F2) in 100 mL volumetric flask. Later, four points of standards calibration are prepared from F2 as below:

- 7 µL of F2 to make 0.5 nM in 25 mL vial
- 14 µL of F2 to make 1.0 nM in 25 mL vial
- 28 µL of F2 to make 2.0 nM in 25 mL vial
- 56 µL of F2 to make 4.0 nM in 25 mL vial

3 Procedures

3.1 Setting-up and cleaning the manifold

- Empty the waste bottle.
- Check the tubes that going through the Gilson Minipuls 3 peristaltic pump are in a good condition and set up the pumping system by putting the pressure on the peristaltic pump tubes. The peristaltic pump is set at speed 9.0, resulting in the flow rates shown in Table A1-1.
- Make sure the auto-analyser controller is in position 1 (Figure A2-2).

Figure A1-2. The auto-analyser controller must be in the position 1 before starting up the analysis

- All reagents and samples 'straw' tubes are in MQ water bottle and turn on the Gilson pump for a few minutes to check if there was any leakage or blockage on the manifold tubing system.
- Then, change the MQ water bottle with 1 M HCl solution bottle.
- Flush 1 M HCl through the manifold for about 20 minutes to remove all manganese residues, followed by a 10 minutes rinse with MQ water. Repeat this step at the end of the analysis or after changing anything in the manifold (*e.g.* tubing, columns, fitting).

3.2 Starting-up

- Switch on all the power supplies, valves and auto-analyser system.

- Switch on the laptop and make sure that the USB cable of the National Instrument DAQ-MX card is plugged in properly.
- Place all the reagent bottles in-line, on the laminar flow bench.
- Open LabView 7.1 program.
- Click 'Open', scroll down and choose file:
  'C:\...Desktop\controller_MX.llb\mx_Mn_CL_pjs.vi'.
  Or one could also create any new file.
- The timing sequence (in ms) menu should appear and look like Figure A2-3. Then check:
    1. Device Sequence – green lights indicate that the valve controllers are 'on'. DO NOT modify the valve sequence (circled red) as it controls the position of the two valves between rinsing, loading and eluting modes.
    2. Time (in ms) – set the time for washing, loading, rinsing and eluting (depending on the samples concentrations. If the concentrations of samples were very low (<1 nM), longer loading time is needed and vice-versa. For example, the sequence time for this analysis is set as follow:
        - 60,000 ms (washing)
        - 260,000 ms (loading)
        - 320,000 ms (rinsing)
        -5 20,000 ms (eluting).
    3. Lines – choose 'Dev2/port0:1'.
    4. Replicates – set to be 2 or 3 (depending on your samples).

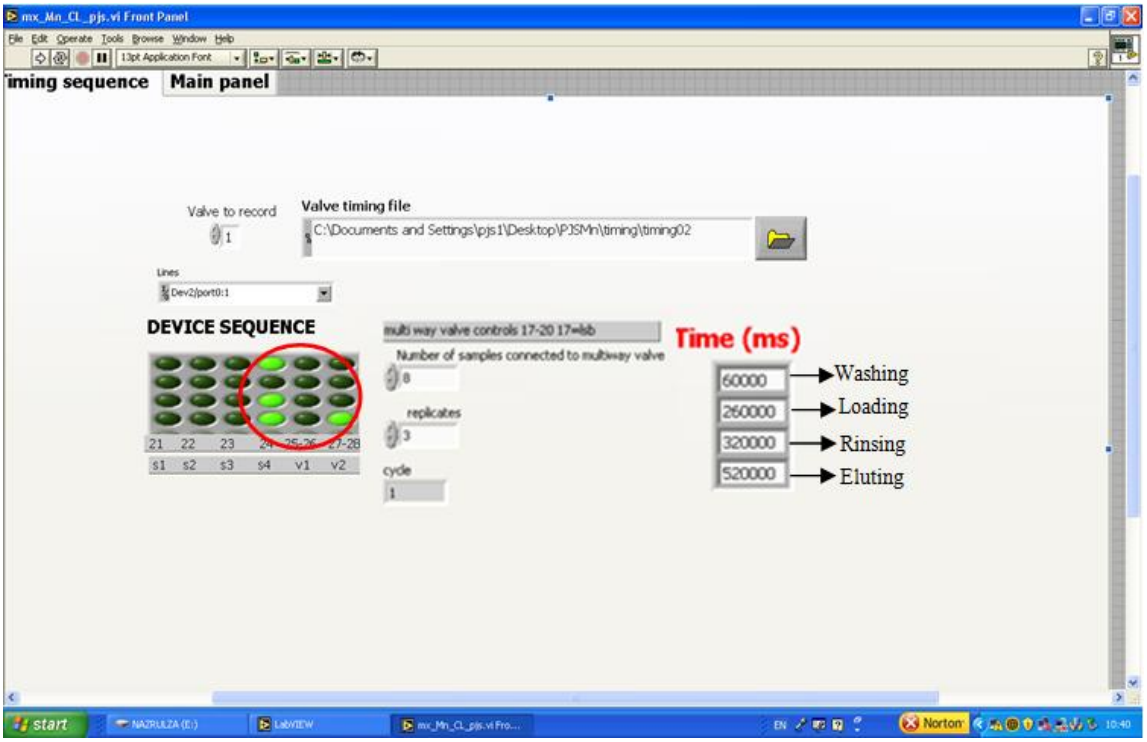

Figure A1-3. Screenshot of LabView 7.1 timing sequence interface.

- Go to 'Main Panel' (Figure A2-4) and check:
    1. Physical Channel – set to Dev2/ai0.
    2. Named the analysis file in 'Save file as' (e.g. C:\Documents and Setting\pjs1\Desktop\PJSMn\Farah10September 2010).
    3. Click 'Log to file' on.
    4. Click the green 'Start' button on.
    5. Click 'Run' button on. The button is show as an arrow at the left top of the screen.
    6. During the analysis, DO NOT click the 'Abort Execution' button (show as red circle), as it would stop the system and contamination might occur, unless if discovered leakage or blockage from the manifold tubing system/columns frits or if there was an electronic faulty. However, it requires starting the whole procedure again (see section 4 of this appendix for troubleshooting).

Figure A1-4. Screenshot of LabView 7.1 main panel interface.

3.3 Running the samples

- Check the pH of the stream is exactly 10.2 (this is the optimum pH for CL reaction). If not, then adjust it by increasing or diluting the ammonia solution concentration depending on which pH is measured.

- Adjust the pH of the standard to ~8.5 (this is the optimum pH for absorption of Mn (II) on the Toyopearl AF-Chelate 650M resin column) by adding ~70 µl of 0.7 M ammonia solution. Run the calibration (2-3 replicates), starting with two blanks and the lowest standard. A few minutes before running a sample, adjust the pH to pH ~8.5 by adding ~70 µl of 0.7 M ammonia solution.
- After the calibration, run the seawater (that used to make up the standard) as an internal standard, then the samples. Periodically, run the SAFe surface and deep certified reference materials, and also NASS-5 or/and CASS-4.
- After each day of analysis, wash the whole system following the procedure described in section 3.1 in this Appendix.
- Release the pressure on all the peristaltic pump tubes after removing the tubing from the reagent bottles (place the tubes in the MQ water bottle to prevent contamination on the tubing system).
- Switch off everything (*i.e.* Gilson peristaltic pump, laptop, power supplies, and valves).

3.4 Peak measurement

- The CL signal (peak) could be measured through the 'Data Processing Area (version 2)'

- Click 'Run' (show as arrow) to choose the require file
- Pick an individual peak to measure by using the small display under of the different options under the chart (as shown in Figure A2-5):
    - The cross + is to drag the axis to the position needed
    - The zoom is to enlarge or reduce the size of the peak
    - The hand is to move from one peak to another by dragging the chart

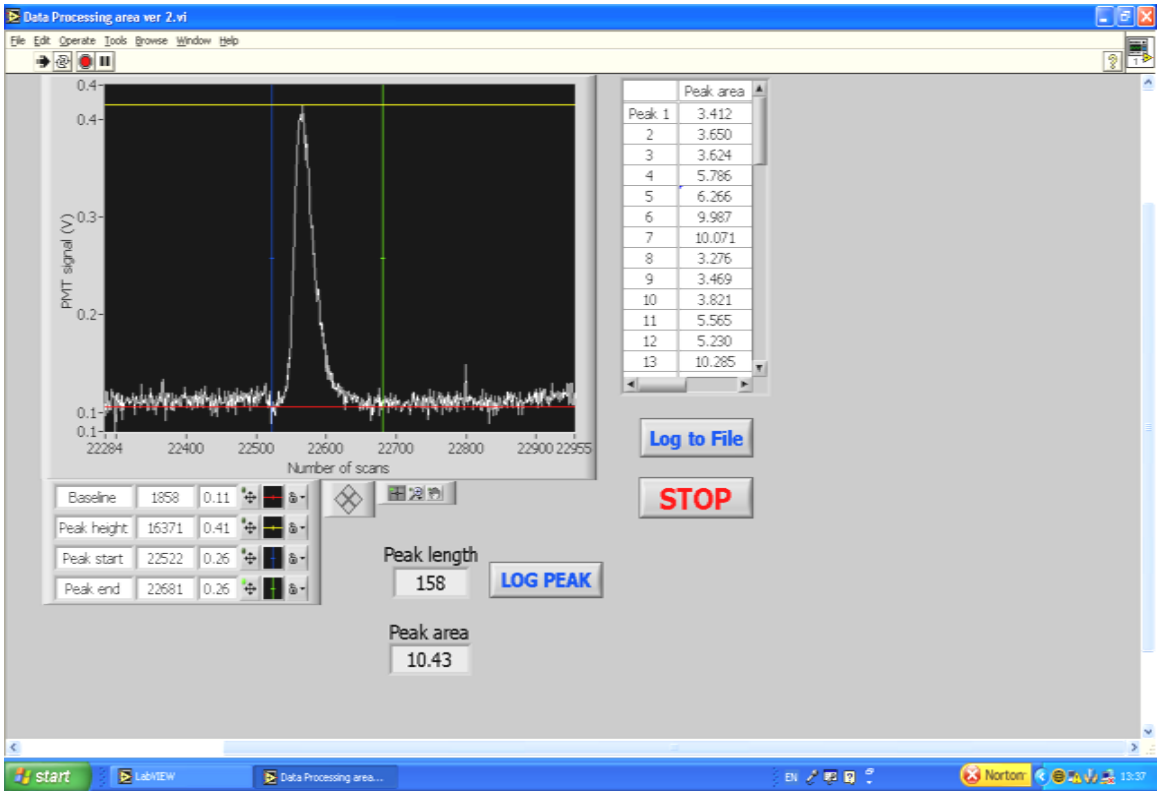

Figure A1-5. Screenshot of LabView Data Processing Area version 2 interface.

- Measure the peak height or/and the peak area by using the different axes on the bottom left of the chart:
    - Red – baseline
    - Yellow – peak height
    - Blue – peak start
    - Green – peak end

  Left-click on the cross of these axis and select 'bring to center'. Then, drag the axis at their position:
    - Baseline – at the baseline level of the peak
    - Peak start – before the peak is formed

- Peak end – after the peak is returned to the baseline level

However, DO NOT analyse the peak if there was a bubble spike on the peak.

- In the middle bottom of the screen are (1) the 'Peak length' (associating to the number of scans between 'peak start' and 'peak end'), (2) the 'peak area' (corresponding to the area of the peak between 'peak start' and 'peak end').
- Log the peak on the log sheet (Figure A2-5) by clicking the 'Log Peak' when axes are properly placed on the chart. Only click once for an individual peak as it will log twice when clicking it twice. In addition, one could manually log the peak measurement in the log book, as a backup.
- Click 'Log to File' to save any change on the log sheet on the file. However, it is preferably to save in different file name to avoid overwritten.
- Click 'Stop' after finishing measuring the peaks.
- All LabView files can be imported in Excel. Raw data files produced 2-column text files where first column is the CL signal (in volt). These files are very big (more than 32000 rows) thus, have to split into some files before imported in Excel spreadsheets.

4.0 Troubleshooting

There are three main troubleshooting, as showed in the next pages, and the solutions related to this analysis:

1. No or very small peak

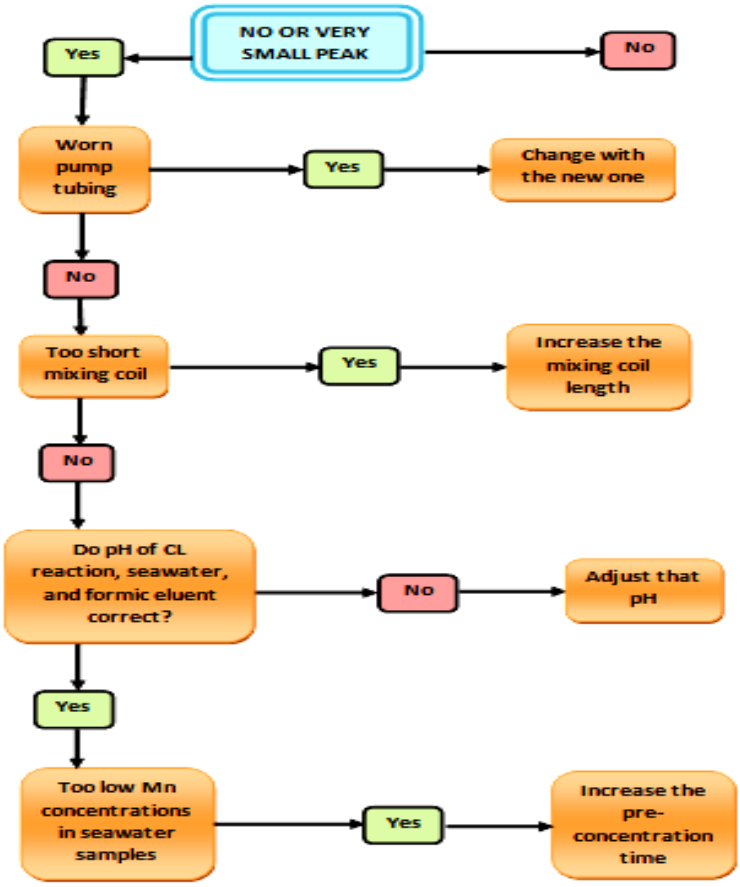

2. Contamination in the manifold

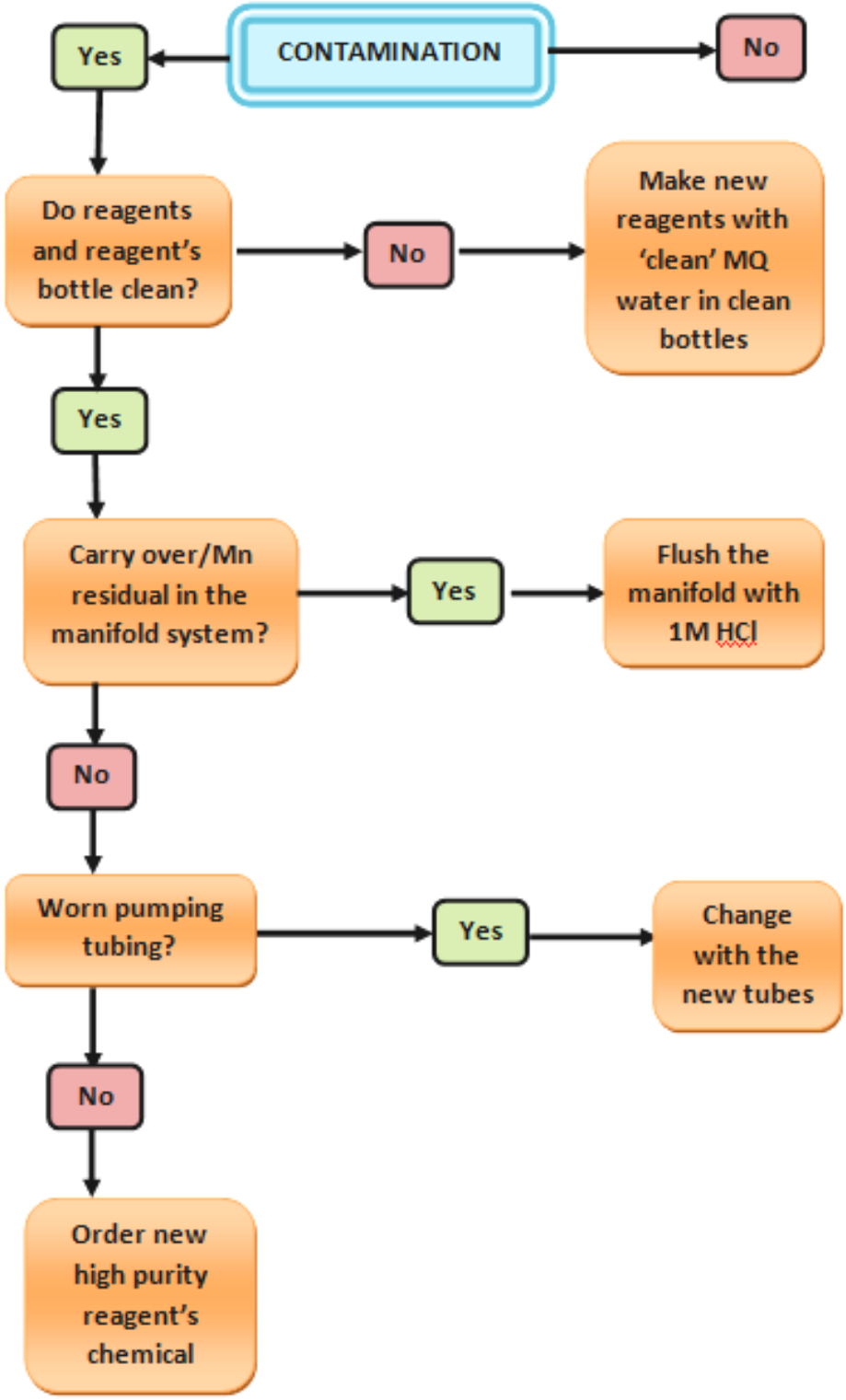

3. Electronic noise and software crash

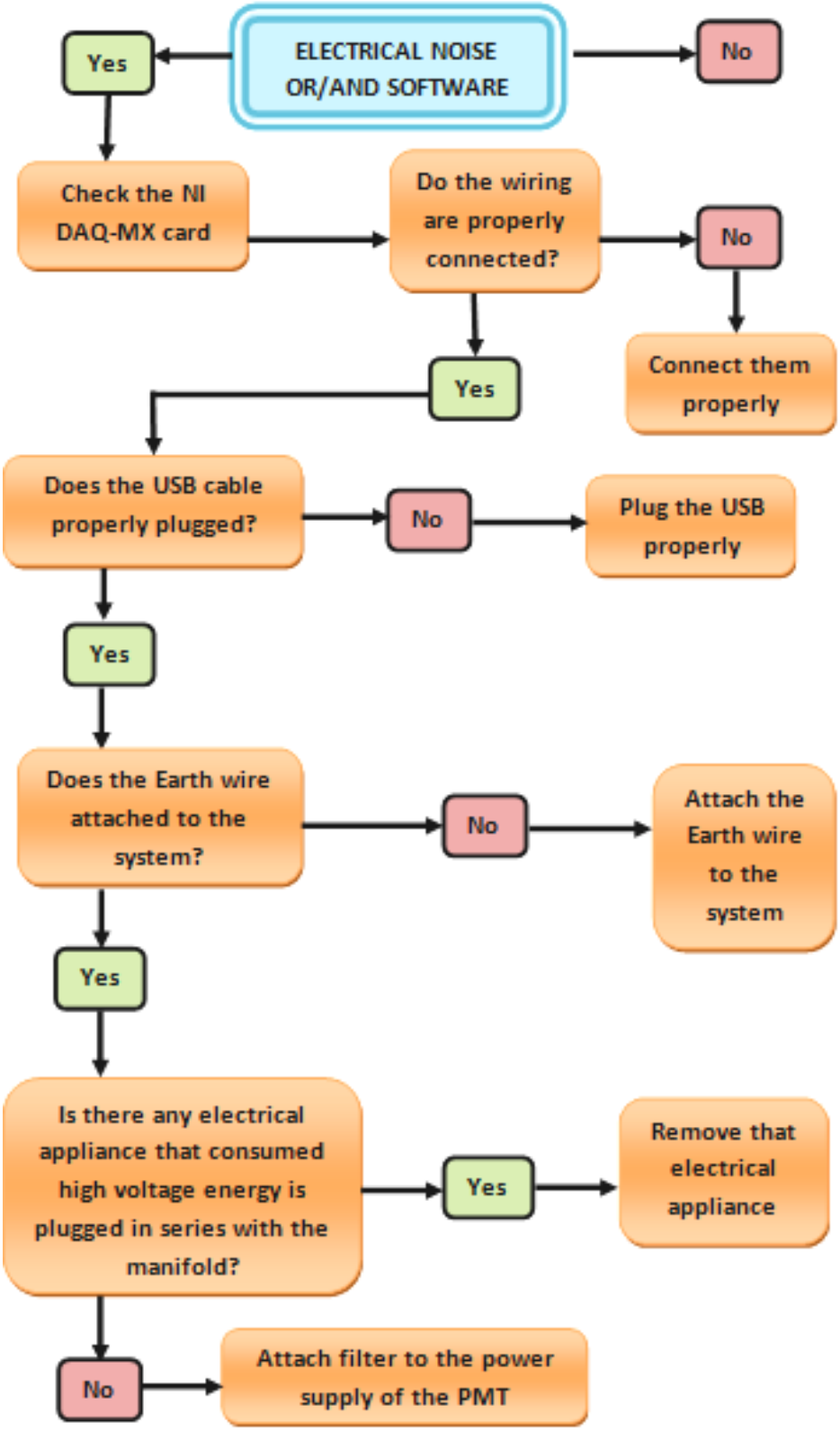

APPENDIX 2:

DISSOLVED MANGANESE, CTD, CHLOROPHYLL *A* AND NUTRIENTS DATA AT EACH OF THE STATIONS AROUND THE CROZET ISLANDS OF THE SOUTHERN OCEAN (*CROZEX* CRUISES: D285 & D286)

TableA2-1. Station locations, depths, dissolved manganese (DMn), Chl-*a*, macronutrients (nitrates, dissolved silicon, phosphates) concentrations, temperatures, salinity, and density values during D285 and D286 cruises. A dash indicates no sample was collected.

Station locations	Depth (m)	DMn (nM)	Chl *a* (mg m $^{-3}$)	Nitrates (µmol L^{-1})	Dissolved silicon (µmol L^{-1})	Phosphates (µmol L^{-1})	Temperature (°C)	Salinity	Density (σ_0)
M3 (496)	*5*	1.24	0.61	23.01	6.12	1.66	4.368	33.828	26.822
13/11/2004	*15*	0.64	0.87	-	-	-	4.371	33.829	26.822
46.06809 °S	*42*	0.85	0.68	22.91	6.11	1.64	4.370	33.829	26.822
51.78529 °E	*100*	0.77	1.10	22.84	6.43	1.60	4.227	33.828	26.839
(bottom depth	*150*	0.47	1.03	-	-	-	3.752	33.828	26.839
2287 m)	*175*	0.78	-	24.77	13.25	1.74	3.125	33.876	26.938
	218	0.41	-	25.56	16.63	1.80	2.990	33.856	26.981
	300	0.83	-	27.90	23.91	1.95	2.858	34.008	27.114
	500	0.72	-	27.90	23.91	1.95	2.855	34.008	27.121
	750	0.60	-	32.39	42.67	2.28	2.846	34.010	27.152
	1000	0.54	-	33.65	79.58	2.34	-	-	-
	1500	0.47	-	29.91	83.14	2.13	-	-	-
	2285	0.13	-	-	-	-	-	-	-
M3 (572)	*5*	1.31	1.01	22.64	1.85	1.53	5.211	33.826	26.720
22/12/2004	*10*	-	0.95	22.86	1.70	1.53	5.211	33.831	26.725
46.06223 °S	*15*	1.23	1.01	22.80	1.77	1.55	5.211	33.831	26.725
51.78169 °E	*25*	0.84	0.95	23.65	5.83	1.71	5.211	33.831	26.725
(bottom depth	*35*	0.65	0.97	27.64	19.98	1.87	5.212	33.831	26.725
2375 m)	*75*	0.72	0.82	32.56	43.25	2.39	4.960	33.835	26.756

	175	0.46	-	-	-	-	4.427	33.852	26.829
	500	-	-	-	-	-	3.108	33.931	27.023
M3 (622)	*5*	-	4.94	17.68	0.19	1.12	6.075	33.831	26.619
10/01/2005	*10*	0.37	5.10	-	-	-	6.075	33.831	26.620
46.03412 °S	*20*	-	4.95	17.78	0.37	1.18	6.075	33.831	26.619
51.86656 °E	*40*	-	3.94	-	-	-	5.661	33.838	26.705
(bottom depth	*50*	-	0.88	-	-	-	4.742	33.871	26.833
2322 m)	*60*	-	-	-	-	-	4.288	33.897	26.889
	80	-	0.29	25.48	15.05	1.81	3.881	33.925	26.945
	100	0.55	-	25.97	17.27	1.84	3.711	33.961	27.006
	150	-	-	27.43	23.80	1.94	3.313	33.997	27.057
	200	0.40	-	-	-	-	3.002	34.056	27.133
	300	-	-	29.95	31.79	2.09	2.742	34.117	27.205
	400	0.24	-	-	-	-	2.700	34.187	27.264
	500	(0.45)a	-	32.78	49.04	2.37	2.641	34.270	27.337
	1000	0.23	-	-	-	-	2.636	34.287	27.451
	1250	0.17	-	-	-	-	2.612	34.291	27.464
	1500	0.12	-	-	-	-	-	-	-
	2000	0.06	-	-	-	-	-	-	-
M1 (491)	*5*	0.64	0.90	-	-	-	5.813	33.727	26.566
11/11/2004	*10*	0.27	0.76	-	-	-	5.803	33.727	26.566
43.92049 °S	*15*	0.43	0.79	18.50	0.74	1.33	5.802	33.727	26.566
50.26742 °E	*25*	0.12	0.77	-	-	-	5.801	33.727	26.567
(bottom depth	*35*	0.33	-	-	-	-	5.761	33.726	26.570
3118 m)	*55*	0.26	0.73	18.38	0.86	1.31	5.769	33.727	26.571
	75	0.31	0.76	-	-	-	5.746	33.730	26.576
	100	0.10	-	27.95	26.18	2.00	4.417	33.890	26.882
	125	0.33	-	28.96	24.46	2.04	3.135	34.085	27.117
	150	0.21	-	32.91	48.98	2.28	2.741	34.301	27.347
	200	0.11	-	-	-	-	2.732	34.289	27.214
	300	0.30	-	-	-	-	-	-	-

	500	0.27	-	-	-	-	-	-	-
M7 (524)	*5*	0.72	1.34	19.05	0.06	1.26	5.530	33.816	26.675
27/11/2004	*10*	0.73	1.34	19.26	0.14	1.38	5.533	33.816	26.675
45.49943 °S	*15*	0.39	1.39	19.69	0.18	1.30	5.533	33.816	26.675
49.00242 °E	*25*	0.65	1.41	19.15	0.11	1.32	5.533	33.817	26.675
(bottom depth	*35*	-	1.38	19.13	0.25	1.32	5.528	33.818	26.677
2749 m)	*55*	0.42	1.22	23.23	6.53	1.79	5.044	33.837	26.748
	75	-	-	25.93	13.88	1.84	3.897	33.897	26.920
	100	-	-	28.13	17.21	1.96	3.444	33.906	26.971
	125	-	-	27.48	18.90	1.87	3.132	33.921	27.013
	150	-	-	28.19	20.14	1.87	3.008	33.939	27.038
	200	0.19	-	29.70	22.99	1.99	2.969	34.016	27.103
	300	-	-	32.15	29.70	2.23	2.872	34.143	27.214
	400	-	-	32.83	39.41	2.36	2.706	34.233	27.293
	500	0.20	-	35.05	48.75	2.44	2.650	34.294	27.355
	1000	0.17	-	-	-	-	-	-	-
	1500	0.23	-	-	-	-	-	-	-
	2000	0.14	-	-	-	-	-	-	-
	2500	0.20	-	-	-	-	-	-	-
	3000	0.14	-	-	-	-	-	-	-
M10 (563)	*5*	0.14	0.80	21.75	3.87	1.48	6.126	33.786	26.578
21/12/2004	*10*	0.29	0.73	-	-	-	6.132	33.786	26.577
44.52528 °S	*20*	-	-	21.69	3.91	1.46	6.142	33.786	26.576
49.96059 °E	*40*	0.38	0.80	-	-	-	6.125	33.786	26.578
(bottom depth	*60*	0.32	0.81	22.01	3.00	1.51	5.998	33.787	26.595
2943 m)	*80*	0.22	-	-	-	-	5.432	33.79	26.666
	125	0.22	-	-	-	-	-	-	-
	175	0.23	0.20	23.27	5.90	1.68	4.459	33.806	26.789
	250	0.20	-	26.15	15.16	1.80	3.700	33.902	26.943
	500	0.19	0.04	29.03	22.54	1.97	3.195	34.007	27.075
	750	0.21	-	-	-	-	-	-	-
	1000	0.19	-	-	-	-	-	-	-

	1500	0.16	-	-	-	-	-	-	-
	2000	0.15	-	-	-	-	-	-	-
	2500	0.11	-	-	-	-	-	-	-
	3000	0.10	-	-	-	-	-	-	-
M2 (502)	*5*	0.61	0.34	25.06	15.49	1.78	3.279	33.793	26.871
19/11/2004	*10*	0.11	0.39	23.93	15.90	1.75	3.155	33.787	26.881
47.79537 °S	*20*	0.64	0.35	23.83	15.89	1.79	3.174	33.79	26.890
52.86216 °E	*40*	0.41	0.42	24.38	15.86	1.83	3.159	33.791	26.903
(bottom depth	*60*	0.27	0.43	24.43	15.61	1.75	3.16	33.801	26.912
3870 m)	*80*	0.21	0.43	24.64	16.00	1.78	3.161	33.805	26.914
	125	0.27	-	-	-	-	3.16	33.805	26.914
	175	0.25	-	-	-	-	3.156	33.805	26.915
	250	0.22	-	-	-	-	3.511	33.804	26.915
	500	0.22	-	-	-	-	3.497	33.803	26.918
	750	0.21	-	-	-	-	3.498	33.804	26.920
	1000	0.21	-	-	-	-	-	-	26.919
	1500	0.15	-	-	-	-	-	-	26.918
	2000	0.16	-	-	-	-	-	-	-
	2500	0.16	-	-	-	-	-	-	-
	3000	0.10	-	-	-	-	-	-	-
	3500	0.13	-	-	-	-	-	-	-
	3800	0.07	-	-	-	-	-	-	-
M6 (511)	*5*	0.31	0.27	24	18.40	1.75	4.368	33.842	26.948
22/11/2004	*10*	0.21	0.25	-	-	-	4.370	33.842	36.948
49.00557 °S	*20*	0.24	0.25	-	-	-	4.369	33.842	26.960
51.50046 °E	*40*	0.36	0.45	25.28	18.67	1.83	4.227	33.841	26.966
(bottom depth	*60*	0.13	0.27	24.56	18.18	1.77	3.875	33.862	26.974
4275 m)	*80*	-	0.38	24.62	18.52	1.81	3.621	33.872	26.974
	250	-	-	-	-	-	3.516	33.878	26.976
	750	0.24	-	35.86	76.53	2.62	3.505	33.881	27.129
	1000	0.16	-	33.68	79.35	2.36	3.501	33.880	27.135
	1250	0.25	-	30.59	82.80	2.27	-	-	-

	1750	0.13	-	29.40	88.23	2.21	-	-	-
	2500	0.09	-	30.37	111.08	2.35	-	-	-
	3000	-	-	31.75	125.33	2.42	-	-	-
	3500	0.13	-	32.59	137.71	2.43	-	-	-
	4000	0.12	-	31.96	150.65	2.49	-	-	-
	4273	0.19	-	31.68	161.01	2.46	-	-	-
M6 (598)	*5*	0.19	0.39	-	-	-	2.71	33.794	26.826
03/01/2005	*10*	0.13	0.39	-	-	-	2.687	33.794	26.826
48.9990 °S	*40*	0.16	0.38	-	-	-	2.705	33.809	26.826
51.5380 °E	*60*	0.13	0.31	-	-	-	2.53	33.811	26.841
(bottom depth	*80*	0.33	0.31	-	-	-	2.572	33.812	26.894
4214 m)	*100*	0.14	0.39	-	-	-	2.469	33.82	26.895
	160	0.11	-	-	-	-	1.661	33.911	26.928
	255	0.24	-	-	-	-	-	-	26.929
	750	0.10	-	-	-	-	-	-	-
	1500	0.07	-	-	-	-	-	-	-
	2000	0.03	-	-	-	-	-	-	-
	3000	0.09	-	-	-	-	-	-	-
	4000	0.09	-	-	-	-	-	-	-
	4168	(0.42)a	-	-	-	-	-	-	-
BA (567)	*5*	2.42	0.57	23.95	7.91	1.71	4.563	33.871	26.830
22/12/2004	*25*	2.03	0.56	24.03	7.83	1.70	4.520	33.872	26.834
46.36854 °S	*50*	2.44	0.54	24.04	8.74	1.72	4.370	33.883	26.863
51.82754 °E	*80*	2.01	0.47	24.43	10.25	1.71	4.248	33.889	26.874
(bottom depth 83 m)									
BA+1 (568)	*5*	1.87	0.60	22.28	5.13	1.61	4.633	33.870	26.819
22/12/2004	*25*	1.30	0.62	22.42	4.91	1.60	4.644	33.870	26.819
46.32332 °S	*50*	0.69	0.62	22.14	4.68	1.64	4.605	33.870	26.823
51.89459 °E	*100*	0.45	0.27	23.77	8.77	1.68	3.956	33.908	26.924
(bottom depth	*200*	0.99	0.30	28.35	25.27	2.00	3.435	33.982	27.034

379 m)	*300*	1.92	0.19	-	-	-	2.986	34.075	27.151
	376	0.63	0.06	30.34	35.99	2.14	2.760	34.190	27.262
BA+2 (569)	*5*	0.36	0.88	22.52	3.75	-	4.662	33.855	26.796
22/12/2004	*25*	0.57	1.00	22.58	4.00	1.56	4.678	33.864	26.810
46.26997 °S	*50*	0.60	0.45	24.80	10.73	1.68	4.049	33.898	26.899
51.97083 °E	*100*	0.31	0.18	26.32	15.61	1.81	3.669	33.962	27.007
(bottom depth	*300*	0.71	0.04	29.59	29.26	2.08	2.803	34.112	27.199
1491 m)	*750*	0.34	-	-	-	-	2.606	34.438	27.476
	1000	0.49	-	-	-	-	2.523	34.438	27.476
	1250	0.22	-	-	-	-	2.505	34.446	27.477

( )a indicates contamination sample

APPENDIX 3:

STATIONS, DISSOLVED MANGANESE, CHLOROPHYLL *A*, NITRATE+NITRITE, PHOSPATE DATA, AND RESIDENCE TIMES IN SURFACE WATERS OF THE TROPICAL NE ATLANTIC OCEAN (*UK SOLAS* CRUISE: D326)

Table A3-1. Stations, locations, dissolved manganese (DMn), Chl-*a* concentrations, nitrate+nitrite, phosphate, and residence time (considering the average mixed layer is 50 m) during D326 cruise (Chl-*a* data: courtesy of Dr. Duncan Purdie of NOCS).

Station (UT)	DMn (nM)	DMn S.D. (nM)	Chl-a (µg/L)	Nitrate+nitrite (nM)	Phosphate (nM)	Residence Time (year)
1	3.31	0.12	0.18	51	100	2.70
2	1.83	0.04	0.79			1.50
3	1.79	0.05	0.41			1.50
4	1.74	0.10	0.61			1.40
5	1.49	0.05	0.44			1.20
6	1.26	0.01	0.42			1.00
7	0.93	0.01	0.56	18	50	0.80
8	1.04	0.02	0.46			0.90
9	0.92	0.03	0.69	16	32	0.80
10	0.81	0.04	0.31			0.70
11	0.75	0.01	0.20			0.60
12	0.70	0.03	0.19			0.60
13				12	8	
14	0.57	0.03	0.19			0.50
15	0.54	0.03	0.25	10	9	0.40
16	0.50	0.05	0.36			0.40
17	0.50	0.36	0.39			0.40
18	0.52	0.02	0.20			0.40
19	0.52	0.11	0.30			0.40
20	0.39	0.17	0.27			0.30
21	0.54	0.01	0.23	6	5	0.40
22	0.59	0.06	0.13			0.50
23	0.35	0.02	0.02			0.30
24	0.53	0.04		9	4	0.40
25	0.41	0.02	0.08			0.30
26	0.61	0.01	0.11			0.50
27	0.59	0.02	0.11			0.50
28	0.39	0.03	0.11	9	6	0.30
29	0.32	0.04	0.11			0.30
29	0.33	0.03	0.09	11	12	0.30
30	0.32	0.03	0.09	19	15	0.30
31	0.34	0.02	0.15	8.5	8	0.30
32	0.37	0.03	0.16	7.5	9	0.30

33	0.57	0.02	0.15	8	13	0.50
34	0.59	0.08	0.15	9	9	0.50
35	0.58	0.31	0.15	9	22	0.50
36	0.62	0.02	0.18	5	23	0.50
37	0.58	0.08	0.16	7	30	0.50
38	0.42	0.02	0.15	9	15	0.30
39	0.64	0.04	0.16			0.50
40	0.55	0.09	0.18			0.50
41	0.66	0.07	0.18			0.50
42	0.78	0.04	0.35			0.60
43	0.67	0.03	0.22	9	60	0.60
44	0.78	0.02	0.16	15	61	0.60
45	0.95	0.03	0.18			0.80
46	1.07	0.02	0.15	19	75	0.90
47	1.33	0.01	0.19			1.10
48	1.64	0.04				1.30
49	1.71	0.03	0.16			1.40
50	2.22	0.05	0.22	16	90	1.80
51	2.22	0.08	0.18	38	100	1.80
52	1.75	0.15	0.18			1.40
53	0.66	0.12	0.24			0.50
54						
55	0.94	0.01	0.27			0.70
56	0.82	0.01	0.21	16.5	88	0.70
57	2.12	0.02	0.25			1.70
58	3.31	0.03	0.29			2.70
59						
60	3.87	0.05	0.33			3.20
61	3.48	0.10	0.30	51	60	2.90
62	2.01	0.06	0.37	48	53	1.70
63	1.94	0.00	0.37	3	26	1.60
64	1.09	0.08	0.37	5	12	0.90
65	1.42	0.04	0.43	6	11	1.20
66	2.23	0.02	0.34	5	9	1.80
67	1.16	0.07	0.31	6	5	1.00
68	1.60	0.02	0.20	5	8	1.30
69	1.58	0.13	0.33	6	9	1.30
70	1.47	0.08	0.38	5	11	1.20
71	1.77	0.01	0.31	6	12	1.50
72	1.97	0.11	0.26	7	7	1.60
73	0.78	0.07	0.26	8.5	5	0.60
74	0.92	0.01		9	8	0.80
75	1.75	0.01	0.58	9.5		1.40
76	1.29	0.05	0.57			1.10
77	0.63	0.02	0.52	5	5	0.50
78	1.48	0.07	0.41			1.20
79	0.57	0.02	0.45	6	7	0.50
80	0.69	0.01	0.33	8	15	0.60

81				6	20	
82	0.76	0.02	0.33	9	12	0.60
83	0.76	0.01	0.35	7.5	7	0.60
84	1.08	0.03	0.16	8	5	0.90
85	0.93	0.03	0.16	7.5	6	0.80
86	0.94	0.00	0.16	5	11	0.80
87	0.56	0.02	0.17	10	5	0.50
88	0.51	0.04	0.19	9	7	0.40
89	3.02	0.00	0.22	6.5	6	2.50
90	0.74	0.00	0.10	9	5	0.60
91	0.71	0.02	0.20	6.5	13	0.60
92	0.50	0.01	0.21	7	24	0.40
93	0.50	0.02	0.18	7.5	13	0.40
94	1.88	0.01	0.24	9	12	1.50
95	0.55	0.02	0.19	10	11	0.50
96	0.53	0.01	0.19	10.5	9	0.40
97	0.61	0.03	0.41	9	8	0.50
98	0.61	0.01	0.37	9	15	0.50
99			0.31	10	14	0.00
100	1.50	0.03	0.25	8.5	10	1.20
101	0.58	0.01	0.28	13	11	0.50
102	0.56	0.02	0.19	9.5	12	0.50
103	0.51	0.01	0.23	12	15	0.40
104	0.62	0.03	0.24	7.5	13	0.50
105	1.00	0.03	0.28	6.5	8	0.80
106	0.68	0.01	0.24	6.5	14	0.60
107	0.60	0.02	0.28	6	13	0.50
108	0.59	0.01	0.24	9.5	11	0.50
109	1.12	0.06	0.22	12.5	13	0.90
110	0.58	0.03	0.34	9.5	20	0.50
111	0.51	0.01	0.21	10	10	0.40
112	0.54	0.02	0.17	10	9	0.40
113	0.69	0.00	0.28	9.8	7	0.60
114	0.68	0.01	0.22	10	11	0.60
115	0.52	0.01	0.22	9		0.40
116	0.65	0.02	0.29	8	11	0.50
117	1.08	0.02	0.25	6.5	12	0.90
118	0.57	0.02	0.24	5	11	0.50
119	0.63	0.07	0.24	6	12	0.50
120	0.67	0.02	0.23	9.5	9	0.50
121	0.57	0.01	0.15	6	11	0.50
122	0.59	0.00	0.19	9	12	0.50
123	0.59	0.02	0.20	8.5	13	0.50
124	0.50	0.01	0.18	8	22	0.40
125	1.55	0.08	0.19	6	40	1.30
126	1.89	0.02	0.20	5.5	40	1.50
127	1.94	0.12	0.20	5	45	1.60
128	0.81	0.03	0.21	5.5	50	0.70

129	1.70	0.04	0.20	5	15	1.40
130	1.24	0.29	0.18	5	35	1.00
131	0.51	0.02	0.15	5	90	0.40
132	1.59	0.01	0.14	5	60	1.30
133	0.59	0.01	0.15	23	70	0.50
134	0.58	0.01	0.10	9.5	80	0.50
135	0.55	0.01	0.14	30	100	0.50
136	1.68	0.01	0.12	51	102	1.40
137	1.57	0.00	0.13	50	101	1.30
138	1.62	0.02	0.12	9	103	1.30
139	1.52	0.00	0.14	8	104	1.20
140	1.53	0.02	0.16	9.5	102	1.30
141	1.58	0.01	0.16	8	90	1.30
142	1.53	0.02	0.17	7.5	88	1.30
143	0.93	0.04	0.16	9.8	77	0.80
144	0.97	0.02	0.17	9	78	0.80
145	0.50	0.03	0.27	8.5	56	0.40
146	3.07	0.25	0.13	9.7	58	2.50
147	1.62	0.01	0.25	12	60	1.30
148	0.65	0.03	0.19	9.5	65	0.50
149	0.54	0.00	0.17	9.7	62	0.40
150	0.55	0.00	0.18	9.5	37	0.50
151	0.57	0.02	0.12	8	41	0.50
152	0.51	0.05	0.16	9		0.40
153	0.53	0.03	0.19	7.5	28	0.40
154	0.60	0.01	0.15	7	12	0.50
155	0.51	0.06	0.18	9.5	13	0.40
156	0.54	0.01	0.13	9	13	0.40
157	0.58	0.00	0.16	9	8	0.50
158	0.60	0.05	0.14	9.5	12	0.50
159	0.47	0.01	0.12	19	13	0.40
160	0.33	0.00	0.18	31	9	0.30
161	0.56	0.01	0.11	18	9	0.50
162	1.18	0.14	0.18	17.5	15	1.00
163	0.50	0.01	0.20	10	11	0.40
164	1.22	0.06	0.26	8.5	12	1.00
165	0.52	0.00	0.21		11	0.40
166	0.53	0.01	0.21	11	12	0.40
167	1.08	0.04	0.23	15	11	0.90
168	1.14	0.03	0.25	8.5	9	0.90
169	0.58	0.00	0.19	11	11	0.50
170	0.51	0.04	0.19	20	9	0.40
171	1.08	0.06	0.20	9	5	0.90
172	0.53	0.01	0.18	7.5	5	0.40
173	0.51	0.02	0.20	7	6	0.40
174	0.50	0.04	0.21	12.5	6	0.40
175	1.13	0.01	0.17	11	3	0.90
176	0.50	0.02	0.15	7.6	7	0.40

177	0.54	0.01	0.22	9.6	5	0.40
178	0.56	0.01	0.24	20	12	0.50
179	0.51	0.01	0.20	18	12	0.40
180	0.65	0.01	0.22	8.5	5	0.50
181	1.32	0.02	0.23	9.5	5	1.10
182			0.19	5	6.5	0.00
183	0.52	0.01	0.19	7.5	7	0.40
184	1.71	0.11	0.19	48	5	1.40
185	1.81	0.02	0.13	8.5	7	1.50
186	1.17	0.00	0.18	46.3	3	1.00
187	1.23	0.01	0.17	47	12	1.00
188	1.36	0.02	0.21	9.5	3	1.10
189	1.22	0.01	0.17	7	3	1.00

APPENDIX 4:

REPORT ON THE PARTICIPATION ON THE DISCOVERY D351 RESEARCH CRUISE

Samples collection for dissolved manganese analysis

Farah Idrus (NOCS)

1 Introduction

Manganese is a key element in photosynthesis (Sunda *et al.,* 1983; Peers and Price, 2004), and also involved through redox processes (Sunda and Huntsman, 1988) in cycles of many elements in oceanic waters. It is also a good tracer of atmospheric and terrestrial inputs. In addition, the recent volcanic eruption in Iceland could supply a massive atmospheric input of manganese from the volcanic ash plume. Manganese can be dissolved from volcanic ash dust and thus may be a useful indicator of volcanic dust inputs to the surface ocean. The general aim of this cruise was to improve the knowledge of the clean sampling of manganese and other trace metals onboard ship.

2 Method

Sampling –Low Density Poly Ethylene (LDPE) bottles (Nalgene, Fisher Scientific UK) were used for the storage of the seawater samples for Mn analysis, which have been thoroughly acid-washed. Water column samples were collected at four selected CTD stations along the transect using the titanium-frame CTD, which was fitted with trace metal clean 10L OTE (Ocean Technology Equipment) sampling bottles with external springs, modified for trace metal work. At these stations LDPE sample bottles were used to collect seawater samples at up to twelve depths, depending on water depth at each station. The trace metal sample bottles were then transferred to a clean van on the back deck for sample processing. The underway surface sampling was conducted every one to two hours during transit between stations along transect. However, only six samples of underway samples were collected during this cruise for manganese analysis. This was done with a towfish deployed off the port side of the ship. Water was pumped into the clean van with a diaphragm pump connected to the ship's compressed air.

Sample processing – Filtered samples were collected (for dissolved manganese) in 1L Nalgene LDPE bottles from the titanium frame rosette bottles. Filtered samples were collected through a Sartobran 300 MF 0.2πm filter cartridge under slight positive pressure (oxygen-free N_2). Underway samples were also collected in 1L Nalgene LDPE bottles, using a Sartobran 300MF 0.2πm filter cartridge. All water samples were acidified to pH~2 with 1mL Hydrochloric acid per 1L seawater sample (Romil UpA) within 24 hours of collection.

These were carried out on a laminar flow clean bench to minimize the risk of contamination.

Data analysis – Samples from underway and vertical profiles are to be analysed using a flow injection system that was set up in the laboratory at the NOCS. The method is based on a flow injection analysis (FIA) chemiluminescene technique (Doi *et al.*, 2004) where manganese catalyses the peroxide oxidation of luminol in the presence of hydroxide salt as an activator. However, the method as used here has some important modifications, including using a commercially available complexing resin, Toyopearl AF Chelate-650M to pre-concentrate the manganese, and using the nitrilotriacetic acid (NTA) to remove interfering iron ions in the carrier solution.

3 Results

Four profiles were sampled (see Figure A4-1 and Table A4-1) from the Ti-frame CTD and 6 underway samples (Figure A4-1 and Table A4-2) from the tow-fish. The samples will be analysed in the lab at NOCS (Southampton).

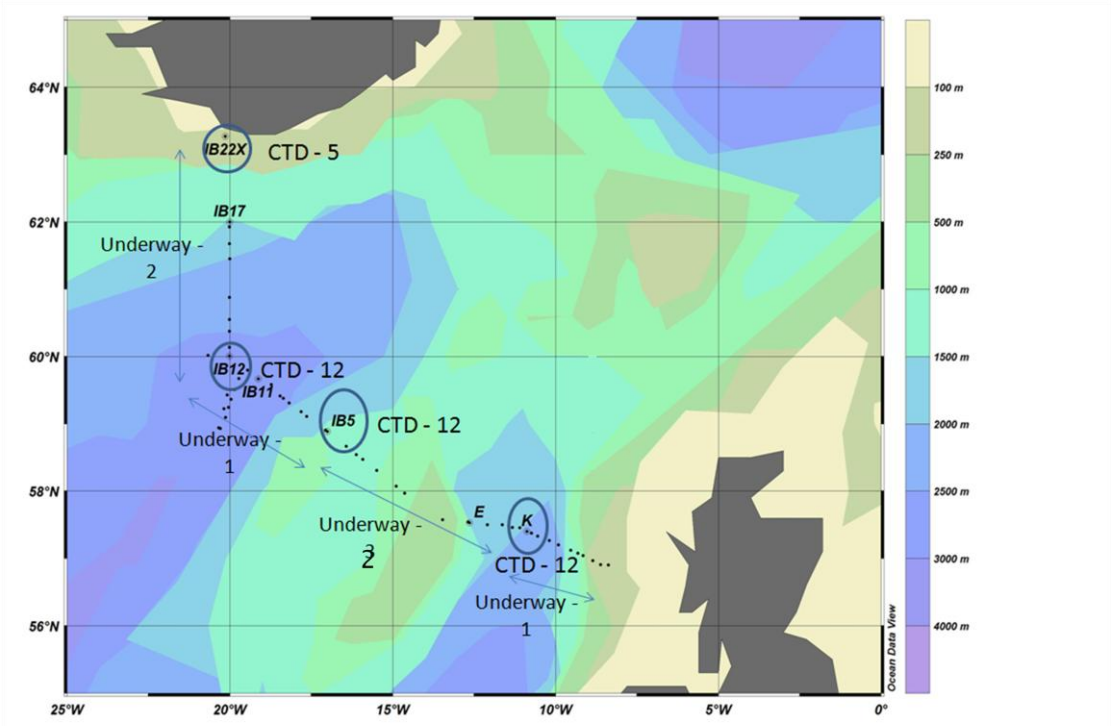

Figure A4-1: Cruise track with positions of Ti-frame CTDs and underway samples. Blue circles are the sampling stations for CTDs and numbers indicate the samples taken at each station.

Table A4-1: List of stations which were sampled for vertical profiles of dissolved manganese

Date	Time in water (GMT)	Station	Latitude (North)	Longitude (West)	Depths (m)
12/05/10	10:59	IB22X	63˚ 13.132	20˚03.760	22, 32, 42, 102, 201, 351, 500, 653
16/05/10	03:00	IB12	60˚00.280	19˚59.873	27, 47, 62, 88, 158, 268, 406, 606, 1007, 1507, 2004, 2709
17/05/10	20:13	IB5	58˚53.174	17˚01.214	22, 42, 57, 77, 103, 202, 300, 397, 597, 746, 998, 1135
20/05/10	01:10	K	57˚23.799	10˚52.223	22, 32, 53, 103, 152, 202, 262, 302, 402, 501

Table A4-2. List of stations which were sampled for the surface underway of dissolved manganese

Date	Time (GMT)	Station	Latitude (North)	Longitude (West)
12/05/10	17:24	U75	63˚ 13.132	20˚03.760
15/05/10	12:43	U84	60˚59.965	20˚00.524
17/05/10	09:45	U93	59˚20.028	18˚14.412
18/05/10	07:19	U99	59˚30.055	15˚58.911
18/05/10	22:34	U105	57˚33.840	13˚20.250
21/05/10	20:11	U129	56˚40.085	06˚08.130

References

Doi, T., Obata, H., & Maruo, M. (2004) Shipboard analysis of picomolar levels of manganese in seawater by chelating resin concentration and chemiluminescence detection. *Analytical and Bioanalytical Chemistry,* 378**,** 1288-1293.

Peers, G. & Price, N. M. (2004) A role for manganese in superoxide dismutases and growth of iron-deficient diatoms. *Limnology and Oceanography,* 49**,** 1774-1783.

Sunda, W. G. & Huntsman, S. A. (1988) Effect of sunlight on redox cycles of manganese in the Southwestern Sargasso Sea. *Deep-Sea Research Part a-Oceanographic Research Papers,* 35**,** 1297-1317.

Sunda, W. G., Huntsman, S. A. & Harvey, G. R. (1983) Photo-reduction of manganese oxides in seawater and its geochemical and biological implications. *Nature,* 301**,** 234-236.